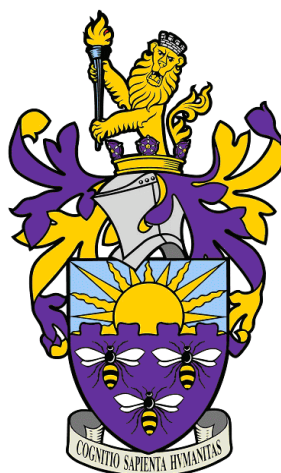


# **New applications of Peroxidases in Biotechnology and Nanotechnology**



A thesis submitted to the University of Manchester for the degree of  
Doctor of Philosophy (PhD) in the Faculty of Science and Engineering

**2016**

**Joseph Hosford**

School of Chemistry

## Table of contents

	<b>Page</b>
<b>Table of contents</b> .....	<b>2</b>
<b>List of Figures</b> .....	<b>8</b>
<b>List of Schemes</b> .....	<b>13</b>
<b>List of Tables</b> .....	<b>17</b>
<b>Abstract</b> .....	<b>18</b>
<b>Declaration</b> .....	<b>19</b>
<b>Copyright Statement</b> .....	<b>20</b>
<b>List of Abbreviations</b> .....	<b>21</b>
<b>List of Abbreviations – Amino Acids</b> .....	<b>23</b>
<b>1.0 Introduction and literature review</b> .....	<b>24</b>
<b>1.1 Biocatalysis</b> .....	<b>25</b>
<b>1.2 Oxidoreductases</b> .....	<b>25</b>
<b>1.2.1 Peroxidases</b> .....	<b>26</b>
<b>1.2.2 Heme-dependent peroxidases</b> .....	<b>27</b>
<b>1.2.3 Redox potential</b> .....	<b>29</b>
<b>1.3 Horseradish peroxidases (HRP)</b> .....	<b>30</b>
<b>1.3.1 Horseradish peroxidase isoenzyme C1A</b> .....	<b>31</b>
<b>1.3.1.1 Prosthetic heme group</b> .....	<b>31</b>
<b>1.3.1.2 Active site</b> .....	<b>33</b>
<b>1.4 Enzyme mechanism and catalytic cycle</b> .....	<b>34</b>
<b>1.5. Enzyme expression and Isolation</b> .....	<b>37</b>
<b>1.5.1 Native expression</b> .....	<b>37</b>
<b>1.5.2 Heterologous expression</b> .....	<b>38</b>
<b>1.5.2.1 Bacterial host</b> .....	<b>39</b>
<b>1.5.2.2 Eukaryotic host</b> .....	<b>39</b>
<b>1.6 Biotransformations performed by HRPs</b> .....	<b>40</b>
<b>1.6.1 Oxygen insertion</b> .....	<b>40</b>

1.6.1.1 Sulfoxidation .....	40
1.6.1.2 Epoxidation .....	41
1.6.1.3 Hydroxylation .....	42
1.6.2 Nitration .....	42
1.6.3 <i>N</i> -dealkylation .....	43
1.6.4 Oxidative dehydrogenation .....	45
1.6.4.1 Oxidation to quinonoid systems .....	45
1.6.4.2 Oxidative polymerisation .....	47
1.6.4.2.1 Phenolic polymerisation .....	47
1.6.4.2.2 Polymerisation of anilines, pyrroles and thiophenes .....	50
1.6.4.2.2.1 Electronically conducting polymers .....	50
1.6.4.2.2.2 Aniline polymerisation .....	51
1.6.4.2.2.3 Thiophene polymerisation .....	54
1.6.4.2.2.4 Pyrrole polymerisation .....	56
1.7 Nanolithography .....	56
1.7.1 Scanning probe nanolithography .....	57
1.7.1 Nanotechnological applications of peroxidases .....	59
1.7.2 Nanolithographic applications of peroxidases .....	60
1.7.3 Scanning probe nanolithography .....	60
1.7.4 Biocatalytic nanolithography .....	62
1.8 Aims .....	64
2.0 Advancing biocatalytic nanolithography .....	65
2.0.1 Catalytic probe nanolithography .....	65
2.0.2 Biocatalytic probes .....	66
2.0.3 Multiplexed nanolithography .....	67
2.1 Aims and objectives .....	68
2.2 Cloning and expression of horseradish peroxidase isoenzyme C1A .....	69
2.2.1 <i>ybbR</i> -C1A activity assays .....	72
2.2.2 Polyaniline formation .....	73

2.2.3 <i>Sfp</i> mediated C1A immobilisation .....	75
2.3 Single probe biocatalytic nanolithography .....	77
2.3.1 <i>Sfp</i> mediated ybbR-C1A immobilisation .....	77
2.3.2 Confinement of ybbR-C1A to the apex of cantilever .....	79
2.3.3 Nanolithography with ybbR-C1A functionalised probe on mica .....	80
2.3.4 Nanolithography with C1A functionalised probe on 4-aminothiophenol functionalised surfaces .....	82
2.4 Multiplexed wide area lithography .....	85
2.4.1 Probe array alignment to substrate .....	86
2.4.1.1 Probe alignment algorithm .....	87
2.4.1.2 Alignment algorithm validation .....	89
2.4.2 Biocatalytic probe array preparation .....	91
2.4.2.1 Linker assembly on PDMS .....	92
2.4.2.2 Confinement of C1A to probe array tip apex .....	93
2.4.2.3 Enzyme functionalised probe arrays activity assay.....	96
2.4.3 Lithography with enzyme probe arrays .....	97
2.4.3.1 4-ATP functionalised glass .....	98
2.4.3.2 Lithography via <i>o</i> -methoxyaniline polymerisation and deposition .....	98
2.4.3.2 Raman mapping on gold 4-ATP functionalised surfaces .....	102
2.4.3.3 Wide area post polymerisation florescence (with alkyne-aniline) .....	104
2.5 Conclusions.....	107
3.0 Fused aromatics from peroxidase catalysed quinonoid intermediates and tandem cyclisation reaction .....	108
3.1 Introduction .....	108
3.1.1 Aims .....	110
3.2 Peroxidase-catalysed <i>o</i> -benzoquinone imine generation .....	111
3.2.2 Development of the biocatalytic synthesis of 1,4-benzoxazines .....	112
3.2.3 Tandem reaction substrate scope - (100mg scale) .....	117
3.3 Peroxidase-catalysed <i>o</i> -quinone methide generation .....	119

<b>3.3.1 Development chromane biocatalytic synthesis .....</b>	<b>121</b>
<b>3.3.2 Optimisation of reaction .....</b>	<b>125</b>
<b>3.4 Conclusions .....</b>	<b>128</b>
<b>4.0 Assay for enzymatic aryl-amine halogenation based on a peroxidase-mediated quinone-amine coupling .....</b>	<b>130</b>
<b>4.1 Introduction .....</b>	<b>130</b>
<b>4.2 Aims .....</b>	<b>132</b>
<b>4.3 Development of halogenation assay .....</b>	<b>133</b>
<b>4.4 Substrate range .....</b>	<b>134</b>
<b>4.5 Quantitative analysis .....</b>	<b>135</b>
<b>4.6 Coupling with a flavin dependent halogenase system .....</b>	<b>138</b>
<b>4.7 Conclusions .....</b>	<b>140</b>
<b>5.0 Concluding remarks .....</b>	<b>142</b>
<b>6.0 Experimental .....</b>	<b>144</b>
<b>6.1 General .....</b>	<b>144</b>
<b>6.1.1 General materials .....</b>	<b>144</b>
<b>6.1.1.1 Growth Media .....</b>	<b>146</b>
<b>6.1.1.2 Buffers .....</b>	<b>146</b>
<b>6.1.2 General apparatus .....</b>	<b>147</b>
<b>6.1.3 General molecular biology methods .....</b>	<b>148</b>
<b>6.1.3.1 Polymerase chain reaction (PCR) .....</b>	<b>148</b>
<b>6.1.3.2 DNA electrophoresis .....</b>	<b>149</b>
<b>6.1.3.3 SDS-PAGE .....</b>	<b>150</b>
<b>6.1.3.4 Extraction of DNA from Agarose gel .....</b>	<b>150</b>
<b>6.1.3.5 Gibson assembly .....</b>	<b>151</b>
<b>6.1.3.6 Transformation of chemically competent bacterial cells .....</b>	<b>152</b>
<b>6.1.3.7 Preparation of chemically competent bacterial cells .....</b>	<b>152</b>
<b>6.1.3.8 Plasmid DNA isolation and purification .....</b>	<b>153</b>
<b>6.1.3.9 Glycerol stock preparation .....</b>	<b>153</b>


6.1.3.10 Restriction digestion of DNA .....	153
6.2 Methods for Chapter 2 .....	155
6.2.1 Production of ybbR-C1A .....	155
6.2.2 Purification of ybbR-C1A .....	155
6.2.3 Synthesis of agarose Immobilised 2-naphylhydroxamic acid .....	156
6.2.4 Peroxidase activity assay (ABTS) .....	156
6.2.5 Conducting polymer enzyme synthesis .....	157
6.2.6 Conducting polymer chemical synthesis .....	157
6.2.7 Fluorescent labelling of ybbR-C1A .....	157
6.2.8 Surface Linker synthesis on silicon nitride (AFM probes) .....	158
6.2.9 ABTS assay on silicon nitride surfaces .....	159
6.2.10 Tip apex CoA confinement on silicon nitride (AFM probes) .....	159
6.2.11 Single probe biocatalytic nanolithography (on mica and ATP surface) .....	159
6.2.12 Synthesis of enzyme substrates: 3-(prop-2-yn-1-yloxy)aniline .....	160
6.2.13 4-aminobenzenethiol functionalised gold surface preparation .....	161
6.2.14 4-aminobenzenethiol functionalised silicon oxide surface preparation .....	161
6.2.14.1 <i>tert</i> -butyl (4-mercaptophenyl)carbamate .....	161
6.2.14.2 4-ATP surface modification .....	162
6.2.15 Surface Linker synthesis on polydimethylsiloxane (PDMS) probe arrays .....	163
6.2.16 ybbR-C1A enzyme immobilisation .....	163
6.2.17 Probe apex CoA confinement on PDMS probe arrays .....	164
6.2.18 Activity assay on HRP immobilised PDMS probe arrays .....	164
6.2.19 Multiplexed biocatalytic nanolithography (on 4-ATP surfaces) .....	165
6.2.20 Raman mapping experiments .....	165
6.2.21 Post lithography florescence functionalisation (3-(prop-2-yn-1-yloxy)aniline substrate) .....	166
6.2.22.1 Z-position measurement .....	166
6.2.22.2 The detection of the amount of force .....	166
6.2.22.3 Selection of z-position step lengths .....	167

6.2.22.4 Tilt angle and data analysis .....	167
6.2.23 Polymer pen nanolithography of 16-mercaptohexadecanoic acid on gold substrates .....	168
6.3 Methods from Chapter 3 .....	169
6.3.1 Quinone Imine product standard and precursor synthesis .....	169
6.3.2 Quinone Imine enzyme assays methods .....	171
6.3.2.1 General analytical assay procedure .....	171
6.3.2.2 General larger scale assay procedure for NMR analysis .....	172
5.3.3 Quinone methide product standard and precursor synthesis .....	175
5.3.4 Quinone methide general analytical enzyme assay .....	181
6.4 Methods from Chapter 4 .....	182
6.4.1 Halogenation assay general assay procedure .....	182
6.4.2 HPLC assay analysis .....	182
6.4.3 Cofactor recycling system enzyme production .....	182
6.4.4 Tryptophan-7-halogenase (RebH) production .....	183
6.4.5 Purification of RebH, Fre and GDH2 .....	183
6.4.6 RebH-catalysed halogenation .....	184
6.4.7 RebH-catalysed halogenation assay analysis .....	184
6.4.8 RebH-catalysed halogenation HPLC Analysis .....	185
6.4.9 Synthesis of 1-bromonaphthalen-2-amine .....	185
7.0 References .....	186
8.0 Appendix .....	193
8.1 ybbR-C1A Sequences .....	193
8.2 Sfp sequences .....	194
8.3 RebH Sequences.....	195
8.4 Fre Sequences.....	196
8.5 GDH2 Sequence.....	197

**List of figures**

	<b>Page</b>
<b>Figure 1.1.</b> Depiction of the partial structure of plant Lignin, reported to be HRP's natural catalytic product .....	<b>30</b>
<b>Figure 1.2</b> Crystallographic structure of horseradish peroxidase isoenzyme C1A, highlighting heme B group (in yellow) and calcium ions (in green) .....	<b>32</b>
<b>Figure 1.3.</b> Structure of iron (III) protoporphyrin IX (heme B) .....	<b>33</b>
<b>Figure 1.4. (A)</b> Stick model of the side view of Heme B structure within the active site of HRP C1A. <b>(B)</b> Side view of the structure and composition of key active site residues. <b>(C)</b> Cartoon model highlighting active site gatekeeper residues in orange. <b>(D)</b> Space filling model highlighting active site gatekeeper residues in orange .....	<b>34</b>
<b>Figure 1.5. (A)</b> Model of crystal structure of isoenzyme C1A with <i>N</i> -hydroxybenzamide bound. Protein databank reference: 1GX2, <b>(B)</b> Depiction of bonding residues of isoenzyme C1A with agarose-naphthylhydroxamic acid .....	<b>38</b>
<b>Figure 1.6.</b> Depiction of the general ring structures of known conducting polymers .....	<b>49</b>
<b>Figure 1.7.</b> Diagrammatic representation of dip-pen nanolithography, with zoomed inlay of molecular deposition at AFM tip apex .....	<b>58</b>
<b>Figure 1.8</b> Stylised depiction of polymer pen lithography probe array and lithographic ink deposition .....	<b>59</b>
<b>Figure 2.1</b> Diagram depicting the issue with non-uniform probe array alignment, whereby misalignment cause probes to reach the surface at different heights .....	<b>67</b>
<b>Figure 2.2. (A)</b> Schematic map of vector pET28a_ybbR_C1A <b>(B)</b> Photo of agarose gel showing fluorescent DNA fragments from PCR with vector template pPpT4_Alpha_S_C1A .....	<b>70</b>
<b>Figure 2.3.</b> Images of SDS-PAGE gels of: <b>(A)</b> ybbR-C1A over the course of isolation of inclusion bodies by nickel affinity chromatography. <b>(B)</b> Refolded ybbR-C1A purification during purification by nickel affinity chromatography .....	<b>71</b>
<b>Figure 2.4</b> Image of SDS-PAGE gel of refolded ybbR-C1A fractions collected from ligand affinity chromatography .....	<b>72</b>



<b>Figure 2.5.</b> Substrates polymerised by enzyme oxidation with ybbR-C1A/hydrogen peroxide .....	<b>73</b>
<b>Figure 2.6</b> IR spectrum of poly-2-methoxyaniline synthesised by chemical oxidation with ammonium persulfate (-) and poly-2-methoxyaniline synthesised by enzyme oxidation with ybbR-C1A/H <sub>2</sub> O <sub>2</sub> (-) and 2-methoxyaniline monomer (-) for comparison .....	<b>75</b>
<b>Figure 2.8.</b> (A) Photo of SDS-PAGE gel of reaction mixtures (B) SDS-PAGE gel of reaction mixtures developed using a fluorescent imager at 488 nm .....	<b>77</b>
<b>Figure 2.9.</b> Graph showing absorbance at 420 nm over time for different functionalised silicon nitride surfaces, constituting ABTS activity assay of any enzyme present .....	<b>79</b>
<b>Figure 2.10.</b> AFM recorded topographic images of mica surfaces with control and full reaction conditions after probe resting for 60 seconds .....	<b>81</b>
<b>Figure 2.11.</b> AFM images of control recorded topographic images, full reaction and control reaction without H <sub>2</sub> O <sub>2</sub> from lithography and expected .....	<b>83</b>
<b>Figure 2.12.</b> AFM images of control, full reaction from lithography and expected. Conditions; 240 s per feature, 0.1 mM aniline, 0.1 mM H <sub>2</sub> O <sub>2</sub> .....	<b>84</b>
<b>Figure 2.13.</b> AFM images of control, full reaction from lithography and expected. Conditions; 30 s per feature, 0.1 mM aniline, 0.1 mM H <sub>2</sub> O <sub>2</sub> .....	<b>84</b>
<b>Figure 2.14.</b> Depiction of the instrument setup; (A) side view with labels, (B) bottom view, highlighting force sensors (C) definition of 5 degrees of freedom .....	<b>86</b>
<b>Figure 2.15.</b> Graphs illustrating the relationships between the tilt angles and z position. Where  indicates the actual values measured and + indicates the best fit with the least-squares method .....	<b>88</b>
<b>Figure 2.16.</b> (A) Depiction of tilt angles sequence of measured angles. (B) Graph of $\phi$ against $\theta$ with the plots of the four points where the maximum z-position was reached. The intersection is calculated as the final overall optimum tilt angle across both axes .....	<b>88</b>
<b>Figure 2.17.</b> Diagram illustrating sites of size measurements with the insets showing the microscopy images, size measurements taken from a sample size of 15 for each site .....	<b>89</b>
<b>Figure 2.18.</b> Images showing sequential magnifications of the pattern produced by PPL deposition of MHA on to gold .....	<b>90</b>

<b>Figure 2.19.</b> Optical microscopy images of gold substrates that were patterned by the aligned PPL arrays and subsequently etched .....	<b>91</b>
<b>Figure 2.20. (A)</b> Depiction of surface components for each surface that the activity assay was performed on. <b>(B)</b> Graph showing absorbance at 420 nm over time for different functionalised arrays, constituting ABTS activity assay of any enzyme present .....	<b>97</b>
<b>Figure 2.21.</b> AFM imaged topography of surface that lithography had been performed on and expected result from lithography. Conditions; 20 s per feature, 2.6 mM aniline, 1 mM H <sub>2</sub> O <sub>2</sub> .....	<b>100</b>
<b>Figure 2.22</b> AFM imaged topography of surface that lithography had been performed on and expected result from lithography. Conditions; 2 s per feature, 80 features per line, 2.6 mM <i>o</i> -methoxyaniline, 1 mM H <sub>2</sub> O <sub>2</sub> .....	<b>101</b>
<b>Figure 2.23.</b> AFM imaged topography of surface that lithography had been performed on and expected result from lithography. Conditions; 1 s per feature, 160 features per line, 2.6 mM <i>o</i> -methoxyaniline, 1 mM H <sub>2</sub> O <sub>2</sub> .....	<b>102</b>
<b>Figure 2.24. (A)</b> Raman micro-spectroscopy surface map at 1398cm <sup>-1</sup> (red showing the highest intensity with black showing no peak) and <b>(B)</b> microscope image of the same area of the surface. Scale Bar 20 μm .....	<b>103</b>
<b>Figure 2.25.</b> Representative Raman spectra of the surface. <b>(A)</b> Taken from unpattern area of surface (black). <b>(B)</b> Taken from patterned area of surface (red) .....	<b>104</b>
<b>Figure 2.26.</b> Fluorescent microscope images collected by excitation at 488 nm of post polymerisation functionalisation, with insets showing expected patterns. <b>(A)</b> 10x10 locations in a 3x3 grid, scale bar 100 μm and <b>(B)</b> Lines of 50 locations per line, scale bar 100 μm .....	<b>106</b>
<b>Figure 3.1</b> Examples <i>o</i> -quinonoid systems, that can be utilised as synthetic intermediates .....	<b>109</b>
<b>Figure 3.2</b> Molecules synthesised from 1,4-benzoxazines and chromanes .....	<b>111</b>
<b>Figure 3.3.</b> Overlaid HPLC chromatograms tracking absorbance at 280 nm of the reaction quenched mixture for the full reaction and control reactions .....	<b>114</b>
<b>Figure 3.4.</b> Product formation after 60 mins from varying concentrations of enzyme, with substrate concentration, 2,3-dihydrofuran and H <sub>2</sub> O <sub>2</sub> constant .....	<b>115</b>

<b>Figure 3.5.</b> Product formation after 60 mins with reactions varying 1-4mM substrate, 50-200 mM 2,3-dihydrofuran and 1.5-4 mM H <sub>2</sub> O <sub>2</sub> concentration, with HRP concentration constant 0.25 U mL <sup>-1</sup> .....	<b>116</b>
<b>Figure 3.6.</b> Percentage conversion to product <b>1</b> over time .....	<b>117</b>
<b>Figure 3.7.</b> Substituted 2-aminophenol compounds tested as substrates and dienophiles tested under reaction conditions. Isolated yields for substrates tested under reaction conditions; 2 mM 2-aminophenol ( <b>2-6</b> ), 100 mM dienophile ( <b>7-9</b> ), 2.5 mM H <sub>2</sub> O <sub>2</sub> and 0.25 U HRP mL <sup>-1</sup> . n.d. = not determined, compounds experienced significant product degradation .....	<b>118</b>
<b>Figure 3.8.</b> (A) Leaving groups identified as substrates to screen with HRP for <i>o</i> -quinone methide generation. (B) Synthesis scheme for starting materials .....	<b>120</b>
<b>Figure 3.9.</b> Overlaid HPLC chromatograms tracking absorbance at 280 nm vs. time for the reaction quenched mixture for the full reaction and control reactions .....	<b>123</b>
<b>Figure 3.10.</b> Compounds produced by oxidation by hydrogen peroxide. Sulfoxide <b>32</b> and sulfone <b>33</b> .....	<b>123</b>
<b>Figure 3.11.</b> Overlaid HPLC chromatograms tracking absorbance at 280 nm vs time for substrate <b>31</b> , sulfoxide <b>32</b> and sulfone <b>33</b> .....	<b>124</b>
<b>Figure 3.12.</b> Percentage conversion of <b>28</b> to <b>31</b> , varying concentration of 50-200 mM dienophile <b>7</b> , 1-5 mM substrate <b>28</b> and 1-3 mM hydrogen peroxide with constant pH (7.4) and 2.5 U HRP mL <sup>-1</sup> .....	<b>125</b>
<b>Figure 3.13.</b> Percentage conversion of <b>28</b> to <b>31</b> , varying concentration of 50-100 mM dienophile <b>7</b> , 0.25-2 mM hydrogen peroxide and 2.5-25 U HRP mL <sup>-1</sup> with constant pH (7.4) and 1 mM substrate <b>28</b> .....	<b>126</b>
<b>Figure 3.14.</b> Percentage conversion of <b>28</b> to <b>31</b> varying concentration of 50-100 mM dienophile <b>7</b> , 2-3 mM hydrogen peroxide, 1-3 mM substrate <b>28</b> and pH 9-5 using a constant 2.5 U HRP mL <sup>-1</sup> .....	<b>127</b>
<b>Figure 4.1.</b> Examples of biologically active chemicals synthesised from halogenated arylamines .....	<b>131</b>

- Figure 4.2.** UV-visible spectra of adduct formed from 4-methyl-catechol (4-MC) with either 0.5 mM 2-aminobenzoic acid (X = H) or 0.5 mM 2-amino-6-chlorobenzoic acid (X = Cl) and controls in 50mM K<sub>2</sub>HPO<sub>4</sub> pH 7.4 ..... **133**
- Figure 4.3.** Structures of substrates tested with the coupled assay. X = H, Cl, Br, I ..... **134**
- Figure 4.4.** Illustrative data for mixtures of 2-aminobenzoic acid and 2-amino-6-chlorobenzoic acid solutions. **(A)** Photograph of one row of wells in a microtitre plate with adducts produced from ratios of 2-aminobenzoic acid:2-amino-6-chlorobenzoic acid (total concentration 0.5 mM). **(B)** UV-visible spectra for the mixtures in range of ratios to a total concentration of 5 mM. **(C)** The calibration graph produced by plotting the absorbance of the peak at 535 nm against the concentration of 2-amino-6-chlorobenzoic acid ..... **137**
- Figure 4.5.** Graph of the increase in the concentration 1-chloronaphthalen-2-amine against length of time of the halogenation reaction. Inset assay graph calibration plot for assay analysis produced using RebH halogenation reagents and conditions ..... **140**

**List of Schemes**

	<b>Page</b>
<b>Scheme 1.1</b> Classification hierarchy of heme-dependent peroxidases. Showing families of enzymes .....	<b>28</b>
<b>Scheme 1.2.</b> Scheme showing the general peroxidase (highlighted in red) and oxidase (highlighted in blue) catalytic cycle .....	<b>35</b>
<b>Scheme 1.3.</b> Scheme showing the complete catalytic mechanism of HRP C1A, from binding and reduction of H <sub>2</sub> O <sub>2</sub> and single electron oxidation of organic substrate .....	<b>36</b>
<b>Scheme 1.4.</b> Representative examples of sulfoxidation reactions catalysed by HRP .....	<b>41</b>
<b>Scheme 1.5.</b> Scheme showing the synthesis of tyrosine to L-DOPA by HRP and molecular oxygen as its oxidation partner .....	<b>42</b>
<b>Scheme 1.6.</b> Scheme showing representative examples of nitrations catalysed by HRP oxidation of NaNO <sub>2</sub> .....	<b>43</b>
<b>Scheme 1.7.</b> Scheme showing the mechanistic steps of HRP catalysed <i>N</i> -dealkylation .....	<b>43</b>
<b>Scheme 1.8.</b> Scheme showing representative examples of <i>N</i> -dealkylations catalysed by HRP .....	<b>44</b>
<b>Scheme 1.9.</b> Scheme showing the mechanistic steps of the HRP catalysed cyclisation of <i>N</i> -cyclopropyl- <i>N</i> -methylaniline .....	<b>44</b>
<b>Scheme 1.10</b> Scheme showing HRP catalysed semiquinone formation and dismutation of semiquinone to starting material and <i>o</i> -benzoquinone .....	<b>45</b>
<b>Scheme 1.11.</b> Scheme showing synthesis of neurotrophic americanol A and isoamericanol by HRP catalysis .....	<b>45</b>
<b>Scheme 1.12.</b> Scheme showing the synthetic step and reaction mechanism towards of melanin-like pigments catalysed by HRP .....	<b>46</b>
<b>Scheme 1.13.</b> Scheme showing the synthesis of aniline-catechol adduct by catalysed by HRP with intermediate <i>o</i> -benzoquinone undergoing Michael addition by aniline .....	<b>46</b>
<b>Scheme 1.14</b> Scheme showing the synthesis of 2-amino-phenoxazin-3-one catalysed by HRP .....	<b>47</b>
<b>Scheme 1.15</b> Scheme showing the synthesis of phenazine-2,3-diamine catalysed by	

HRP .....	47
<b>Scheme 1.16.</b> Scheme showing possible resonance forms of .....	48
<b>Scheme 1.17.</b> Scheme showing potential coupling products from radical polymerisation of phenol .....	48
<b>Scheme 1.18.</b> Scheme showing the synthesis of phenolic polymers catalysed by HRP .....	49
<b>Scheme 1.19.</b> Scheme showing the different outcomes of chemical and enzyme catalysis on 3-ethynylphenol .....	50
<b>Scheme 1.20.</b> Scheme showing possible insulating and conducting doped states of polyaniline. With the highly conductive emeraldine salt highlighted in green .....	52
<b>Scheme 1.21.</b> Scheme showing reaction route of aniline oxidation and subsequent polymerisation catalysed by HRP .....	53
<b>Scheme 1.22.</b> Scheme showing the synthesis of substituted polyaniline, using ring substituents to direct <i>para</i> -ring coupling .....	53
<b>Scheme 1.23.</b> Scheme showing steps of HRP catalysed polymerisation of aniline in the presence of template. Oxidation followed by polymerisation .....	54
<b>Scheme 1.24.</b> Scheme showing structure and conducting and insulating forms of polythiophene .....	54
<b>Scheme 1.25.</b> Scheme showing steps of EDOT polymerisation reaction catalysed by HRP .....	55
<b>Scheme 1.26.</b> Scheme showing steps of co-polymerisation of EDOT and terthiophene with SBP .....	55
<b>Scheme 1.27.</b> Scheme showing polypyrrole polymerisation reaction catalysed by HRP .....	56
<b>Scheme 1.28.</b> Scheme showing steps towards PPL array fabrication .....	59
<b>Scheme 1.29.</b> Scheme showing the conditions for fabrication of polyaniline using DNA as a guiding template .....	60
<b>Scheme 1.30.</b> Scheme showing the steps towards HRP catalysed poly(4-ATP) formation .....	61
<b>Scheme 1.31.</b> Scheme showing the steps towards HRP catalysed surface modification .....	62
<b>Scheme 1.32.</b> Scheme showing the general overview of the workflow for reported biocatalytic	

nanolithography .....	63
<b>Scheme 2.1.</b> Depiction of the general overview for the work flow to set up biocatalytic nanolithography .....	68
<b>Scheme 2.2.</b> Single electron oxidation reaction of ABTS by HRP with product $\lambda_{\text{max}}$ absorbance at 420 nm .....	72
<b>Scheme 2.3.</b> Sfp-mediated immobilisation of ybbR tagged protein .....	76
<b>Scheme 2.4.</b> Depiction of the reaction in the <i>Sfp</i> catalysed, ybbR-C1A fluorescent labelling assay .....	76
<b>Scheme 2.5.</b> Depiction of the reactions for silicon nitride probe construction .....	78
<b>Scheme 2.6.</b> Depiction of the procedure for confining enzyme to the apex of the AFM tip .....	80
<b>Scheme 2.7.</b> Depiction of biocatalytic nanolithographic catalysed formation and deposition of polyaniline on the negatively charged surface of freshly cleaved mica .....	81
<b>Scheme 2.8.</b> Overview of lithography with ybbR-C1A functionalised probes on 4-ATP functionalised surfaces .....	82
<b>Scheme 2.9</b> Depiction of alignment procedure, showing the relationship between z-axis extension and degree of alignment to the probe arrays .....	87
<b>Scheme 2.10.</b> General workflow for probe array enzyme functionalisation .....	91
<b>Scheme 2.11.</b> Reaction scheme for amino functionalisation of the PDMS surface modification .....	92
<b>Scheme 2.12.</b> Reaction scheme for coenzyme A ligation .....	93
<b>Scheme 2.13.</b> Depiction of the procedure for coenzyme A probe apex confinement .....	94
<b>Scheme 2.14.</b> Depiction of different outcomes from varying levels of probe contact with coenzyme A coated surface .....	95
<b>Scheme 2.15.</b> Depiction of <i>Sfp</i> catalysed ybbR-C1A immobilisation reaction step of forming enzyme functionalised probe arrays .....	96
<b>Scheme 2.16.</b> Reaction scheme for the functionalisation of silicon glass with 4-ATP .....	98
<b>Scheme 2.17.</b> Depiction of the lithographic procedure for the deposition of polyaniline via catalytic probes .....	99

<b>Scheme 2.18.</b> Depiction of the HRP catalysed polymerisation reaction to form lithographic patterns, followed by washing to remove non-covalently attached short chain polymers .....	<b>100</b>
<b>Scheme 2.19.</b> Workflow for multiplexed biocatalytic lithography on gold surfaces .....	<b>103</b>
<b>Scheme 2.20.</b> Synthesis of 3-(prop-2-yn-1-yloxy)aniline .....	<b>105</b>
<b>Scheme 2.21.</b> Reaction sequence for post polymerisation functionalisation with fluorophore .....	<b>105</b>
<b>Scheme 3.1 (A)</b> Potential reactions routes of <i>o</i> -quinonoid systems, with potential reactions including Michael addition and cycloaddition. <b>(B)</b> Selected routes to <i>o</i> -quinone methide systems, highlighting diverse methodologies towards generation .....	<b>109</b>
<b>Scheme 3.2</b> Literature known reactions with HRP; Oxidation of 2-aminophenol forming <i>o</i> -quinone imine. Oxidation of <i>o</i> -cresol does not proceed to <i>o</i> -quinone methide .....	<b>110</b>
<b>Scheme 3.3</b> Reaction scheme of potential reaction pathways. Unsubstituted 2-aminophenol not undergoing cycloaddition .....	<b>112</b>
<b>Scheme 3.4</b> Reaction scheme showing HRP-catalysed oxidation followed by cycloaddition to form <b>1</b> .....	<b>113</b>
<b>Scheme 3.5.</b> Scheme showing potential oxidation routes towards <i>o</i> -quinone methides and reaction not proceeding with <i>o</i> -cresol .....	<b>120</b>
<b>Scheme 3.9.</b> Reaction selectivity of <i>o</i> -quinone methide with dienophiles and water. Where LG = leaving group. In the presence of a dienophile, cycloaddition reaction will proceed preferentially over nucleophilic attack by H <sub>2</sub> O .....	<b>121</b>
<b>Scheme 4.1.</b> General scheme illustrating the HRP-catalysed oxidation of catechols to their corresponding <i>ortho</i> -quinone (upper pathway) and the formation of the arylamine-catechol adduct. This reaction can be coupled to a biocatalytic halogenation reaction (lower pathway) .....	<b>122</b>
<b>Scheme 4.2.</b> Reaction sequence for RebH halogenation followed by <i>in situ</i> HRP oxidation of 4-MC and coupling of the naphthylamine(s) .....	<b>139</b>



**List of Tables**

	<b>Page</b>
<b>Table 1.1.</b> Table of subclasses of oxidoreductases and a description of the reaction they catalyse .....	<b>26</b>
<b>Table 1.2.</b> Table of grouped peroxidase-catalysed reactions with the reaction name and scheme for the reaction .....	<b>27</b>
<b>Table 1.3.</b> Table of heme Fe(III)/Fe(II) redox potential of a variety of commonly studied heme peroxidases at pH 7.....	<b>29</b>
<b>Table 2.1.</b> Table detailing the activity units of enzyme per mg of protein .....	<b>73</b>
<b>Table 2.2.</b> Table detailing the percentage yield of insoluble polymer produced by polymerisation with HRP .....	<b>74</b>
<b>Table 2.3</b> Assignments for Raman shift of bond vibrations for 4-ATP and poly 2-methoxyaniline .....	<b>104</b>
<b>Table 3.1</b> E-factor calculated for the peroxidase catalysed and DIAB catalysed methods of synthesising compound 1 .....	<b>119</b>
<b>Table 3.2.</b> HPLC data summary, <b>y</b> indicates the presence of a peak at 9.4 mins the same retention time as the product standard and <b>n</b> indicating no peak present .....	<b>122</b>
<b>Table 4.1.</b> UV-visible $\lambda_{\max}$ and $\epsilon$ values of the aniline-catechol adducts formed by the assay. "--" = not determined .....	<b>135</b>
<b>Table 4.2.</b> Parameters calculated from the best-fit of calibration plots for the binary mixtures of the halogenated and non-halogenated aryl-amine-catechol adducts .....	<b>138</b>
<b>Table 6.1</b> PCR reaction profile .....	<b>148</b>
<b>Table 6.2</b> PCR master mix (2 $\mu$ l total) .....	<b>149</b>
<b>Table 6.3</b> SDS-PAGE gel components .....	<b>150</b>
<b>Table 6.4</b> 5X ISO buffer components .....	<b>151</b>
<b>Table 6.5</b> Gibson assembly master mix components .....	<b>151</b>
<b>Table 6.6</b> Restriction digest mix .....	<b>154</b>
<b>Table 6.7</b> Fluorescent labelling master mix .....	<b>157</b>
<b>Table 6.8</b> ybbR_C1A immobilisation master mix .....	<b>163</b>

**Abstract**

Biocatalysis can offer advantages over traditional chemical synthesis, offering chemical orthogonality. The size range of biocatalysts makes them particularly suitable in nanotechnology applications, however their potential is yet to be fully explored.

One of the key requirements in the development of nanotechnological devices is the need to generate nanometre-sized features on a variety of surfaces. However, current methods of nanofabrication largely rely on methods derived from the microelectronics sector, which are energetically intensive, costly and are extremely limited in the chemical complexity they can achieve. The work presented here includes development of a new wide area method of synthesising nanometre-sized features by constructive deposition of material. Biocatalytic nanolithography combines the control of polymerising biocatalyst and the precision of scanning probe microscopy. In this work horseradish peroxidase has been immobilised to probe arrays and was used for the *in situ* generation and deposition of aryl amine polymers. Lithography was carried out with nanometre resolution and on a wide area for the first time.

Additionally, research was carried out utilising peroxidase for the synthesis of fine chemicals. Specifically, their ability to catalyse the formation of quinoid systems, which often require harsh chemical conditions to generation. Quinoid systems can be used as reactive intermediates of the syntheses of organic backbones. Horseradish peroxidase was used to catalyse the formation of *o*-quinone methide, *o*-quinone imine and *o*-quinone systems. Novel tandem one-pot cycloadditions with dienophiles were carried out with *o*-quinone methide and *o*-quinone imine systems to form fused ring aromatics, on a synthetically relevant scale. Tandem 'one-pot' Michael additions with aryl amines were carried out on *o*-quinone systems. The adducts formed with non/halogenated aryl amines had significantly different UV/Vis spectrum and could be used to assay halogenation by this difference. It was shown this detection could be coupled with a flavin dependent halogenase which currently lack a high throughput assay, in a 'one-pot' workflow.

**Declaration**

I declare that no portion of the work referred to in the thesis has been submitted in support of an application for another degree or qualification of this or any other university or other institute of learning.

### **Copyright Statement**

- i. The author of this thesis (including any appendices and/or schedules to this thesis) owns certain copyright or related rights in it (the “Copyright”) and s/he has given The University of Manchester certain rights to use such Copyright, including for administrative purposes.
- ii. Copies of this thesis, either in full or in extracts and whether in hard or electronic copy, may be made only in accordance with the Copyright, Designs and Patents Act 1988 (as amended) and regulations issued under it or, where appropriate, in accordance with licensing agreements which the University has from time to time. This page must form part of any such copies made.
- iii. The ownership of certain Copyright, patents, designs, trade marks and other intellectual property (the “Intellectual Property”) and any reproductions of copyright works in the thesis, for example graphs and tables (“Reproductions”), which may be described in this thesis, may not be owned by the author and may be owned by third parties. Such Intellectual Property and Reproductions cannot and must not be made available for use without the prior written permission of the owner(s) of the relevant Intellectual Property and/or Reproductions.
- iv. Further information on the conditions under which disclosure, publication and commercialisation of this thesis, the Copyright and any Intellectual Property and/or Reproductions described in it may take place is available in the University IP Policy, in any relevant Thesis restriction declarations deposited in the University Library, The University Library’s regulations and in The University’s policy on Presentation of Theses.

**List of Abbreviations**

2D	Two-dimensional
4-ATP	4-Aminothiophenol
4-MC	4-Methylcatechol
ABTS	2,2'-Azino-bis(3-ethylbenzothiazoline-6-sulphonic acid)
AFM	Atomic force microscopy
APTES	(3-Aminopropyl)triethoxysilane
CoA	Coenzyme A
DIAB	(Diacetoxyiodo)benzene
DLL	Dynamic Linking Library
DMF	Dimethylformamide
DMSO	Dimethyl sulfoxide
DNA	Deoxyribonucleic acid
DPN	Dip-pen nanolithography
EDOT	3,4-Ethylene-dioxithiophene
ee	Enantermeric excess
FAD	Flavin adenine dinucleotide disodium salt
FPLC	Fast protein liquid chromatography
FWHM	Full width half maximum
H <sub>2</sub> O <sub>2</sub>	Hydrogen peroxide
heme B	Iron (III) protoporphyrin IX
HEPES	4-(2-Hydroxyethyl)-1-piperazineethanesulfonic acid
HPLC	High pressure liquid chromatography
HRP	Horseradish peroxidases
IBs	Inclusion bodies
IMAC	Immobilised metal affinity chromatography
IPTG	$\beta$ -D-1-thiogalactopyranoside
IR	Infrared
MHA	16-Mercaptohexadecanoic acid

MWCO	Molecular weight cut off
NAD	$\beta$ -Nicotinamide adenine dinucleotide dipotassium salt
PANI	Polyaniline
PCR	Polymerase chain reaction
PDMS	Polydimethylsiloxane
PEDOT:PSS	Poly(3,4-ethylene-dioxithiophene)-polystyrene sulphonate
pI	Isoelectric points
PPL	Polymer pen lithography
RZ	Reinheitszahl
SBP	Soybean peroxidase
SCU	Simple Control Unit
SDS-PAGE	Sodium dodecyl sulfate polyacrylamide gel electrophoresis
SERS	Surface enhanced Raman scattering
SHE	Standard hydrogen electrode
SPL	Scanning probe nanolithography
SPM	Scanning probe microscopy
TCEP	Tris(2-carboxyethyl)phosphine
TEMED	Tetramethylethylenediamine
Terthiophene	2,5-Di(2-thienyl)thiophene
TLC	Thin layer chromatography
$\epsilon$	Absorption coefficient

**List of Abbreviations – Amino Acids**

<b>Amino acids</b>	<b>3 letters</b>	<b>1 letter</b>
Alanine	Ala	A
Arginine	Arg	R
Asparagine	Asn	N
Aspartic acid	Asp	D
Cysteine	Cys	C
Glutamic acid	Glu	E
Glutamine	Gln	Q
Glycine	Gly	G
Histidine	His	H
Isoleucine	Ile	I
Leucine	Leu	L
Lysine	Lys	K
Methionine	Met	M
Phenylalanine	Phe	F
Proline	Pro	P
Serine	Ser	S
Threonine	Thr	T
Tryptophane	Trp	W
Tyrosine	Tyr	Y
Valine	Val	V

---

## Chapter 1

### Introduction and literature review

#### 1.1 Biocatalysis

Biocatalysis, the use of enzymes to perform chemical transformations on organic compounds, has considerably grown in significance over recent years.<sup>1-3</sup> Wide-ranging industrial applications and low environmental impact have spurred on interest and development. Biocatalysis was formerly overlooked in favour of chemocatalysis, due to lack of tools to identify enzymes and isolate them in any reasonable quantity for practical application. Additionally, essential structural and mechanistic studies of enzymes were similarly impeded. These difficulties were widely addressed with the introduction of recombinant DNA technology in the early 1980s.<sup>4</sup> Enzymes could be more easily identified using genome sequencing and produced more cheaply by recombinant protein expression. Recombinant DNA technology also enabled protein engineering, a set of techniques essential to addressing the catalytic limitations of wild type enzymes. More than 100 industrial enzymatic processes have been since been introduced using such techniques.<sup>5, 6</sup>



Most enzymes are active at mild pH (6-8), ambient temperature and favour reactions in aqueous media. These criteria are frequently considered advantageous. Goals for industrial processing such as “environmentally sustainable development” and “green chemistry” are an increasingly important boundary condition for industrial activity in a large part of the world. These goals would be significantly more difficult without the increasing prominence of biocatalysis in industry.<sup>7, 8</sup>

However, with this explosion of new potential biocatalysts it is important not to overlook classic enzymes, which often already display features that would put them in a prime position for development in new applications. These include good stability, high efficiency and broad substrate scope with structure and mechanism fully expounded. These enzymes could also benefit retrospectively from new technologies. Increasing their utility by tailoring, engineering and design to build on their baseline catalysis.<sup>5, 9</sup>

## 1.2 Oxidoreductases

Oxidoreductases are one such class of enzymes widely distributed among all organisms.<sup>10,</sup>

<sup>11</sup> They are responsible for catalysing the exchange of electrons or redox equivalents between donor and acceptor molecules within reactions involving electron transfer, proton abstraction, oxygen insertion, hydrogen extraction or hydride transfer. Generally, this takes place by two half reactions (one oxidative and one reductive), and a minimum of two substrates (one reducing and one oxidising). Oxidoreductases utilise numerous redox-active centres to complete their catalytic function. Common redox centres involve amino acid side chains, coenzymes, metal ions, metal complexes (e.g. heme) or a combination of these.

These centres are protected by the peptide backbone of the protein, which is also responsible for controlling redox potential, substrate selectivity and enzyme stability.

Oxidoreductases can be grouped according to the type of reaction they catalyse. Some of these reactions are highlighted in Table 1.1.<sup>12</sup>

<b>Subclass</b>	<b>Description of reaction</b>
<b>Oxidases</b>	Molecular oxygen is the hydrogen or electron acceptor
<b>Dehydrogenases</b>	Oxidise substrate by transferring one or more hydride ion ( $H^-$ )
<b>Peroxidases</b>	Reduction of hydrogen peroxide and alkyl peroxides
<b>Oxygenases</b>	Incorporate molecular oxygen into organic substrates
<b>Reductases</b>	Catalyse reductions
<b>Hydroxylase</b>	Add hydroxyl groups to a substrate

**Table 1.1.** Table of subclasses of oxidoreductases and a description of the reaction they catalyse.

Many chemical and biochemical processes utilise redox reactions, subsequently a significant amount of literature generated about oxidoreductases, and developing practical biocatalytic applications.<sup>13-15</sup>

### 1.2.1 Peroxidases

Peroxidases are oxidoreductases that exploit hydrogen peroxide and/or alkyl peroxides as redox partners to oxidise a wide variety of organic and inorganic compounds.<sup>16</sup> They are amongst the first enzymes to have been reported, with references from the 19th century documenting peroxidase activity in biological systems, with descriptions of the oxidation of a variety of organic compounds by hydrogen peroxide ( $H_2O_2$ ).<sup>17</sup> There are four categories of peroxidase-catalysed reactions, given in Table 1.2.<sup>18, 19</sup>

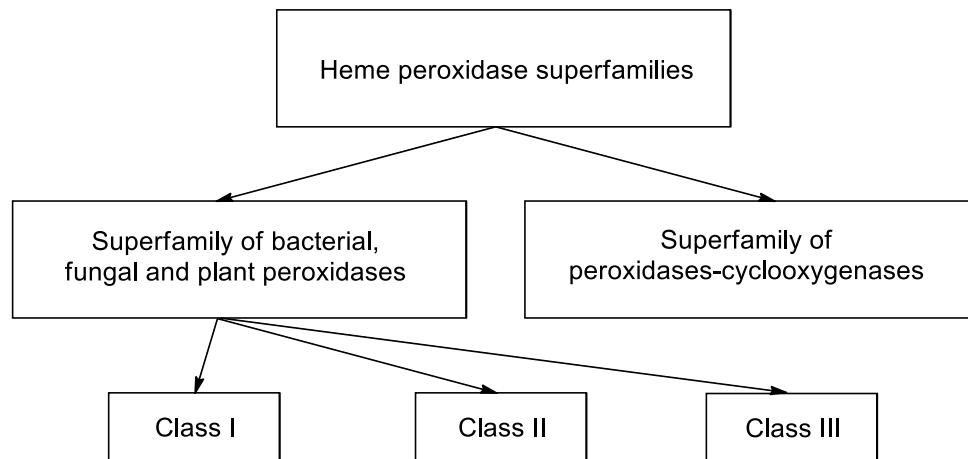
Reaction name	Reaction scheme
Oxidative dehydrogenation	$2S-H + H_2O_2 \rightarrow 2S + 2H_2O$
Oxidative halogenation	$S-H + H_2O_2 + X^-H^+ \rightarrow SX + 2H_2O$
Hydrogen peroxide dismutation	$2H_2O_2 \rightarrow 2H_2O + O_2$
Oxygen-transfer	$S-H + H_2O_2 \rightarrow S-OH + H_2O$

**Table 1.2.** Table of grouped peroxidase-catalysed reactions with the reaction name and scheme for the reaction, S-H = Substrate and X = Cl, Br, I.

These enzymes can also be categorised into heme-dependent peroxidases - which constitute the bulk of peroxidase redox-centres - and non- heme-dependent peroxidases that use different redox-centres such as vanadium (vanadate-dependent haloperoxidases)<sup>20</sup>, cysteine (glutathione peroxidases, NADH peroxidase),<sup>21, 22</sup> selenocysteine (glutathione peroxidases)<sup>23</sup> and manganese (manganese catalase).<sup>24</sup>

### 1.2.2 Heme-dependent peroxidases

Heme-dependent peroxidases<sup>25</sup> have been widely reported in nature. There are two superfamilies of peroxidases (Scheme 1.1): those of animal origin (peroxidase-cyclooxygenase superfamily) or fungal, plant and bacterial origin.<sup>18, 26</sup> Fungal, plant and bacterial peroxidases evolved independently of animals and have been categorised based on primary sequence similarity.<sup>27</sup>



**Scheme 1.1** Classification hierarchy of heme-dependent peroxidases. Showing families of enzymes.

The superfamily of bacterial, fungal and plant peroxidase is made up of three classes:

Class I is comprised of intracellular peroxidases, exemplified by yeast cytochrome c peroxidase, ascorbate peroxidase and bacterial catalase–peroxidase. Class I peroxidases are not glycosylated and contain no disulfide bridges or diaxial calcium ions.<sup>28</sup>

Class II is comprised of secretory fungal peroxidases, illustrated by lignin peroxidases and manganese-dependent peroxidases. Class II peroxidases are monomeric glycoproteins, containing four conserved disulfide bridges and two diaxial calcium-binding sites.<sup>28</sup>

Class III is comprised of secretory plant peroxidases, exemplified by horseradish peroxidases (HRPs) and soybean peroxidases (SBP). Class III peroxidases are monomeric glycoproteins, containing four conserved disulfide bridges (whose position differs from that observed in Class II enzymes) and two diaxial calcium ions. Their physiological functions involve tissue-specific tasks, such as removal of  $\text{H}_2\text{O}_2$  from chloroplasts and cytosol, oxidation of toxic compounds, biosynthesis of cell walls and defence towards wounding.<sup>28</sup>

Understanding of the structure-function relationships and catalytic mechanisms of heme-dependent peroxidases is principally based on work with HRPs.<sup>29</sup>

### 1.2.3 Redox potential

Redox potential is an important physiochemical property of heme-dependent peroxidases. It controls the range of oxidisable substrates that can be converted by determining the limit for the oxidative capacity of the enzyme. In solution the Fe(III)/Fe(II) couple has a standard redox potential of 770 mV; when complexed to protoporphyrin IX forming heme B and surrounded by a protein matrix its redox potential can vary by up to approximately 1000 mV (Table 1.3).<sup>25, 30</sup>

In theory, peroxidases can only catalyse the oxidation of substrates with a lower redox potential. This, however is not the only factor. Electrostatic interactions between substrate and active site, substrate orientation and structural features also influence activity. For example, lignin processing peroxidase is able to oxidise substrates containing a 2-methoxyphenol substituent with higher redox potentials than the native enzyme versus standard hydrogen electrode (SHE).<sup>31</sup> This effect is mostly attributed to favourable binding within the enzyme active site.

<b>Protein</b>	<b>Redox potential vs. SHE (V)</b>	<b>Function</b>
<b>Soybean peroxidase</b>	1.156	Cell wall formation
<b>Cytochrome c peroxidase</b>	0.717	Hydrogen peroxide metabolism
<b>Horseradish peroxidase C1A</b>	0.900	Lignification, cell wall formation
<b>Horseradish peroxidase A2A</b>	0.920	Lignification, cell wall formation
<b>Lactoperoxidase</b>	1.090	Innate immune system
<b>Myeloperoxidase</b>	1.350	Innate immune system

**Table 1.3.** Table of heme Fe(III)/Fe(II) redox potential of a variety of commonly studied heme peroxidases at pH 7<sup>30</sup>.

### 1.3 Horseradish peroxidases (HRP)

HRP are the most heavily studied peroxidases. In 1976, Welinder determined the first complete amino acid sequence of an HRP.<sup>32</sup> After extensive studies in involving isolation and sequencing it was accepted that horseradish peroxidases are a large family of isoenzymes.<sup>33, 34</sup> Isoenzymes are different molecular forms of enzymes with very similar catalytic function within the cell (all involved in the synthesis of lignin (Figure 1.1)), but have individual physical, chemical and kinetic properties originating from differences in primary structure. Isoenzymes have as low as 40% sequence identity to each other, however retain very similar tertiary structures.<sup>35</sup>

The first evidence of multiple isoenzymes came in 1958 when five different isoforms of peroxidase were isolated from horseradish using a form of ion-exchange chromatography.<sup>34</sup> These isoenzymes were subsequently designated as A, B, C, D and E, by the sequence they were eluted. Later reports confirmed these results and additionally reported that isoform A could be further resolved, these new isolates were assigned as A1, A2 and A3. Proteins within group A have acidic isoelectric points (pI). Later the Morita group isolated five neutral (B1, B2, B3, C1 and C2) and six basic (E1, E2, E3, E4, E5 and E6) isoforms, again groupings were made based on isoelectric points.<sup>17, 36</sup>

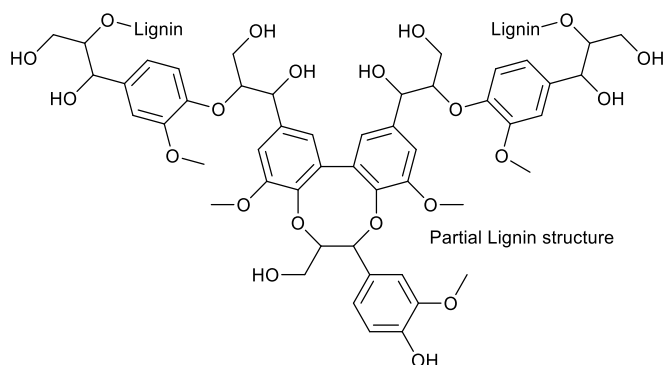


**Figure 1.1.** Depiction of the partial structure of plant Lignin, reported to be HRPs natural catalytic product.

### 1.3.1 Horseradish peroxidase isoenzyme C1A

Isoenzyme C1A, a monomer consisting of 308 amino acids, has the highest cellular abundance and is the most widely studied.<sup>37, 38</sup> The crystallographic structure<sup>39</sup> (Figure 1.2) showed that there are four disulfide bridges between cysteine residues 11-91, 44-49, 97-301 and 177-209, and a salt bridge between Asp99 and Arg123. Nine N-glycosylation sites have been identified from the primary sequence, from the series Asn-X-Ser/Thr (x = any amino acid residue), of which eight are occupied. 75-80% of glycosylation is accounted for by branched heptasaccharides, but HRP C1A has a heterogeneous carbohydrate profile.<sup>40</sup> Further complications arise from variation in the type of glycan present at any of the glycosylation sites, therefore the total carbohydrate content of HRP C is determined by the source of enzyme. Typical values are between 18 and 22%. Glycosylation plays an important role in the stability and solubility of the enzymes, 'shielding' surface amino acid residues and peptide bonds from harsh solution conditions.<sup>41</sup>

There are two distinct types of metal centre contained within HRP C1A, a prosthetic iron (III) protoporphyrin IX (heme B) group and two calcium atoms. The structural and functional integrity of the enzyme are dependent on both of these. The heme-binding region is linked to the calcium ions by a network of hydrogen bonds, loss of calcium results in a markable decrease in activity and stability of the enzyme.<sup>42</sup>

#### 1.3.1.1 Prosthetic heme group

HRP C1A contains heme B (Figure 1.3) as a prosthetic group in its active site. Heme B iron has two free axial coordination sites in addition to the four planar sites occupied by nitrogen atoms from the porphyrin. Heme B is directly coordinated to the protein backbone by a bond between His170 and iron (Figure 1.4).<sup>39</sup> The other coordination site is unoccupied when the enzyme is in its resting state. Heme B position is maintained through hydrogen bonds between the carboxyl substituents of Glu176, Ser73, Ser35 and Arg31 side chains.<sup>34</sup>

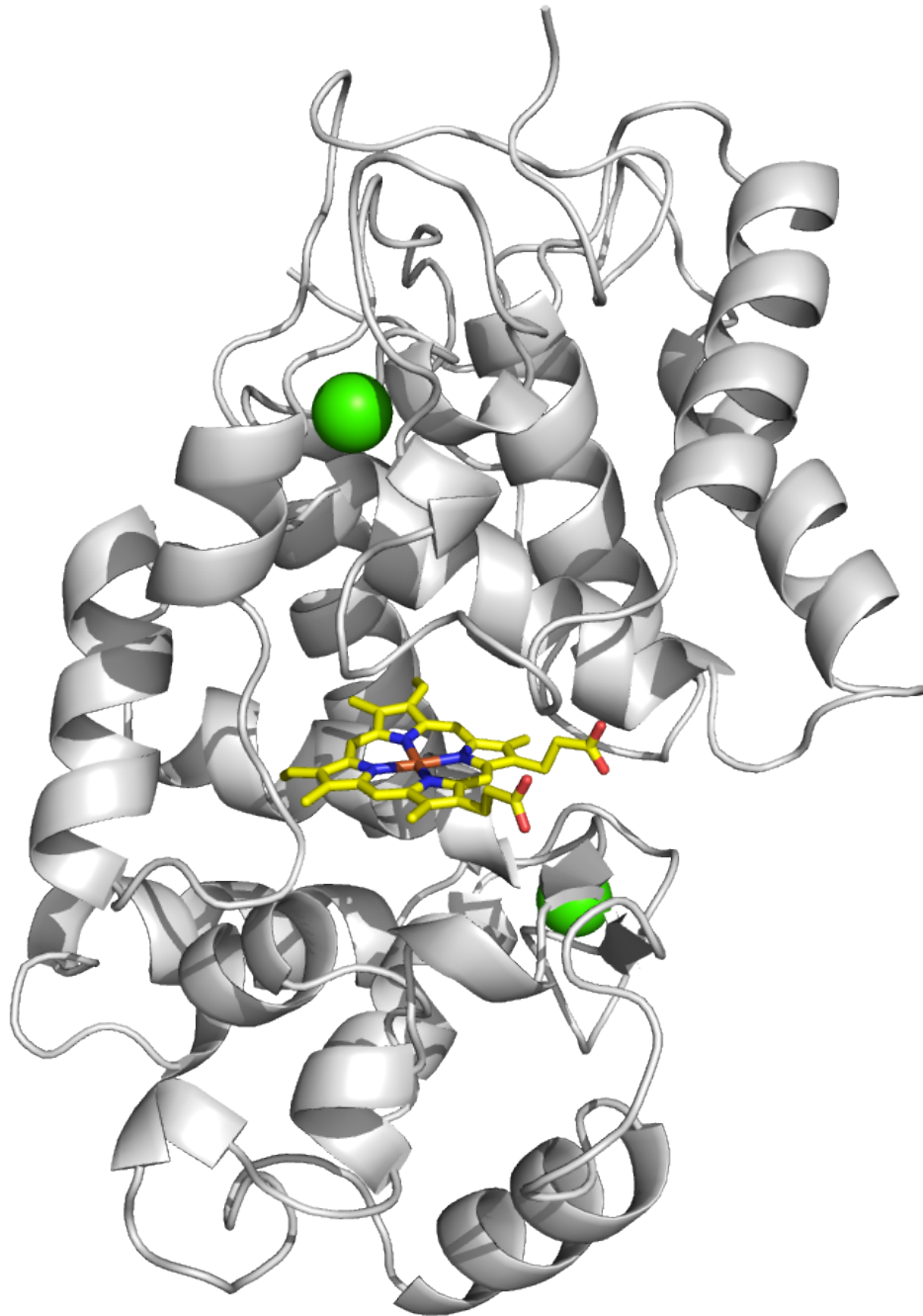


**Figure 1.2** Crystallographic structure of horseradish peroxidase isoenzyme C1A, highlighting heme B group (in yellow) and calcium ions (in green). Protein databank reference: 1HCH.<sup>39</sup>



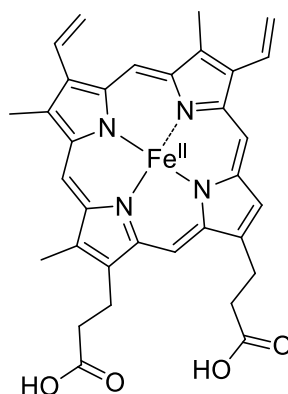


**Figure 1.3.** Structure of iron (III) protoporphyrin IX (heme B).

### 1.3.1.2 Active site

The crystal structure of the active site, in Figure 1.4A, shows the key amino acid residues for an active enzyme.<sup>43</sup> Figure 1.4B shows the active site of HRP C1A, which constitutes a distal domain (area above the plane of heme) and proximal domain (below the plane of heme), containing residues essential for catalytic activity. Within the proximal domain, His170 is coordinated to heme and a hydrogen bond to Asp247 controls its basicity. H170A mutants show no enzymatic activity with  $H_2O_2$ .<sup>44</sup> Activity can be partially restored, by addition of imidazole. Within the distal domain, Arg38 and His42 are conserved in all plant peroxidases. Arg38, used in substrate binding and His42 in peroxide bond cleavage. Mutating residues to alanine each of the key residues (Arg38 and His42) show a dramatically decreased activity.<sup>44</sup>

Phenyl active site gatekeeper residues highlighted in mustard in Figure 1.4C/D provide  $\pi$ -interactions to guide aromatic substrates towards the active site of the enzyme. Figures 1.4C/D show the large steric space of the gateway to the active site, this lack of steric control contributes to the significant substrate promiscuity of aromatics active with this peroxidase.<sup>43, 45</sup>

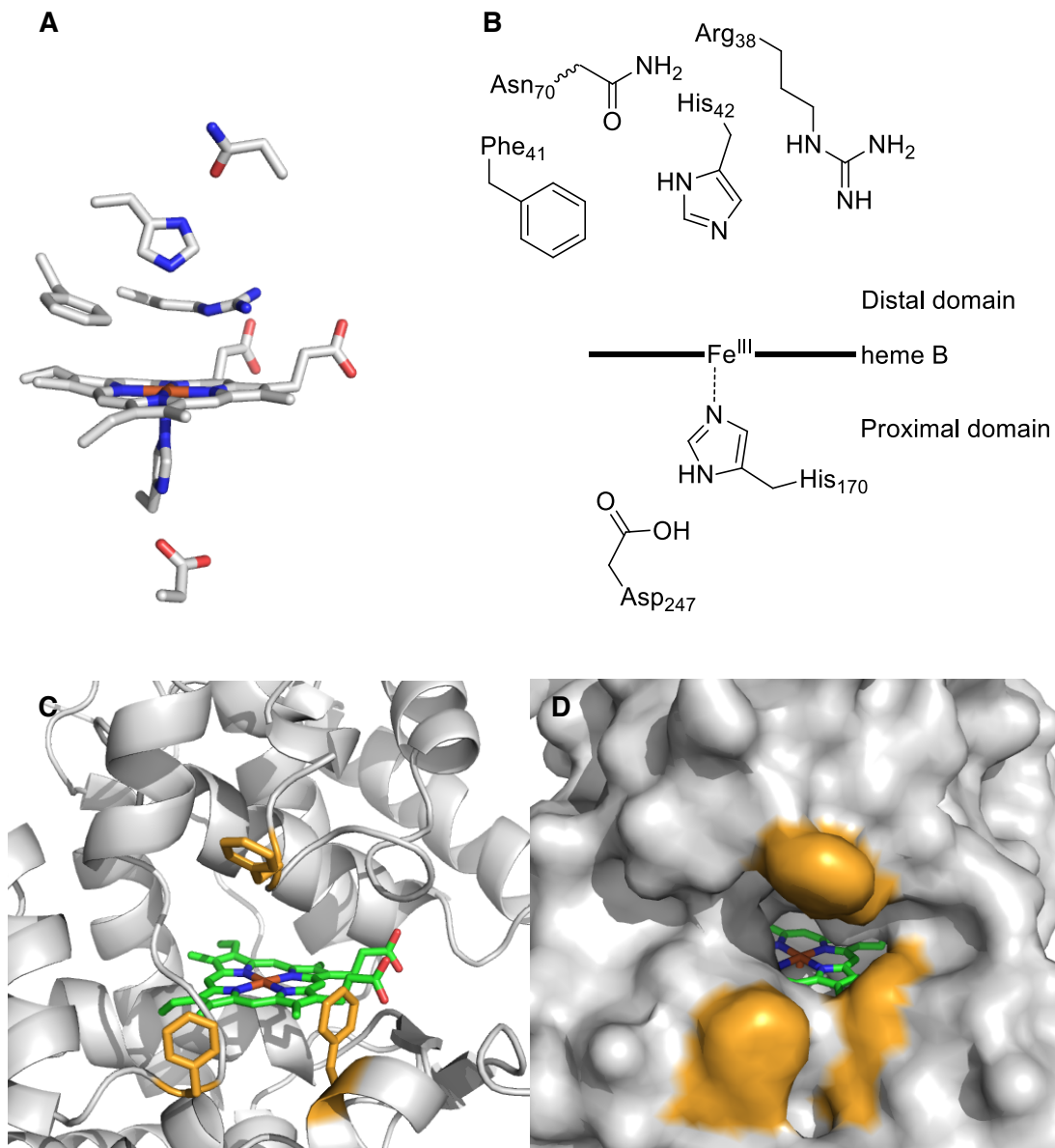
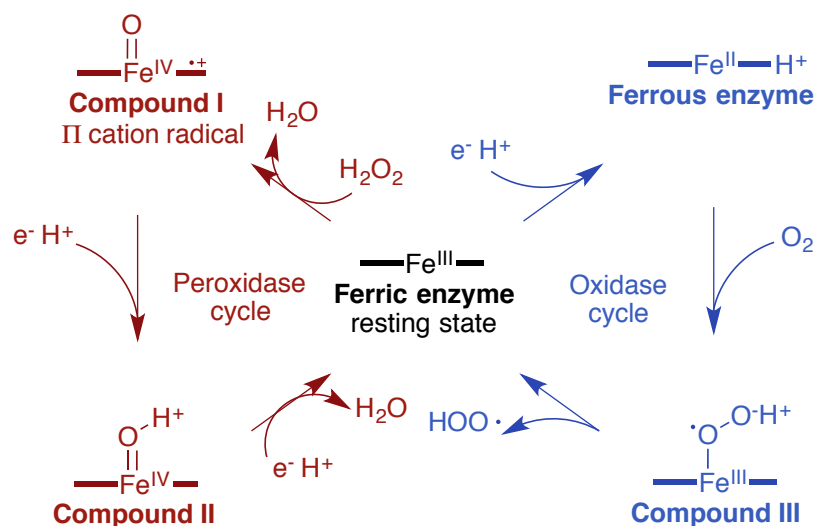


**Figure 1.4.** (A) Stick model of the side view of Heme B structure within the active site of HRP C1A. Protein databank reference: 6ATJ.<sup>43</sup> (B) Side view of the structure and composition of key active site residues. (C) Cartoon model highlighting active site gatekeeper residues in orange. (D) Space filling model highlighting active site gatekeeper residues in orange. Protein databank reference: 6ATJ.<sup>43</sup>

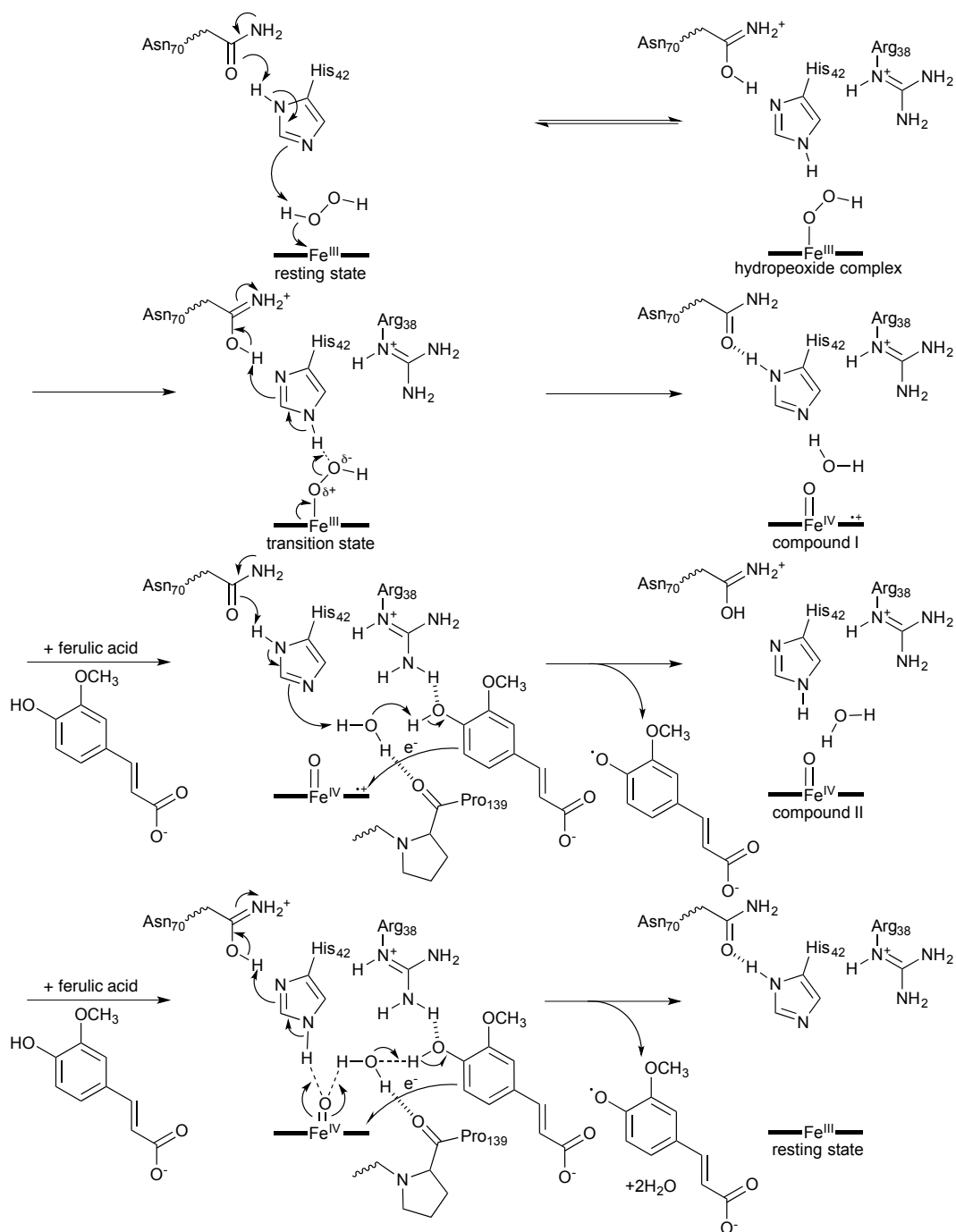
## 1.4 Enzyme mechanism and catalytic cycle

The general catalytic cycle for oxidase and peroxidase enzymes is shown in Scheme 1.2.<sup>19</sup> this diagram seeks to illustrate the potential catalytic pathways heme dependent enzymes can take. Examples in the literature have shown heme-dependent enzymes exhibiting both cycles.<sup>13, 46</sup>



**Scheme 1.2.** Scheme showing the general peroxidase (highlighted in red) and oxidase (highlighted in blue) catalytic cycle. Where  $e^-$  = electron and  $\text{H}^+$  = hydrogen cation.

The full oxidation mechanism of C1A and its natural substrate, ferulic acid, was deduced in 2002.<sup>38, 39</sup> The catalytic cycle commences by the reaction between hydrogen peroxide and the iron(III) resting state of the enzyme. This reaction generates compound I, a high oxidation state intermediate, consisting of an iron(IV) oxoferryl centre and a porphyrin-based radical cation. The accepted mechanism has His42 accepting a proton from hydrogen peroxide and Arg38 helping to stabilise the charged intermediate. This mechanism can be more clearly viewed in Scheme 1.3 below.



**Scheme 1.3.** Scheme showing the complete catalytic mechanism of HRP C1A, from binding and reduction of  $\text{H}_2\text{O}_2$  and single electron oxidation of organic substrate. Where  $e^-$  = electron.

Heme oxidation state compound I is considered in formal terms two oxidising equivalents ( $2e^-$ ) above the resting state of the enzyme. compound I is converted to compound II by a one-electron reduction step by the participation of a reducing substrate. compound II is an

iron(IV) oxoferryl species that is one oxidising equivalent above the enzyme resting state, which can then oxidise a second substrate molecule.

compound I and II are powerful oxidants, with combined redox potentials close to 1000 mV.<sup>30</sup>

## 1.5. Enzyme expression and Isolation

HRPs are available commercially as purified, native and heterologous expressed, proteins. Much effort has been put into heterologous expression in academia and commercial enterprise for numerous reasons including protein engineering and improving activity/yield due to its many biotechnological applications.<sup>38, 47</sup>

### 1.5.1 Native expression

Typically, peroxidases are extracted from the homogenised roots of horseradish (*Armoracia rusticana*) and purified to varying levels. Commercial preparations contain a mixture of isoenzymes, thus preparations from different sources contain different ratios of isoenzymes, due to transient enzyme expression within the root. Native expression is induced in response to external factors such as wounding, stress, and attack by pathogens.<sup>36, 41</sup>

These preparations are measured by quantity of enzyme needed to oxidise a particular substrate in a particular time, to give a figure in units of enzyme activity per milligram of enzyme preparation. These commercially available preparations are currently the cheapest source of horseradish peroxidases, per weight basis. Another measure of purity used is the Reinheitszahl (RZ) ratio, the absorbance ratio  $A_{403}/A_{275}$  determined at 0.5-1.0 mg/ml in deionised water. The absorbance at 403 nm ( $A_{403}$ ) arises from absorption from the heme cofactor, the so-called Soret peak. The absorbance 275 nm ( $A_{275}$ ) arises from absorption of aromatic residues. Thus the ratio  $A_{403}/A_{275}$  gives an indication of heme content. As a spectrophotometric measure of heme content, it is not a measure of enzymatic activity and

thus even preparations with high RZ may have low enzymatic activity (due to heme being in an inactivated state), although generally higher RZ correlates to higher enzyme activity.<sup>48</sup>

Purification and isolation of individual isoenzymes from root extractions has also been accomplished extensively in an academic setting using a combination of ammonium sulphate precipitation, size exclusion chromatography (on a variety of media) and ion exchange chromatography. For example, ligand affinity chromatography has been used effectively to purify preparations of C1A to a high RZ. In this case naphthylhydroxamic acid ligand was utilised due to its high affinity for binding holo-C1A by binding key residues which can be observed in the crystal structure (Figure 1.5) of isoenzyme C1A co-crystallised with *N*-hydroxybenzamide. Naphthyl hydroxamic acid modified agarose was submerged in impure preparations of C1A, after washing highly purified C1A could be dissociated and recovered by washing with boronic acid.<sup>33</sup>

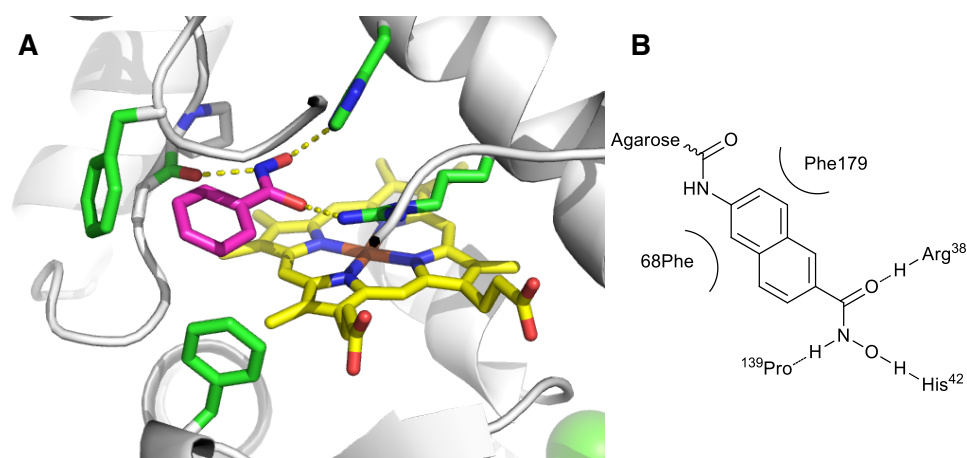


**Figure 1.5. (A)** Model of crystal structure of isoenzyme C1A with *N*-hydroxybenzamide bound. Protein databank reference: 1GX2, **(B)** Depiction of bonding residues of isoenzyme C1A with agarose-naphthylhydroxamic acid

### 1.5.2 Heterologous expression

Recombinant production of individual horseradish peroxidase isoenzymes is complicated by their complex tertiary structure, the presence of disulphide bonds, prosthetic heme group

and calcium metal centres.<sup>49</sup> However, structure and activity studies require defined homogeneous enzyme preparations avoiding other isoenzymes and heterogeneous surface glycans that are present from the native plant. Efforts have been focused on expression in bacterial and yeast systems although other systems have been employed.<sup>44, 48, 50</sup>

#### 1.5.2.1 Bacterial host

Initially (cytoplasmic) expression studies of isoenzyme C1A in *E. coli* showed protein to be formed exclusively in inclusion bodies (IBs). This was thought to be because of their complex structure,<sup>51</sup> therefore investigations then focused on the purification and refolding of the inclusion bodies into functional protein using conventional methods. The typical workflow would include separating IBs from soluble proteins, IB solubilisation in a chaotropic agent and purification followed by refolding of the pure IBs in buffer containing necessary cofactors, metal ions necessary for active protein and disulphide bond forming reagents. Further purification is then required to isolate active protein. This methodology has been very inefficient with final yields of 3% being reported, however protein produced showed to be homogeneous. Significant improvements have recently been reported with yields of 24% using a design of experiments approach to refolding buffer component concentrations.<sup>52</sup>

#### 1.5.2.2 Eukaryotic host

In contrast to prokaryotic protein expression, good yields have been achieved through expression and purification of individual isoenzymes using the methylotrophic yeast *Pichia pastoris*. Functional expression could be achieved due to eukaryotic post translational modification machinery being suited to produce proteins from eukaryotic organs. The drawback of using *P.pastoris* for recombinant protein production is *N*-linked hyperglycosylation of non-native proteins and unpredictability of *O*-linked glycosylation. This can affect downstream purification and further utilisation of the enzyme, due to masking of amino acid residues in the primary protein sequence.<sup>53-55</sup>

## 1.6 Biotransformations performed by HRP

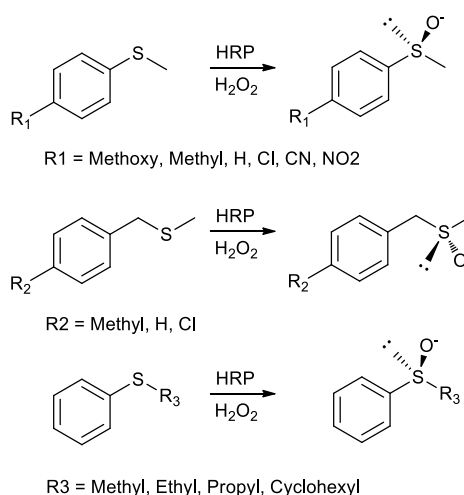
Horseradish peroxidases currently have several industrial and medical applications, in waste water treatment, chemical synthesis, coupled enzyme assays, biosensors, diagnostic kits and immunoassays.<sup>34</sup> These broad applications draw HRP from different sources (heterologous or native expression) and are generally chosen based on the needs of the specific task (often related to purity of the enzyme preparation). In terms of applications in synthetic organic chemistry, native horseradish peroxidases or mutants have been applied to dealkylations, epoxidation, hydroxylation, and sulfoxidation reactions with varying regioselectivity and/or stereoselectivity, which are discussed in later later text. In general, design of these reactions is carefully planned to avoid side reactions due to the very board substrate scope of HRP.

### 1.6.1 Oxygen insertion

#### 1.6.1.1 Sulphoxidation

HRPs are commonly able to perform the sulfoxidation of dialkyl or alkyl aryl sulfides. Compared with P450 enzymes, HRP reactivity is normally slow, due primarily to conformational restrictions brought about by inherent differences in the substrate-binding pocket compared to oxidase enzymes. There have been several studies focused on asymmetric sulfoxidation by HRP, with examples of substrates applied to this reaction in Scheme 1.4 with literature ee of greater than 90 for each reaction.<sup>56</sup>





**Scheme 1.4.** Representative examples of sulfoxidation reactions catalysed by HRP.

There is no general agreement in the literature regarding the best method for maximising the yield and the enantiomeric excess (ee) of the formed sulphoxide. The most significant factor affecting ee is the way in which H<sub>2</sub>O<sub>2</sub> is added to the reaction. Primarily either by very slow addition or *in situ* production (using an enzyme such as glucose oxidase), thus spontaneous oxidation of the thioether by H<sub>2</sub>O<sub>2</sub> is significantly decreased. However a major confounding factor is that studies have mostly been carried out using a mixture of isoenzymes thus structural differences in the active sites of enzymes may have played a greater part in the ee of the product.<sup>57</sup>

The reaction has been proposed to proceed via a direct oxygen transfer from compound I to the substrate or via a P450-like mechanism (single electron transfer from the substrate to compound I, with the substrate forming a radical species that is tightly bound to compound II, followed by oxygen transfer from compound II to the sulphur (Scheme 1.2).)<sup>58</sup>

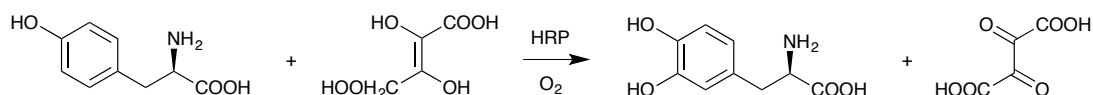
### 1.6.1.2 Epoxidation

Native HRP isoenzymes do not catalyse the epoxidation of allyl substrates, however mutants of isoenzyme C1A (F41L, F41T, F41A, H42V) have been used to produce optically

active phenylethene-oxide derivatives. The synthetic impact of this reaction is restricted because most of the phenylethene-oxide derivatives produced undergo rearrangement to phenylethene-aldehyde by-products. Reactions have been shown to proceed with low enantio-selectivity.<sup>59</sup>

### 1.6.1.3 Hydroxylation

HRP has been able to catalyse CH-bond oxidation of limited phenolic substrates, by molecular oxygen, in the presence of dihydroxyfumaric acid, as a hydrogen donor. The reaction is exemplified by the hydroxylation of L-tyrosine to L-DOPA (Scheme 1.5).<sup>60</sup>



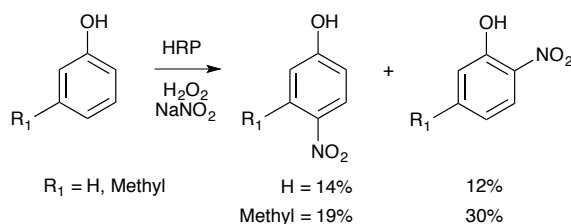
**Scheme 1.5.** Scheme showing the synthesis of tyrosine to L-DOPA by HRP and molecular oxygen as its oxidation partner.

### 1.6.2 Nitration

Synthesis of nitro containing compounds is useful, mostly due to the functional group's reactivity to derivatisation (such as reduction to amine).<sup>61</sup> It has been shown extensively that HRP is able to oxidise  $\text{NO}_2^-$  in the presence of  $\text{H}_2\text{O}_2$  to nitrate aromatic compounds (Scheme 1.6).<sup>62</sup>

Most examples of nitrations involve the oxidation of sodium nitrite and a phenolic substrate,<sup>63</sup> however nitration of tryptophan derivatives also been reported.<sup>61</sup>

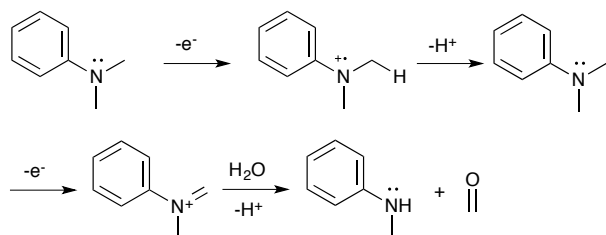
Due to nitration occurring outside the active site of HRP regiocontrol is provided by the electron and structural properties of the aromatic to be nitrated.



**Scheme 1.6.** Scheme showing representative examples of nitrations catalysed by HRP oxidation of  $\text{NaNO}_2$ .

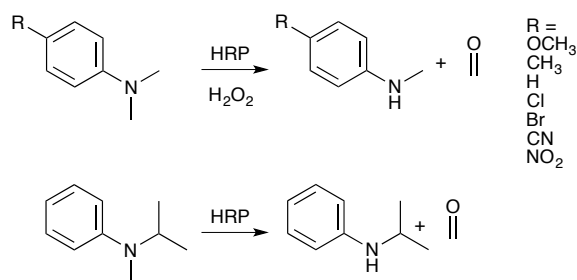
### 1.6.3 *N*-dealkylation

Oxidative *N*-dealkylations have been achieved using HRP in the presence hydrogen peroxide. The reaction proceeds by a single electron transfer oxidation of the nitrogen centre forming a highly reactive aminium radical cation (Scheme 1.7).<sup>64</sup>



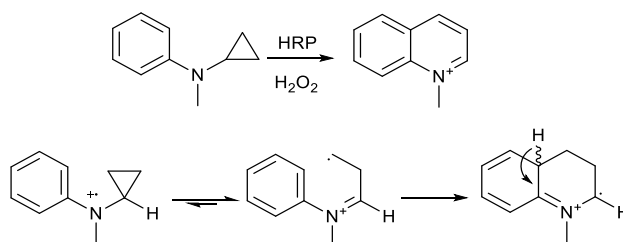
**Scheme 1.7.** Scheme showing the mechanistic steps of HRP catalysed *N*-dealkylation.

This reaction has been applied to several substrates, examples including those in Scheme 1.8 which proceed with quantitative yield. Active substrates are however limited to *N,N*-dialkylanilines due to the redox potential of *N*-alkylanilines substrates being too high for HRP. Therefore *N*-dealkylation will only occur once on tertiary nitrogens.



**Scheme 1.8.** Scheme showing representative examples of *N*-dealkylations catalysed by HRP. Conditions; 0.5 mM substrate, 0.816  $\mu\text{g/mL}$  HRP, 1 mM  $\text{H}_2\text{O}_2$  in 0.4 M potassium phosphate pH 5.5.

An interesting variation on this reaction occurs upon the oxidation of *N*-cyclopropyl-*N*-methylaniline (Scheme 1.9). In this case the aminium ion, produced, undergoes cyclopropyl ring fragmentation, which preforms a unimolecular cyclisation leading, after further oxidation, to a *N*-methylquinolinium cation.<sup>64</sup>



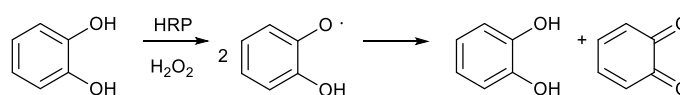
**Scheme 1.9.** Scheme showing the mechanistic steps of the HRP catalysed cyclisation of *N*-cyclopropyl-*N*-methylaniline.

## 1.6.4 Oxidative dehydrogenation

### 1.6.4.1 Oxidation to quinonoid systems

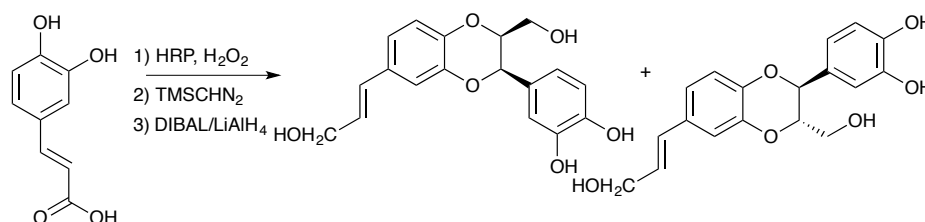
Catechols are converted into semiquinone radicals upon single-electron oxidation.

Semiquinones are innately unstable and undergo dismutation to the corresponding quinone and original catechol (Scheme 1.10).<sup>65</sup>



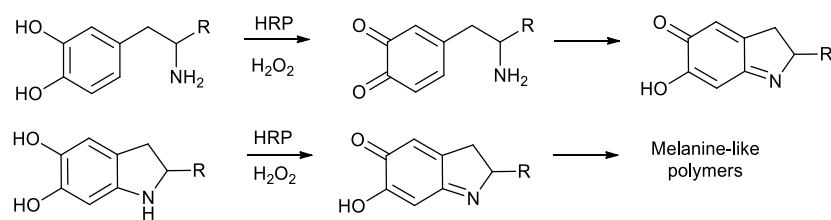
**Scheme 1.10** Scheme showing HRP catalyzed semiquinone formation and dismutation of semiquinone to starting material and *o*-benzoquinone.

Some *o*-benzoquinones with bulky substituents can be isolated, but due to the highly unstable nature of quinonoid systems, they rapidly undergo other reactions such as Michael addition by nucleophiles present in solution. This reaction has been employed in the synthesis of the neurotrophic compounds americanol A and isoamericanol by HRP-catalysed coupling of caffeic acid. The reaction proceeds via oxidation of caffeic acid to *o*-benzoquinone, followed by tandem cycloaddition of the quinone and alkene pendent (Scheme 1.11).<sup>66</sup>



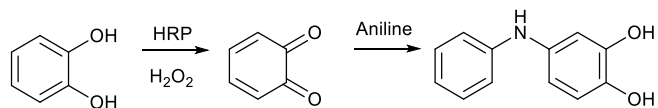
**Scheme 1.11.** Scheme showing synthesis of neurotrophic americanol A and isoamericanol by HRP catalysis.

Investigation with *L*-DOPA and dopamine as substrates has shown that upon oxidation catalysed by HRP, attack by a nucleophilic side chain occurs, causing ring closure. These indolinediols then react further to form melanin-like pigments (Scheme 1.12).<sup>67</sup>



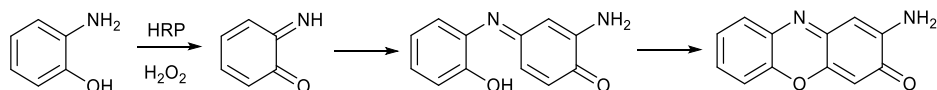
**Scheme 1.12.** Scheme showing the synthetic step and reaction mechanism towards of melanin-like pigments catalysed by HRP.

An intermolecular variation of this reaction has also been shown, where the HRP catalysed oxidation of catechol to *o*-benzoquinone can be combined with subsequent Michael addition of aniline to the quinone (Scheme 1.13). Since the resulting catechol-aniline adduct is highly coloured, this reaction sequence has been previously used as an assay for peroxidase activity.<sup>68</sup>

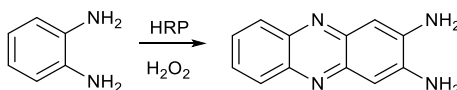


**Scheme 1.13.** Scheme showing the synthesis of aniline-catechol adduct by catalysed by HRP with intermediate *o*-benzoquinone undergoing Michael addition by aniline.

Horseradish peroxidase has also been found to catalyse the formation of both *o*-benzoquinone imine (Scheme 1.14)<sup>69</sup> and *o*-benzoquinone diimine (Scheme 1.15).<sup>70</sup> Both quickly dimerise and, again, upon prolonged reaction times polymerisation occurs. Regioselectively is exhibited with *o*-benzoquinone imine, due to semi-quinone stabilisation.<sup>69</sup>



**Scheme 1.14** Scheme showing the synthesis of 2-amino-phenoxazin-3-one catalysed by HRP.



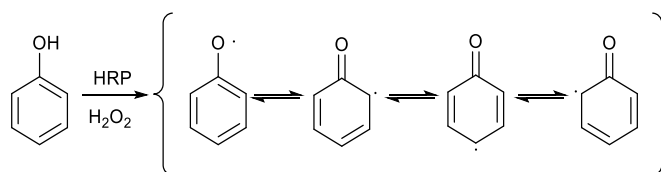
**Scheme 1.15** Scheme showing the synthesis of phenazine-2,3-diamine catalysed by HRP.

#### 1.6.4.2 Oxidative polymerisation

Single electron oxidation of electron rich aromatic substrates is the central usage of HRP.<sup>71</sup> The radical species produced, whether phenolic or aryl amine in origin, can be directed to free radical polymerisation under the appropriate conditions. Over the years a vast and diverse volume of research concerning polymerisation reactions, using HRP as a catalyst, has been carried out. HRP has been found to have a broad substrate scope being able to produce a variety of interesting compounds including electronically conducting polymers and antistatic coatings.<sup>72</sup>

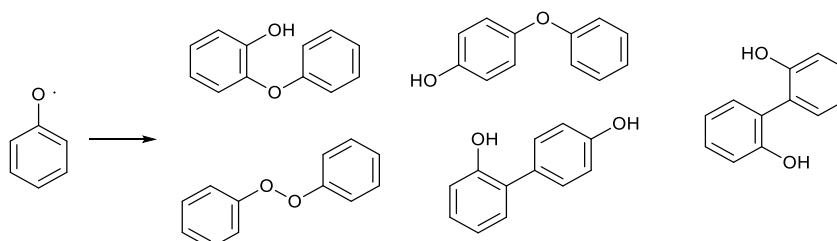
##### 1.6.4.2.1 Phenolic polymerisation

The polymerisation of phenoxyl radicals produced in the presence of peroxidases was first characterised in the 1940s.<sup>73</sup> The reaction proceeds by single electron oxidation of the phenol into phenoxyl radical (Scheme 1.16), which polymerises in successive reactions. Consequently, chain initiation and propagation is an enzyme-independent process, resulting in dimers, trimers, oligomers and high molecular weight polymers.<sup>74</sup>



**Scheme 1.16.** Scheme showing possible resonance forms of phenoxyl radicals.

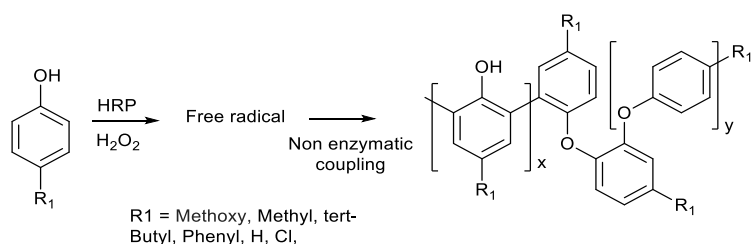
The chemical composition of the final polymer is determined by the reactivity of the phenoxyl radicals and other compounds in the reaction. In phenoxyl radicals the unpaired electron may delocalise, stabilising the aromatic ring (Scheme 1.16). Unless directed by ring substituents, coupling can occur at any of these locations. Consequently, oligomers and polymers contain a random mixture of the linkages shown in Scheme 1.17 with significant branching of polymers taking place.<sup>75, 76</sup>



**Scheme 1.17.** Scheme showing potential coupling products from radical polymerisation of phenol.

Additionally, phenoxyl radicals may react with other non-substrate molecules present in the reaction mixture, forming adducts and subsequently heteropolymers. Examples of phenolic polymers produced are vast. An illustrative example of *para*-substituted substrates is shown in Scheme 1.18.

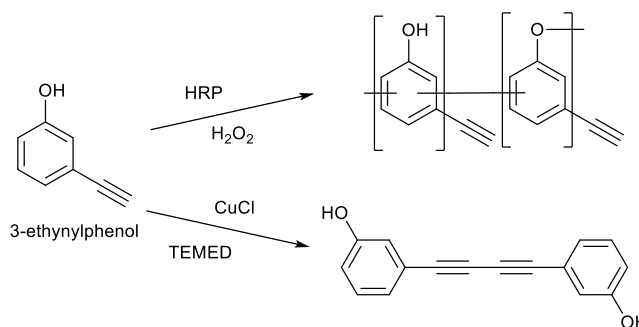




**Scheme 1.18.** Scheme showing the synthesis of phenolic polymers catalysed by HRP.

Due to the polymerisation reaction proceeding as a non-enzymatic reaction, to synthesise high molecular weight polymers with a regular structure (low branching, homogenous bonding) efforts have been concentrated on directing non-specific free radical reactions. Adjusting reaction conditions, such as concentration of HRP can reduce the short chain oligomers produced, this reduces the free radicals in solution making a termination reaction less likely to occur. Blocking positions on the aromatic ring where the radical is stabilised to stopping branching has also been used effectively.<sup>76</sup>

An interesting example, useful for post-polymerisation modifications (such as click coupling to the polymer backbone), is the polymerisation of 3-ethynylphenol, shown in Scheme 1.19. Here it is shown HRP produces exclusively poly(phenol) (thus providing alkyne functional groups for post-polymerisation reactions). It is also shown that copper catalysed coupling conversely leads to dimerisation of the substrate.<sup>77</sup>



**Scheme 1.19.** Scheme showing the different outcomes of chemical and enzyme catalysis on 3-ethynylphenol; formation of 3-ethynylphenol polymer by HRP and cross coupling by CuCl.

#### 1.6.4.2.2 Polymerisation of anilines, pyrroles and thiophenes

As for the oxidation of phenols, the peroxidase reaction with aniline, pyrrole and thiophene derivatives will form polymers under the appropriate conditions. These polymers are of particular interest as they can allow the flow of electrons through their polymer chain and are therefore classed as 'electronically conducting polymers'.<sup>78, 79</sup>

##### 1.6.4.2.2.1 Electronically conducting polymers

Electronically conducting polymers, or intrinsically conducting polymers, are organic polymers that conduct electricity. Generally conductivity is dependent on the number of charge carriers in the material and their mobility. Metals conduct electricity through freely dissociable outer electrons in the conduction band that travel across atoms in the atomic lattice (of the given metal). In organic materials conductivity is principally transmitted using delocalised  $\pi$ -electrons. Electronically conducting polymers have in common a substantial overlap of delocalised  $\pi$ -electrons down the polymer chain. Shown below, in Figure 1.6, are general structures of highly conjugated polymers.<sup>78</sup>

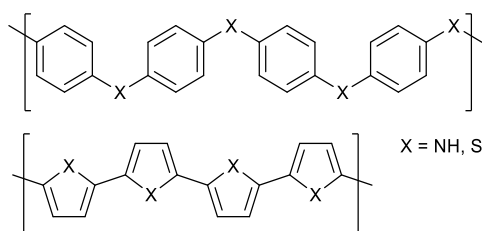
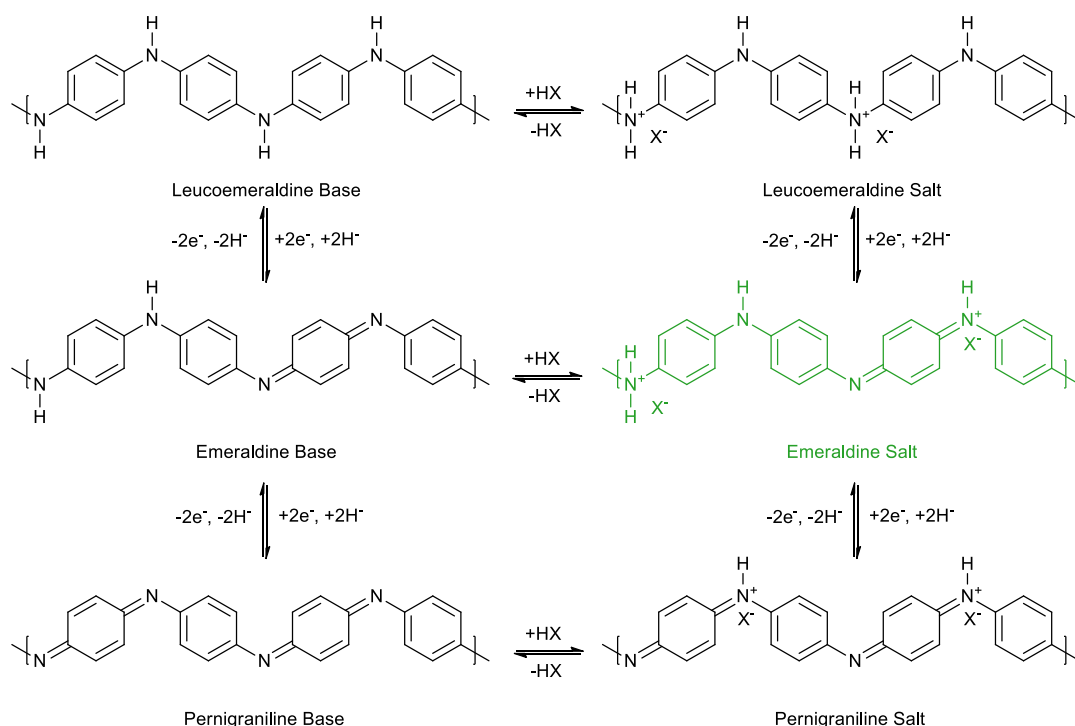


**Figure 1.6.** Depiction of the general ring structures of known conducting polymers.

Conductance is dependent on the doping of cation salts to the highly conjugated polymer base. The cation salts are obtained by oxidation of the monomer, coupled with doping with an anion such as chlorine or bromine. The purpose of doping is to reduce the band gap energy between highest occupied and lowest unoccupied molecular orbital and make charge carrier movement easier. Electronically conducting polymers have found applications in lithography, electrostatic discharge protection of electronic components, sensors and biosensors.<sup>80-83</sup> Depending on polymer composition (dopants/organic backbone) organic conducting polymers have a conductivity range of  $10^4$ - $10^{-10}$  S  $\text{cm}^{-1}$ , ranging from highly conductive like metals such as iron ( $\sim 10^4$  S  $\text{cm}^{-1}$ ) to the conductivity of insulators such as diamond ( $\sim 10^{-10}$  S  $\text{cm}^{-1}$ ).<sup>78</sup>

#### 1.6.4.2.2.2 Aniline polymerisation

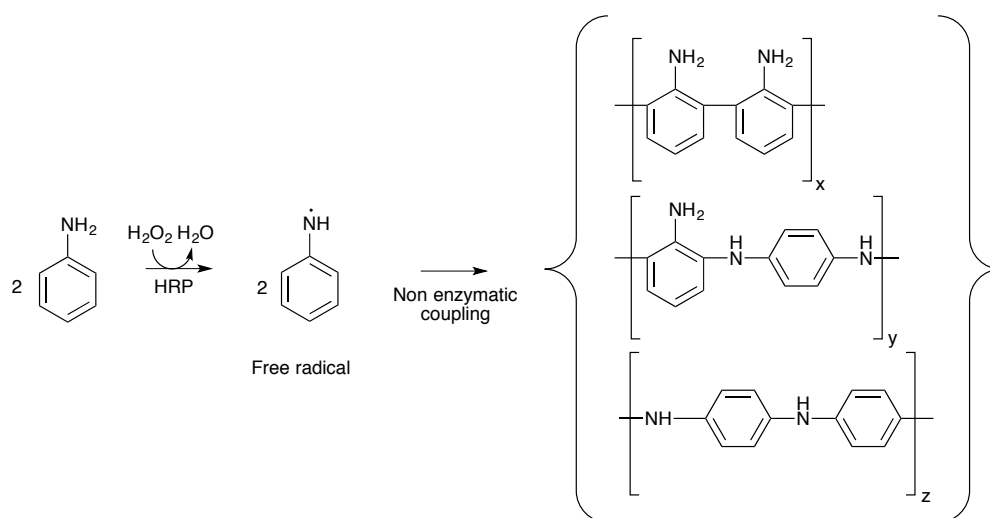
Polyaniline (PANI) is a conducting member of the semi-flexible rod polymer family. Generally, PANI consists of two types of structural units, Quinoid and Benzenoid. These two units are interchangeable by redox changes. Not all types of doped PANI are conductors. Only when benzenoid:quinoid are 1:1 can they efficiently conduct an electrical current (Scheme 1.20).<sup>84</sup> Substituted anilines have been used to influence the electronic and physical properties both as heteropolymers when co-polymerised, with aniline, and homopolymers.<sup>85</sup> Un-doped emeraldine base has a conductivity of  $\sim 10^{-10}$  S  $\text{cm}^{-1}$ , whereas emeraldine salts doped with camphorsulfonic acid or HCl have conductivities in the range of  $\sim 10^3$  S  $\text{cm}^{-1}$ .<sup>78</sup>



**Scheme 1.20.** Scheme showing possible insulating and conducting doped states of polyaniline. With the highly conductive emeraldine salt highlighted in green.

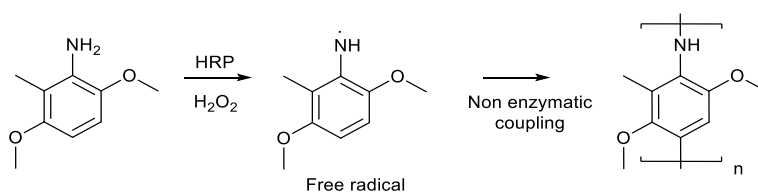
Aniline polymerisation with HRP progresses much like phenol, but the reaction only proceeds at a useful rate at pH less than 4.5.<sup>86, 87</sup> The redox potential of HRP is pH dependent.<sup>86</sup> Therefore due to the greater oxidation potential of aniline over phenol (aniline  $E^\circ = 1.02 \text{ V}^{88}$  and phenol  $E^\circ = 0.860 \text{ V}^{89}$ ) the redox potential of HRP must be greater to oxidise aniline.<sup>90</sup> The reduction of HRP compound II to compound I is usually the rate-determining step for many substrates and the redox potential of HRP compound II decreases at higher pH, this is attributed to the loss of a hydrogen bond which is present between the oxygen ligand and an amino acid residue in the heme pocket at higher pH.<sup>91</sup> The reaction starts with enzyme activation by hydrogen peroxide, in a two-electron redox reaction, to the oxidised form compound I which oxidises two molecules of aniline to yield two aniline radicals. This proceeds through two sequential one-electron redox reactions by the intermediate compound II (see scheme 1.2). After the second oxidation HRP is returned to its initial state and cycle can be repeated. As with phenolic polymerisation, after free

radical formation, formation of aniline polymers occurs outside of the HRP active site (Scheme 1.21) again leading to branched chain polymers (leading to low conductivity).<sup>92</sup>



**Scheme 1.21.** Scheme showing reaction route of aniline oxidation and subsequent polymerisation catalysed by HRP.

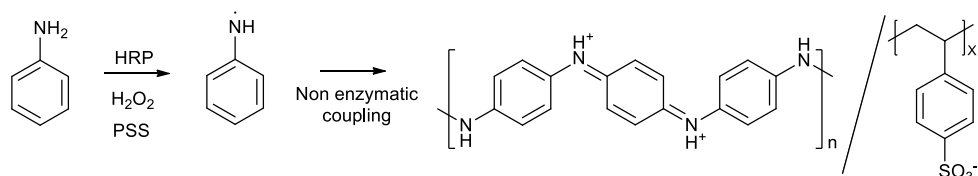
Many different methods have been used to produce linear unbranched chains, first by using ring substituents to prevent coupling at *ortho*-ring positions (Scheme 1.22) and only allow coupling at the *para*-ring position.<sup>93, 94</sup>



**Scheme 1.22.** Scheme showing the synthesis of substituted polyaniline, using ring substituents to direct *para*-ring coupling.

Most success has been found by conducting the polymerisation in the presence of a polyanionic template (Scheme 1.23), sulphonated polystyrene. This provides an electrostatic interaction to align the growing polymer chain in a specific orientation favoured for chain

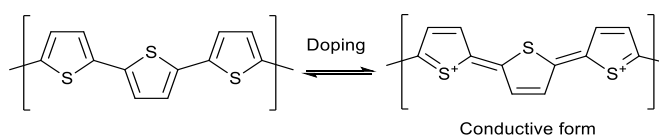
growth and solubilises the polymer, preventing undesirable precipitation of the polymer chain and ensuring only low molecular weight polymers are formed. It also provides counter ions to dope the polymer. An alternative method to prevent precipitation is use of an organic co-solvent in the reaction, such as 2-pyrrolidone.<sup>86, 95</sup>



**Scheme 1.23.** Scheme showing steps of HRP catalysed polymerisation of aniline in the presence of template. Oxidation followed by polymerisation.

#### 1.6.4.2.2.3 Thiophene polymerisation

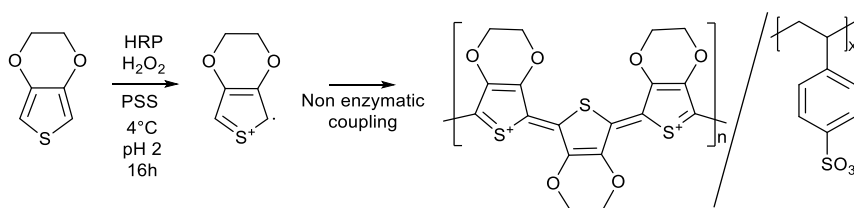
Polymers of thiophene also conduct electricity when doped, allowing electrons to be added or removed from the conjugated  $\pi$ -orbitals (Scheme 1.24).<sup>96</sup>



**Scheme 1.24.** Scheme showing structure and conducting and insulating forms of polythiophene.

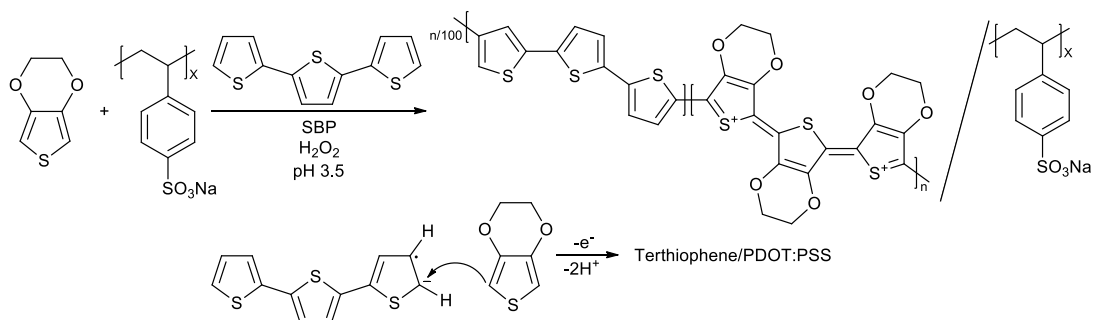
Of particular interest, poly(3,4-ethylene-dioxithiophene)-polystyrene sulphonate, (PEDOT:PSS) has seen use commercial applications. However polymerisation by HRP has been problematic due to the high oxidation potential of thiophenes ( $\sim 1.1$  V respect to SHE) to that of HRP.<sup>97</sup>

There have been reports of the synthesis of PEDOT:PSS using commercial HRP under harsh conditions (pH 2 and at 4°C). This reaction proceeds very slowly, taking 16 hours to synthesise a good yield of polymer (Scheme 1.25). As previously mentioned HRP oxidation potential is pH dependent, reducing the pH lowers the activation energy allowing the reaction to proceed.<sup>91</sup>



**Scheme 1.25.** Scheme showing steps of EDOT polymerisation reaction catalysed by HRP.

It remains unclear how the enzyme remains active, resisting denaturation, over 16 hours in strongly acidic conditions but the low temperature has been suggested as a potential factor. There have been other reports of enzymatic polymerisation using SBP, another plant peroxidase (with a higher oxidation potential than HRP, as shown in table 1.3) (Scheme 1.26).

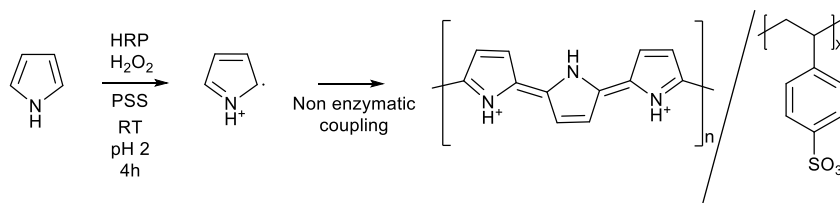


**Scheme 1.26.** Scheme showing steps of co-polymerisation of EDOT and terthiophene with SBP.

This method was carried out at room temperature and at pH 3.5, but employed 1% 2,5-di(2-thienyl)thiophene (terthiophene) with a lower oxidation potential than EDOT (3,4-ethylenedioxythiophene). It is proposed that terthiophene can therefore act as a redox initiator facilitating the polymerisation.<sup>98</sup>

#### 1.6.4.2.2.4 Pyrrole polymerisation

Polypyrrole is a conducting polymer of the same class as polythiophene but has reduced conductivities, copolymers (of pyrrole and thiophene) can therefore offer tuneable conductivity.<sup>98</sup> Synthesis of polypyrrole has also be carried out by HRP, but the synthesis encounters the same problems as polythiophene eg the higher oxidation potential requires a very low pH to achieve polymerisation (Scheme 1.27). The reaction does achieve good yield in 4 hours at room temperature, these conditions would also render the enzyme inactive.<sup>99</sup>



**Scheme 1.27.** Scheme showing polypyrrole polymerisation reaction catalysed by HRP.

## 1.7 Nanolithography

Nanolithography is the fabrication of nanometre-scale structures, below 100 nm in at least one dimension.<sup>100</sup> Progress in nanotechnology is dependent on the development of techniques capable of efficiently and reliably fabricating nanoscale features on to surfaces. Due to their nanometre size range, enzymes are perfectly suited to utilisation in nanolithography,<sup>101</sup> either directly as structural units or indirectly to catalyse the assembly of nanometre sized units into structures.<sup>102</sup> However, generating nanoscale features is not a



trivial endeavour, with most existing techniques derived from the semiconductor industry, relying on ablative photolithography to fabricate 'hard' materials.<sup>103</sup> More recently, lithographic techniques derived from scanning probe microscopy (SPM) have emerged as a convenient and versatile approach for the rapid prototyping of nanoscale designs.<sup>104</sup> Predominantly due to the capability to actuate the location of the probe with subnanometre resolution with SPM such as atomic force microscopy (AFM).

### 1.7.1 Scanning probe nanolithography

Scanning probe nanolithography (SPN) based techniques are able to conveniently and rapidly 'write' any user-defined pattern. The most well-known of these is dip-pen nanolithography (DPN),<sup>105</sup> whereby a scanning probe is used as a 'pen' to transfer a molecular 'ink' onto a surface, producing features in a fashion analogous to writing. Under ambient conditions, as a probe is scanned across a surface the 'ink' molecules are transferred to the surface via a water meniscus that forms between the probe and the surface (Figure 1.7). DPN thus allows the nanolithographic deposition of a wide range of materials, most commonly a thiol-containing molecule on to a gold surface, to take advantage of the bond forming (with gold) driving force of deposition. Feature resolutions of less than 10 nm have been reported.<sup>106</sup>

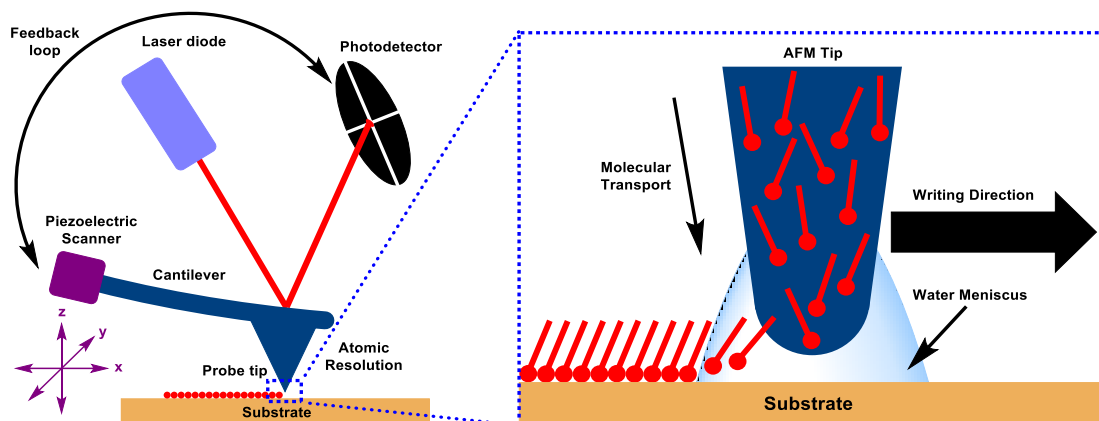


**Figure 1.7.** Diagrammatic representation of dip-pen nanolithography, with zoomed inlay of molecular deposition at AFM tip apex.

The main obstacle to the wider application of SPM-derived lithography is throughput, due to the serial-write nature of standard single probe instrumentation. Early efforts to address this issue focused on the parallelisation of cantilever-based DPN, with both ‘one-dimensional’ and ‘two-dimensional’ (2D) probe arrays being reported for the lithography of  $\text{cm}^2$  areas.<sup>107</sup> However, these cantilever arrays are produced through non-trivial multistep fabrication methods and are fairly fragile.

The development of polymer pen lithography (PPL) (Figure 1.8) addressed this issue by replacing the standard SPM cantilevers with a 2D array of soft siloxane elastomer probes bonded to a glass slide (Scheme 1.28).<sup>108, 109</sup> Feature resolutions of less than 50 nm being reported this technique has delivered a wide area alternative to cantilever based lithography. The simple probe setup significantly decreases the cost and complexity of patterning large areas and has opened up nanolithography to a wider range of applications.<sup>110</sup>

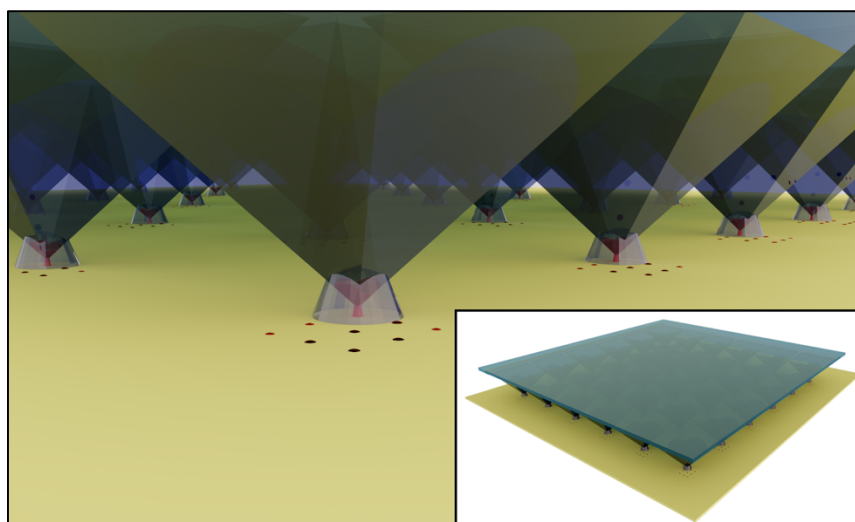
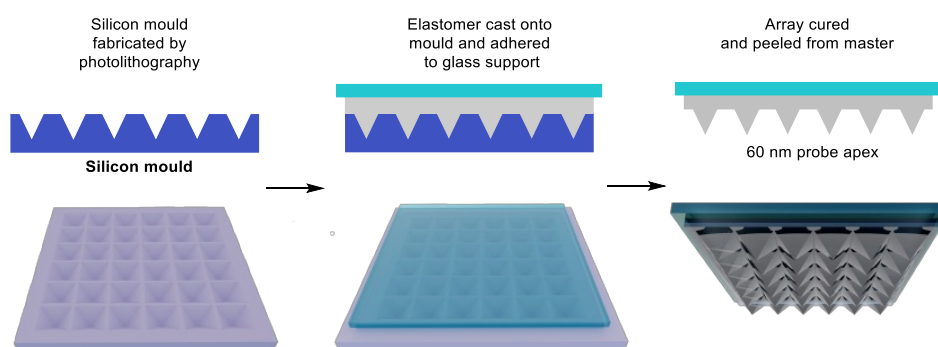


**Figure 1.8** Stylised depiction of polymer pen lithography probe array and lithographic ink deposition.



**Scheme 1.28.** Scheme showing steps towards PPL array fabrication. Steps; silicon mould filled with elastomer and cured before peeling probe array away from mould.

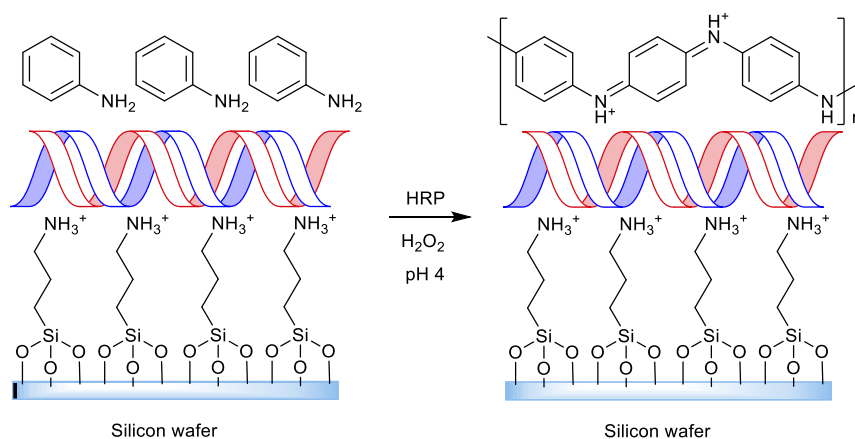
### 1.7.1 Nanotechnological applications of peroxidases

Horseradish peroxidase has been utilised as a catalyst within many nanotechnological applications.<sup>111, 112</sup> The wide array of reactions it can carry out and its large substrate scope are appealing features. Most applications involve its ability to catalyse the polymerisation of aromatic substrates either for their conductive properties or for use as structural building blocks.

### 1.7.2 Nanolithographic applications of peroxidases

In one of the first reports of HRP application to nanolithography, conducting polymer 'nanowires' were fabricated on a silicon wafer using DNA as a guiding template (Scheme 1.29).<sup>113</sup>

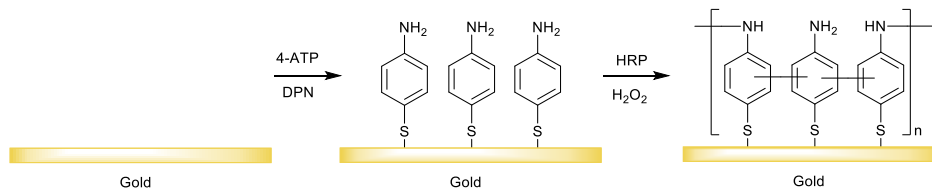
A solution of double stranded DNA and aniline was applied to an amine functionalised silicon wafer. Analysis by AFM showed the DNA strands were unwound and immobilised. It was hypothesised that the agglomeration of DNA was stopped by the coordination of aniline to the phosphodiester bond backbone of DNA. Aniline polymerisation could then be catalysed by HRP with the 'nanowire' polymers orientation and position determined by DNA location.



**Scheme 1.29.** Scheme showing the conditions for fabrication of polyaniline using DNA as a guiding template.

### 1.7.3 Scanning probe nanolithography

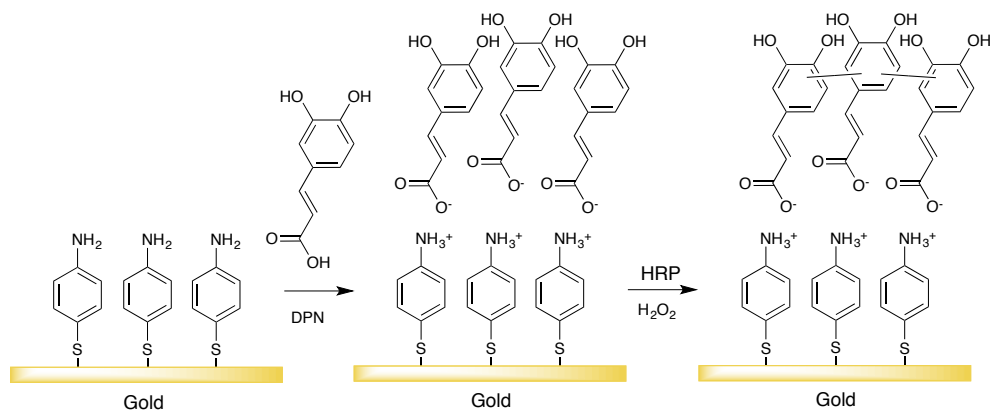
Lithographic techniques derived from SPM have been combined with HRP catalysis. In the first example DPN was used to deposit 4-aminothiophenol (4-ATP) onto gold substrates and HRP could subsequently be used to catalyse polymerisation of the monolayer (scheme 1.30).<sup>114</sup>



**Scheme 1.30.** Scheme showing the steps towards HRP catalysed poly(4-ATP) formation. Steps; 4-ATP functionalised gold surfaces subsequently polymerised by HRP catalysis.

In this report, DPN was first used to produce lines of deposited 4-ATP with dimensions of 4  $\mu\text{m}$  x 170 nm on gold surfaces with an average height of 35 nm. The surface was then submerged in a solution of HRP and hydrogen peroxide. Post polymerisation the surface analysis showed an average width of 210 nm and average height of 25 nm. The line width increased and the line height decreased, with the deduction being successful polymerisation would cause the monolayer to become disordered. X-ray photoelectron spectroscopy analysis also supported successful polymerisation was achieved on these surfaces.

In another interesting combination of HRP and DPN, the fabrication polycaffeic acid structures (scheme 1.31) is shown.<sup>115</sup> Caffeic acid could be deposited on to self-assembled monolayer of 4-ATP by DPN using the electrostatic interaction between carboxyl and amine groups. The patterns could then be submerged in HRP/H<sub>2</sub>O<sub>2</sub> to polymerise the monomer. It was found the 4-ATP surface also acted as a template to orient the monomer and as a result the subsequent polymerisation with HRP proceeded with a high selectivity to ring-ring coupling rather than a mixture couplings as with solution based polymerisation.



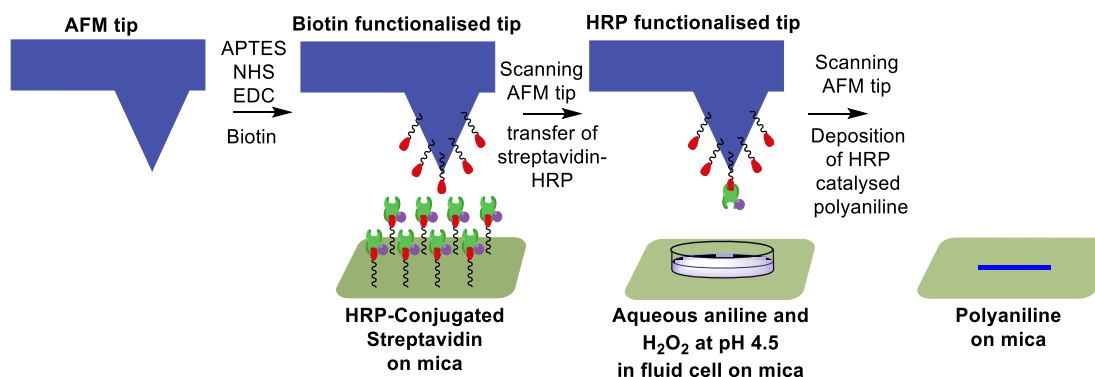
**Scheme 1.31.** Scheme showing the steps towards HRP catalysed surface modification.

Steps; deposition and subsequently polymerised by HRP catalysis of substrate.

#### 1.7.4 Biocatalytic nanolithography

HRP has also been used directly in the combination of scanning probe lithography by its immobilisation of to the apex of a scanning probe. The biocatalytic probe could then be used to carry out constructive ‘biocatalytic nanolithography’, where catalysis can only take place at the point of probe-substrate contact, to form polymer features on a surface.<sup>116</sup>

This was achieved (scheme 1.32) by first functionalising a probe with biotin, then transferring streptavidin–HRP to the tip using the biotin-streptavidin interaction. This probe could then be traced in an arbitrary pattern on a mica surface in the presence of aqueous aniline and hydrogen peroxide (pH 4), to catalyse the formation and precipitation of polyaniline. Thus confining polyaniline to probe locations.<sup>117</sup> Confinement of the catalyst to the apex of the tip was essential for low resolution lithography as polymer is produced in solution.



**Scheme 1.32.** Scheme showing the general overview of the workflow for reported biocatalytic nanolithography. Steps; Biotin functionalisation of probe followed by HRP immobilisation at probe apex and finally biocatalytic nanolithography on mica.

However, this approach had several drawbacks. The use of a homogeneous mix of isoenzymes means that isoenzymes with low or no activity could be attached, additionally variation in streptavidin-HRP conjugates means HRP molecules to streptavidin is not necessarily 1:1. Furthermore the immobilisation offers no orientation of the enzyme as HRP is conjugated to streptavidin in by surface residues, using non-selective bioconjugation reactions.

The non-covalent immobilisation means that once emerged in solution the enzymes may dissociate from biotin. While the interaction between biotin and streptavidin extremely strong, the strongly acidic conditions necessary for aniline polymerisation could cause dissociation (by changing the tertiary structure or cleavage of amide bonds).

The tetrameric structure of streptavidin (211.2 kDa) means not only can dissociation into monomers can occur but due to its size the link between HRP and the probe is increased and thus the possible resolution of the resulting pattern is decreased.

## 1.8 Aims

The strategic aims for this body of work are to increase synthetic utility and understanding of biocatalysis, in particular focused on heme peroxidases from horseradish. These are a well-established and investigated group of enzymes and have previously shown attributes that make them a good target for further investigation. Attributes such as broad reaction and substrate scope which make a solid starting points for further biocatalyst development and research.

Specific areas of interest are the biocatalytic formation of quinoid systems by HRP and the subsequent properties these systems possess. These systems can be directed towards both carbon-heteroatom and carbon-carbon bond forming reactions, for example either Michael or cyclo-additions. Efforts were made to develop these reactions or find new uses for existing known reaction. One aim was to utilise HRP to generate quinonoid systems (such as quinone methides and quinone imines), and use them as intermediates in tandem cycloaddition reactions, to produce fused aromatics ring systems. A key objective was to conduct these reactions in environmentally benign aqueous reaction media as use of organic solvents, particularly chlorinated hydrocarbons contribute to pollution.

Another area of interest is that certain quinoid systems have also shown their ability to conduct electricity and HRP has been shown to catalyse their formation, directing this catalytic activity towards nanotechnological uses in particularly nanolithography. Expanding on previous work could provide an alternative to traditional semiconductor manufacturing. Specifically, to advance biocatalytic nanolithography by first validating uni-probe methodology and then by extending it to a multi-probe approach. This it is aimed to tackle drawbacks of previous approaches by recombinantly expressing enzymes for homogeneity and using covalent and site specific attachment which will provide reliable catalysis.



## **Advancing biocatalytic nanolithography**

### **2.0.1 Catalytic probe nanolithography**

Lithographic techniques<sup>118</sup> derived from scanning probe microscopy (SPM), in particular those derived from atomic force microscopy (AFM) have been widely implemented due to their nanometre scale resolution and registry.<sup>100</sup> These nanolithographic methods use the probe tip to direct a chemical transformation to a specific location. There are many instances of direct physical manipulation of surfaces by the probe tip to produce nanoscale features: nanoshaving, local anodic oxidation and thermochemical nanolithography among them.<sup>116</sup> Probes have also been extensively utilised for the local deposition of ‘molecular inks’ to the surface, in so called dip pen nanolithography (DPN).<sup>105,108,119</sup> The drawback of these techniques being that they all rely on the physical manipulation of materials and surfaces by the probe tip.

Techniques combining the precision of scanning probe lithography with catalysis, whereby probes functionalised with a catalyst are able to directly carry out chemical transformations at the probe tip locality to generate nanoscale features have been widely reported.<sup>116</sup> While this approach can simply be carried out using DPN and a catalyst-containing ink,<sup>104</sup> a more elegant approach is to employ a probe that itself has been rendered catalytically active. This has the advantage of allowing the catalytic probe to be repeatedly reused and avoiding the need to transport the catalyst to the surface therefore contaminating the surface the catalyst. Examples of catalytic probes include functionalisation with transition metal coatings/complexes, organic catalysts photocatalysts or enzymes.<sup>116</sup>

### 2.0.2 Biocatalytic probes

The immobilisation of the enzyme onto a probe is an attractive prospect as it brings the advantages of enzyme catalysis (high catalytic turnover, operational under mild conditions) with the spatial resolution of scanning probe lithography. However, implementations of this concept have been few. The first demonstration; a covalently functionalised endoproteinase tip was used to digest polypeptide chains linked to a surface. At low tip speed the proteinase could catalyse the cleavage of a surface immobilised peptide to expose fluorescence, thereby forming nanoscale features on the surface. Probe immobilised enzymes have also been used to demonstrate constructive nanolithography.<sup>116</sup> Alkaline phosphatase functionalised was tip used to catalyse the precipitation of reduced nitro-blue tetrazolium, producing feature resolutions of 150–170 nm. Previously discussed (section 1.7.4) was the use of HRP to produce features of polyaniline, this was particularly notable as it was the first example of the deposition of a potentially functional material.<sup>117</sup> These techniques all suffer from the same limitation, that single probe lithography is low throughput due to only small areas able to be patterned at a time (~100  $\mu\text{m}$  x 100  $\mu\text{m}$ ). These methods also rely on non-site selective protein immobilisation, which provide inherently heterogeneous probes thus reducing reproducibility.

### 2.0.3 Multiplexed nanolithography

The issue of throughput has been addressed with multiplexed techniques such as the use of 2D-cantilever probe arrays<sup>107</sup> and cantilever free methods such as polymer pen lithography (PPL)<sup>108</sup> used for patterning  $\text{cm}^2$  areas with DPN (Figure 1.8). However, 2D-array techniques have the drawback that all probes must be exactly parallel to the surface to carry out uniform lithography<sup>120</sup> (Figure 2.1).

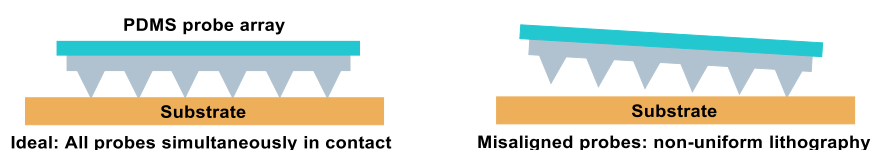


**Figure 2.1** Diagram depicting the issue with non-uniform probe array alignment, whereby misalignment cause probes to reach the surface at different heights.

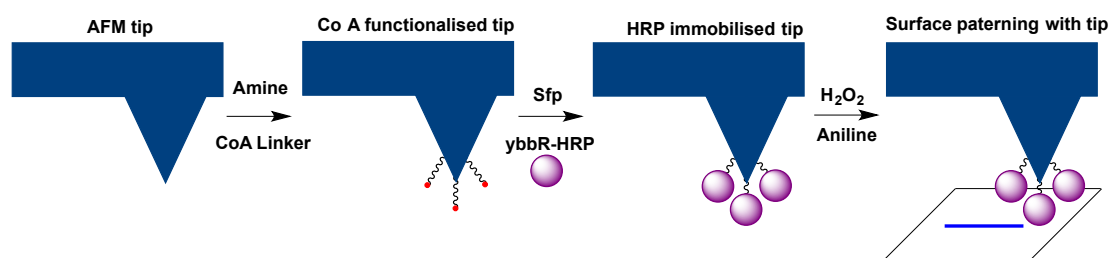
Even a small misalignment can cause a large difference in feature size from one side of the array to the other since some probes will come into contact with the surface earlier during the descent of the array, while others will come into contact later or not at all. Exact alignment is especially important with PPL due to the compressibility of the soft elastomer probes, where the probes contacting the surface earlier will be compressed, resulting in larger feature sizes.<sup>121</sup> Early work on PPL employed purely visual inspection to guide the alignment process, using a camera mounted above the array to observe the deformation of the pyramidal probes as they were brought into contact with the surface. Following adjustment the relative tilt angle, the procedure is repeating in an iterative fashion until the difference in contact on each side of the probe was indistinguishable to the eye.<sup>121</sup>

Subsequently, a more systematic approach was developed, consisting of a force sensor mounted beneath the substrate to measure the force applied upon contact of the probes on the surface. Alignment was thus achieved by adjusting the tilt angles to maximise the force exerted, which indicated that all the probes were simultaneously in contact. This method

showed that alignment to within  $0.004^\circ$  of the surface parallel was possible.<sup>122</sup> The primary limitation of SPL is therefore the need to carry out this repetitive process, which is not only exceptionally tedious for the operator but very time-consuming. In fact, the process of alignment is often several-fold longer (2-4 hours) than the lithographic patterning (usually < 1 hour).

## 2.1 Aims and objectives

The planned aims of this project were to advance biocatalytic nanolithography, first through refinement and validation of single probe biocatalytic nanolithography using horseradish peroxidase functionalised probes catalysing the formation and subsequent deposition of polyaniline (Scheme 2.1). Then extending it to multi-probe PPL to demonstrate parallelised large area nanolithography.



**Scheme 2.1.** Depiction of the general overview for the work flow to set up biocatalytic nanolithography. Steps; Functionalisation with coenzyme A, site-selective immobilisation of ybbR-tagged HRP, biocatalytic nanolithography producing polyaniline features.

It was planned to address shortcomings of previously reported methods by recombinantly expressing enzymes for homogeneity and using covalent and site specific attachment which will provide reliable catalysis. Previous studies have shown that site specific immobilisation of proteins give improved activity (compared to non-site specific)<sup>123</sup> this is especially important when confined to a probe tip as there are only a small number of protein molecules present.

The project then sought to challenge the biggest shortcoming of scanning probe lithography; low throughput, by multiplexing the biocatalytic probes to facilitate patterning over a wide area. In order to progress with multiplexed lithography, the necessity for perfect alignment of arrays to the lithographic substrate surface to produce uniform lithography required improvement as current techniques were slow and could have improved accuracy. Multiplexed biocatalytic nanolithography could then be refined to produce high resolution patterns over a wide area.

## 2.2 Cloning and expression of horseradish peroxidase isoenzyme C1A

The DNA of 26 peroxidase enzymes from horseradish (*Armoracia rusticana*) in the expression vector pPpT4\_Alpha\_S were kindly donated by Professor Glieder and co-workers (Technische Universität Graz, Austria).<sup>35, 37</sup> The constructs were sequenced before use to confirm they were received as expected. Isoenzyme C1A, being the most extensively studied isoenzyme, was selected as the primary candidate for immobilisation.

In order to enable the site specific attachment of HRP to the probes, the enzyme immobilisation technique previously developed in the group was chosen.<sup>124, 125</sup> This technique utilises a 12-mer peptide known as a ybbR tag which is recognised by the phosphopantetheinyl transferase *Sfp*. This *Sfp* enzyme then catalyses the ligation of the phosphopantetheine group from an immobilised coenzyme A (discussed in section 2.2.3).

Insertion of the ybbR tag was carried out by Gibson assembly. Assembly of the pPpT4\_alpha\_ybbR\_C1A vector was confirmed by double digestion and Sanger sequencing.

Protein production was initially conducted using *Pichia pastoris* as an expression host, soluble protein was isolated and purified. However, trials of immobilisation showed that the protein was unable to load a coenzyme A molecule using *Sfp* whereas controls showed the *Sfp* to be active. The produced ybbR\_C1A was heavily glycosylated by the expression host. It was hypothesised that either the key serine residue on the ybbR tag was glycosylated or

surrounding glycosylation provided significant enough steric bulk to stop *Sfp* binding the ybbR tag. Following this protein production in *E. coli* was conducted as this expression host lacks machinery for protein glycosylation.

In order to heterologously produce this protein in *E. Coli*, the vector pET28a\_ybbR\_C1A was constructed by restricting the previously constructed ybbR\_C1A gene with enzymes *XhoI* and *NcoI* and ligating the fragment in to the bacterial protein production vector pET28a (Figure 2.2). The assembled vector was then confirmed by Sanger sequencing.

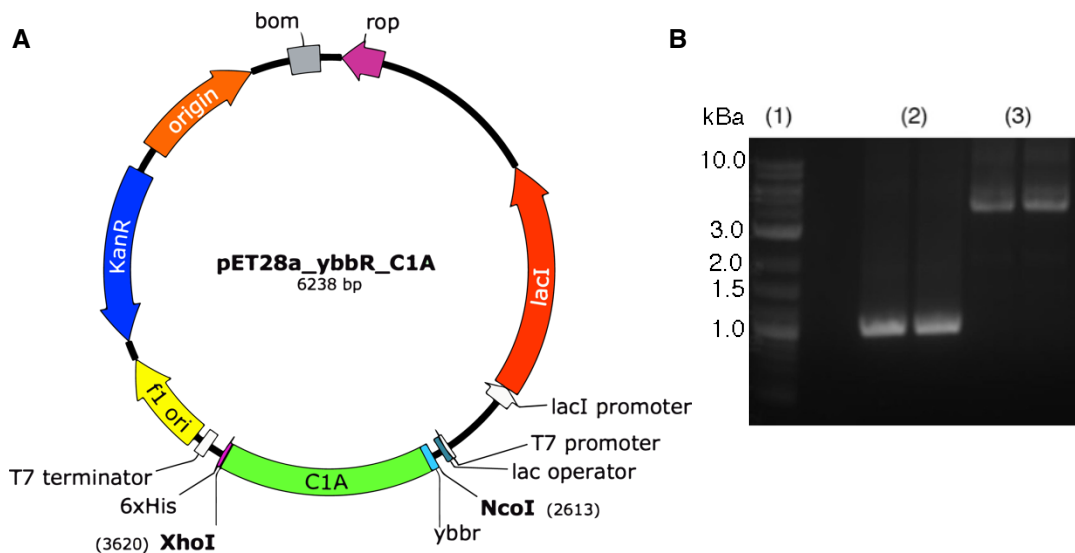


**Figure 2.2.** (A) Schematic map of vector pET28a\_ybbR\_C1A (B) Photo of agarose gel showing fluorescent DNA fragments from PCR with vector template pPpT4\_Alpha\_S\_C1A (1) Ladder (2) ybbR\_C1A and (3) pET28a\_ybbR.

The vector was then transformed into *E. coli* BL21 (DE3) and the polypeptide produced upon IPTG induction. The inclusion bodies produced were then solubilised in urea and purified by immobilised metal affinity chromatography (IMAC) (Figure 2.3A). The purified inclusion bodies were then refolded by drop-wise addition to refolding buffer according to previously reported procedures<sup>51</sup> and the refolded protein was then purified by IMAC (Figure 2.3B). The

isolated protein was then reconstituted with heme by drop-wise addition of hemin and repeated assaying of protein aliquots with 2,2'-azino-bis(3-ethylbenzothiazoline-6-sulphonic acid) (ABTS) until enzyme activity was found to have reached a maximum (reaction rate reached a plateau).

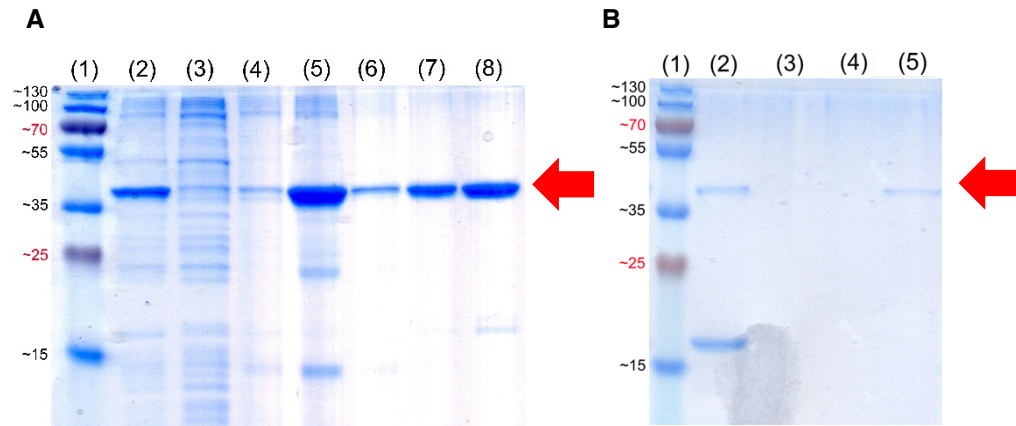


**Figure 2.3.** Images of SDS-PAGE gels of: **(A)** ybbR-C1A over the course of isolation of inclusion bodies by nickel affinity chromatography; (1) Molecular weight markers, (2) total protein, (3) soluble protein, (4) solubilised inclusion bodies (5) unbound flow through, (6) 20 mM imidazole wash, (7) 60 mM imidazole wash, (8) 250 mM imidazole wash. **(B)** Refolded ybbR-C1A purification during purification by nickel affinity chromatography. (1) Molecular weight markers, (2) unbound flow through, (3) 20 mM imidazole wash, (4) 60 mM imidazole wash, (5) 250 mM imidazole wash.

To further ensure that protein was correctly folded and had correctly bound a heme group, ligand affinity chromatography was utilised.<sup>33</sup> *N*-hydroxy-2-naphthamide functionalised agarose was prepared and used to purify the *holo*-protein (Figure 2.4), giving an RZ of 2.93 from an original RZ of 1.10 (theoretical maximum RZ 3.42<sup>126</sup>)

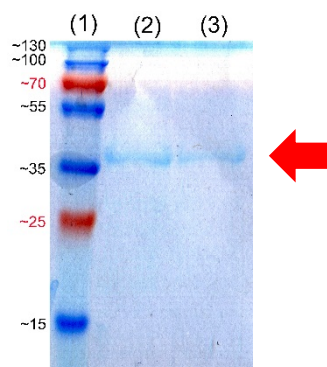
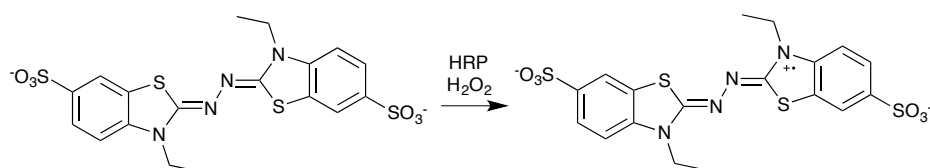


**Figure 2.4** Image of SDS-PAGE gel of refolded ybbR-C1A fractions collected from ligand affinity chromatography (1) Molecular weight markers, (2) unbound flow through, (3) boronic acid wash.

### 2.2.1 ybbR-C1A activity assays

Enzyme activity assays were performed on the fully purified and reconstituted ybbR-C1A (ybbR-C1A) using the standard literature procedure with ABTS as a substrate. In this assay the colour change from the starting material to the oxidised product could then be tracked at 420 nm using UV/Vis spectroscopy (Scheme 2.2).



**Scheme 2.2.** Single electron oxidation reaction of ABTS by HRP with product  $\lambda_{\max}$  absorbance at 420 nm.

To draw comparison for recombinant enzyme activity a commercial available HRP preparation (c-HRP) was acquired. While this is not a perfect comparison, as commercial HRP preparations contain a mixture of isoenzymes it provided a baseline for activity. Preparations of ybbR-C1A before purification by ligand affinity (BL-ybbR-C1A) were also



assayed and compared (Table 2.1). Results showed that the purified enzyme showed comparable activity with the commercially sourced HRP, ybbR-C1A did show a slightly higher activity but this is within error of protein quantification. Therefore, protein produced was deemed active enough to proceed with.

	<b>ybbR-C1A</b>	<b>BL-ybbR-C1A</b>	<b>c-HRP</b>
	<b>(purified and reconstituted enzyme)</b>	<b>(before purification by ligand affinity chromatography)</b>	<b>(commercially sourced mixture of isoenzyme)</b>
<b>U/mg</b>	491.2	9.7	407.1

**Table 2.1.** Table detailing the activity units of enzyme per mg of protein. Units are determined by activity assay with ABTS. One activity unit will oxidise 1  $\mu$ mole of ABTS per minute at 25°C at pH 5.0.

### 2.2.2 Polyaniline formation

After activity assays with ABTS, the refolded ybbR-C1A was assayed with aniline and several of its derivatives (Figure 2.5) to check that it was still able to oxidise anilines which would then in turn polymerise (see section 1.6.4.2.2). Polymerisation by HRP catalysis, and by chemical oxidation as a comparison were carried out by adapting existing methods.<sup>84, 86</sup>

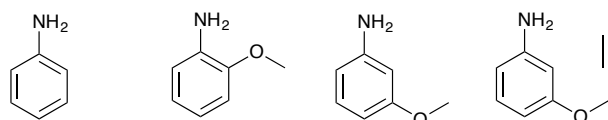


**Figure 2.5.** Substrates polymerised by enzyme oxidation with ybbR-C1A/hydrogen peroxide.

Characterisation was carried out by IR<sup>86</sup> due to polymers being insoluble in all available solvents. Insoluble material was isolated from the reaction mixtures, by filtration and washing. The IR spectra for each synthesis method were then compared, and dry weight of the polymer used to ascertain approximate turnover numbers. All aniline derivatives polymerised in the presence of HRP/H<sub>2</sub>O<sub>2</sub>, giving IR spectra consistent with those reported in the literature therefore showing that they were all suitable substrates.<sup>127</sup> The IR spectra produced for each method for each compound had comparable peaks when comparing chemo and bio-catalytic methods. A representative IR spectrum for poly-2-methoxyaniline is shown in Figure 2.6. Dry weights of the polymer produced (Table 2.2) showed that poly-2-methoxyaniline had the highest yield. All others produced a good yield with aniline being the lowest. The low yield of aniline was most likely due to its higher oxidation potential compared to the other substrates, due to lacking electron rich ring substituents.<sup>128</sup>

<b>Substrate</b>	<b>Percentage yield (%)</b>
Aniline	<b>48%</b>
2-Methoxyaniline	<b>89%</b>
3-Methoxyaniline	<b>75%</b>
3-(Prop-2-yn-1-yloxy)aniline	<b>71%</b>

**Table 2.2.** Table detailing the percentage yield of insoluble polymer produced by polymerisation with HRP. Percentage yield calculated by dry weight of insoluble polymer compared to monomer weight.

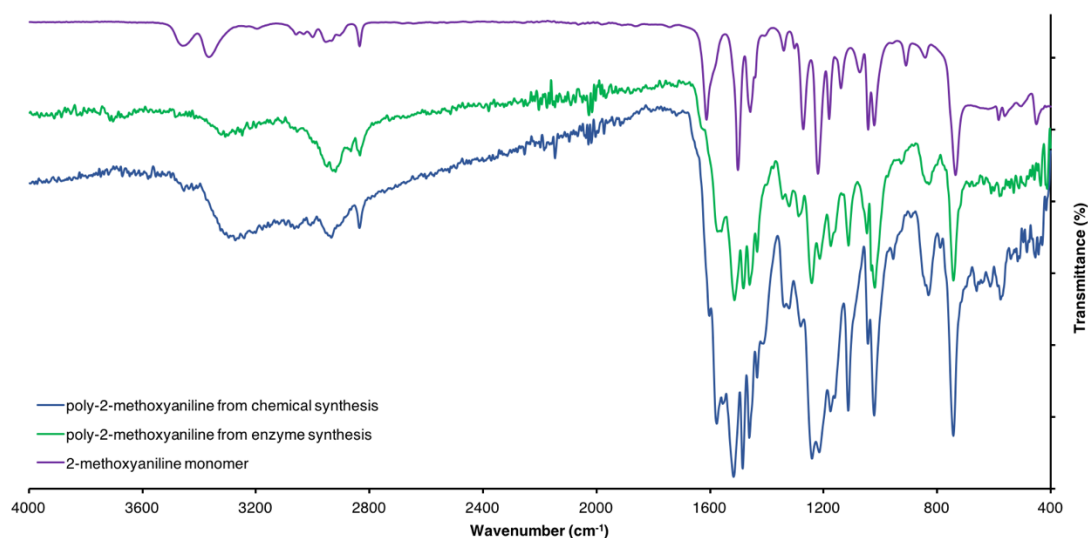
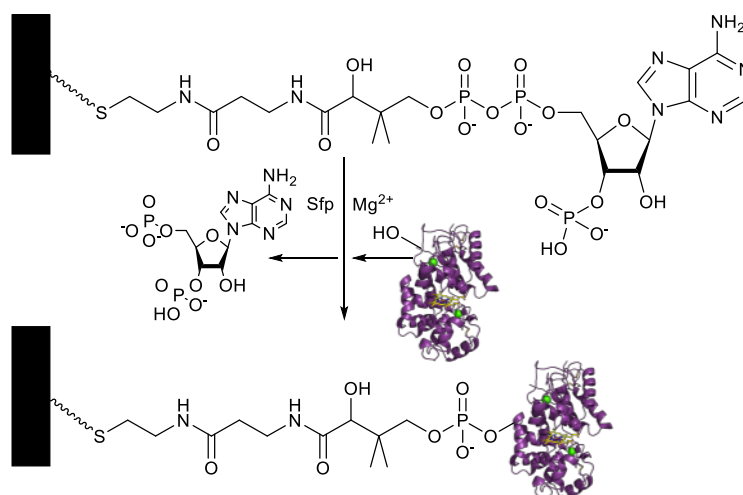


**Figure 2.6** IR spectrum of poly-2-methoxyaniline synthesised by chemical oxidation with ammonium persulfate (-), poly-2-methoxyaniline synthesised by enzyme oxidation with ybbR-C1A/H<sub>2</sub>O<sub>2</sub> (-) and 2-methoxyaniline monomer (-) for comparison.

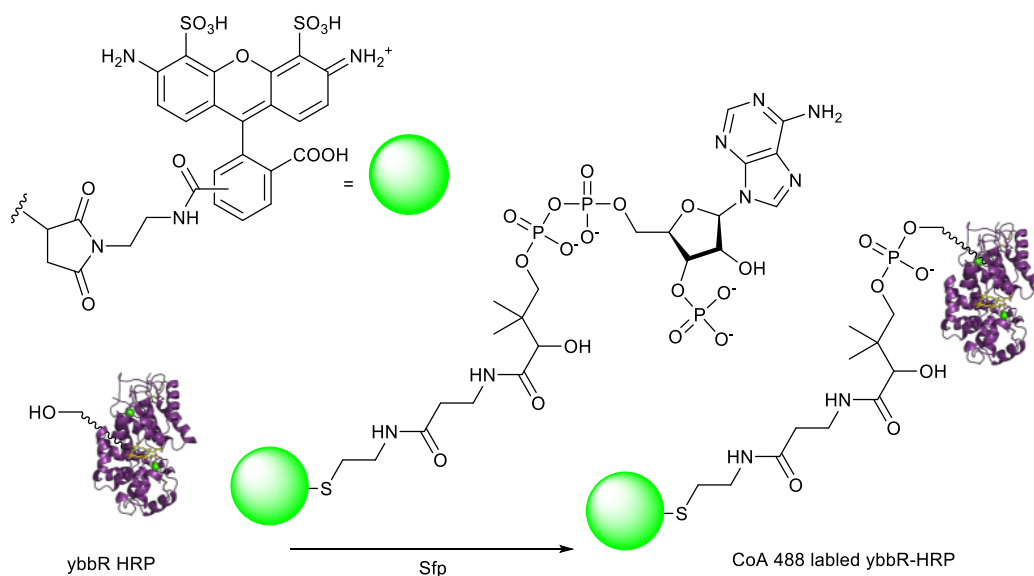
### 2.2.3 *Sfp* mediated C1A immobilisation

Site specific covalent attachment of the ybbR-tagged C1A isoform of HRP (ybbR-C1A) to the tip of an AFM cantilever was then performed. This was to be accomplished by using the 4'-phosphopantetheinyl transferase (*Sfp*) from *B.subtilis* which binds ybbR tagged proteins and transfers phosphopantetheine to a serine in the tag<sup>125</sup> (Scheme 2.3). In cases where the coenzyme A is attached to a solid support via its sulphur atom the phosphopantetheine transfer results in the attachment to the support.



**Scheme 2.3.** Sfp-mediated immobilisation of ybbR tagged protein.

In order to determine whether the ybbR-tagged C1A peroxidase (ybbR-C1A) was a substrate for *Sfp* an assay was carried out based on the fluorescent labelling of the protein with CoA-coupled fluorophore using the standard literature procedure<sup>129</sup> (Scheme 2.4). This fluorophore coupled ybbR-C1A was then subjected to SDS-PAGE. *Sfp* was prepared using the same construct.<sup>124</sup>



**Scheme 2.4.** Depiction of the reaction in the *Sfp* catalysed, ybbR-C1A fluorescent labelling assay.

Results of the labelling showed that CoA 488 was successfully conjugated (Figure 2.8). In comparison, the results also show no loading has taken place in control reactions that lacked one of the four reaction components as expected.

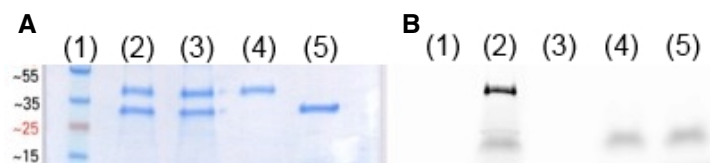
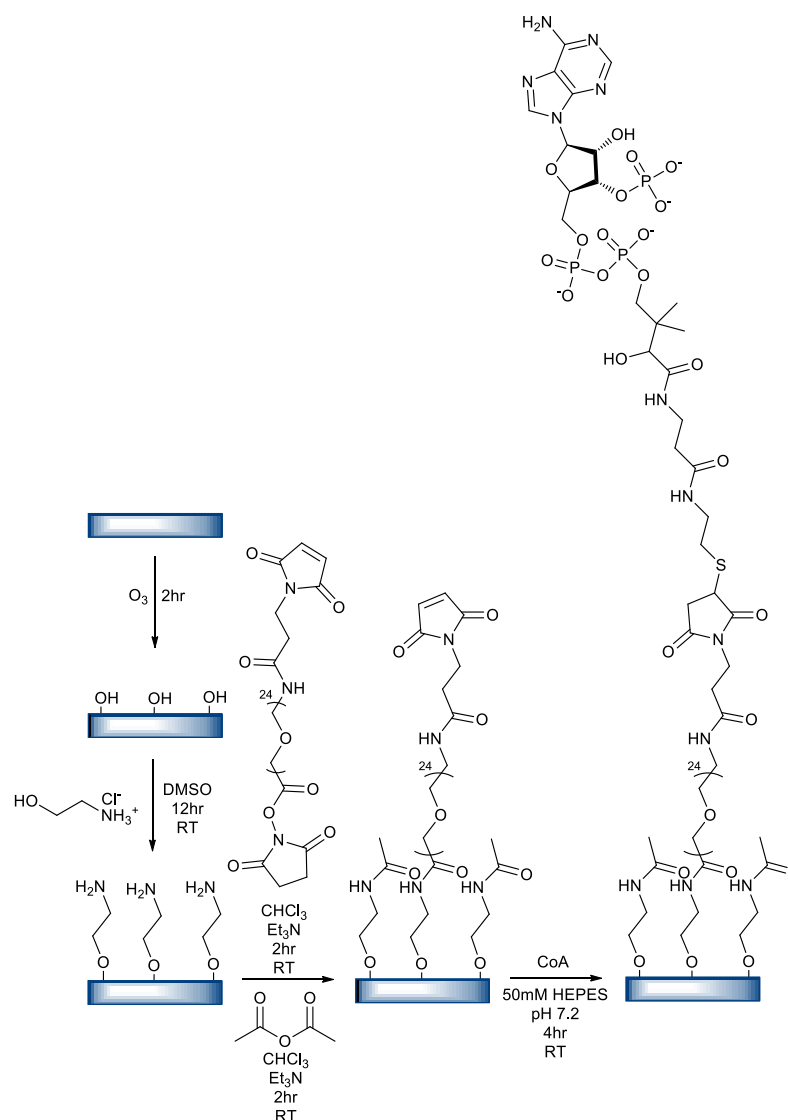


**Figure 2.8.** (A) Photo of SDS-PAGE gel of reaction mixtures (B) SDS-PAGE gel of reaction mixtures developed using a fluorescent imager at 488 nm. Lanes (1) Molecular weight markers, (2) Full reaction (ybbR-C1A+Sfp+CoA), (3) CoA omitted, (4) Sfp omitted, (5) ybbR-C1A omitted.

## 2.3 Single probe biocatalytic nanolithography

### 2.3.1 Sfp mediated ybbR-C1A immobilisation

Having demonstrated ybbR-C1A can be conjugated with CoA the next step was to immobilise it on to the surface of an AFM cantilever tip. A number of surface amino functionalisation methods were tested but it was found that surface functionalisation with ethanolamine<sup>130</sup> gave the best results. The amino functionalised probes were then ligated with CoA using a procedure similar to that previously reported<sup>131</sup> (Scheme 2.5).



**Scheme 2.5.** Depiction of the reactions for silicon nitride probe construction. First by oxidation of silicon nitride and amino functionalisation. Followed by ligation of PEG linker by NHS-ester. Finally, addition of Coenzyme A.

Silicon nitride surfaces (discarded AFM chips) functionalised with linker were subjected to *Sfp*-catalysed enzyme. Additionally, control reactions with reactions lacking *Sfp* or HRP or CoA (where the maleimide was blocked with 2-mercaptoethanol) were carried out. The silicon nitride surfaces were then washed until no HRP activity was detected in the washings. The silicon nitrite surfaces were then attached to a microtitre plate and assayed with ABTS by following absorbance at 420 nm. Results showed that immobilisation had

taken place, with a positive result recorded only when *ybbR-C1A*, *Sfp* and the CoA-functionalised surface was used (Figure 2.9).

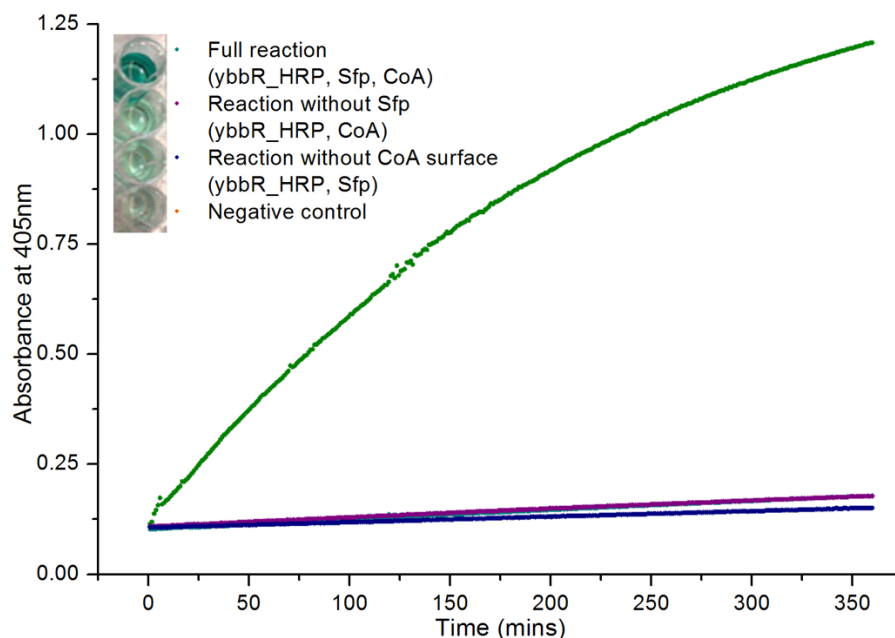
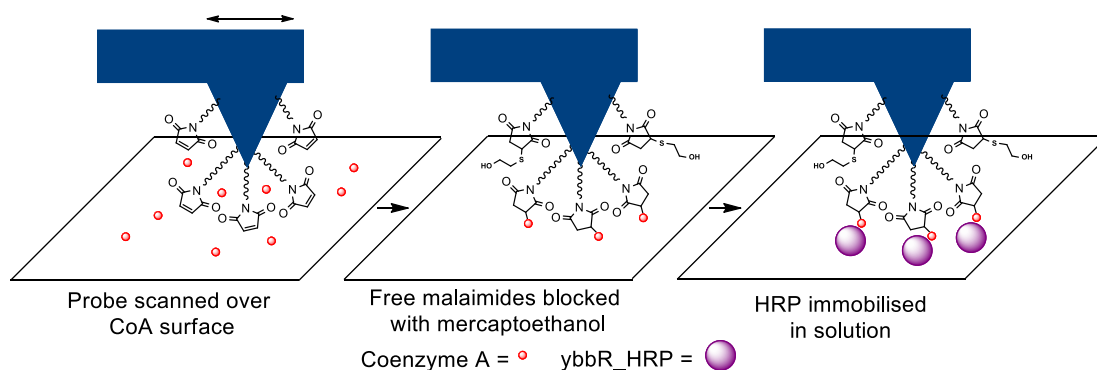


**Figure 2.9.** Graph showing absorbance at 420 nm over time for different functionalised silicon nitride surfaces, constituting ABTS activity assay of any enzyme present.

### 2.3.2 Confinement of *ybbR-C1A* to the apex of cantilever

In order to achieve the highest resolution patterns the enzymes need to be confined to only the very apex of the probe. The methodology consisted of initial surface functionalisation with linker but leaving the maleimide group unreacted. Coenzyme A was then spin coated to a silicon surface and the cantilever functionalised with maleimide was very slowly scanned over the surface (in contact mode) (Scheme 2.6). It was conceived that the motion would be slow enough and the concentration of Coenzyme A on the surface to be sufficient for the 'pick-up' reaction to take place.



**Scheme 2.6.** Depiction of the procedure for confining enzyme to the apex of the AFM tip.

First by scanning the maleimide functionalised probe over a Coenzyme A covered surface, unreacted maleimide are then blocked with mercaptoethanol. *Sfp* catalysed HRP immobilisation can then be carried out in solution.

After scanning the surface for 1 hour at 60% humidity, the probe was then transferred to a solution of 2-mercaptoethanol to block the remaining unreacted maleimide groups from reacting with the protein. The probe was then subjected to the immobilisation procedure and finally washed with PBS/tween until no activity with ABTS was seen in the wash buffer.

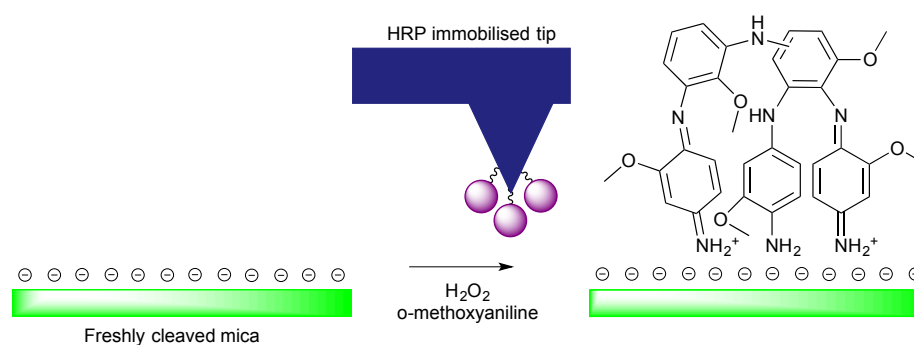
### 2.3.3 Nanolithography with ybbR-C1A functionalised probe on mica

The probe with attached ybbR-C1A was used to attempt patterning of a mica surface with polyaniline (Scheme 2.7). Freshly cleaved mica was used as the surface substrate as it has a negatively charged surface and it was hypothesised that this would attract the positivity charged polyaniline that would be produced, as proposed by previous literature reports.<sup>117</sup>

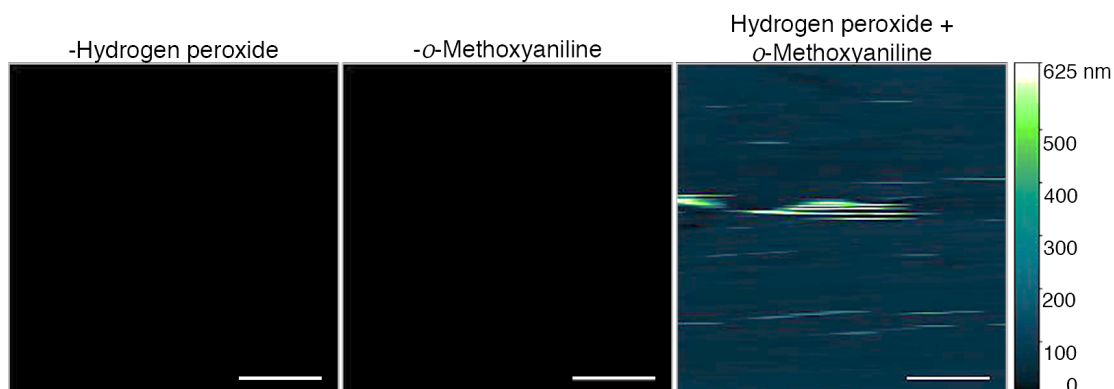
The freshly cleaved mica was imaged by AFM in topography mode using the enzyme immobilised probe immersed in phosphate buffered saline which showed no features on the surface, then a solution of 5 mM *o*-methoxyaniline and 1 mM hydrogen peroxide were added. The AFM probe was rested on the mica for 60 seconds, to allow the polymerisation reaction to take place and the surface was then imaged. It was expected that corresponding to the deposited a feature polyaniline expected in the centre of the image. The resulting



image showed apparently rough surfaces consistent with particles/aggregates being dragged over the surface (Figure 2.10). Control experiments without either *o*-methoxyaniline or  $\text{H}_2\text{O}_2$  showed featureless surfaces (Figure 2.10). It was concluded that polyaniline was being produced at the location of the probe, however polymer produced was not significantly attracted to the negatively charged surface, and was instead adsorbing to the protein covered probe. This coating then caused the images of an apparently rough surface due to the cantilever sticking and slipping on the surface.



**Scheme 2.7.** Depiction of biocatalytic nanolithographic catalysed formation and deposition of polyaniline on the negatively charged surface of freshly cleaved mica.



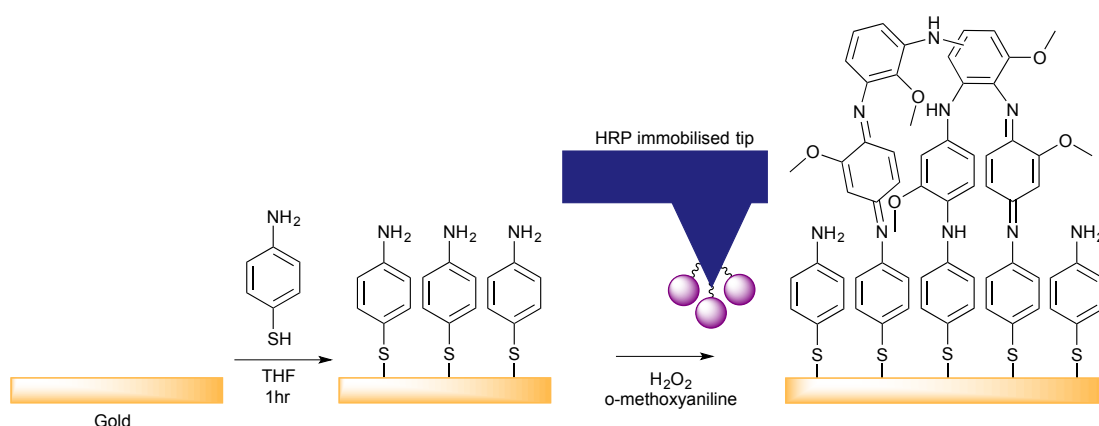
**Figure 2.10.** AFM recorded topographic images of mica surfaces with control and full reaction conditions after probe resting for 60 seconds. Scale bar  $20\ \mu\text{m}$ .

Further attempts to produce meaningful patterns of polyaniline on mica, by adjusting the concentrations of polyaniline,  $\text{H}_2\text{O}_2$  and probe dwell times and patterns were attempted. Imaging parameters were also considered and probe speed and force constant applied to

the probe varied. However, all attempts on mica were unsuccessful resulting in either noise consistent with polymer being absorbed to the tip or no patterns being produced.

### 2.3.4 Nanolithography with C1A functionalised probe on 4-aminothiophenol functionalised surfaces.

The earlier experiments suggested that polymer was apparently produced but was failing to be deposited to the negatively charged surface. This was perhaps due to the charge density not being sufficiently high compared to charged amino acid residues on the enzyme functionalised tip to enable preferential deposition of the polymer on the mica. As an alternative 4-aminothiophenol functionalised surfaces were investigated as previous report<sup>114</sup> has shown they could be polymerised by HRP. This report was stimulus for utilising a functional surface as a covalent tether for polymers. The hypothesis was that free radicals produced by HRP and subsequent radical propagating chains could react with the surface. HRP could also oxidise the surface directly if the proximity of probe tip is close enough. It was also found this approach has also been utilised successfully in electrochemical polymerisation.<sup>132</sup> 4-ATP functionalised gold surfaces were readily prepared by submerging clean gold surfaces in a solution of 4-ATP followed by scanning probe lithography as described in the previous section (Scheme 2.8).



**Scheme 2.8.** Overview of lithography with ybbR-C1A functionalised probes on 4-ATP functionalised surfaces. Steps; 4-ATP surface functionalisation followed by lithography.

Similar to the previous experiments, the 4-ATP functionalised surface imaged with a C1A functionalised probe (in phosphate buffered saline) showed no features on the surface. To initiate lithography a solution of 5 mM *o*-methoxyaniline and 1 mM hydrogen peroxide were added (Scheme 2.8) and the AFM probe scanned across a 25  $\mu\text{m}$  line for 120 s (Figure 2.11). The surface was then imaged and showed a new feature in the area of the scanned line.

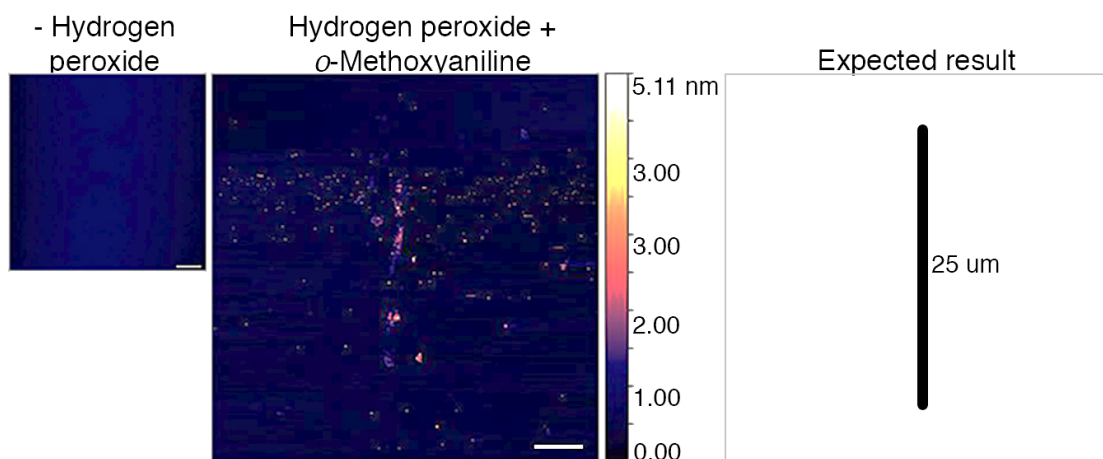


**Figure 2.11.** AFM images of control recorded topographic images, full reaction and control reaction without  $\text{H}_2\text{O}_2$  from lithography and expected. Conditions; 120 s per feature, 5 mM aniline, 1 mM  $\text{H}_2\text{O}_2$ . Scale bar 5  $\mu\text{m}$ .

Further improvements were achieved by reducing the concentration of both aniline and  $\text{H}_2\text{O}_2$ . This change increased the resolution of the feature produced by reducing the spread of polymer aggregates, although this also meant the write speed (the speed at which the probe was scanned across the surface) had to be increased. For example, lithography conducted in 0.1 mM *o*-methoxyaniline and 0.1 mM hydrogen peroxide by scanning a line of 12  $\mu\text{m}$  in length over 240 s ( $0.05 \mu\text{m s}^{-1}$ ) gave a feature of average full width half maximum (FWHM) of  $443 \pm 24 \text{ nm}$  (Figure 2.12).

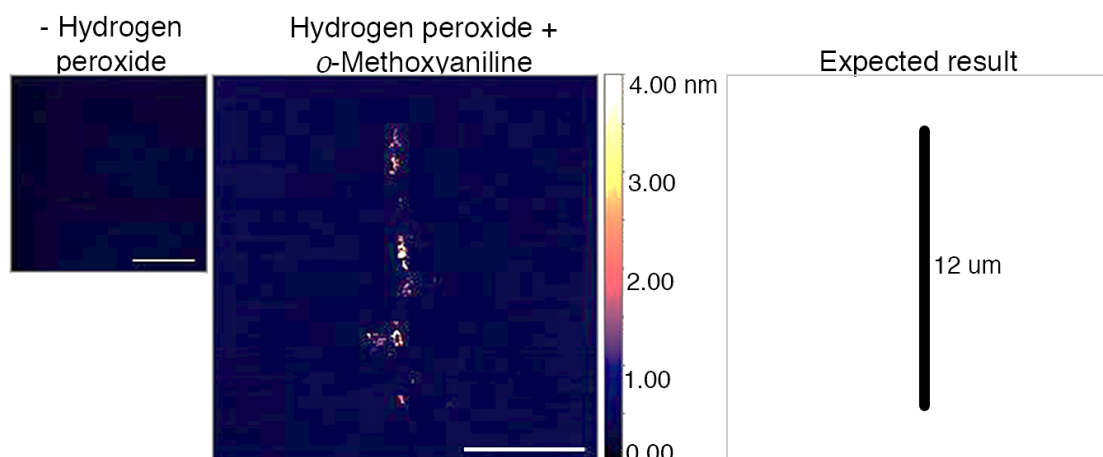


**Figure 2.12.** AFM images of control, full reaction from lithography and expected. Conditions; 240 s per feature, 0.1 mM aniline, 0.1 mM H<sub>2</sub>O<sub>2</sub>. Scale bar 5  $\mu$ m.

Similarly, lithography carried out by positioning the probe in three sequential locations (Figure 2.13) 15  $\mu$ m apart with a 30 s dwell time in each location generated 'dot' features at the correct locations and with little diffusion of polymer to the surrounding area (clean background). Interestingly feature size decreased (90%) from the first dwell position to the second indicating that less polymer was being deposited in the later features. This could either indicate that the immobilised enzymes quickly become deactivated or that the probe becomes covered in adsorbed polyaniline.

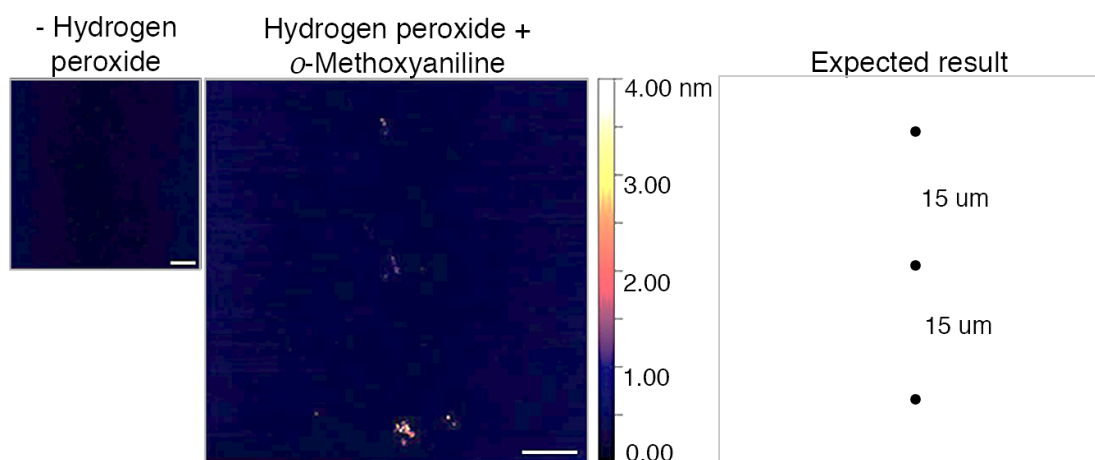


**Figure 2.13.** AFM images of control, full reaction from lithography and expected. Conditions; 30 s per feature, 0.1 mM aniline, 0.1 mM H<sub>2</sub>O<sub>2</sub>. Scale bar 5  $\mu$ m.

The current major drawback is that imaging the surfaces with the functionalised probe was the only practical method of finding the features produced. This meant that the enzyme was continuously reacting with substrate and therefore polymer was still produced as the tip moved over the surface during imaging. Although the tip moved significantly faster when imaging ( $20 \mu\text{m s}^{-1}$  versus  $0.05 \mu\text{m s}^{-1}$ ) any polymer produced could still contribute to the quality of patterns produced.

Encouraged by these initial single probe lithography results, efforts then moved to multiplexing this lithography.

#### **2.4 Multiplexed wide area lithography**

The multiplexing of any new nanolithography method is essential for wider applications due to the inherently low-throughput nature of single probe nanolithography. Wide area ( $\text{cm}^2$ ) lithography could also address practical considerations, such as enabling more convenient post-lithography processing, imaging and characterisation.

Cantilever free elastomer probe arrays developed for the dip-pen nanolithography technique known as polymer pen lithography (PPL) is a very attractive candidate for development into multiplexed biocatalytic nanolithography.<sup>108</sup> PPL arrays are made from a polydimethylsiloxane (PDMS) elastomer, which is cured in a silicon mould and mounted on a flat substrate. They can therefore be produced cheaply and are readily functionalised with a range of chemistries. The arrays can therefore be functionalised with enzyme, mounted in an AFM and used in the same way as a conventional cantilever.

As previously mentioned,<sup>122</sup> crucial to the execution of 2D array technologies is that the probe array must be exactly parallel to the surface substrate so that when lithography is conducted, all the probes come into contact with the surface simultaneously. To get the best result from multiplexed biocatalytic nanolithography this limitation of the instrumentation would need to be addressed. An algorithm that automates the iterative alignment process on a modified AFM system, employing the detection of force using multiple force sensors to

determine probe-surface contact, was developed in collaboration with Dr Shuai Wang and Dr William Heath (School of Electrical and Electronic Engineering, University of Manchester)

#### 2.4.1 Probe array alignment to substrate

The hardware setup consisted of a 3-axis AFM ( $x$ ,  $y$  and  $z$ ) located above a custom-built translation and goniometer stage with 5 degrees of freedom; lateral, longitudinal, vertical, pitch and roll motion ( $x$ ,  $y$ ,  $z$ ,  $\theta$  and  $\phi$  respectively) (see Figure 6.1 in s for a graphic representation). The three piezoelectric load cell sensors were build into the stage (Figure 2.14).

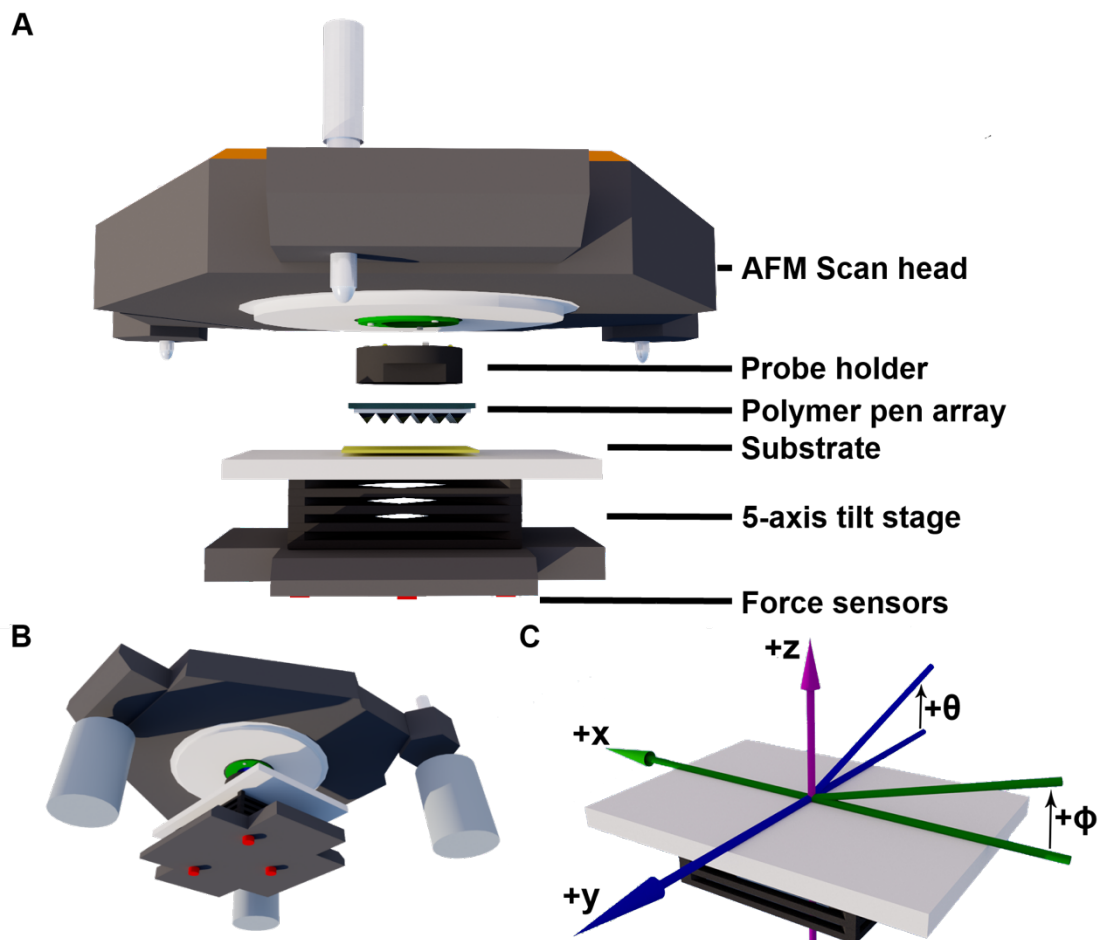
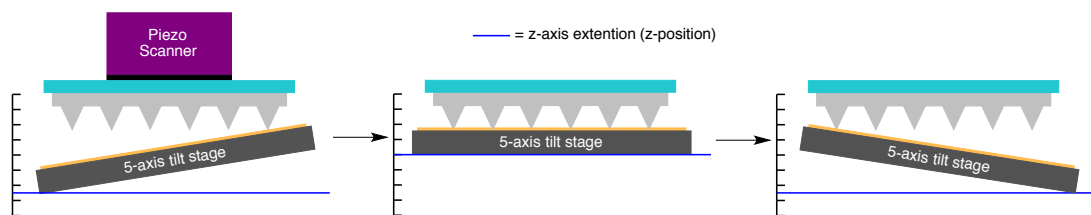


**Figure 2.14.** Depiction of the instrument setup; (A) side view with labels, (B) bottom view, highlighting force sensors (C) definition of 5 degrees of freedom.

### 2.4.1.1 Probe alignment algorithm

This work was undertaken in collaboration with Dr Shuai Wang, to write the source code for the devised algorithm. Essentially this algorithm automates procedures that would have been undertaken by a human operator when performing an alignment: to advance the probe array towards the surface; record the distance travelled in order to apply a pre-determined amount of force on the sensors; ( $490 \mu\text{N}$ , chosen owing to reliably showing probe contact over the background sensor noise of  $\sim 49 \mu\text{N}$ ) then retract the probes and adjust the tilt by a pre-set amount. First recording the point on the z-axis that the probes come into contact with the surface and tilt angle of the stage, then repeating this procedure across a series of tilt angles, the angle that requires the greatest extension of the stage should correspond to the angle of parallel alignment (Scheme 2.9). Repeating this process for the second tilt axis can then complete the alignment of a two-dimensional array of probes.



**Scheme 2.9** Depiction of alignment procedure, showing the relationship between z-axis extension and degree of alignment to the probe arrays.

Example data collected for the relationship between tilt angles  $\theta$  and  $\phi$  and the z-axis extensions 'z position' is shown in Figure 2.15A. This data can then be fitted to two lines to resolve their intersection, which is the point at which  $\theta/\phi$  gives the maximum z-extension. This point termed  $\theta/\phi_{\text{optimal}}$  (Figure 2.16A) is thus the angle at which the stage must be tilted to bring the stage parallel to the probe array along the given axis ( $\theta$  or  $\phi$ ).

It was found that when the optimal for one angle had been set, the change in the z-position as a function of the other tilt angle becomes too small to accurately fit the subsequent angle.

Thus by tilting one axis  $\pm 150\text{ m}^\circ$  away from its 'optimal' angle before alignment of the other axis, (Figure 2.16A) the data fitting could be accurately achieved and thus the 'optimal' could be found. Then by performing this procedure twice for each angle ('optimal'  $+150\text{ m}^\circ$  and 'optimal'  $-150\text{ m}^\circ$ ) the four pairs of angles  $(\theta, \phi)$  (one calculated, one optimal  $\pm 150\text{ m}^\circ$ ) can be represented in a coordinate system (Figure 2.16B). The intersection point of the pairs of coordinates thus represents the overall optimal tilt angle for each axis  $(\theta_{\text{optimal}}, \phi_{\text{optimal}})$ .<sup>133</sup>

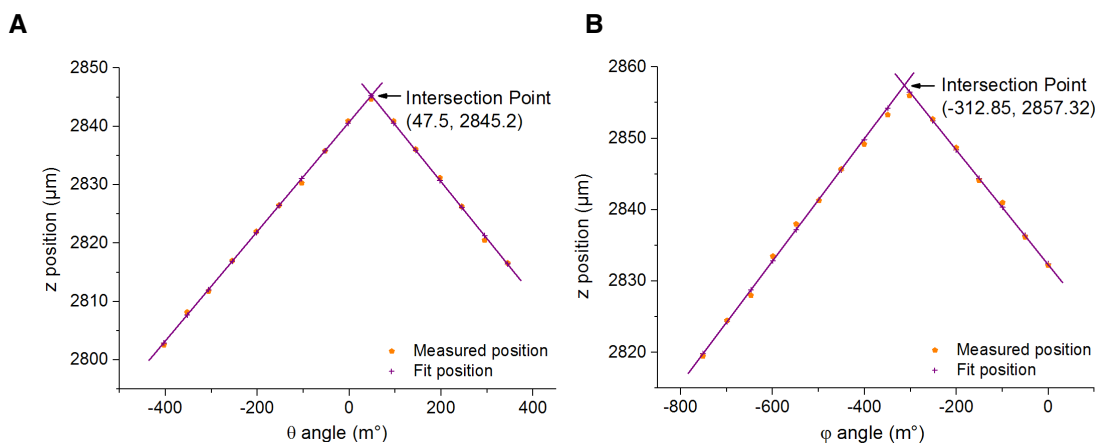


**Figure 2.15.** Graphs illustrating the relationships between the tilt angles and z position.

Where  $\blacklozenge$  indicates the actual values measured and  $+$  indicates the best fit with the least-squares method.

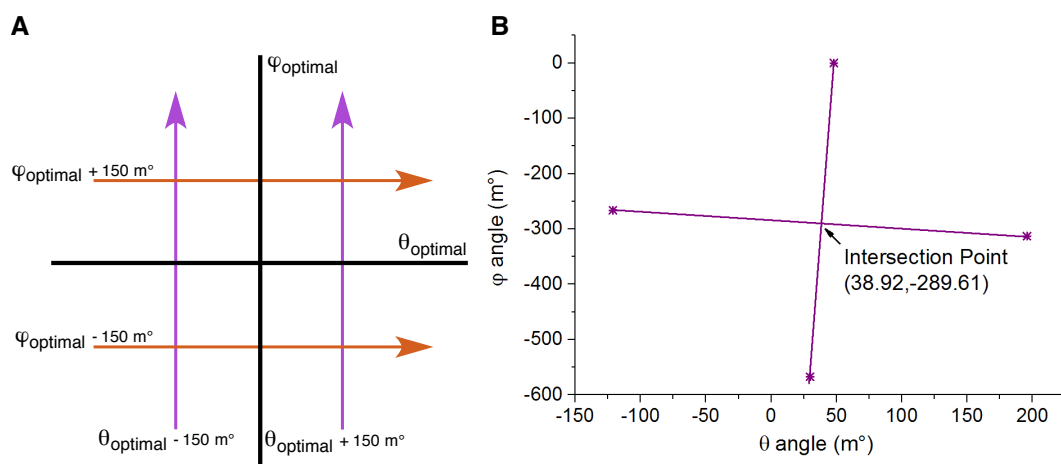




**Figure 2.16.** (A) Depiction of tilt angles sequence of measured angles. (B) Graph of  $\phi$  against  $\theta$  with the plots of the four points where the maximum z-position was reached. The intersection is calculated as the final overall optimum tilt angle across both axes.

#### 2.4.1.2 Alignment algorithm validation

In order to validate the alignment procedure, simple PPL was carried out by depositing 16-mercaptohexadecanoic acid on to a gold substrate as a model system. Surface patterns were either imaged by lateral force AFM or (after chemical etching<sup>105</sup>) by light microscopy. Large-Area Nanolithography was accomplished using a 1.44 cm<sup>2</sup> PPL array. Figure 2.17 represents an example of a produced pattern, 5 locations were imaged and size measurements (half width full maximum) of 15 random features taken from each location. The features were found to have an average size of 1.97  $\mu\text{m}$  with a standard deviation of 7 nm and a range of 40 nm.

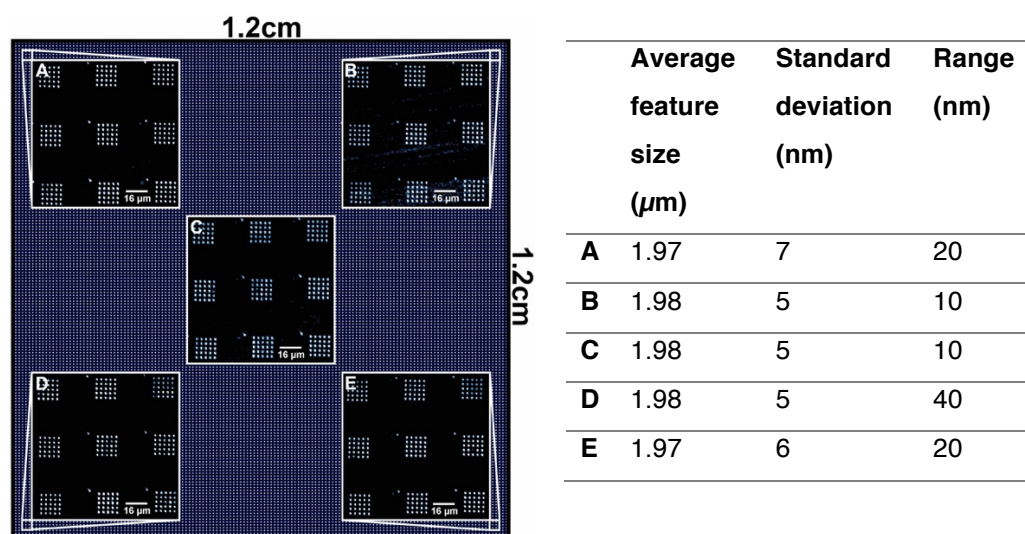


**Figure 2.17.** Diagram illustrating sites of size measurements with the insets showing the microscopy images, size measurements taken from a sample size of 15 for each site.

Efforts were next focussed on achieving the smallest possible features over the printed area.

To make it possible to locate features by lateral force imaging a template consisting of

nested oval features was used (Figure 2.18) was used. Two locations at opposite corners of the patterned area were imaged, and size measurements the features (Figure 2.18C) taken for each area. The features in the areas were measured at  $66.5 \pm 9.8$  nm and  $71.3 \pm 9.3$  nm respectively, which were within experimental error and maximum practical resolution of PPL.<sup>108</sup> This indicated any misalignment was less than the minimum tilt step that can be realised with the hardware setup ( $\leq 0.3$  m°).

Additionally, with respect to the problem of time taken to achieve alignment; for the given example, the pattern of 2500 individual features shown in Figure 2.18 took 55 minutes to complete, with the alignment algorithm taking an average of 35 min to complete. Therefore, the rate limiting step of 2D-SPL is now the lithographic printing rather than the alignment.

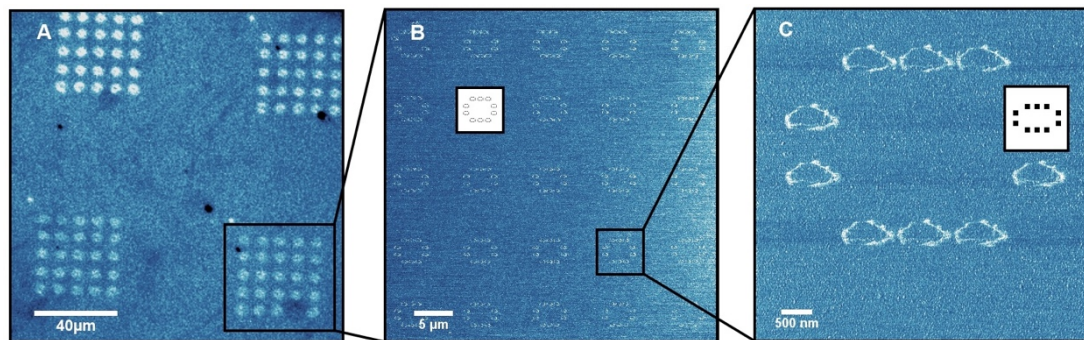


**Figure 2.18.** Images showing sequential magnifications of the pattern produced by PPL deposition of MHA on to gold: **(A)** an optical microscope image taken after 4 minutes' exposure to gold enchan; **(B and C)** Lateral force AFM images of the MHA deposited onto the gold with schematic inlays of the pixel pattern used.

Other more complex templates were also used for patterning over large area, in each case uniform patterns were produced, with Figure 2.19 showing a representative pattern produced with microscope images from etched patterns.

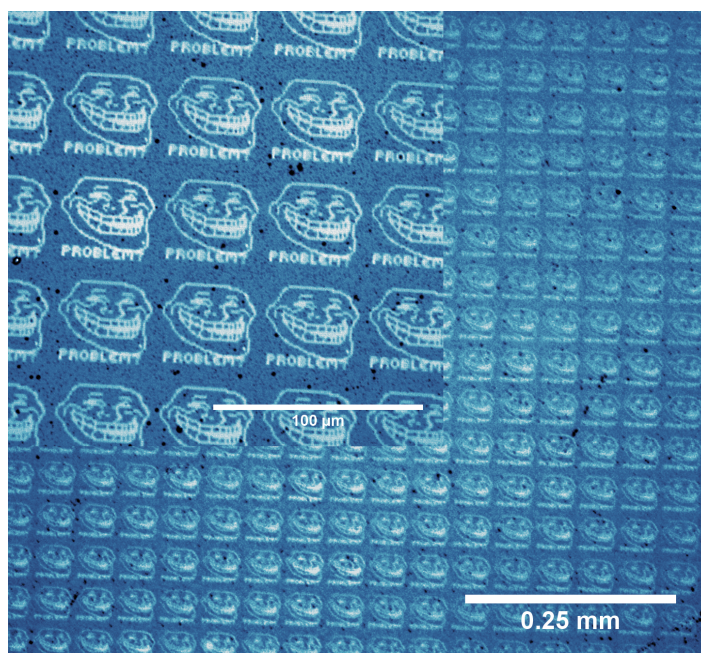
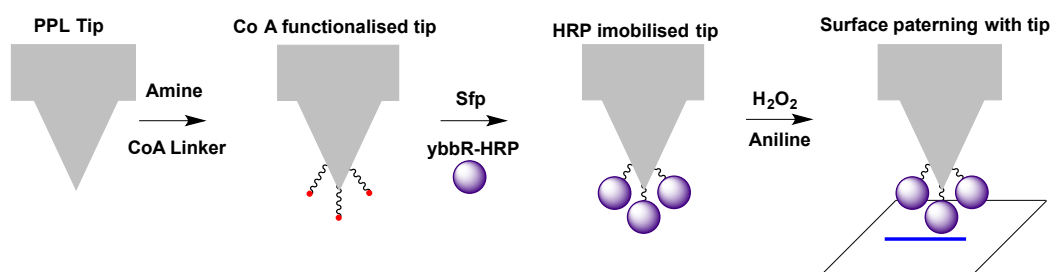


**Figure 2.19.** Optical microscopy images of gold substrates that were patterned by the aligned PPL arrays and subsequently etched.

#### 2.4.2 Biocatalytic probe array preparation

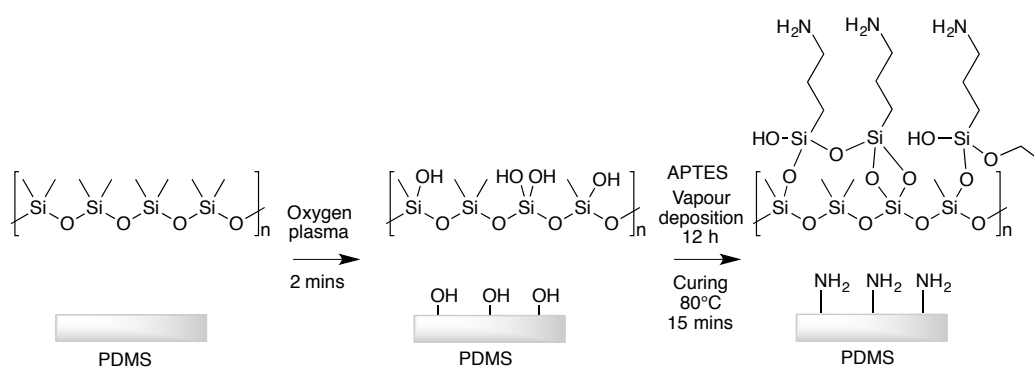
Having successfully developed a system for reproducible and automated large-area nanolithography, work then proceeded to the implementation of multiplexed biocatalytic nanolithography. The preparation of multiplex probe arrays followed a similar work flow to single probe lithography utilising PDMS probe arrays instead of AFM probes (Scheme 2.10).



**Scheme 2.10.** General workflow for probe array enzyme functionalisation. Steps; Amine functionalisation, Linker construction, Site specific enzyme immobilisation and biocatalytic nanolithography.

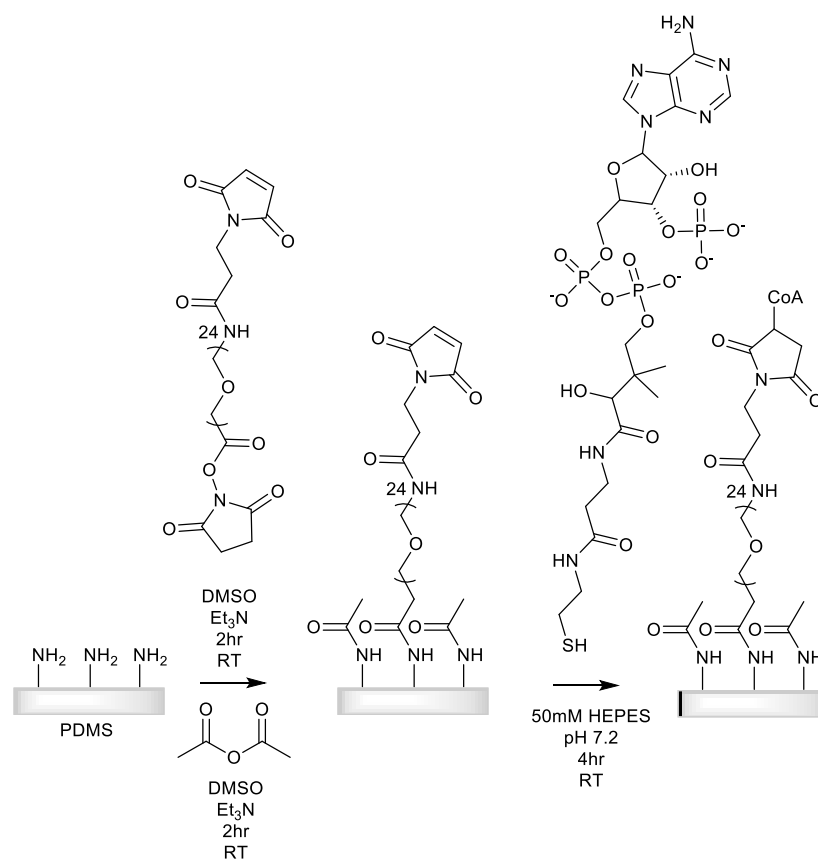
### 2.4.2.1 Linker assembly on PDMS

Due to the change in probe surface material from silicon nitride to PDMS a different amine surface functionalisation was employed. Solvent choice was also considered to avoid any swelling and delamination of the PDMS from their backing support. Amine functionalisation was achieved (Scheme 2.11) by first using oxygen plasma to hydroxylate the PDMS and then vapour deposition of (3-aminopropyl)triethoxysilane (APTES) followed by thermal annealing to maximise covalent bonding to the surface.



**Scheme 2.11.** Reaction scheme for amino functionalisation of the PDMS surface

modification. Steps; surface oxidation by oxygen plasma, vapour deposition of APTES and thermal annealing.



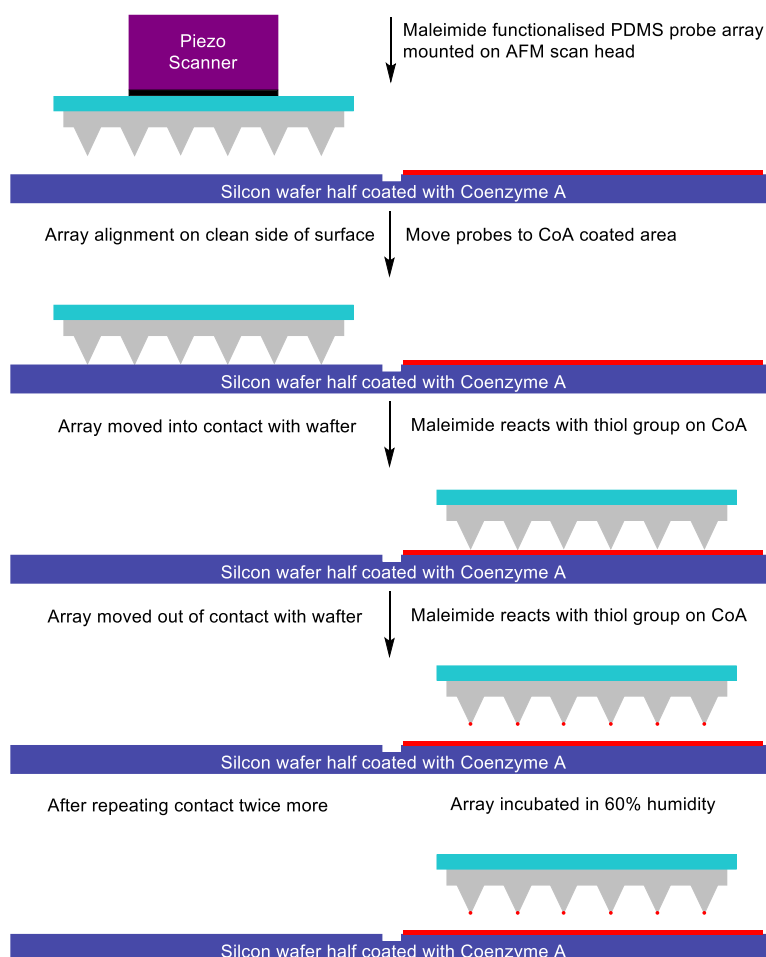
**Scheme 2.12.** Reaction scheme for coenzyme A ligation. Steps; Ligation of NHS-PEG-maleimide to surface by amide bond and maleimide/thiol reaction for coenzyme A.

The amine functionalised PDMS surfaces could then be further elaborated with a bifunctional polyethylene glycol linker leaving a free maleimide for reaction with Coenzyme A (Scheme 2.12). The length of the linker was chosen as this number of ethylene glycol units was found to be sufficiently long to enable access of *Sfp* in the conjugation step.<sup>131</sup>

#### 2.4.2.2 Confinement of C1A to probe array tip apex

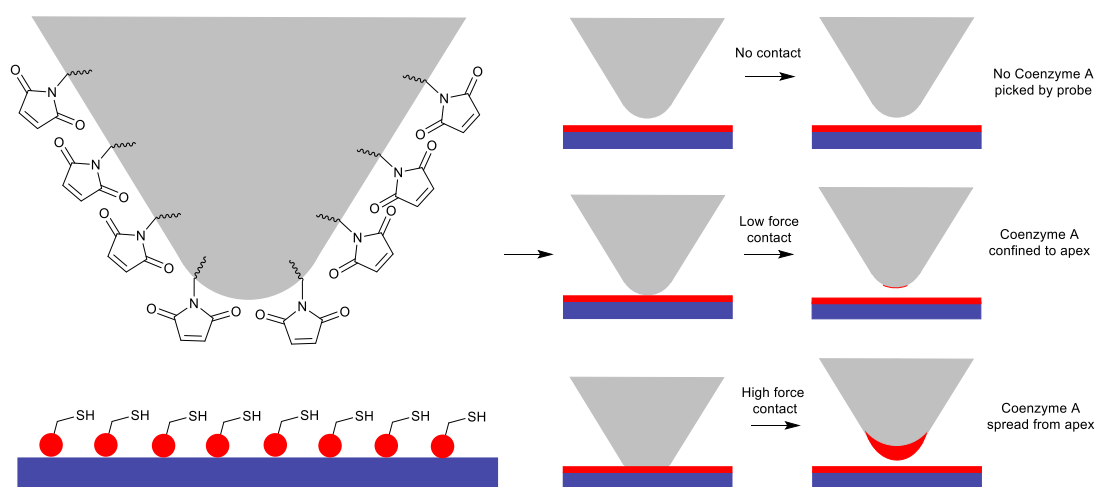
In order to confine the immobilised enzymes to the apex of the probes a method was developed analogous to that previously employed. Enzymes were confined to the probe apex by first the confinement to coenzyme A to the apex of the probes (Scheme 2.13). In

order to stop coenzyme A reacting during the alignment process, a clean silicon wafer was scored down the middle, debris removed and a coenzyme A solution drop coated onto one side of the surface. A maleimide functionalised array was then mounted to the AFM and the partially coenzyme A drop coated silicon wafer attached to the 5-axis stage and aligned to the clean side of the wafer using the automated system previously described. Once aligned, the array could then be moved to the coenzyme A coated area and brought into contact with the surface so the thiol group of coenzyme A could react with the maleimide only at the apex of the probe array. The whole array was then incubated at 60% humidity to facilitate completion of the ligation reaction.



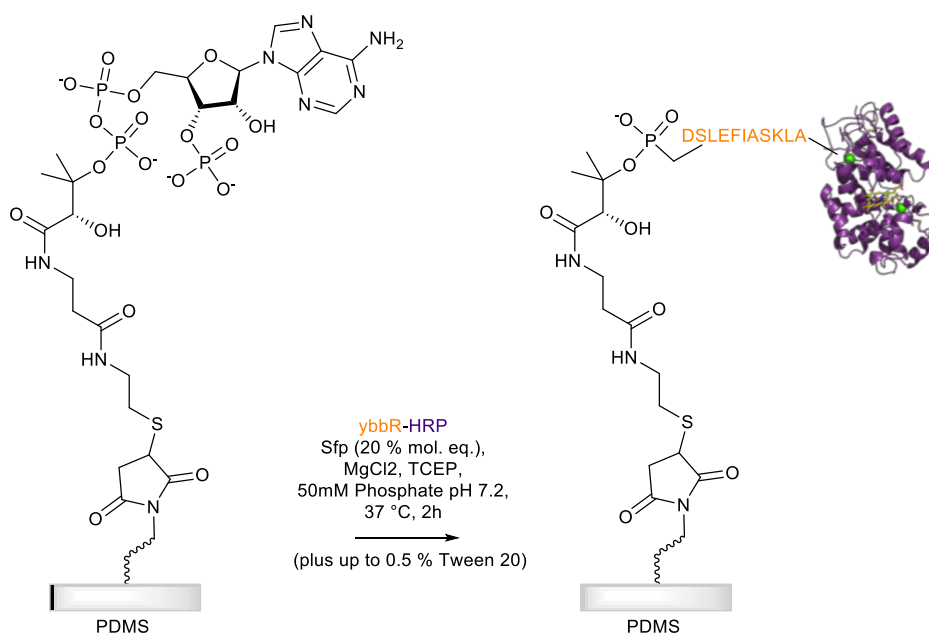
**Scheme 2.13.** Depiction of the procedure for coenzyme A probe apex confinement. Steps; Maleimide functionalised probe array aligned to pristine silicon wafer, array is then moved to area with coenzyme A coating, probe array moved to react with enzyme A.

Alignment of the probes to the surfaces was particularly important in this case as the excessive contact or no contact, in various areas of the array would result in the coenzyme A being coated over a large area of the probes, or not being transferred to the probes at all (Scheme 2.14). Controlling the contact of the probe arrays with the Coenzyme A coated surface was therefore necessary to maximise the resolution of the subsequent nanolithography since probes with a large amount of area coated with enzymes would produce large features.



**Scheme 2.14.** Depiction of different outcomes from varying levels of probe contact with coenzyme A coated surface.

After coenzyme A ligation, the probe arrays functionalised with Coenzyme A were then submerged in a solution of 2-mercaptoethanol to block unreacted maleimide sites. Following washing to remove any unreacted 2-mercaptoethanol, the arrays were finally submerged in solution contain Sfp and ybbR-C1A to allow enzyme conjugation. They were then thoroughly washed to remove any unreacted ybbR-C1A (Scheme 2.15).



**Scheme 2.15.** Depiction of *Sfp* catalysed ybbR-C1A immobilisation reaction step of forming enzyme functionalised probe arrays. Conditions; ybbR-C1A, *Sfp* (20% mol. eq),  $\text{MgCl}_2$ , TCEP in 50 mM sodium phosphate buffer (pH 7.2) at 37°C for 2h.

#### 2.4.2.3 Enzyme functionalised probe arrays activity assay

Following enzyme immobilisation to the PDMS arrays, activity assays using ABTS as the substrate were conducted on the arrays to confirm that the immobilised enzyme remained catalytically competent. Arrays were placed within wells of a 24 well plate and the absorbance at 420 nm recorded over time (Figure 2.20).

In order to ensure signal transduction both arrays with full coverage of Coenzyme A and arrays with Coenzyme A confined to the tip apex were assayed. Control experiments were constructed with arrays where all maleimides were blocked with 2-mercaptoethanol were submerged in *Sfp*/ybbR-C1A. Additionally, arrays with full Coenzyme A coverings were submerged in reaction mixtures where *Sfp* was excluded and ybbR-C1A was excluded. Absorbance 420 nm over 60 mins can be seen in Figure 2.20. The data shows that the control experiments display very little absorbance change (consistent with slow spontaneous oxidation of ABTS). Arrays with full coverage of Coenzyme A show a very rapid increase in



absorbance in accordance with the immobilisation of ybbR-C1A being successful. Arrays that were subject to the Coenzyme A confinement procedure also show a significant increase in absorbance compared to controls indicating that not only had ybbR-C1A immobilisation had been successful but also that confinement was also effective.

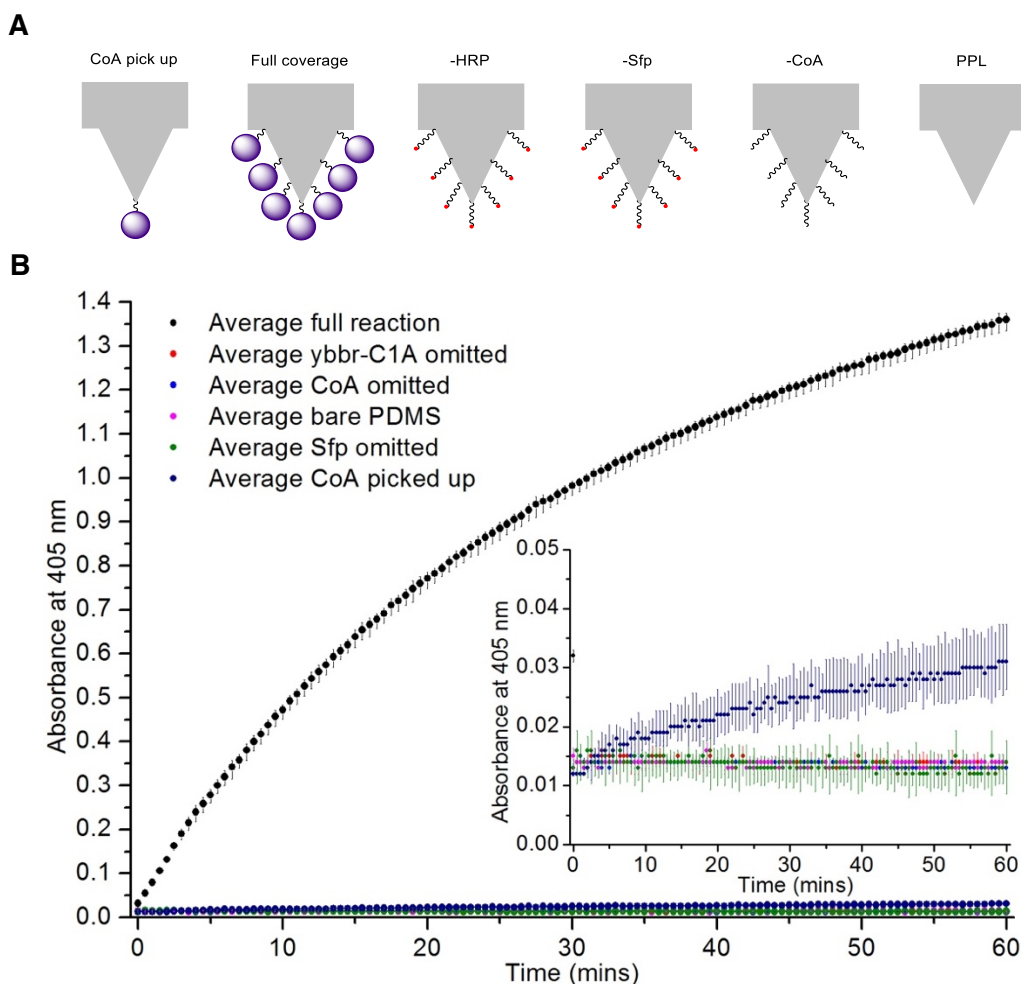


**Figure 2.20.** (A) Depiction of surface components for each surface that the activity assay was performed on. (B) Graph showing absorbance at 420 nm over time for different functionalised arrays, constituting ABTS activity assay of any enzyme present.

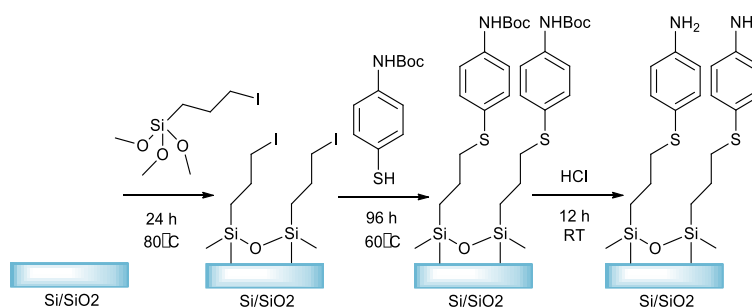
### 2.4.3 Lithography with enzyme probe arrays

Having successfully produced probe arrays with HRP confined to the tips of the probes, multiplexed biocatalytic nanolithography was attempted. From the experiments with single

probe lithography it was decided use similar lithographic conditions (i.e. reagent concentrations and write speeds). Since gold is a conductor it would be unsuitable for fabrication of an electronic device utilising conducting polymers, therefore silicon oxide surfaces were investigated instead.

#### 2.4.3.1 4-ATP functionalised glass

Functionalisation methods for silicon oxide surfaces were adapted from literature. This was carried out first by oxygen plasma cleaning of the surfaces then derivatisation with an iodo terminated siloxane, followed by substitution by Boc-protected 4-ATP and finally Boc deprotection (Scheme 2.16). Surface analysis by AFM showed minimal surface roughening.

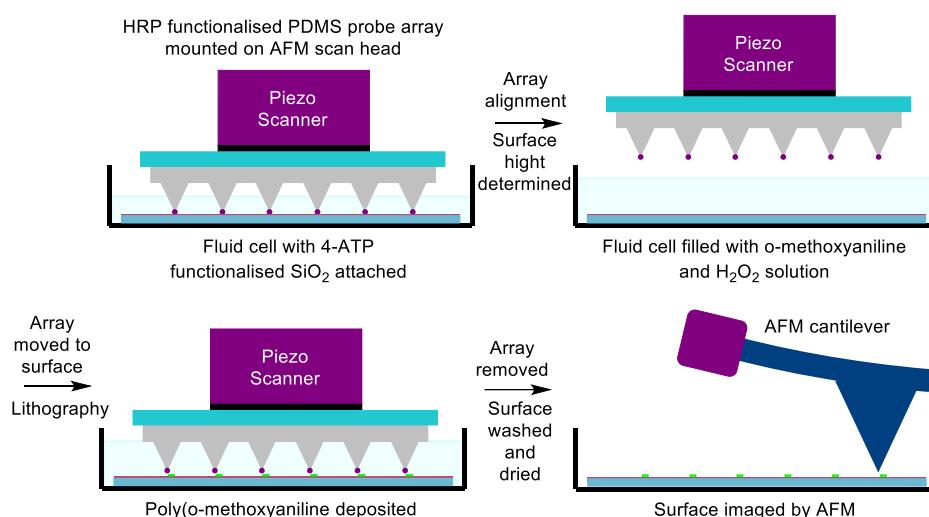


**Scheme 2.16.** Reaction scheme for the functionalisation of silicon glass with 4-ATP. Steps; iodo surface modification, substitution of Boc-protected 4-ATP and finally deprotection of amine.

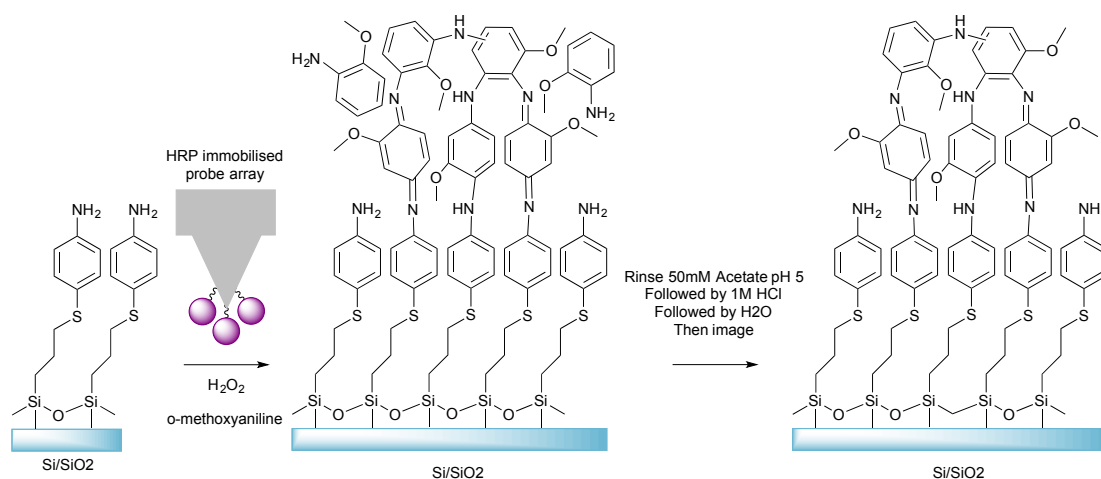
#### 2.4.3.2 Lithography via *o*-methoxyaniline polymerisation and deposition

2-Methoxyaniline was yet again used as the substrate as the methoxy group lowered the oxidation potential of the molecule meaning not only could lithography take place at a higher pH but the turnover rate of the enzyme with 2-methoxyaniline over aniline is much higher. The C1A functionalised array was then mounted to the AFM scan head and the 4-ATP functionalised silicon surface attached to the 5-axis stage and aligned to the surface as per

the automated system previously described. A lithographic pattern consisting of 10x10 dots (20s per dot) 2000 nm apart was written with the probes and surface submerged in a solution containing 1 mM 2-methoxyaniline and 1 mM  $\text{H}_2\text{O}_2$  (Scheme 2.17). The functionalised probes were first aligned to the surface in buffer and the surface height determined by force feedback, then substrate solution was added after alignment to minimise polymerisation before the patterning sequence had been started. Following completion, the array was rapidly removed, solution decanted and surface rinsed to avoid adsorption of any non-covalently bound oligomers. Additionally, Scheme 2.18 provides a molecular depiction of the lithographic patterns. The surface was then analysed by AFM imaging.



**Scheme 2.17.** Depiction of the lithographic procedure for the deposition of polyaniline via catalytic probes. Showing first probe alignment followed by surface height determination and lithography, finally washing and topographic imaging (AFM).



**Scheme 2.18.** Depiction of the HRP catalysed polymerisation reaction to form lithographic patterns, followed by washing to remove non-covalently attached short chain polymers.

The images (Figure 2.21) showed that, an initial pattern was produced with the pattern used. Though lithographic fidelity was poor this initial result was used as a starting point for further refinement of the procedure.

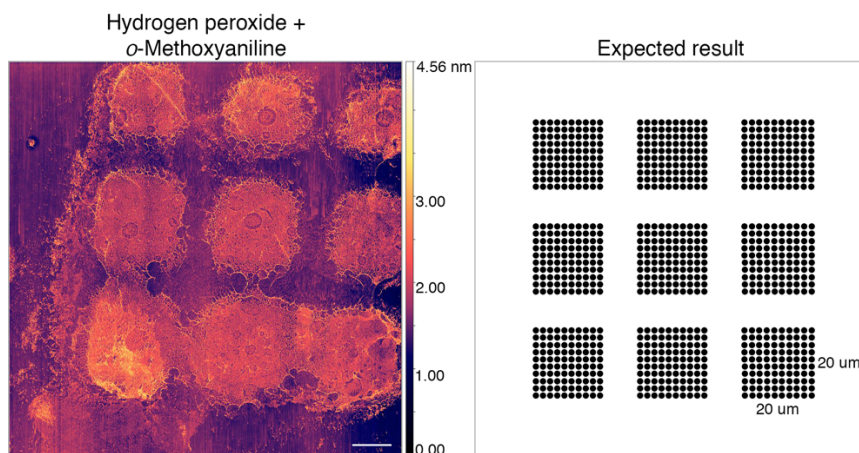


**Figure 2.21.** AFM imaged topography of surface that lithography had been performed on and expected result from lithography. Conditions; 20 s per feature, 2.6 mM 2-methoxyaniline, 1 mM H<sub>2</sub>O<sub>2</sub>. Scale bar 10  $\mu\text{m}$ .

As previously mentioned the method used to confine coenzyme A to the probe apex was dependent on the amount of contact the maleimide functionalised probe has with the

coenzyme A coated surface, i.e. the wider the spread of coenzyme A the wider the spread of enzyme immobilised over the tip. This procedure was gradually refined until a minimum amount of enzyme was immobilised by careful control of PDMS probe preparation and the contact between the probes and the surface during the CoA 'pick up' step. This refined procedure lead to an increased quality of lithography, both in terms of background to noise and feature resolution (Figure 2.22). Size measurements were taken across the line features in 20 representative locations across the printed area ( $1\text{cm}^2$ ) and gave an average FWHM of  $489\text{ nm} \pm 52\text{ nm}$ .

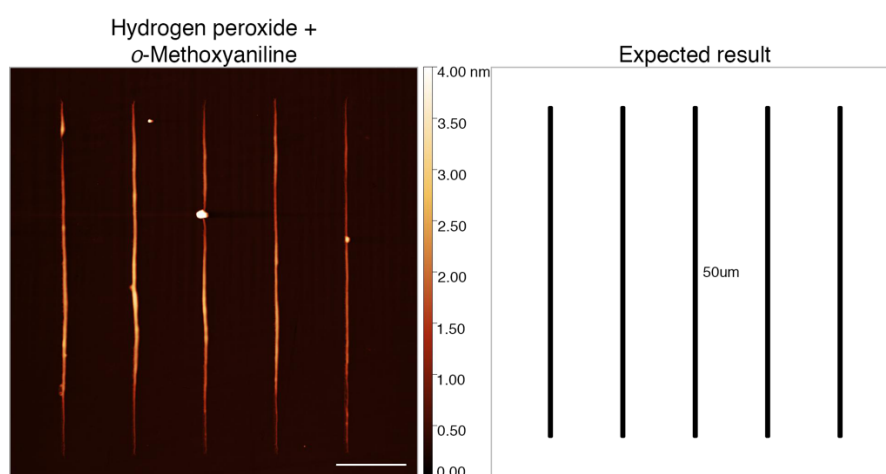


**Figure 2.22** AFM imaged topography of surface that lithography had been performed on and expected result from lithography. Conditions; 2 s per feature, 80 features per line, 2.6 mM 2-methoxyaniline, 1 mM  $\text{H}_2\text{O}_2$ . Scale bar  $10\ \mu\text{m}$ .

Attention was then turned to producing the smallest pattern resolution, with further refinement of probe dwell time (20s to 1s). Size measurements (half width full maximum) were taken across the line features in 20 random locations giving  $162\text{ nm} \pm 24\text{ nm}$ . The theoretical minimum probe tip width of a PPL probe is  $\sim 50\text{ nm}^{108}$  so any pattern produced would be greater than this distance, linker and enzyme add approximately  $\pm 10\text{ nm}$ . Therefore, the highest resolution feature that could be produced is  $\sim 70\text{ nm}$ . With this information it can be determined patterns could potentially be 50% smaller than the current best.

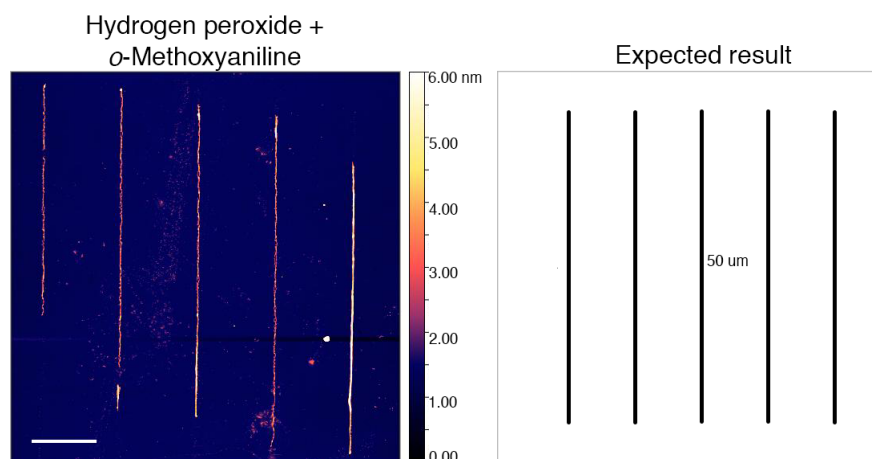
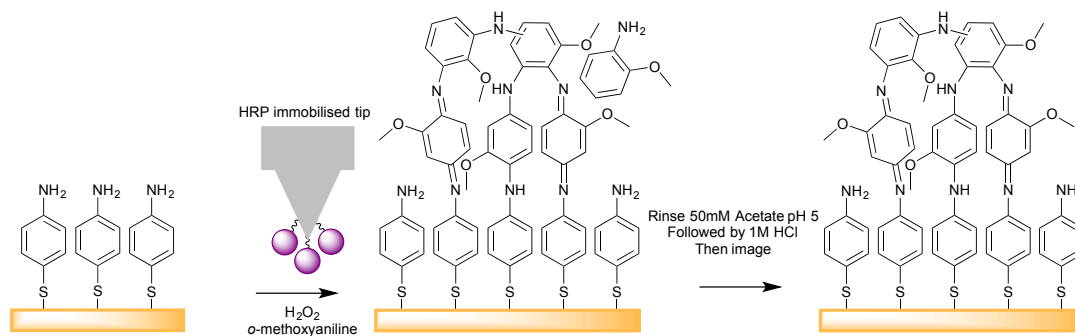


**Figure 2.23.** AFM imaged topography of surface that lithography had been performed on and expected result from lithography. Conditions; 1 s per feature, 160 features per line, 2.6 mM 2-methoxyaniline, 1 mM H<sub>2</sub>O<sub>2</sub>. Scale bar 10 μm.

#### 2.4.3.2 Raman mapping on gold 4-ATP functionalised surfaces.

In order to characterise the chemical composition of the polymers and confirm the production of polyanilines, further surface characterisation was undertaken. Raman microscopy was used as it provides information on chemical bonds, is unaffected by residual water from the lithography and is capable of relatively high resolution (in comparison with IR spectroscopy). Raman microscopes can collect spectra on a very small area ( $< 1 \mu\text{m}^2$ ) and build this information into a spectroscopic map of an area by plotting the intensity at a set frequency. However, Raman spectroscopy generally suffers from low sensitivity. It was known Raman scattering is significantly enhanced by metal surfaces (such as gold) through surface-enhanced Raman scattering (SERS). It was therefore decided to use 4-ATP functionalised gold surfaces to conduct lithography on for characterisation purposes. Lithography experiments were carried out as previously described (Scheme 2.19) and, surfaces washed and analysed by Raman micro-spectroscopy.



**Scheme 2.19.** Workflow for multiplexed biocatalytic lithography on gold surfaces.

The microscope was scanned over the surface over an area of  $100\ \mu\text{m}$  with a spectra collected every  $0.5\ \mu\text{m}$  Figure 2.24 shows a map of the surface at  $1398\ \text{cm}^{-1}$  (which corresponds to Raman shift with no response from 4-ATP but C-N<sup>+</sup> quinoid in poly-2-methoxyaniline) next to a microscope image of the same site. The map shows pattern produced of expected size for the template used. Representative spectra for each area are shown in Figure 2.25 with assignments in Table 2.3, these spectra are equivalent to spectra obtained from control experiments of 4-ATP functionalised surfaces and can be assigned from the literature.<sup>134-136</sup> This data shows that 2-methoxyaniline polymer had been deposited, and that features from topographic AFM images are poly-2-methoxyaniline.

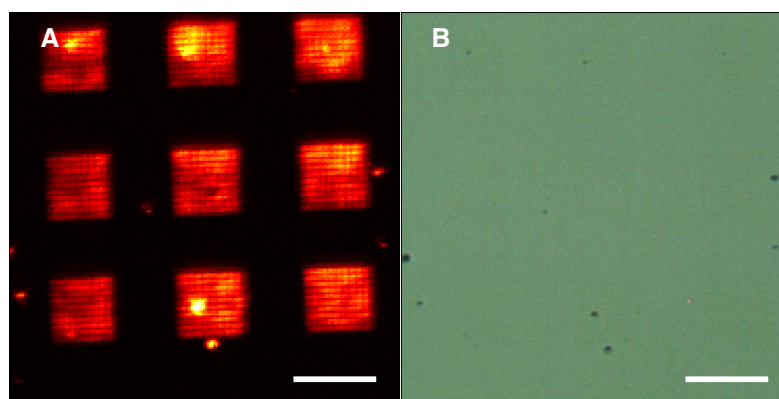


**Figure 2.24.** (A) Raman micro-spectroscopy surface map at  $1398\ \text{cm}^{-1}$  (red showing the highest intensity with black showing no peak) and (B) microscope image of the same area of the surface. Scale Bar  $20\ \mu\text{m}$ .

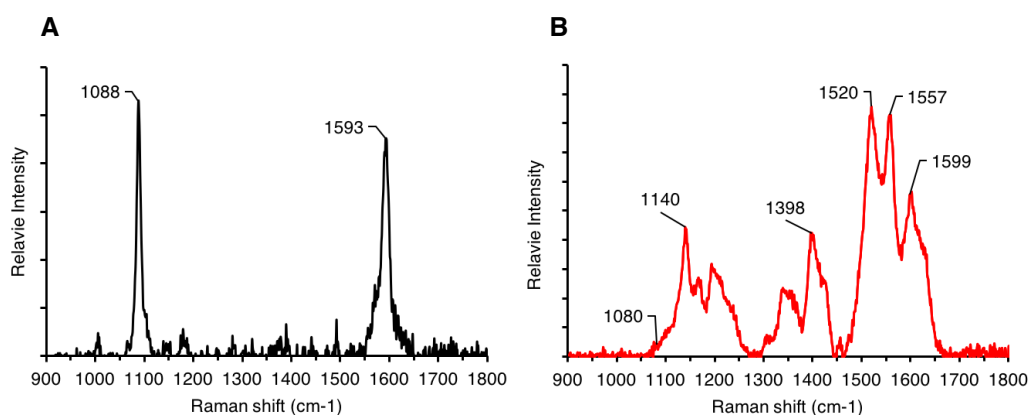


**Figure 2.25.** Representative Raman spectra of the surface. **(A)** Taken from unpatterned area of the surface (black). **(B)** Taken from patterned area of surface (red).

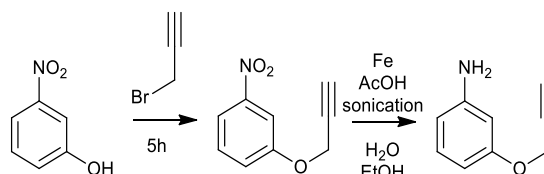
<b>4-aminothiophenol (Figure 2.25A)</b>		<b>poly-2-methoxyaniline (Figure 2.25B)</b>	
<b>Bond vibration</b>	<b>Raman shift (cm<sup>-1</sup>)</b>	<b>Bond vibration</b>	<b>Raman shift (cm<sup>-1</sup>)</b>
$\delta$ (ring)	1088	$\delta$ (ring) (quinoid)	1599
$\nu$ (C–C)	1593	$\nu$ (C=NH+) (quinoid)	1520
		$\nu$ (C–N+) (quinoid)	1398
		$\nu$ (C–O–C)	1140

**Table 2.3** Assignments for Raman shift of bond vibrations for 4-ATP and poly 2-methoxyaniline.

#### 2.4.3.3 Wide area post polymerisation fluorescence (with alkyne-aniline)

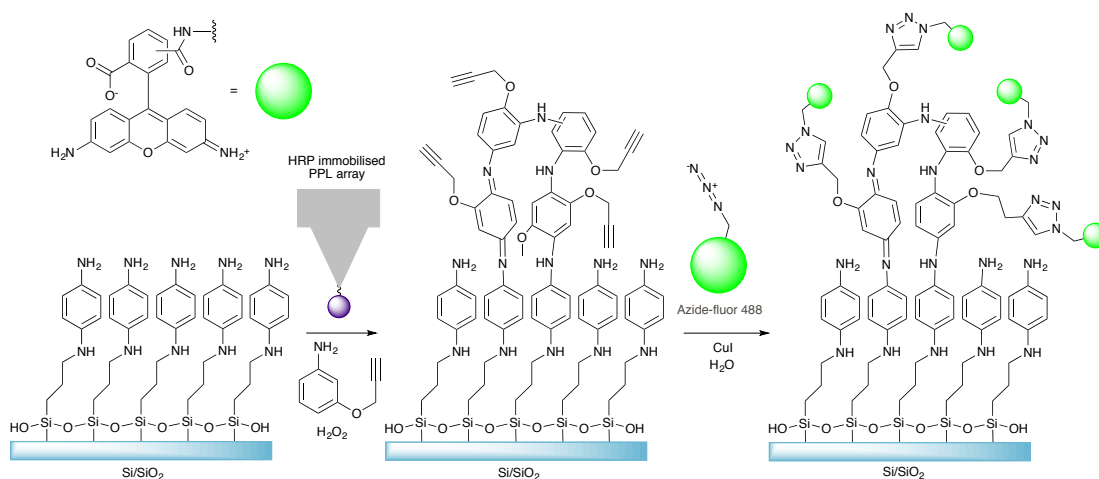
In order to assess the wide area nature of the lithographic patterns, an experiment to fluorescently tag the polymer patterns by post-polymerisation functionalisation was performed. The Huisgen 1,3-dipolar cycloaddition between azide and alkyne was used due to ease of reaction and high yield. For this purpose 3-(prop-2-yn-1-yloxy)aniline was synthesised in two steps (Scheme 2.20) for use as the monomer substrate for HRP. This could then easily be reacted with any azide containing molecule for further functionality.





**Scheme 2.20.** Synthesis of 3-(prop-2-yn-1-yloxy)aniline. Steps; ether synthesis with propargyl bromide followed by nitro reduction with iron.

The lithography was then carried out in the same way as previously. The surfaces could then be submerged in a solution of 'azide-fluor 488' and Cu(I) catalyst (Scheme 2.21). After completion the surfaces could be washed and imaged under a fluorescence microscope. Lithography experiments containing a co-monomer mixture of 2-methoxyaniline and 3-(prop-2-yn-1-yloxy)aniline were also carried out at various ratios but polymers from only 3-(prop-2-yn-1-yloxy)aniline were found to produce fluorescence images of good quality. Functionalised patterns produced with monomer mixtures showed decreased brightness, this was thought to be from the reduced alkyne groups available for reactions.



**Scheme 2.21.** Reaction sequence for post polymerisation functionalisation with fluorophore.

Lithography was conducted over a 1.2 x 1.2 cm area. Patterns were produced where probes were directed to pause in 10 x 10 locations in a 3 x 3 grid (Figure 2.26A). Lithography was also conducted using lines of 50 locations per line (Figure 2.26B). From the microscope images collected by excitation at 488 nm it can be observed that well defined polymer patterns have been produced and subsequently fluorescently tagged over a large area. This result therefore demonstrates that large-area patterning was successfully carried out.

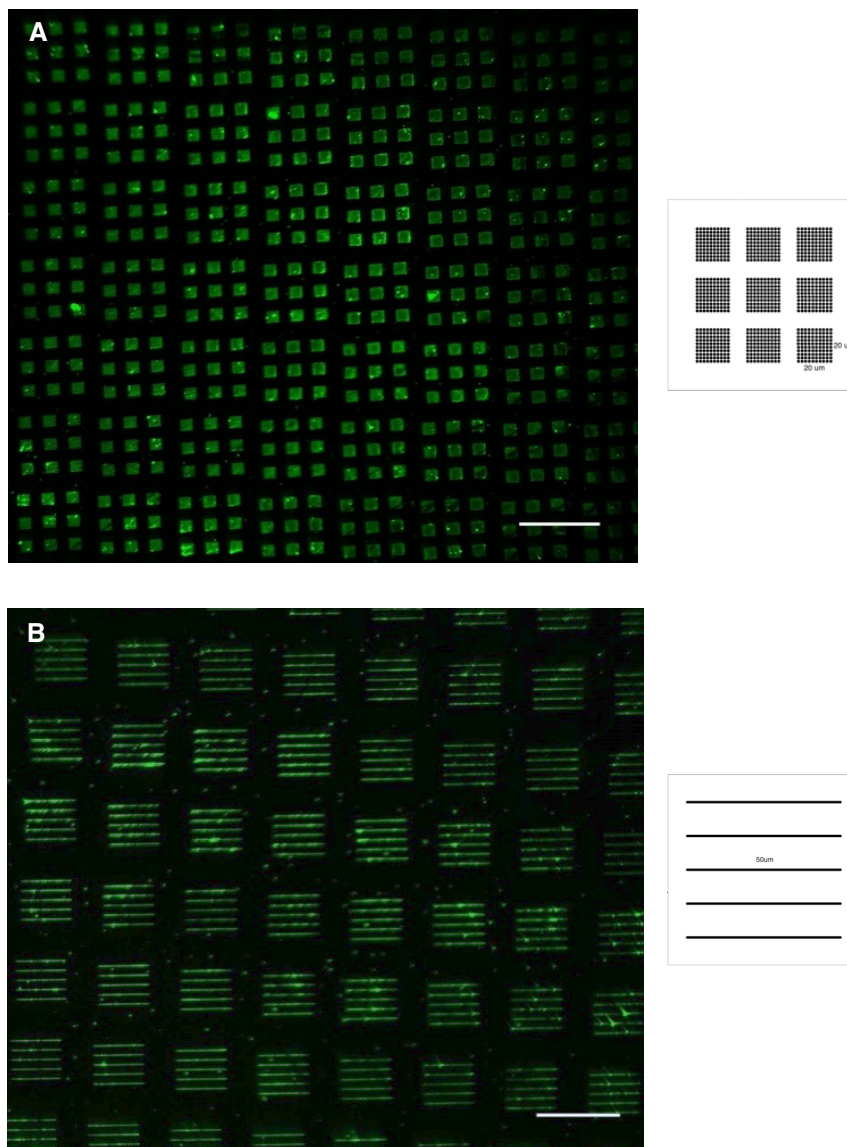


**Figure 2.26.** Fluorescent microscope images collected by excitation at 488 nm of post polymerisation functionalisation, with insets showing expected patterns. **(A)** 10x10 locations in a 3x3 grid, scale bar 100  $\mu\text{m}$  and **(B)** Lines of 50 locations per line, scale bar 100  $\mu\text{m}$ .

## 2.5 Conclusions

To summarise, the aim of this project was to demonstrate constructive biocatalytic nanolithography. This was principally achieved by extending lithography to wide area patterning over a 1.2 x 1.2 cm area through the use of multiplexed lithography. Polyanilines were catalytically formed and subsequently deposited at high resolution, with features of 162 nm  $\pm$ 24 nm in width. These patterns were chemically analysed by Raman spectroscopy, confirming that aniline polymers were being formed from the substrates. Wide area patterning was confirmed by modifying the deposited aniline polymers with a fluorescent moiety, which could then be imaged by fluorescent microscopy. Comparing to previous attempts at biocatalytic nanolithography,<sup>116</sup> patterns were of far higher complexity and with comparable resolution while providing the first example of patterning over wide area. Additional improvements were made by implementing a covalent and site specific attachment, using a homogeneous and highly active enzyme preparation.

Key to implementing wide area biocatalytic nanolithography was the simplification and improvement of existing methods used to align multiplexed probe arrays to an arbitrary substrate. It is capable of rapid, accurate and operator-free alignment of multiplexed probe arrays has been attained.

Further development of scanning probe-based lithography could benefit both of these advances. First as a means for incorporating other enzymes and their chemical reactions to wide area lithography and second to simplifying the hurdles to carry out such lithography.

## **Fused aromatics from peroxidase catalysed quinonoid intermediates and tandem cyclisation reaction**

### **3.1 Introduction**

Quinonoid systems<sup>137</sup> (Figure 3.1) are highly reactive, transient species, that can be useful intermediates for organic synthesis and, potentially, as precursors to complex molecular architectures.<sup>138, 139</sup> Such molecules are known to react with nucleophiles in 1,4-Michael-type addition<sup>140, 141</sup> and with an array of dienophiles to perform [4 + 2] inverse electron demand cycloadditions<sup>142-144</sup> (Scheme 3.1A). Cycloadditions with *o*-quinone methide systems are particularly useful as they constitute new C-C bond formation. However, the synthetic value of quinonoid moieties has not been fully utilised as they are extremely unstable<sup>145</sup>. *c*-Benzoquinones and *o*-benzoquinone imines are especially susceptible to rapid dimerization and polymerisation.<sup>146</sup>

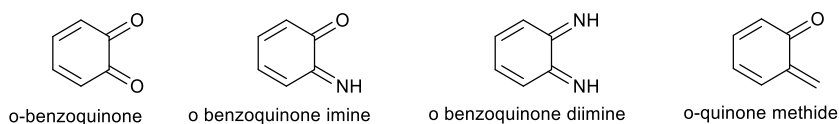
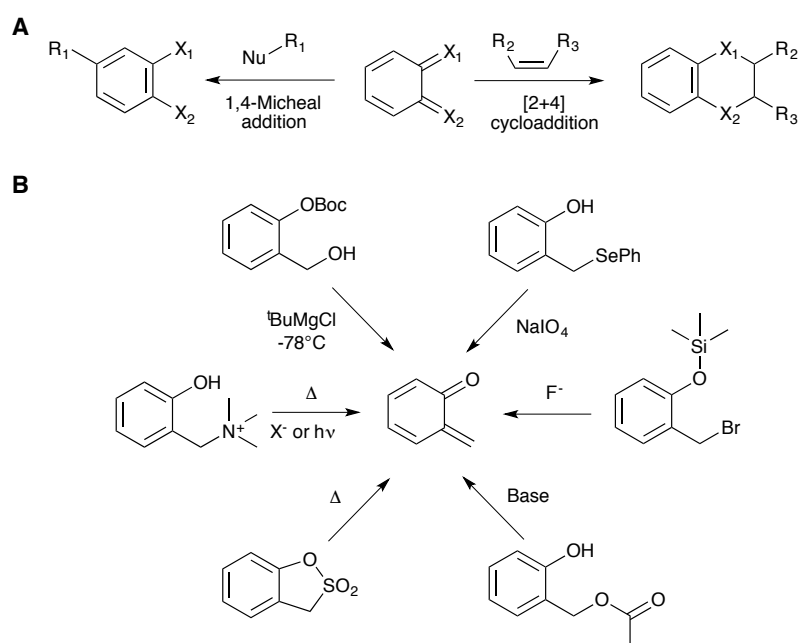


**Figure 3.1** Examples *o*-quinonoid systems, that can be utilised as synthetic intermediates.

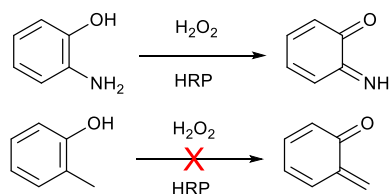
Investigations have provided strategies in order to generate *o*-quinonoid systems *in situ* by both chemical<sup>141, 147, 148</sup> and electrochemical<sup>149</sup> methods (Scheme 3.1B). However, complications with such methodologies often include extremes of temperatures and pH, long reaction times and use of transition-metal catalysis, which can exacerbate problematic side reactions (dimerization and polymerisation).



**Scheme 3.1** (A) Potential reactions routes of *o*-quinonoid systems, with potential reactions including Michael addition and cycloaddition. (B) Selected routes to *o*-quinone methide systems, highlighting diverse methodologies towards generation.

An alternative methodology that avoids the use of harsh and environmentally unfriendly conditions is to harness oxidoreductase enzymes such heme-peroxidases and multicopper

oxidases to generate these systems<sup>10, 71, 150, 151</sup>. Previously, it has been shown that the oxidation of catechols<sup>65</sup>, 2-aminophenol<sup>69</sup> and benzene-1,2-diamines<sup>152</sup> by horseradish peroxidase to their corresponding *o*-benzoquinone, *o*-benzoquinone imine and *o*-benzoquinone diimine, can take place (Scheme 3.2). However, in the case of *o*-cresol the oxidation potential of the enzyme is too low to facilitate the oxidation of *o*-cresol to *o*-quinone methide (Scheme 3.2), instead a single electron oxidation reaction takes place forming a phenoxyl radical, which can then go on to react with other molecules (i.e. polymerisation). In the case of catechols this reaction has been extensively investigated, and *o*-benzoquinones produced for use as intermediates, in a variety of applications<sup>66, 153, 154</sup> (see section 1.6.4.1 for further details).



**Scheme 3.2** Literature known reactions with HRP; Oxidation of 2-aminophenol forming *o*-quinone imine. Oxidation of *o*-cresol does not proceed to *o*-quinone methide.

### 3.1.1 Aims

It was aimed to investigate the HRP catalysed formation of *o*-quinonoid systems. To achieve this HRP was utilised to generate quinonoid systems, and use them as intermediates in tandem cycloaddition reactions, to produce fused aromatics. Choosing ring structures such as 1,4-benzoxazines and chromanes as targets to exemplify the reaction, as they constitute parts of many pharmaceutically active small molecules (Figure 3.2).

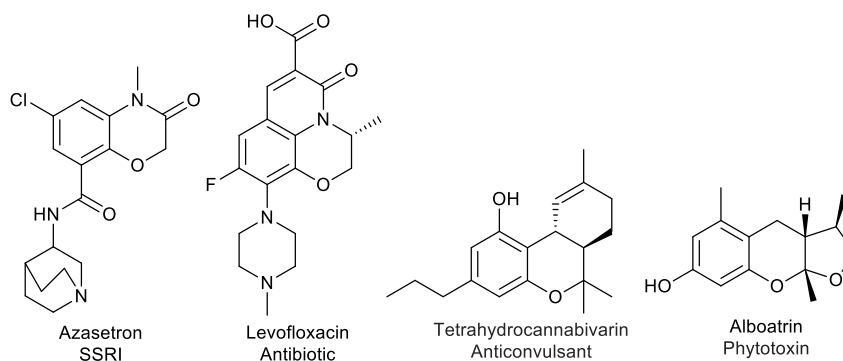
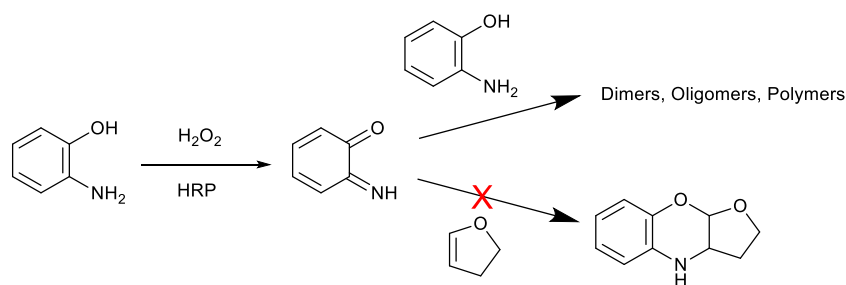


**Figure 3.2** Molecules synthesised from 1,4-benzoxazines and chromanes.

Although, there are many methods for the synthesis of 1,4-benzoxazines most of these methods involve multistep processes.<sup>155</sup> Advantageously the Diels-Alder reaction provides a single step but can also allow the assembly of complex organic bicyclic skeletons. Current reported synthetic routes to 1,4-benzoxazines by *o*-quinone imine intermediate, utilise reduced temperatures (0°C) and dry organic solvents.<sup>156</sup> Performing any enzyme catalysed reactions in water and at room temperature will be a key objective to any development.

### 3.2 Peroxidase-catalysed *o*-benzoquinone imine generation

Previous investigations<sup>69</sup> have found 2-aminophenol to be a substrate of HRP, however the product would rapidly react to form dimers, oligomers and polymers (Scheme 3.3) and consequently was not investigated as an intermediate. It was surmised that in the presence of excess electron rich dienophile (e.g. vinyl ethers), the *o*-benzoquinone imine would undergo a [4 + 2] inverse electron demand cycloaddition and be intercepted before polymer formation (self-condensation).



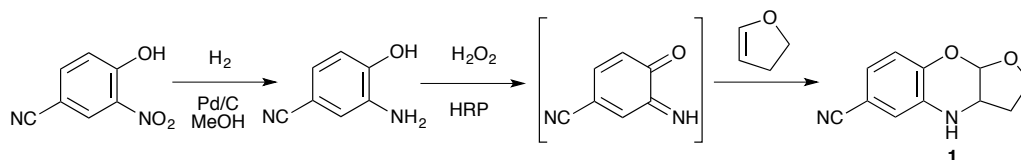
**Scheme 3.3** Reaction scheme of potential reaction pathways. Unsubstituted 2-aminophenol not undergoing cycloaddition.

To investigate this approach, initial small scale (150  $\mu\text{L}$ ) reactions were set up containing 2-aminophenol, 2,3-dihydrofuran,  $\text{H}_2\text{O}_2$  and HRP in pH 7.2 phosphate buffer, with the appropriate controls (reactions lacking one of the four reaction components in each). Analysis by analytical HPLC showed the reaction yielded none of the expected 1,4-benzoxazine, and only polymerisation of the starting material had taken place (no new peaks but consumption of starting material). It was hypothesised that the *o*-benzoquinone imine produced could not undergo a [4 + 2] inverse electron demand cycloaddition as it is not sufficiently electron-deficient to promote the cycloaddition. The Michael addition dimerisation reaction then proceeds, which leads to polymer formation. This was found to be in agreement with previous literature<sup>156</sup>, which also pointed to using electron withdrawing substituents on the 2-aminophenol aromatic ring to provide the correct electronic conditions for the reaction to proceed.

### 3.2.2 Development of the biocatalytic synthesis of 1,4-benzoxazines

With this knowledge, 3-amino-4-hydroxybenzoxazine was synthesised by hydrogenation from the corresponding 2-nitrophenol to be tested for activity as an enzyme substrate. This 2-aminophenol contains a strongly electron withdrawing nitrile ring substituent. This compound was then used as a substrate in small scale reactions using the same conditions (Scheme 3.4).





**Scheme 3.4** Reaction scheme showing HRP-catalysed oxidation followed by cycloaddition to form **1**, Reaction conditions; 1 mM 3-amino-4-hydroxybenzonitrile, 50 mM 2,3-dihydrofuran, 1 mM H<sub>2</sub>O<sub>2</sub> and 2.5 U of HRP mL<sup>-1</sup> in 50 mM phosphate buffer (pH 7.2), RT, 12 hours.

Analysis by HPLC (Figure 3.3) showed the generation of a new compound with the same retention time as the authentic product standard that was synthesised chemically<sup>156</sup> (8.1 min), indicating that 1,4-benzoxazine had been produced, with good conversion (90%). In control reactions where HRP and H<sub>2</sub>O<sub>2</sub> were omitted show a peak at 3.3 min was observed, indicative of the unreacted starting material. Reactions with dienophile omitted show a wide range of peaks, from dimers and trimers formation of the *o*-benzoquinone imine. The reaction to form **1** therefore only proceeds when all components (3-amino-4-hydroxybenzonitrile, 2,3-dihydrofuran, H<sub>2</sub>O<sub>2</sub> and HRP) are present.

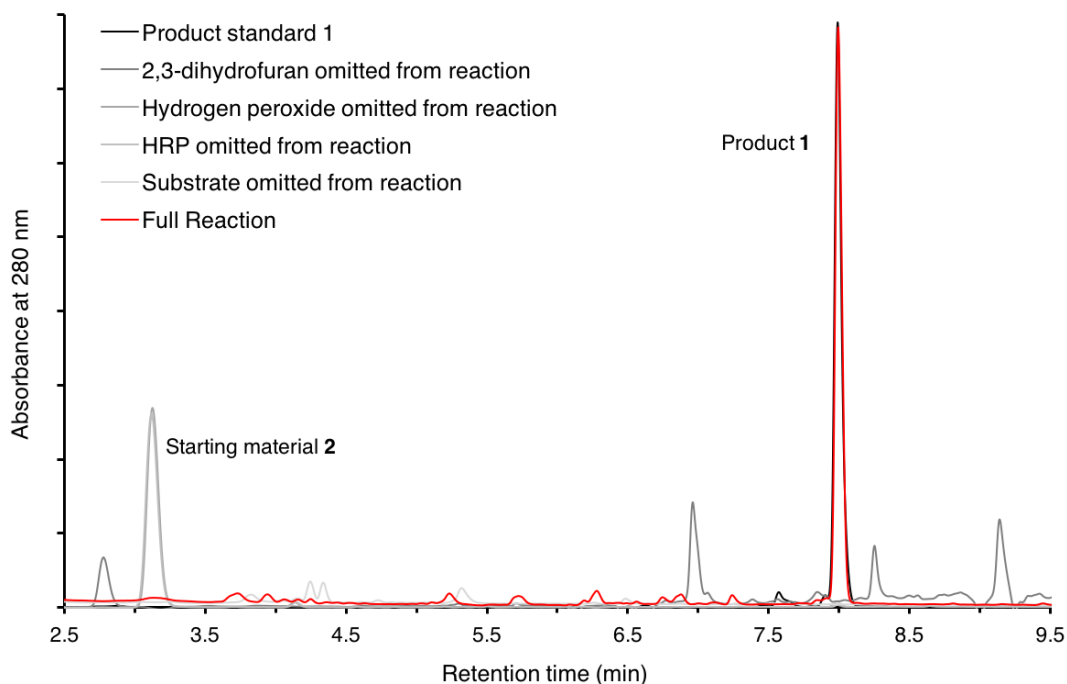


**Figure 3.3.** Overlaid HPLC chromatograms tracking absorbance at 280 nm of the reaction quenched mixture for the full reaction and control reactions. Control reactions omitted one of four reaction components to form the full reaction. Also shown is product standard for compound 1.

Thus the electron poor 2-aminophenol was a good starting point for oxidation by HRP and the tandem cycloaddition reaction then proceeded in aqueous buffer at room temperature due to the frontier orbitals now being favourable for the reaction to proceed.

This successful initial result served as a starting point to further optimise the reaction conditions, efforts were then made to optimise the reaction with 3-amino-4-hydroxybenzotrile to improve conversion by varying substrate, dienophile, hydrogen peroxide and enzyme concentration. The pH and temperature were also considered.

Reactions where the enzyme concentration was varied (Figure 3.4) showed that product formation after 60 mins remains fairly constant with as low as 0.25 U of HRP per mL of reaction with product formation only showing a 7% conversion with a 2 orders of magnitude

decrease at 0.025U. This reduction in conversion is most likely due to starting material not being turned over before enzyme deactivation by  $\text{H}_2\text{O}_2$ .

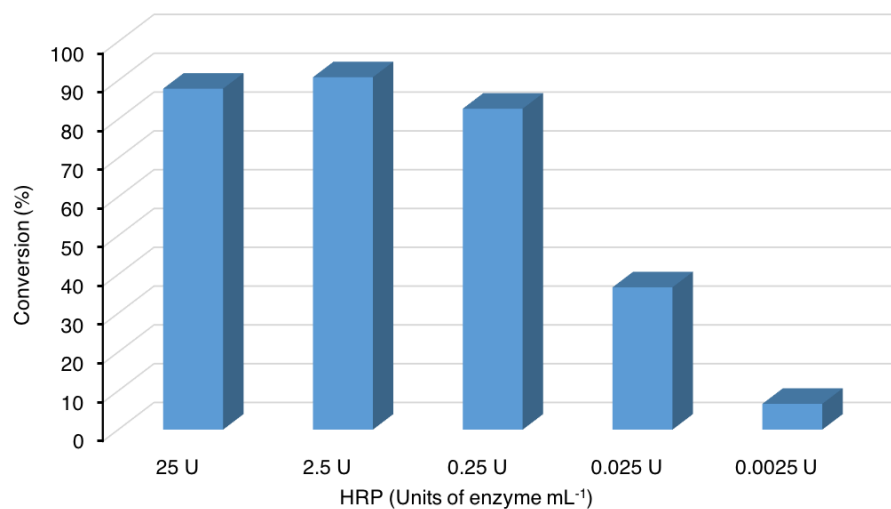


**Figure 3.4.** Product formation after 60 mins from varying concentrations of enzyme, with substrate concentration, 2,3-dihydrofuran and  $\text{H}_2\text{O}_2$  constant.

Reactions show as expected there is a general correlation between concentration of hydrogen peroxide and substrate. Reactions should require 0.5 equivalents (two substrate molecules can be oxidised per hydrogen peroxide molecule) but experimentally reactions require 1.5 equivalents of hydrogen peroxide to reach good conversions (Figure 3.5). This could arise from  $\text{H}_2\text{O}_2$  oxidising amino acid residues or spontaneous decomposition.

However, substrate concentrations of 4 mM show lower conversions even at 4.5 mM  $\text{H}_2\text{O}_2$  possibly pointing to inhibition of the enzyme either by  $\text{H}_2\text{O}_2$  or substrate.<sup>157</sup>

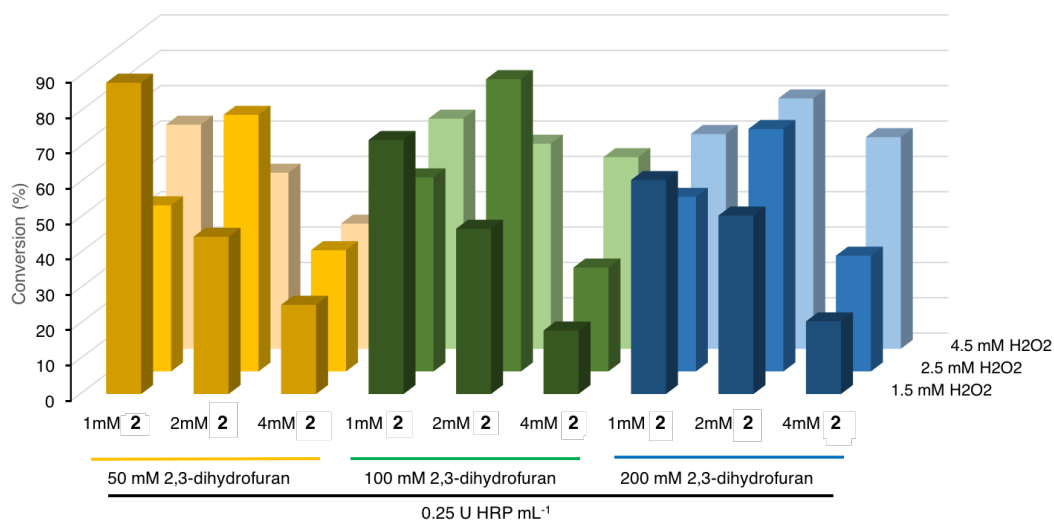


**Figure 3.5.** Product formation after 60 mins with reactions varying 1-4mM substrate, 50-200 mM 2,3-dihydrofuran and 1.5-4 mM H<sub>2</sub>O<sub>2</sub> concentration, with HRP concentration constant 0.25 U mL<sup>-1</sup>.

A time course experiment (Figure 3.6) was conducted using the best conditions tested during the optimisation experiments (2 mM Substrate, 100 mM 2,3-dihydrofuran, 2.5 mM H<sub>2</sub>O<sub>2</sub> and 0.25 U mL<sup>-1</sup> HRP). The data shows that conversion to product reached a plateau at 88±4% before 160 min, this plateau indicated that the reaction had reached completion. It is assumed that therefore 10% of starting material is lost to dimerisation or polymerisation.

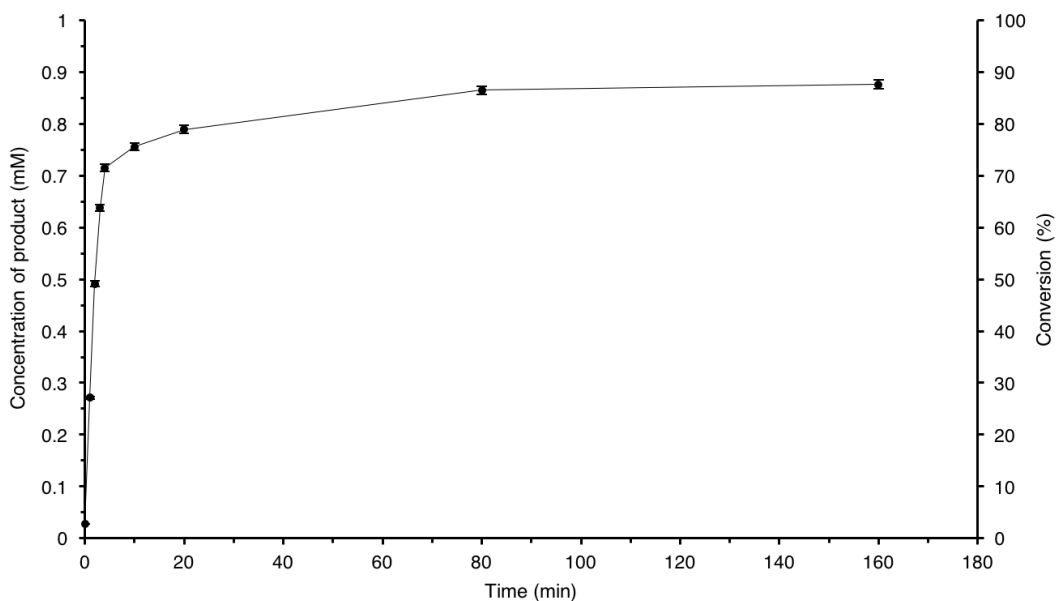


**Figure 3.6.** Percentage conversion to product **1** over time. Reaction conditions 2 mM 3-amino-4-hydroxybenzotrile, 100 mM 2,3-dihydrofuran, 2.5 mM H<sub>2</sub>O<sub>2</sub> and 0.25 U of HRP mL<sup>-1</sup>.

### 3.2.3 Tandem reaction substrate scope - (100mg scale)

To determine reaction scope, a range of 2-aminophenols bearing different electron withdrawing groups at different positions on the aromatic ring **2-6** were used as substrates (Figure 3.7) and the dienophiles expanded to the assessment of ethoxyethene **8** and 3,4-dihydropyran **9**. These reactions were performed at a semi-preparative scale and the isolated product yields were obtained.

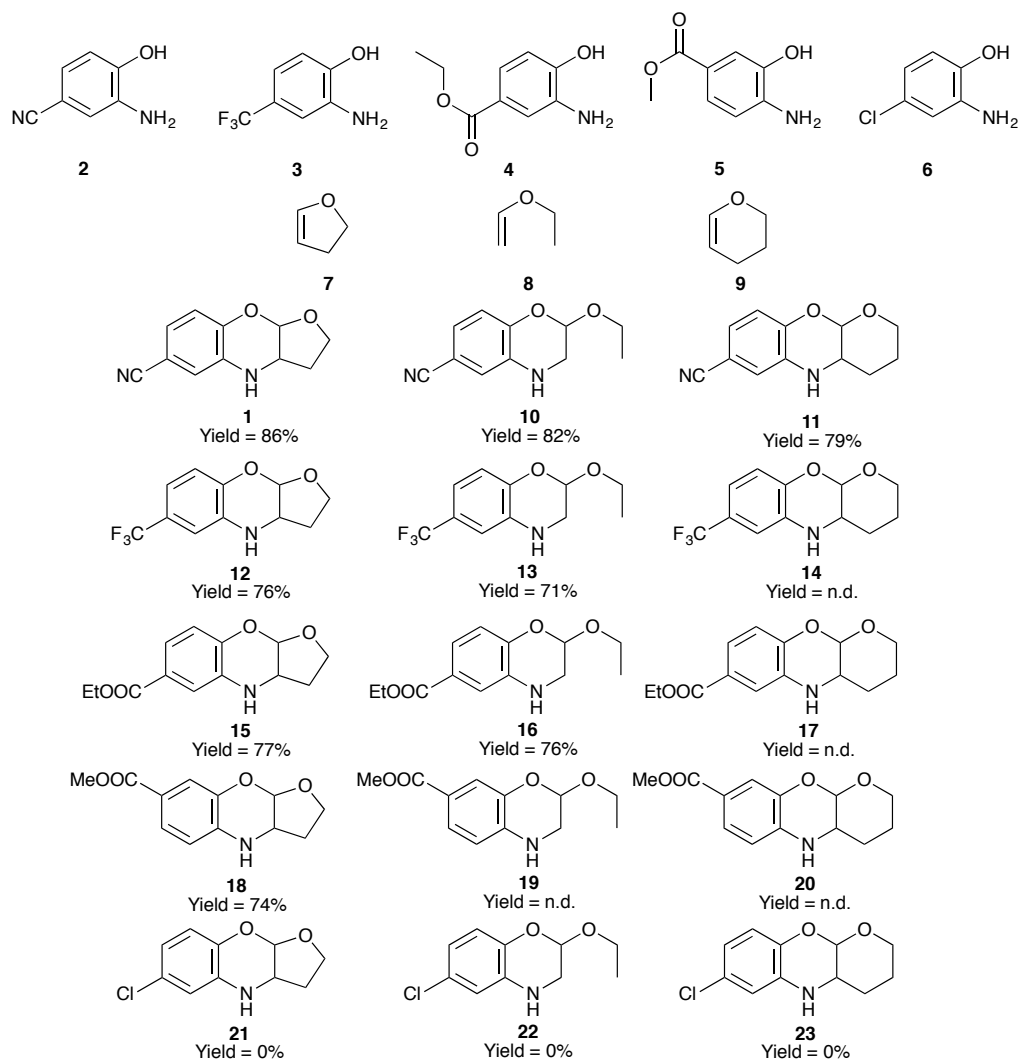


**Figure 3.7.** Substituted 2-aminophenol compounds tested as substrates and dienophiles tested under reaction conditions. Isolated yields for substrates tested under reaction conditions; 2 mM 2-aminophenol (2-6), 100 mM dienophile (7-9), 2.5 mM H<sub>2</sub>O<sub>2</sub> and 0.25 U HRP mL<sup>-1</sup>. n.d. = not determined, compounds experienced significant product degradation.

Substrates with the strongest electron withdrawing groups **2-5** proceeded with all dienophiles used achieving good yields. The chloro- substituted 2-aminophenol **6** failed to undergo cycloaddition with all dienophiles showing that mildly electron withdrawing groups do not provide the correct electronic properties for the reaction to proceed.

Environmental factor (E-factor = total weight waste / weight product)<sup>158</sup> has been calculated for the peroxidase catalysed to compare against the literature (diacetoxyiodo)benzene

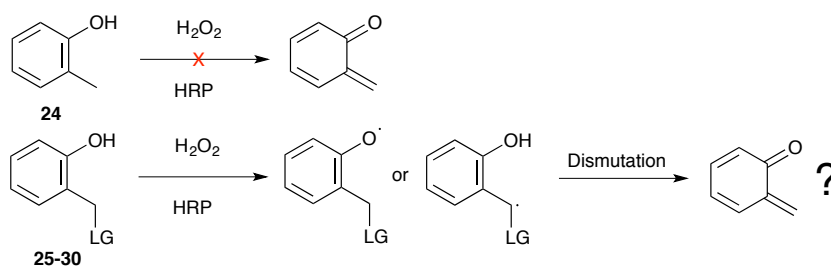
(DIAB)<sup>156</sup> catalysed synthesis of compound **1** (Table 3.1). The E-factor calculation is defined by the ratio of the mass of waste per mass of product (waste is defined as all organic compounds). Fine chemical synthesis typically has reaction E-factors of between 5-50 (the lower E-factor the better, as lower waste). Both catalysed reactions have E-factors within this range, however the peroxidase catalysed reaction is less than half of the DIAB catalysed reaction. The DIAB catalysed reaction uses 1.2 equivalents of DIAB which has the waste products of iodo-benzene and two acetic acid molecules, whereas the peroxidase catalysed reaction use hydrogen peroxide which is reduced to two water molecules. This reduces the environmental impact of the reaction.

	Peroxidase catalysed <b>2a</b>	DIAB catalysed <b>2a</b> <sup>156</sup>
<b>E-factor</b>	17.13	46.66

**Table 3.1** E-factor calculated for the peroxidase catalysed and DIAB catalysed methods of synthesising compound **1**.

### 3.3 Peroxidase-catalysed *o*-quinone methide generation

The approach taken to form *o*-quinone methide intermediates differed from *o*-benzoquinone imine formation as the oxidation potential of 2-aminophenols was significantly lower than that of *o*-cresol which was not within the oxidation range of HRP.<sup>72, 159</sup> Oxidation of *o*-cresol with HRP gives the corresponding alkoxide radical which subsequently undergoes dimerisation, oligomerisation and polymerisation. It was hypothesised that the addition of a suitable leaving group on the alpha position to the aromatic ring (scheme 3.5) could yield *o*-quinone methide upon oxidation with HRP. This approach has shown success in the literature in purely chemical synthetic methods.<sup>139</sup>



**Scheme 3.5.** Scheme showing potential oxidation routes towards *o*-quinone methides and reaction not proceeding with *o*-cresol.

These methods identified three leaving main groups which used quaternary ammonium salts<sup>141</sup>, carboxyl<sup>160</sup> and mercapto<sup>161</sup> substituents (Figure 3.8.A), which were used as precursors to produce *o*-quinone methide by chemical and electrochemical reactions. These starting materials were then chemically synthesised from 2-(hydroxymethyl)phenol in each case (Figure 3.8.B).

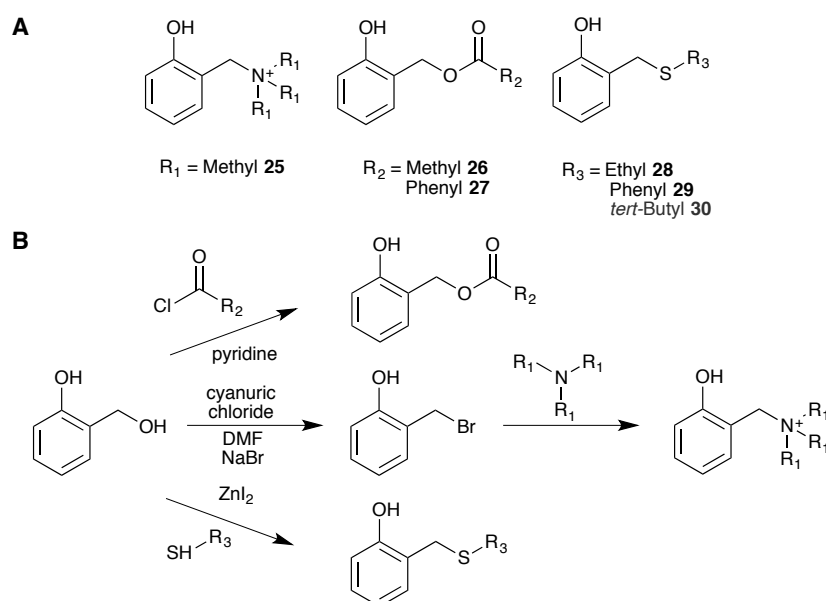
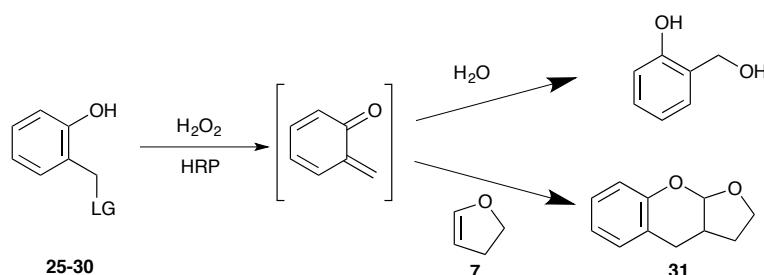


**Figure 3.8.** (A) Leaving groups identified as substrates to screen with HRP for *o*-quinone methide generation. (B) Synthesis scheme for starting materials.



### 3.3.1 Development chromane biocatalytic synthesis

As with *o*-benzoquinone imines it was known that in the presence of excess electron rich dienophile (e.g. vinyl ethers), the *o*-quinone methide would undergo a [4 + 2] inverse electron demand cycloaddition. Literature examples of *o*-quinone methide generation had also been performed in water showing they have a short lived stability (minutes), undergoing addition of water to form 2-(hydroxymethyl)phenol with no dienophile present. These studies also showed that cycloaddition would proceed selectively in the presence of a dienophile (Scheme 3.9) opposed to addition of water due to the cycloaddition being kinetically significantly faster. Thus *o*-quinone methide presence would be inferred by the production of the corresponding chromane product.



**Scheme 3.9.** Reaction selectivity of *o*-quinone methide with dienophiles and water. Where LG = leaving group. In the presence of a dienophile, cycloaddition reaction will proceed preferentially over nucleophilic attack by H<sub>2</sub>O. Reaction conditions 1 mM *o*-cresolic substrate **25-30**, 50 mM 2,3-dihydrofuran **7**, 1 mM H<sub>2</sub>O<sub>2</sub> and 2.5 U HRP mL<sup>-1</sup> in 50 mM phosphate buffer (pH 7.2).

Initial small scale (150  $\mu$ L) reactions were set up each containing *o*-cresolic substrates **25-30**, 2,3-dihydrofuran **7**, H<sub>2</sub>O<sub>2</sub> and HRP in pH 7.2 phosphate buffer, with controls for each reaction. Dienophile **7** was selected as inverse electron demand cycloadditions require dienophiles with electron withdrawing groups. Reactions were analysed by analytical HPLC, comparing retention time using product standard **31** (synthesised by literature methods<sup>160</sup>). These data have been summarised in Table 3.2. Where **y** indicates the presence of a peak

at 9.4 mins the same retention time as the product standard and **n** indicating no peak present.

Substrate	Full reaction (substrate, dienophile, HRP, H <sub>2</sub> O <sub>2</sub> )	HRP omitted from reaction	H <sub>2</sub> O <sub>2</sub> omitted from reaction	Dienophile omitted from reaction	Substrate omitted from reaction
<b>25</b>	<b>n</b>	<b>n</b>	<b>n</b>	<b>n</b>	<b>n</b>
<b>26</b>	<b>n</b>	<b>n</b>	<b>n</b>	<b>n</b>	<b>n</b>
<b>27</b>	<b>n</b>	<b>n</b>	<b>n</b>	<b>n</b>	<b>n</b>
<b>28</b>	<b>y</b>	<b>n</b>	<b>n</b>	<b>n</b>	<b>n</b>
<b>29</b>	<b>n</b>	<b>n</b>	<b>n</b>	<b>n</b>	<b>n</b>
<b>30</b>	<b>n</b>	<b>n</b>	<b>n</b>	<b>n</b>	<b>n</b>

**Table 3.2.** HPLC data summary, **y** indicates the presence of a peak at 9.4 mins the same retention time as the product standard and **n** indicating no peak present.

These results showed that only substrate **28** formed any product. Unsuccessful reactions mostly showed insoluble oxidation product. The control reactions for this substrate **28** showed no peak at the expected product retention time. The HPLC chromatogram from reaction with **28** (Figure 3.9) showed that product conversion was very low (6 %, by comparison with a calibration curve using known amounts of the authentic material). The chromatogram also showed an unexpected peak, with RT of 5.6 mins. This peak was present in the controls, showing the highest absorbance in the control without HRP. The controls also showed a depletion of substrate, with exception of reactions without hydrogen peroxide. It was hypothesised that this new peak was either sulfoxide **32** or sulfone **33** (Figure 3.10) produced by S-oxidation with hydrogen peroxide, which if proved would

contradict previous reports.<sup>57</sup> These literature reports state there is no spontaneous oxidation by hydrogen peroxide only HRP catalysed oxidation.

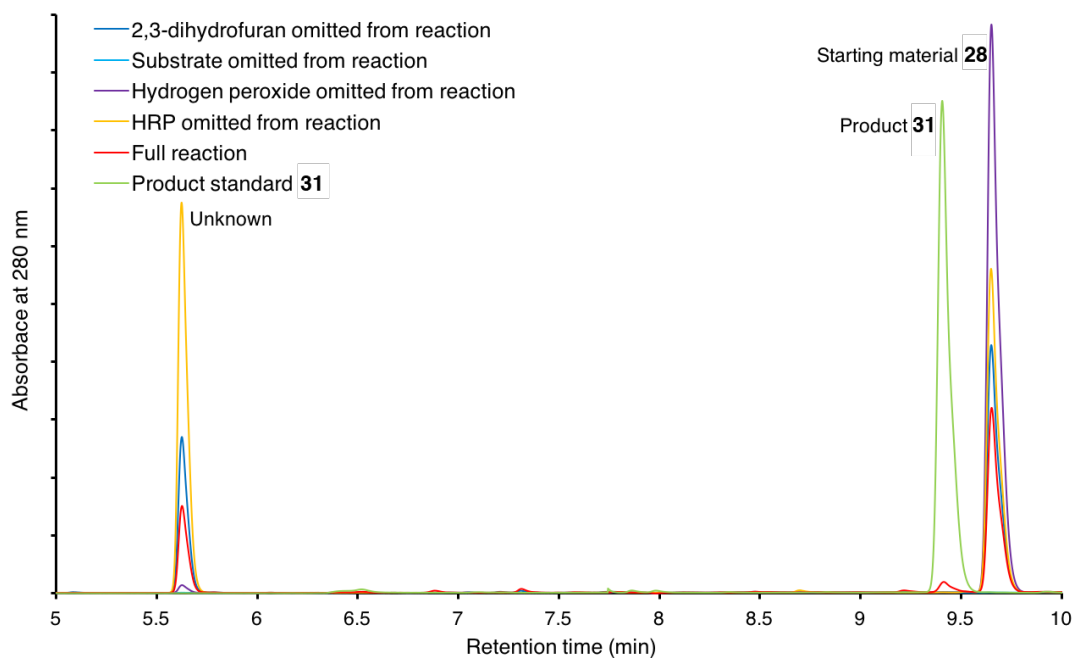


**Figure 3.9.** Overlaid HPLC chromatograms tracking absorbance at 280 nm vs. time for the reaction quenched mixture for the full reaction and control reactions. Control reactions lacked one of four reaction components to form the full reaction. Additionally shown is Product standard for compound **31**.

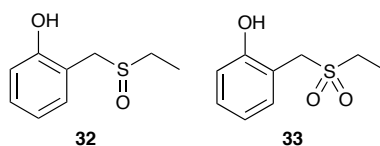


**Figure 3.10.** Compounds produced by oxidation by hydrogen peroxide. Sulfoxide **32** and sulfone **33**.

To investigate the possibility of sulfoxide or sulfone production under these reaction conditions, sulfoxide **32** and sulfone **33** were synthesised by oxidation using concentrated hydrogen peroxide, which was confirmed with spectra equivalent to literature.<sup>162</sup> HPLC analysis of these found that the sulfoxide **32** was the peak at 5.6 mins and sulfone **33** was not present in the chromatogram of the reaction mixture (Figure 3.11). Sulfone **33** not being detected may have been because its formation had not taken place or that its low stability meant that it quickly decomposed upon formation.

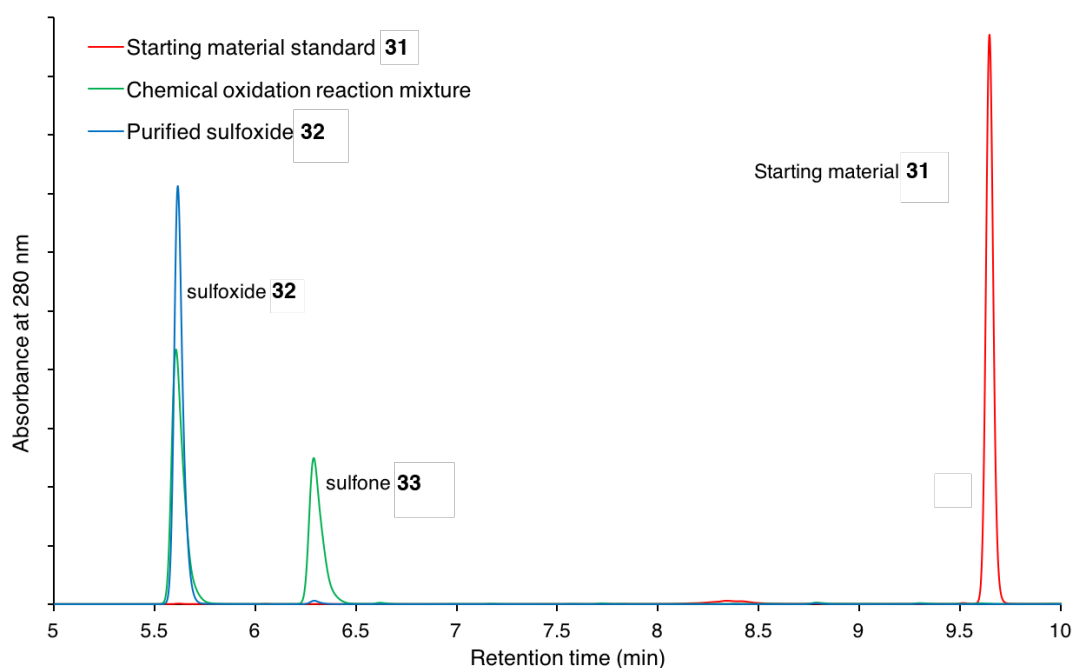


**Figure 3.11.** Overlaid HPLC chromatograms tracking absorbance at 280 nm vs time for substrate **31**, sulfoxide **32** and sulfone **33**.

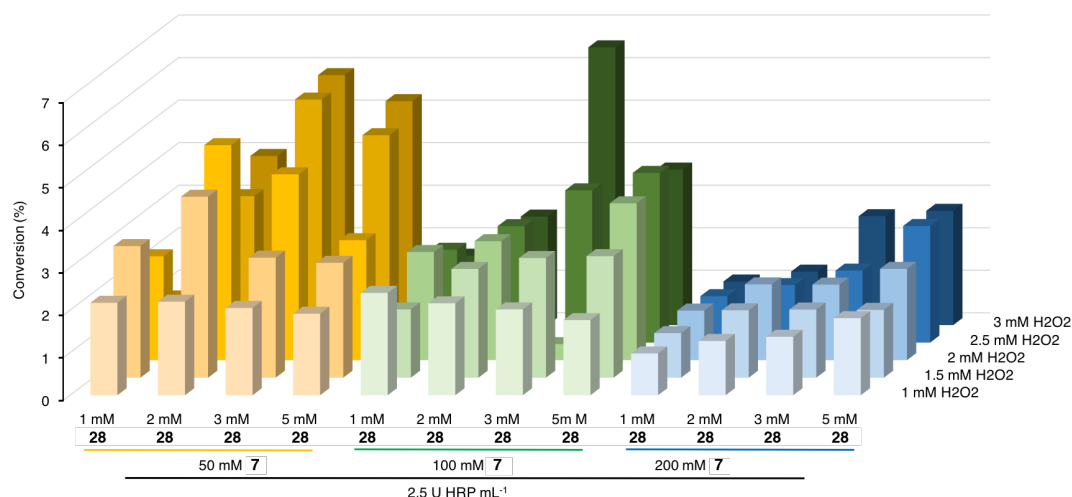
It was then investigated whether **31**, **32** or **33** could be the reactive substrate responsible for *o*-quinone methide generation. Reactions using sulfoxide **32** were hampered by its stability and its isolation in reasonable quantity. The sulfone **33** was particularly unstable and decomposed rapidly and therefore could not be utilised as a substrate (purified **33** also decomposed by polymerisation due to acidic HPLC conditions). Either of these compounds could be the reactive substrate that forms *o*-quinone methide, but the reaction controls show that the *o*-quinone methide forming reaction only proceeds in the presence of HRP.

Consequently, this evidence shows it cannot be a spontaneous event arising from decomposition of **32** or **33** (but could still be HRP catalysing quinone formation from **32** or **33**).

### 3.3.2 Optimisation of reaction

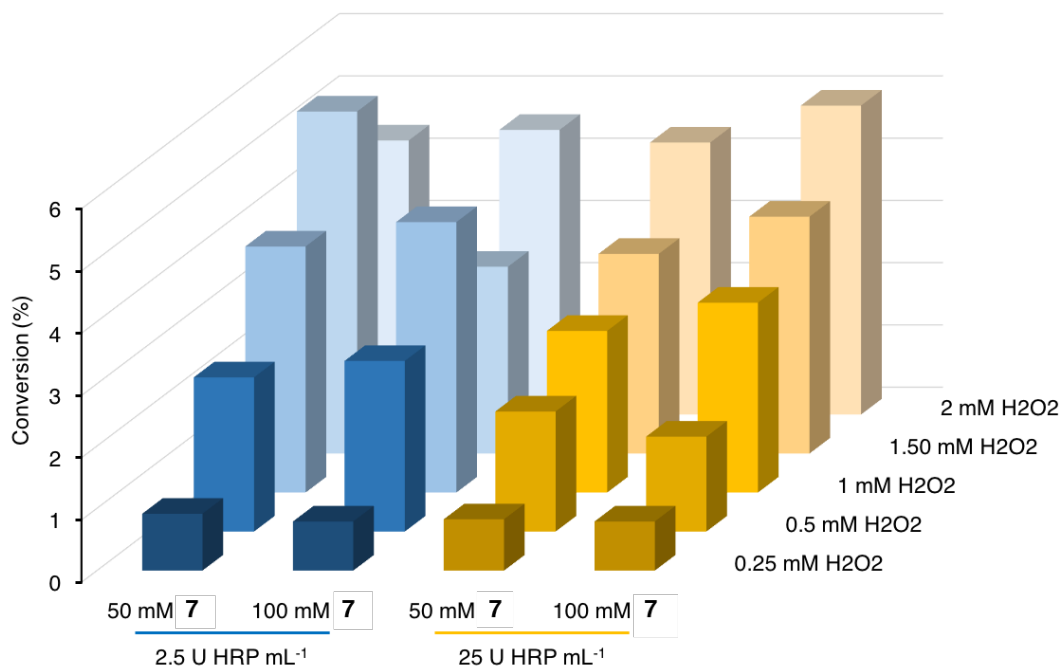
The initial substrate screening showed that the tandem reaction (conversion of **28** to **31**) was feasible, experiments were then designed in an attempt to maximise substrate conversion. Reactions were carried out by varying substrate, dienophile, hydrogen peroxide, enzyme concentrations and pH of the reactions. Results from analytical HPLC analysis using a calibration curve of product concentration to determine conversion in percentage have been summarised in Figures 3.12, 3.13 and 3.14.

Figure 3.12 shows that generally reactions with higher concentrations of dienophile **7** have lower conversions than reactions with lower concentrations of dienophile **7**, despite HRPs innate enzyme stability dienophile **7** is highly reactive could potentially react with nucleophilic amino acids deactivating the enzyme.<sup>141</sup>



**Figure 3.12.** Percentage conversion of **28** to **31**, varying concentration of 50-200 mM dienophile **7**, 1-5 mM substrate **28** and 1-3 mM hydrogen peroxide with constant pH (7.4) and 2.5 U HRP mL<sup>-1</sup>.

At the concentrations of HRP tested there appears to be little effect on the conversion to product (Figure 3.13), therefore substrate inhibition has not occurred to limit conversion. Reactions also show the reaction requires over a stoichiometric quantity of  $\text{H}_2\text{O}_2$  for the reaction to proceed to highest conversion (Figure 3.13).



**Figure 3.13.** Percentage conversion of **28** to **31**, varying concentration of 50-100 mM dienophile **7**, 0.25-2 mM hydrogen peroxide and 2.5-25 U HRP mL<sup>-1</sup> with constant pH (7.4) and 1 mM substrate **28**.

The most interesting observation from these results comes from the variation of pH (Figure 3.14), where reactions conducted at pH 5 and at pH 9 show markedly reduced conversions when compared to the analogous reactions at pH 7.5. Conversion reduction at pH 9 is unsurprising as HRP is deactivated at high pH<sup>72</sup> but at low pH (down to pH 3.5) HRP is very stable.<sup>17</sup> Therefore, the deduction in conversion at pH 5 must be attributed to another variable such as stability of o-quinone methide at decreased pH.<sup>141</sup>

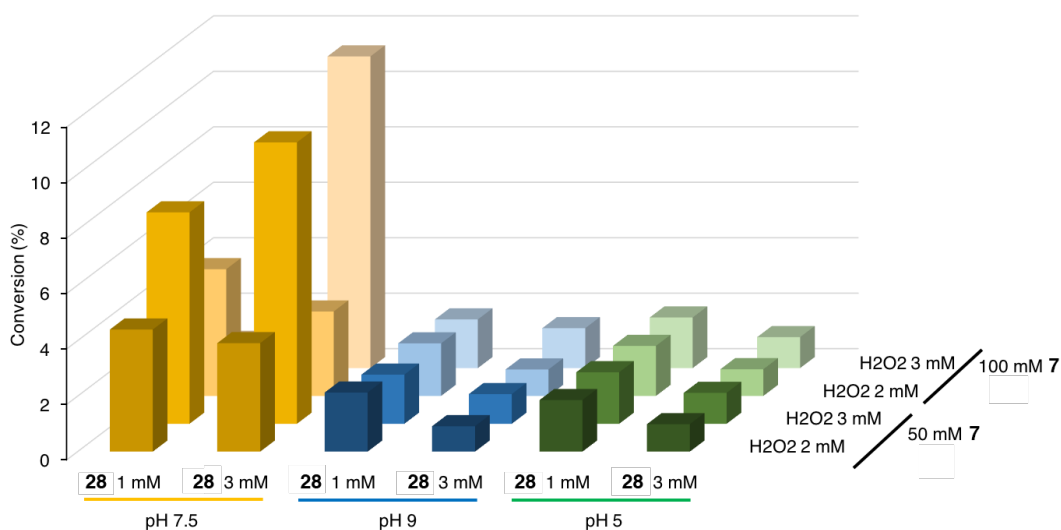


**Figure 3.14.** Percentage conversion of **28** to **31**, varying concentration of 50-100 mM dienophile **7**, 2-3 mM hydrogen peroxide, 1-3 mM substrate **28** and pH 9-5 using a constant 2.5 U HRP mL<sup>-1</sup>.

Overall these experiments show only a modest increase in conversion from 6% to 12%. This shows that a wide variation of reaction conditions is insufficient to make the reaction synthetically viable. Due to the poor product yield efforts to scale this reaction to obtain full characterisation were not viable under the range of tested conditions. Instead work will need to be done expanding the leaving groups screened or using different aromatic ring substituents to influence the quinone methide formation reaction. Substrates with electron withdrawing ring substituents were used to promote the cycloaddition reaction (once the quinone imine was formed) in the work to catalyse production of 1,4-benzoxazine. Unsubstituted *o*-quinone methides are known undergo preferential cycloaddition in water and are stable in water for minutes (without dienophile),<sup>145</sup> the rationale for not initially using electron withdrawing groups was that it was the actually catalysed formation of *o*-quinone methide that was problematic not the subsequent cycloaddition reaction. Therefore, it was unknown what effect any ring substituent would have on formation.

### 3.4 Conclusions

The study set out to generate quinonoid species and utilise them *in situ* as intermediates to form more complex organic skeletons. This was achieved by a tandem biocatalytic oxidation-cycloaddition sequence, forming either in the case of *o*-benzoquinone imines two new carbon-heteroatom bonds or in the case of *o*-quinone methide new carbon-carbon and carbon-heteroatom bonds in a one-pot system.

The *o*-benzoquinone imines formed by HRP catalysis showed a good substrate scope but did rely on electron withdrawing ring substituents on the aminophenol for the cycloaddition reaction to proceed. The benzoxazines formed could be isolated in good yield and fully characterised with reactions carried out on a synthetically useful scale. When compared to current literature methods for the one-step synthesis of benzoxazines by cycloaddition, the enzyme catalysed reaction offers lower E-factor for the reaction and increased product yield. The enzyme reaction also has the additional environmental benefit of being truly catalytic, rather than the chemical method which uses stoichiometric quantities of DIAB to perform the oxidation, with iodo-benzene and acetic acid as waste products.<sup>156</sup>

The major drawback of the enzyme reaction is that the reaction is run at relatively low concentrations due to solubility of substrate and product in aqueous buffer. Further investigations of increased substrate loading per volume and increased tolerance of the reaction to organic solvents will need to take place for reaction to be run at preparative scale.

The production of chromane **31** could infer the generation of *o*-quinone methide. This demonstrates the first enzyme catalysed formation thus a new method for the formation of chromane ring structures. The utilisation of the enzyme generated *o*-quinone methide can be expanded to other reactions than cycloaddition<sup>145</sup>, however the conversion to *o*-quinone methide (inferred by chromane) is very low. Further investigations into increasing the conversion must be undertaken in order to give wider utility to this reaction. This may be undertaken by exploring further leaving groups or by enzyme mutation to increase oxidation potential.



The methods described may also be helpful in expanding the possibilities in quinonoid chemistry, such the coupling of the enzymatic generation of quinonoid systems with a Diels–Alderase enzyme<sup>163, 164</sup> in order to fully control the stereochemistry of a fused ring system produced by cycloaddition rather than relying on the electronic directing effects of the substrate.

## **Assay for enzymatic aryl-amine halogenation based on a peroxidase-mediated quinone-amine coupling**

### **4.1 Introduction**

Halogenated aryl-amine constitute key building blocks in many fine chemicals including pharmaceuticals, polymers and agrochemicals (Figure 4.1).<sup>165, 166</sup> As building blocks, halogenated arenes are frequently employed in transition metal-catalysed cross-coupling reactions.<sup>167</sup> However synthetic routes for production often rely on electrophilic aromatic substitution, but these approaches lack regioselectivity<sup>168</sup> and commonly rely on Lewis acid catalysis, consequently generating large amounts of environmentally unfriendly waste acid.<sup>169</sup> The inherent usefulness of aryl-halide compounds has subsequently generated substantial interest in more efficient and selective routes to their synthesis. It is possible to exploit enzymes to provide an alternative methodology to the use of transition metal catalysis for halogenation. As previously discussed (Section 1.1) biocatalysis can in principle provide efficient synthesis in terms of yields and highly chemo-, regio- and stereo-selective reactions; biocatalysis could also potentially supersede many traditional chemical catalysts, including catalysts that are toxic or have properties that are environmentally unfriendly.<sup>3, 170-172</sup>

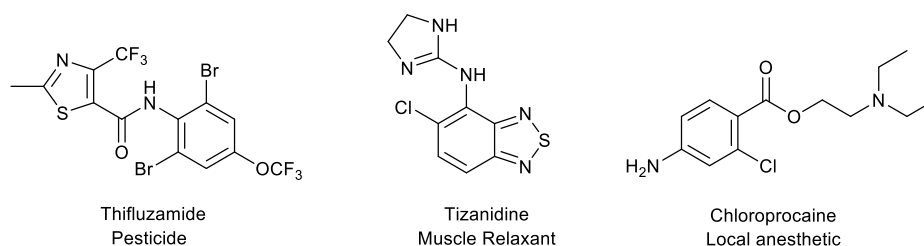


**Figure 4.1.** Examples of biologically active chemicals synthesised from halogenated arylamines.

By classification of their oxidation partner<sup>173</sup> there are currently two distinct classes of enzyme which perform biological halogenation reactions. Oxygen-dependent halogenases, encompassing flavin-dependent and non-heme iron(II)-dependent enzymes requiring oxygen as an electron acceptor. Hydrogen peroxide ( $H_2O_2$ ) utilising enzymes, heme- and vanadium-dependent enzymes are known as haloperoxidases.<sup>174, 175</sup> Recently flavin-dependent halogenases have been investigated for the production of halogenated aryl amines.<sup>176</sup> This group of enzymes are unique in that they have been shown to regioselectively install chlorine/bromine atoms on a variety of aromatic substrates.<sup>177</sup> The deduced mechanism proceeds *via* the *in situ* production of hypohalous acid followed by its association with an active site lysine residue, which is then thought to guide the regioselective attack of the substrate.<sup>178, 179</sup> In contrast heme-dependent enzymes release free hypohalous acid which react with substrates in solution, with only electronic directing effects.<sup>174, 175</sup>

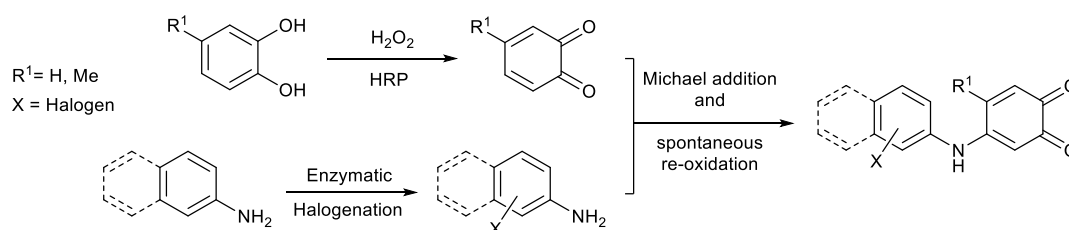
Discovering new halogenases<sup>174, 175</sup> or evolving existing enzymes<sup>180</sup> requires the capacity to detect and quantify halogenation activity. This has traditionally been attempted by assaying free hypohalous acid in solution,<sup>181, 182, 183</sup> however this is an indirect method of detecting enzyme turnover and would not be applicable to halogenating enzymes that bind hypohalous acid in their active site such as the FAD-dependent enzymes. Consequently, most analyses of substrate conversion have relied on intrinsically low throughput methods such as HPLC, LC-MS and NMR.<sup>176, 184</sup> Further development of halogenation enzymes

would thus benefit from a high-throughput screen which could aid in the screening of enzyme libraries.

As previously mentioned (section 1.12) it has been shown that the oxidation of catechols by horseradish peroxidase to their corresponding 1,2-benzoquinone (*ortho*-benzoquinone) can be combined with a successive 1,4- Michael addition of aniline to the quinone in a tandem reaction.<sup>140</sup> The formation of a highly coloured quinone-aniline adduct has previously been applied to the development of an assay for peroxidase activity.<sup>68</sup> In assays with different anilines it was observed that even those closely related in structure result in the formation of adducts that have significantly different UV-visible spectra. When comparing halogenated anilines to their parent compounds, these spectral differences were sufficiently large to even be visually distinguishable.

#### 4.2 Aims

The aims of this work was therefore to investigate and develop this reaction sequence into a colorimetric assay for the detection and quantification of halogenated aryl-amines. Key objectives were that the assay would be generally applicable to a wide range of aryl-amines, whilst being rapid and high-throughput. Additionally, because the coupling is enzyme driven it was hoped to be utilised sequentially after an enzymatic halogenation reaction in a “one-pot” procedure (Scheme 4.1).



**Scheme 4.1.** General scheme illustrating the HRP-catalysed oxidation of catechols to their corresponding *ortho*-quinone (upper pathway) and the formation of the arylamine-catechol adduct. This reaction can be coupled to a biocatalytic halogenation reaction (lower pathway).

### 4.3 Development of halogenation assay

The foundation for the assay is the distinct UV-visible spectrum of the quinone-aniline adduct that is produced by the stoichiometric 1,4-Michael addition of the amino-constituent to the *ortho*-benzoquinone (produced by the oxidation of catechol by HRP).<sup>68</sup> Whilst previously this adduct formed has been used to quantify the concentration of peroxidase in solution, by using an excess of HRP it is instead possible to use the adduct produced by the reaction for quantification of the amino-constituent. If the reaction mixture contains multiple amino-constituents, each resulting adduct can be distinguished by their individual  $\lambda_{\max}$  peaks in the overall UV-visible spectra. In the case of aryl-amines and halogenated aryl-amines it was found the  $\lambda_{\max}$  values were predictably in the range of  $\sim 520$  nm and  $\sim 425$  nm, respectively (Figure 4.2). In contrast, the 4-methylcatechol (4-MC) prior to the reaction does not absorb much above 350 nm

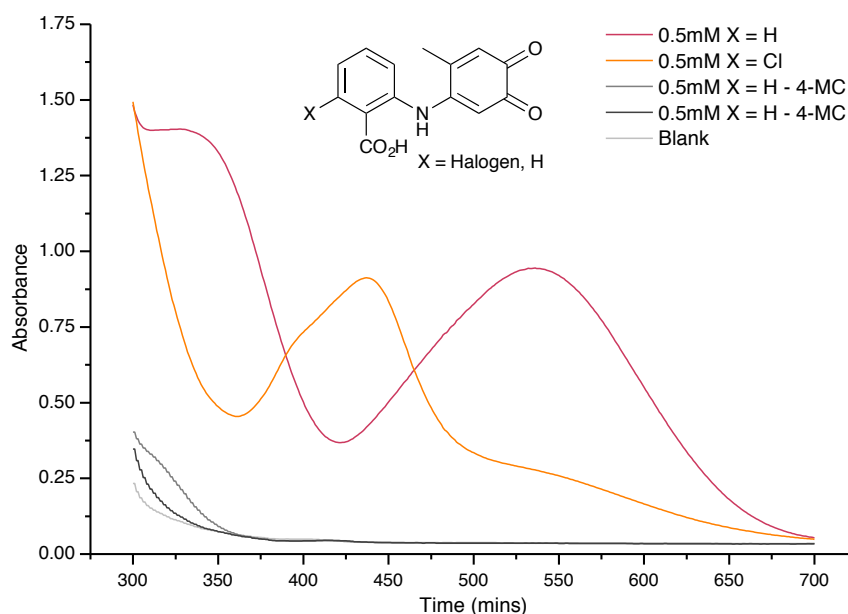


**Figure 4.2.** UV-visible spectra of adduct formed from 4-methyl-catechol (4-MC) with either 0.5 mM 2-aminobenzoic acid (X = H) or 0.5 mM 2-amino-6-chlorobenzoic acid (X = Cl) and controls in 50 mM K<sub>2</sub>HPO<sub>4</sub> pH 7.4.

First, a series of experimental considerations were taken into account in order to simplify the spectral analysis and permit a 'one-pot' process. As shown above 4-methyl-catechol (4-MC) was used to form the quinone component as it was also known to be a good substrate for HRP, and when converted to a *ortho*-benzoquinone it only allows a single conjugated product since the 4-methyl substituent blocks further addition at this position.<sup>185, 186</sup> In order to prevent oxidation of the aryl-amine product by HRP that occurs at low pH,<sup>86</sup> all assays were carried out in pH 7.4 buffered conditions. Additionally, to confirm that only the desired product was formed under these conditions, test reactions were carried out with 4-MC and either 2-aminobenzoic acid or 2-amino-6-chlorobenzoic acid. HPLC and MS analysis of the reaction mixtures confirmed single product formation and that the reaction was complete within 5 minutes.

#### 4.4 Substrate range

To confirm the trend that the  $\lambda_{\max}$  values of adducts formed from the Michael addition were lower than the corresponding non-halogenated aryl-amines, a series of further analogues were tested (Figure 4.3). From the spectral data collected it was observed that halogenated substrates have a lower  $\lambda_{\max}$  than their non-halogenated counterparts throughout the series (Table 4.1). The results show that the trend is also observed with more highly substituted aryl-amines as well as the pyridine tested.

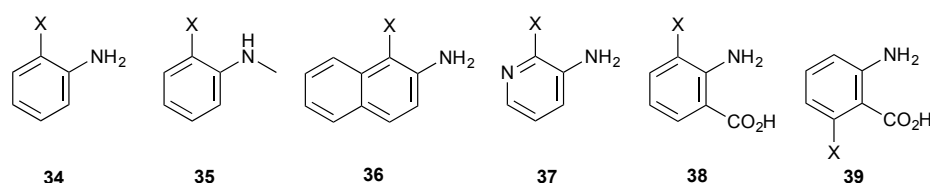


**Figure 4.3.** Structures of substrates tested with the coupled assay. X = H, Cl, Br, I.

Aryl-amine (see Figure 3 for structure)	X = H		X = Cl		X = Br		X = I	
	$\lambda_{\max}$ (nm)	$\epsilon$ ( $M^{-1}$ $cm^{-1}$ )	$\lambda_{\max}$ (nm)	$\epsilon$ ( $M^{-1}$ $cm^{-1}$ )	$\lambda_{\max}$ (nm)	$\epsilon$ ( $M^{-1}$ $cm^{-1}$ )	$\lambda_{\max}$ (nm)	$\epsilon$ ( $M^{-1}$ $cm^{-1}$ )
<b>34</b>	508	4141	441	2386	432	1964	431	2029
<b>35</b>	537	5050	403	1027	400	1108	--	--
<b>36</b>	516	1966	438	1489	437	1086	--	--
<b>37</b>	500	1919	398	1710	413	1244	--	--
<b>38</b>	535	4706	436	3789	436	2770	--	--
<b>39</b>	535	4706	437	4548	--	--	--	--

**Table 4.1.** UV-visible  $\lambda_{\max}$  and  $\epsilon$  values of the aniline-catechol adducts formed by the assay.

“--” = not determined.

#### 4.5 Quantitative analysis

The molar absorption coefficients ( $\epsilon$ ) for the  $\lambda_{\max}$  values that were determined in Table 4.1 allowed for the qualification of binary mixtures of the the halogenated aryl-amines and their non-halogenated analogues. Towards this aim, calibration curves were constructed for each of the selected aryl-amines by known using concentrations of the halogenated and non-halogenated aryl-amine. Whereby the halogenated and non-halogenated aryl-amine were added in ratios of 10:0 to 0:10 to a total concentration 0.5mM (Figure 4.4A).

For instance, the UV-visible spectra were recorded for mixtures of 2-aminobenzoic acid and 2-amino-6-chlorobenzoic acid that were subjected to the assay. It was observed that as the ratio of 2-amino-6-chlorobenzoic acid increased, the absorbance at 437 nm increased with a concomitant decrease at 535 nm. A calibration curve was then constructed by plotting the absorbance of the peak in the 500-550 nm region corresponding  $\lambda_{\max}$  of the aryl-amine-catechol adduct produced (which in the case of 2-amino-6-chlorobenzoic acid was at 535 nm), against concentration of the halogenated component (Figure 4.4B). Calibration curve

construction was then extended to a range of other halogenated and un-halogenated mixture pairs and in all cases the resulting calibration plot fitted a linear relationship with a high statistical significance ( $R^2 > 0.99$ , table 4.2). The detection limit for halogenated product was dependent on the sensitivity of the UV-visible assay, which in these cases were able to detect conversion rates as low as 5% (0.025 mM in 0.5 mM of total adduct).



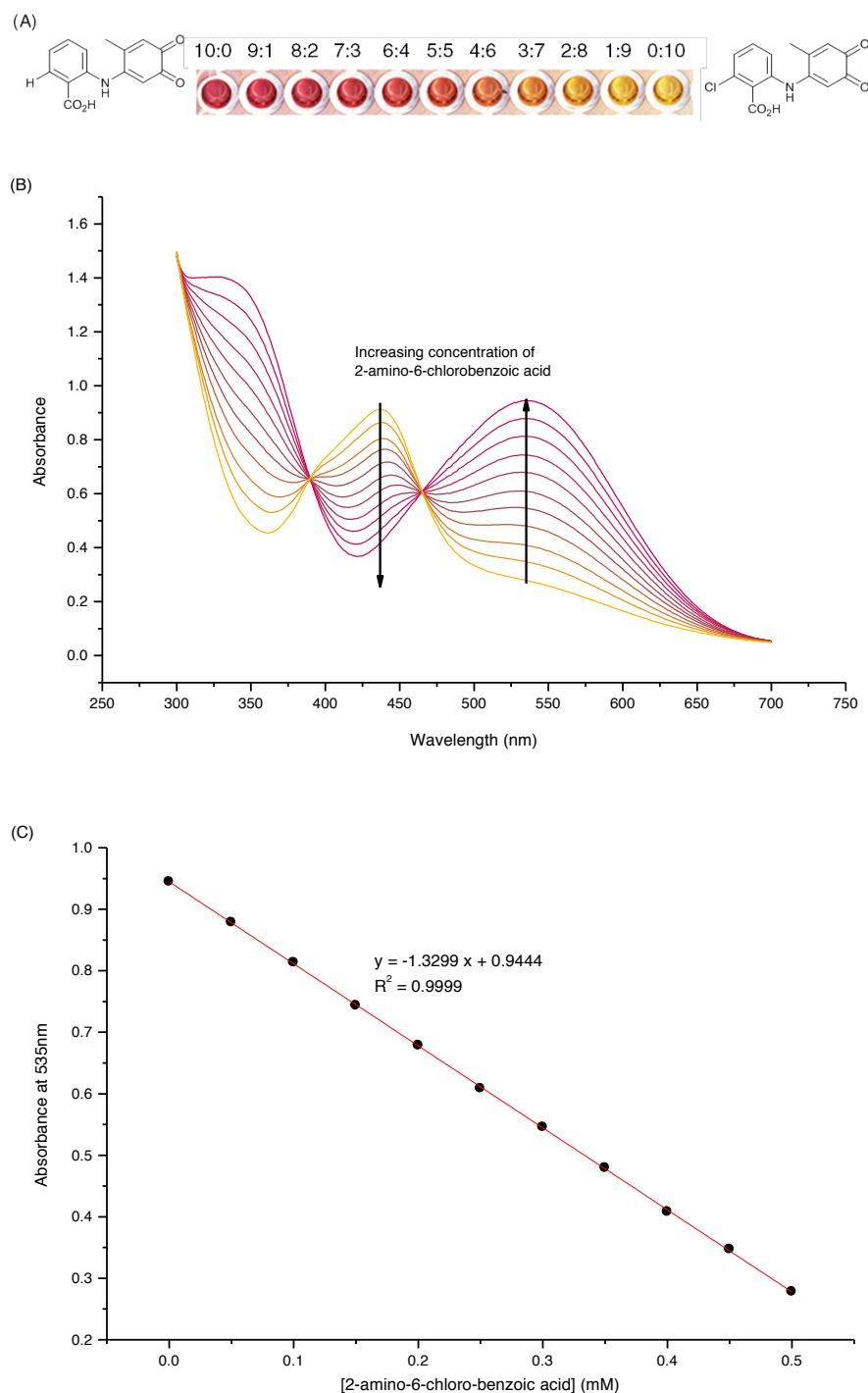


**Figure 4.4.** Illustrative data for mixtures of 2-aminobenzoic acid and 2-amino-6-chlorobenzoic acid solutions. **(A)** Photograph of one row of wells in a microtitre plate with adducts produced from ratios of 2-aminobenzoic acid:2-amino-6-chlorobenzoic acid (total concentration 0.5 mM). **(B)** UV-visible spectra for the mixtures in range of ratios to a total concentration of 5 mM. **(C)** The calibration graph produced by plotting the absorbance of the peak at 535 nm against the concentration of 2-amino-6-chlorobenzoic acid.

<b>Arylamine (Figure 4.3 for structure)</b>	<b>Ring substituent X</b>	<b>Gradient</b>	<b>y-intercept</b>	<b>Coefficient of determination (R<sup>2</sup>)</b>
<b>34</b>	H vs. Cl	-0.9916	0.8139	0.9977
	H vs. Br	-1.2304	0.8099	0.9951
	H vs. I	-0.9916	0.8139	0.9977
<b>35</b>	H vs. Cl	-1.706	1.0078	0.9997
	H vs. Br	-1.7988	1.0479	0.9992
<b>36</b>	H vs. Cl	-0.4588	0.4082	0.9982
	H vs. Br	-0.6210	0.4132	0.9910
<b>37</b>	H vs. Cl	-0.3803	0.3973	0.9906
	H vs. Br	-0.7111	0.4744	0.9933
<b>38</b>	H vs. Cl	-1.4900	0.9705	0.9921
	H vs. Br	-1.5853	0.9781	0.9910
<b>39</b>	H vs. Cl	-1.3299	0.9444	0.9999

**Table 4.2.** Parameters calculated from the best-fit of calibration plots for the binary mixtures of the halogenated and non-halogenated aryl-amine-catechol adducts.

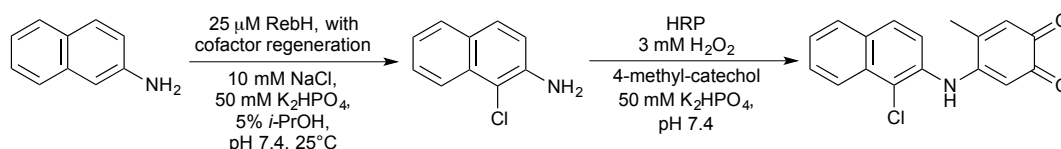
#### 4.6 Coupling with a flavin dependent halogenase system

In order to establish the application of this assay to biocatalytic halogenation reactions, efforts were then directed to the development of an end point assay that could be conducted sequentially in the same reaction vessel.

Tryptophan-7-halogenase RebH from *Lechevalieria aerocolonigenes* was employed as a model halogenase. It was chosen as it was known to catalyse the chlorination of 2-naphthylamine to 1-chloronaphthalen-2-amine.<sup>176</sup> As RebH is a flavin-dependent enzyme, the biocatalytic halogenation system required the inclusion in the reaction mixture of a co-factor regeneration system comprising of a flavin reductase<sup>187</sup> (Fre, from *E. coli*) and glucose

dehydrogenase<sup>188</sup> (GDH2, from *Bacillus megaterium*). Molecular cloning of RebH and Fre was carried out by Dr Sarah Shepard. The overall sequential biocatalytic halogenation and assay procedure thus involved the execution of the halogenation, which was terminated at the pre-determined time points by heating to 95°C.

HRP, H<sub>2</sub>O<sub>2</sub> and 4-MC were then added and the mixtures were incubated for a further 5 minutes (Scheme 4.2). Each mixture was then analysed to quantify the amount of the respective halogenated and non-halogenated 4-MC adducts by the UV-visible method described above, and the time course of the biotransformation was plotted (Figure 4.5). The quantifications were also conducted by HPLC as a comparator. A good correlation between both analysis methods was observed, thus validating the spectrometric method. It was subsequently discovered that due to the rapidity of the quinone generation and adduct formation, it was also found that it is possible to perform the second step of the assay without the need to stop the halogenation reaction beforehand.



**Scheme 4.2.** Reaction sequence for RebH halogenation followed by *in situ* HRP oxidation of 4-MC and coupling of the naphthylamine(s).

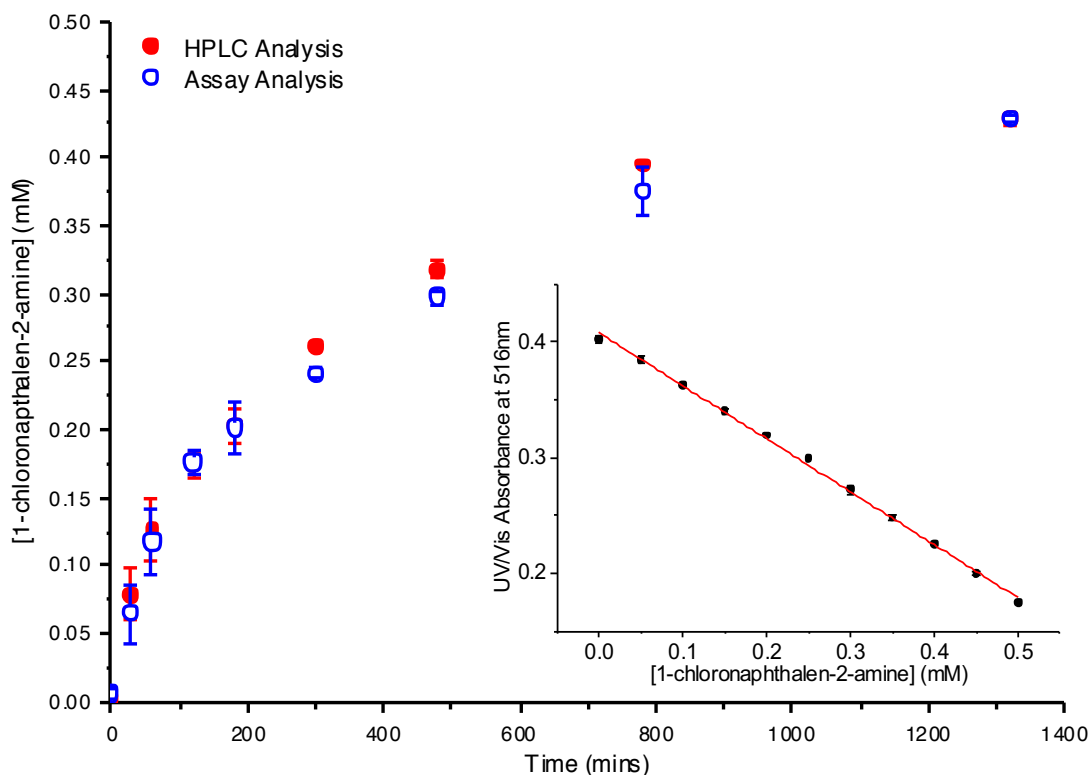


**Figure 4.5.** Graph of the increase in the concentration 1-chloronaphthalen-2-amine against length of time of the halogenation reaction. Inset assay graph calibration plot for assay analysis produced using RebH halogenation reagents and conditions.

#### 4.7 Conclusions

To summarise, a UV-visible spectrometric assay for the halogenation of arylamines based on *in situ* oxidation of 4-methylcatechol by HRP and coupled conjugate addition has been developed. The assay is rapid (5 minutes), sensitive (25  $\mu\text{M}$  detection limit) and provides both qualitative and quantitative analysis. In all the examples described, the reaction results in a sufficiently large  $\lambda_{\text{max}}$  shift that it can even be visually observed, making it a genuine colorimetric assay. It has also been shown to be amenable to coupling with reactions carried out by flavin-dependent halogenase enzymes in a one-pot procedure and can be applied in a high-throughput multi-well format. Since the assay functions under mild physiological conditions, this assay can in principle be used in a similar manner with halogenation reactions catalysed by other classes of enzymes. Going forward it is hoped the key purpose

of this assay will be its utilisation in efforts to discover and reengineer new halogenase enzymes for synthetic applications, and is an improvement over previously described methods that only identify enzyme activity indirectly by the detection of hypohalous acid production. Reports suggest previous efforts in the development of new biocatalysts have shown that the availability of a suitable high-throughput screening methodology has been crucial to their success.<sup>189</sup>

Ideally, an authenticated sample of the desired product is required in order to provide accurate quantification, but in most cases standards can be obtained through conventional (non-enzymatic) chemistry. Even in cases where information on the product is limited, a simple absorbance measurement of any wavelength in the 500–550 nm range can serve as a qualitative test, which is usually sufficient as a first-pass library screening tool.

Though the original intention was to develop a colorimetric assay for enzymatic aryl-amine halogenations, it could also be equally applied to any halogenation reaction of aryl systems that possess an exocyclic nucleophile.<sup>140, 190</sup> Thus, this general procedure of *in situ* HRP-mediated quinone oxidation followed by conjugate addition has substantial scope for further development into assays for a wide range of substrates.

---

## Chapter 5

### Concluding remarks

This work has encompassed three different projects, with the overall goal of applying peroxidase enzymes in new ways to the context of both biotechnology and nanotechnology. This has primarily been achieved by utilising both commercial preparations and recombinantly expressed peroxidases from Horseradish.

Firstly, an HRP isoenzyme was used to expand current techniques for biocatalytic nanolithography in the catalytic formation of polyaniline with nanometre resolution. Features were characterised by AFM, Raman and functionalised by the post-polymerisation addition of a fluorescent moiety. A refinement in resolution was also achieved compared to previous biocatalytic probe lithography. Lithographic patterning was also extended to a wide area (1.2 cm x 1.2 cm) this constitutes the first example of multiplexed biocatalytic nanolithography. Overall the approach developed to functionalise probe arrays with enzymes could also be extended to other enzyme classes. Due to the use of site specific immobilisation any ybbR tagged protein could be used to functionalise arrays. This would enable the expansion of

reaction types possible perform constructive lithography or direct the use of arrays to perform localised reactions with nanometre resolution.

Readily available commercial preparations of HRP were also utilised to catalyse the formation of quinoid systems. *o*-Quinone methides and *o*-quinone imines were exploited to perform tandem [2+4] cycloadditions to produce aromatic fused ring systems in water. HRP showed a good substrate scope to the generation of benzoquinone imines but did rely on electron withdrawing ring substituents on the aminophenol derivatives for the sequential cycloaddition reaction to proceed. The benzoxazines produced in this one pot process could be isolated in good yields characterised with reactions carried out on a synthetically useful scale. Comparison to current literature for one-step synthesis of benzoxazines showed higher yields but reaction volumes were significantly higher, for this reaction to be useful on an industrial scale this would need to be addressed. *o*-Quinone methide generation was inferred by the production of furo-chromane, however further development work will need to take place for this reaction to reach its full potential.

A *o*-quinone 1,4-Michael addition to aryl amines was used to detect the formation of halogenated aryl amines. This was based on the significantly different UV/Visible spectra of halogenated conjugates and non-halogenated conjugates. The assay provided a fast (5 minutes), sensitive (25  $\mu$ M detection limit) and both qualitative and quantitative means of calculating reaction conversions. This halogenation assay was then applied to following the reaction kinetics of a flavin dependent halogenase, as a one-pot procedure it is amenable to a high-throughput multi-well format. This being critical to the application of the assay to the detection new halogenases and reengineer these enzymes for industrial chemical processes.

---

## Chapter 6

### Experimental

This section details methods, materials and apparatus used throughout this work.

#### 6.1 General

##### 6.1.1 General materials

**Organic chemistry:** All compounds are racemic unless *R*, *S* descriptors are given. Starting materials were purchased from Sigma Aldrich unless otherwise stated. Solvents were of analytical or HPLC grade. Column chromatography was performed on silica gel (Fluka, 220–440 mesh). Analytical thin layer chromatography (TLC) was carried out on Polygram Silica G/UV254 plates, with visualisation at 254 nm or the following agents: ninhydrin, iodine or potassium permanganate. Ultrapure water (18.2 MΩ·cm at 25 °C) was used throughout and was prepared by Milli-Q filtration (Merck Millipore).



**Molecular biology:** All chemicals were purchased from Sigma Aldrich unless otherwise stated. Restriction enzymes and DNA ladder were purchased from New England Biolabs. Protein ladder was PageRuler Plus from Fermentas. Protein stain was instant blue stain from Expedeon. *E. coli* ArcticExpress (DE3) cells were purchased from Agilent and BL21 (DE3) cells were purchased from Thermo Fisher Scientific. Nickel NTA column used for FPLC based IMAC was HisTrap HP column (GE Healthcare, USA). Peroxidase from horseradish (Type VI-A),  $\beta$ -nicotinamide adenine dinucleotide dipotassium salt (NAD), flavin adenine dinucleotide disodium salt (FAD) and sequencing primers were purchased from Sigma Aldrich (UK) Ltd. The *ybbR-C1A* gene was amplified from the vector pPpT4\_Alpha\_S\_ybbR-C1A using primers 5'-ACTTTAAGAAGGAGATATACCATGGATTCTTTGGAGTTCATTG-3' and 5'-GACTTTGTTAGCAGCATGCTCGAGCACCACCACCACCACCACC-3' with *XhoI* and *NcoI* restriction sites. The gene was cloned into the corresponding restriction sites of pET28a. The *rebH* gene was amplified from the genomic DNA of *Lechevalieria aerocolonigenes* using primers 5'-GTACGTCATATGTCCGGCAAGATTGACAAG-3' and 5'-GTCAGCAAGCTTTCAGCGGCCGTGCTGTGCC-3' with *NdeI* and *HindIII* restriction sites. The gene was cloned into the corresponding restriction sites of pET28a.<sup>191</sup> The *fre* gene was amplified from the genomic DNA of *E. coli* BL21 (DE3) using primers 5'-AAAAAAGGTACCATGACAACCTTAAGCTGTAAA-3' and 3'-AAAAAAGGTACCATGACAACCTTAAGCTGTAAA-3' and 3'-AAAAAAGGTACCATGACAACCTTAAGCTGTAAA-3' and 3'-AAAAACTCGAGTCAGATAAATGCAAACGCATC-5', and digested using *KpnI* and *XhoI* before ligating into the pET45b expression vector. The pET28a plasmid encoding *Sfp*<sup>124</sup> was a kind gift from Prof J. Micklefield laboratory. The pET21b plasmid encoding GDH2 plasmid<sup>188</sup> was a kind gift from Prof. N. S. Scrutton's laboratory. All vectors were confirmed by DNA sequencing.

**Nanolithography:** N-hydroxysuccinimidyl-75-N-(3-maleimidopropionyl)-amido-4,7,10,13,16,19,22,25,28,31,34,37,40,43,46,49,52,55,58,61,64,67,70,73-tetracosaoxapentaheptacontanoate, (Quanta BioDesign, USA). Atomically flat microarray slides were SuperClean 2 (Arrayit Corp, USA). AFM lateral force imaging was performed on

the same instrument using ContAI-G cantilevers (Budget Sensors, Bulgaria) under ambient conditions.

The PPL arrays were prepared according to previously reported procedures.<sup>108</sup> with silicon masters purchased from NIL Technology ApS (Kongens Lyngby, Denmark). Silicon masters had a probe to probe pitch of 100  $\mu\text{m}$  and a probe base diameter of 40  $\mu\text{m}$ . The gold substrates were constructed of 2 nm titanium adhesion layer, 10 nm gold on aluminasilicate glass microscope slides (Sigma Aldrich, UK). 16-mercaptohexadecanoic acid, thiourea, iron (III) nitrate nonahydrate and hydrochloric acid (37%) were also purchased from Sigma Aldrich and used as received.

#### 6.1.1.1 Growth Media

- SOB media: 20 g L<sup>-1</sup> tryptone, 5 g L<sup>-1</sup> yeast extract, 2 mL L<sup>-1</sup> of 5 M NaCl, 2.5 mL L<sup>-1</sup> of 1 M KCl, 10 mL L<sup>-1</sup> of 1 M MgCl<sub>2</sub>, 10 mL L<sup>-1</sup> of 1 M MgSO<sub>4</sub>, H<sub>2</sub>O.
- SOC media: 20 g L<sup>-1</sup> tryptone, 5 g L<sup>-1</sup> yeast extract, 2 mL L<sup>-1</sup> of 5 M NaCl, 2.5 mL L<sup>-1</sup> of 1 M KCl, 10 mL L<sup>-1</sup> of 1 M MgCl<sub>2</sub>, 10 mL L<sup>-1</sup> of 1 M MgSO<sub>4</sub>, 20 mL L<sup>-1</sup> of 1 M glucose, H<sub>2</sub>O.
- LB media: 10 g L<sup>-1</sup> tryptone, 5 g L<sup>-1</sup> yeast extract, 10 g L<sup>-1</sup> NaCl, H<sub>2</sub>O, pH 7.0.
- LB agar: 10 g L<sup>-1</sup> tryptone, 5 g L<sup>-1</sup> yeast extract, 10 g L<sup>-1</sup> NaCl, H<sub>2</sub>O 15g L<sup>-1</sup> Agar, pH 7.0.

#### 6.1.1.2 Buffers

- Inoue transformation buffer: 10.88 g L<sup>-1</sup> MnCl<sub>2</sub>, 2.2 g L<sup>-1</sup> CaCl<sub>2</sub>, 18.65 g L<sup>-1</sup> KCl, 20 mL L<sup>-1</sup> of 500 mM 1,4-piperazinediethanesulfonic acid (pH 6.7), H<sub>2</sub>O.
- Buffer A: 50mM Tris-HCl, pH 8, 1 mM EDTA, 10 mM DTT.
- Buffer B: 50mM Tris-HCl, pH 8, 1 mM EDTA, 10 mM DTT, 2 M urea.
- Buffer C: 50 mM Tris-HCl, pH 8, 1 mM DTT and 6 M urea.

- 5x Laemmli buffer: 0.312 M Tris-Cl pH 6.8, 0.05 % bromophenol blue, 50 % glycerol, 10 % SDS, 25 %  $\beta$ -mercaptoethanol.
- SDS buffer: 25 mM Tris-base pH 8.8, 192 mM glycine, 0.1 % SDS.
- TAE: 40mM Tris, 20mM Acetate, pH 8.6, 1mM EDTA.
- 5x DNA loading dye: 10mM Tris-Cl pH 7.6, 0.03% bromophenol blue, 0.03% xylene cyanol FF, 60% glycerol, 60mM EDTA.

### 6.1.2 General apparatus

**Organic chemistry:** IR spectra were recorded using a Bruker Alpha FTIR spectrometer. NMR spectra were recorded at 400MHz for 0.2mol L<sup>-1</sup> solutions in CDCl<sub>3</sub> or *d*6-DMSO, on a Bruker Avance 400MHz. <sup>13</sup>C NMR spectra were acquired at 101 MHz. All analytical High pressure liquid chromatography (HPLC) was carried out on an Agilent Technologies 1200 Infinity with a Kinetex 5  $\mu$ m XB-C18 100 Å, Column 100 x 4.6 mm (Solvent system specified for particular compounds/experiments).

**Molecular biology:** Protein and DNA concentrations were determined using a Thermo Scientific Nanodrop 2000 spectrophotometer. Cell lysis was carried out using a Bandelin Sonopuls HD2070 probe sonicator. The fluorescent gel scanner used was a Typhoon 8600 Variable Mode Imager. Fast protein liquid chromatography (FPLC) was carried out on ÄKTAFPLC system (GE healthcare, UK)

**Nanolithography:** The AFM used was a FlexAFM with a C3000 controller (Nanosurf, Liestal, Switzerland) and has a nominal translation range of 100  $\mu$ m in *x*- and *y*-axes and 10  $\mu$ m in the *z*-axis. The probe arrays were mounted on a custom made array holder in place of a conventional cantilever chip holder. The AFM was placed above a custom built (by Nanosurf) five-axis translation stage with a maximum *x*, *y* and *z* traverse of 72 mm, 46 mm and 5 mm, respectively; and a step resolution of 0.3  $\mu$ m, 0.3  $\mu$ m and 0.1  $\mu$ m, respectively. The stage is able to tilt in both  $\theta$  and  $\phi$  axes across 10 ° with a maximum resolution of 0.3 m°.

Incorporated into the sample stage are three metal foil strain gauge load cell sensors (FUTEK, Irvine, CA, USA), each with a sensitivity of 2  $\mu\text{N}$ . The software code was written in LabVIEW V13.0 (32-bit). A user interface is built up to allow the operator to define as inputs the coarse and fine step lengths, angle step, and the path for data storage. The outputs are given by a real-time amplitude figure and an Excel file containing the results and all the force and positional data gathered during the alignment procedure. In order to incorporate the force measurements into the routine above, the USB DLL (Dynamic Linking Library) supplied by FUTEK is used for the LabVIEW software to acquire the data input from the sensors. The output from the software algorithm is used to control the  $z$ ,  $\theta$  and  $\phi$  of the sample stage through an existing DLL for the Simple Control Unit (SCU) product family (USB version). Ramen microscope used was inVia confocal (Renishaw plc, UK). Microscopy with fluorescent excitation was Fluorescent Stereo Microscope, (Leica Microsystems GmbH, Germany).

### 6.1.3 General molecular biology methods

#### 6.1.3.1 Polymerase chain reaction (PCR)

Generally, PCR was carried out by employing the following conditions, although primer annealing temperature and concentration of DMSO were varied in each individual reaction, as per the manufacturers protocol.

Polymerase chain reaction conditions	Temperature ( $^{\circ}\text{C}$ )	Time (s)	Cycles
Initial denaturation	98	90	1
Denaturation	98	10	
Annealing	Variable	20	30
Extension	72	180	
Final extension	72	300	1

**Table 6.1** PCR reaction profile.

<b>Polymerase chain reaction reagents</b>	<b>Volume (<math>\mu</math>l)</b>
Water	14.75
5x Phusion HF Buffer	5
10 mM dNTPs	0.5
10 mM Forward Primer	0.5
10 mM Reverse Primer	0.5
Template DNA	2
DMSO	1
Additional MgCl <sub>2</sub>	0.5
Phusion polymerase	0.25

**Table 6.2** PCR master mix (2  $\mu$ l total).

### 6.1.3.2 DNA electrophoresis

Agarose (1.0 g) was dissolved in TAE (100 mL) on heating. After cooling to 50°C ethidium bromide (2  $\mu$ l, 10 mg/ml) was added to the mixture and thoroughly mixed. This was then poured into a gel casting cassette along with a well comb. Once the gel had set, the well comb was detached and the gel immersed in TAE in a gel electrophoresis tank. DNA samples were loaded along with 5x DNA loading dye and subject to gel electrophoresis alongside a 1 kb DNA ladder. Usually, gel electrophoresis was performed at 110 V for 35 minutes. Gels were visualised using a UV transilluminator.

### 6.1.3.3 SDS-PAGE

SDS-PAGE gels were made up according to the procedure below:

Stock solution	Separating gel (10 %)	Stacking gel (4 %)
Water	3.8 mL	3.1 mL
1.5M Tris-Cl pH 8.3	2 mL	-
0.5M Tris-Cl pH 6.8	-	1.25 mL
30% Acrylamide	2mL	0.5 mL
10% APS	80 $\mu$ L	50 $\mu$ L
TEMED	8 $\mu$ L	5 $\mu$ L
10% SDS	80 $\mu$ L	50 $\mu$ L

**Table 6.3** SDS-PAGE gel components.

Protein samples were mixed with 5x Laemmli buffer to 1x concentration and were denatured at 95°C for 7 minutes then loaded. SDS-PAGE electrophoresis was then conducted in 1x SDS buffer in a SDS-PAGE tank at 150 V until the dye had reached the bottom of the gel before staining with protein stain.

### 6.1.3.4 Extraction of DNA from Agarose gel

The anticipated DNA fragments were cut from the gels using a razor blade and extracted using a QIAquick Gel Extraction Kit. Protocols followed were as described in the QIAquick Gel Extraction kit manual. DNA was eluted with 50  $\mu$ l nuclease free H<sub>2</sub>O.

### 6.1.3.5 Gibson assembly

Gibson assembly<sup>192</sup> was carried out by employing the following conditions:

<b>5X ISO buffer</b>	
1 M Tris-HCl pH 7.5	3 ml
2 M MgCl <sub>2</sub>	150 $\mu$ L
100 mM dGTP	60 $\mu$ L
100 mM dATP	60 $\mu$ L
100 mM dTTP	60 $\mu$ L
100 mM dCTP	60 $\mu$ L
300 $\mu$ L	1 M DTT
PEG-8000	1.5 g
100 mM NAD	300 $\mu$ L
Water	to 6 ml

**Table 6.4** 5X ISO buffer components.

<b>Gibson assembly master mix</b>	
5X ISO buffer	320 $\mu$ L
10 U/ $\mu$ L T5 exonuclease	0.64 $\mu$ L
2 U/ $\mu$ L Phusion polymerase	20 $\mu$ L
40 U/ $\mu$ L Taq ligase	160 $\mu$ L
Water	to 1.2 ml

**Table 6.5** Gibson assembly master mix components.

To a 1.5mL tube, 100 ng of each of the gel purified DNA fragments for assembly were added together and water added to a final volume of 10  $\mu$ l. 10  $\mu$ l Gibson assembly master mix was then added. This mixture was gently mixed and incubated at 50 °C for 60 min. The resulting mixture was then used directly for transformation.

#### **6.1.3.6 Transformation of chemically competent bacterial cells**

Generally, a 30  $\mu\text{L}$  aliquot of chemically competent bacterial cells (of the appropriate strain) were thawed on ice and subsequently added to 1  $\mu\text{L}$  of plasmid DNA (1-25 ng in water) or 4  $\mu\text{L}$  of assembly product (40 ng). This mixture was then incubated on ice for 30 min then at 42°C. The mixture was then placed back on ice for 2 min, after which 950  $\mu\text{L}$  of room temperature SOC media was added and the cells subject to incubation at 37 °C with shaking at 200 rpm for 1 h. Aliquots of the incubated cells (10  $\mu\text{L}$ , 50  $\mu\text{L}$ , 300  $\mu\text{L}$ ) were then spread onto pre-warmed LB agar plates (containing the appropriate selection antibiotic) and incubated overnight at 37 °C.

#### **6.1.3.7 Preparation of chemically competent bacterial cells**

In a sterile environment, 5  $\mu\text{L}$  aliquots of the bacterial cells (of the appropriate strain) were streaked onto LB agar plates (containing appropriate antibiotic if necessary) and incubated overnight at 37 °C. Single colonies were inoculated into SOB media (25 mL) then incubated overnight at 37 °C with shaking at 200 rpm. 1 mL of starter culture was then inoculated into SOB media (250 mL) and incubated at 20°C with shaking at 200 rpm until the  $\text{OD}_{600}$  reached 0.55. The cultures were then placed on ice for 10 min and pelleted by centrifugation (2500 x g, 10 min, 4 °C). The supernatants were discarded and the cells gently resuspended in Inoue transformation buffer (80 mL), the washed cells were then harvested by centrifugation (2500 x g, 10 min, 4 °C). The supernatants were again discarded and the cells gently resuspended in Inoue transformation buffer (20 mL), with swirling DMSO (at 37 °C) was added to a final concentration of 7% (v/v) and the cells incubated on ice for 10 min. The resulting solutions were then aliquoted (50  $\mu\text{L}$ ) into chilled (0 °C) tubes, flash-frozen with liquid nitrogen and stored at -80 °C.



#### **6.1.3.8 Plasmid DNA isolation and purification**

Single colonies of *E. coli* cells (of various strains, transformants from antibiotic selection) were used to inoculate 5 mL LB (containing appropriate selection antibiotics) and incubated with shaking (37 °C, 200 rpm over 12 h), plasmid DNA was extracted using using a QIAprep Spin Miniprep kit. Protocols followed were as described in QIAprep Spin Miniprep kit manual. DNA was eluted with 50  $\mu$ l EB (10 mM Tris-Cl pH 8.5) buffer. The eluted DNA was sequenced and the concentration determined by spectrophotometer.

#### **6.1.3.9 Glycerol stock preparation**

Single colonies of *E. coli* cells (of various strains, transformants from antibiotic selection) were used to inoculate 5 mL LB (containing appropriate selection antibiotics) and incubated with shaking (37 °C, 200 rpm over 12 h), a 50 % (v/v) solution glycerol was added to a final concentration of 25 % glycerol. This solution was then aliquoted (1000  $\mu$ L) into chilled (0 °C) tubes, flash-frozen with liquid nitrogen and stored at -80 °C.

#### **6.1.3.10 Restriction digestion of DNA**

Generally, restriction digestions were carried out by employing the following conditions although specific digestion buffer (NEB 1.1, 2.1, 3.1 and 'CutSmart', New England Biolabs) and reaction temperature/time (commonly 37 °C, 1 h) were varied depending on optimal conditions specified by the manufacturer for the specific restriction enzyme combination.

<b>Restriction digest mix</b>	
DNA	2.5 ug
10x Digestion buffer	5 µL
1st Restriction enzyme	2.5 µL
2nd Restriction enzyme	2.5 µL
Water	to 50 µL

**Table 6.6** Restriction digest mix.

Once the reaction reacted competition, the reaction mixture would be subject to DNA electrophoresis and analysed or purified as described elsewhere.

## 6.2 Methods for Chapter 2

### 6.2.1 Production of ybbR-C1A

ybbR-C1A (see plasmid map Figure 2.2A) was heterologously produced as *N*-terminal hexahistidine tagged proteins using standard methods in *E. coli*.<sup>193</sup> Briefly, the plasmid pET28a\_ybbR\_C1A was transformed into *E. coli* BL21(DE3). Cells were grown to an optical density of 0.6 OD<sub>600</sub>, then gene expression was induced by the addition of  $\beta$ -D-1-thiogalactopyranoside (0.1 mM) at 37 °C for 3 h after which the cells were collected by centrifugation (4000 g for 15 min) and the supernatant removed.

### 6.2.2 Purification of ybbR-C1A

Cells from cultures were resuspended in Buffer A (section 6.1.1.2) , left to stand for 1h at 4°C then lysed by sonication (5 x 30 s). The suspension was then collected by centrifugation (8000 g for 40 min) and supernatant removed. The pellet was then solubilised in Buffer B and subjected to centrifugation (8000 g for 40 min) and supernatant removed. The washed inclusion bodies were finally solubilised in Buffer C and subjected to centrifugation (8000g for 40 min). The solubilised inclusion bodies were then purified by IMAC under denaturing conditions in Buffer C. The purified denatured protein (final concentration 0.18 mg/mL) were then added drop-wise to refolding buffer (1.7 M urea, 2 mM CaCl<sub>2</sub>, 7% glycerol, 0.35 mM oxidised glutathione 0.044 mM dithiothreitol) and stirred for 16 h. The solution was then filtered (0.2  $\mu$ m pore) to remove aggregated protein and purified by IMAC.

Refolded apoprotein was then reconstituted with heme by drop wise addition of hemin (1 mM solution in 20 mM NaOH). Dropwise addition of hemin was continued until rate with peroxidase activity assay (section 6.2.4) showed no increase. Aliquots of 1  $\mu$ L were diluted with assay buffer (50 mM NaOAc pH 4.5) 1:100 and 10  $\mu$ L used.

The refolded holoprotein was then buffer exchanged by centrifugal filtration (10,000 molecular weight cut off (MWCO) into 50 mM succinate buffer pH 5.5 and then further

purified applying it to 2-naphylhydroxamic acid functionalised agarose at a flow rate of 1mL per minute. The protein was then eluted with 50mM succinate buffer, pH 5.5, 200 mM borate. The pure protein was then buffer exchanged into TBS and concentrated. Giving an RZ ( $A_{404}/A_{280}$ ) of 2.93 from an original RZ of 1.10 (maximum RZ 3.42<sup>126</sup>)

### 6.2.3 Synthesis of agarose Immobilised 2-naphylhydroxamic acid

Method adapted from literature.<sup>33</sup> Affi-Gel 10 (Bio-Rad) (6 g) was washed with water then suspended in a solution of 6-amino-2-naphthoic acid (300mM) dissolved in 50 mM succinate buffer pH 4.5 (100 mL) and DMF (100 mL). The suspension was the gently mixed for 15 h at room temperature. The gel was washed with 50% DMF/succinate buffer (200 mL), then water (200 mL). The gel was then suspended in a solution of p-nitrophenol (40 mM) and EDAC (12.6 mM) in 25% (v/v) aqueous acetone and stirred for 1 h maintaining the pH at 5 using HCl (1 M). The gel was then washed with aqueous HCl (pH 5) on a sintered-glass funnel until no p-nitrophenol could be detected in the filtrate. The gel was then suspended in water (300 mL) and added to a solution of hydroxylamine hydrochloride (41 g) in NaOH (1M, 300 mL) and stirred for 2 h. The gel was washed thoroughly with water followed by 50 mM succinate buffer pH 4.5 and analysed by UV/Vis using methods from the original synthesis.<sup>33</sup>

### 6.2.4 Peroxidase activity assay (ABTS)

In a 96 well plate, assay solution (150  $\mu$ L) consisted of 50 mM NaOAc pH 4.5, 0.77 mM hydrogen peroxide, 1.00 mM, 2,2'-azino-bis(3-ethylbenzothiazoline-6-sulfonic acid) (ABTS), peroxidase (10  $\mu$ L) was dispensed. The reaction was then shaken for 5 s and the absorption at 405 nm monitored for 15 minutes.

### 6.2.5 Conducting polymer enzyme synthesis<sup>86</sup>

A solution of 6 mM aniline monomer (aniline, 2-methoxyaniline, 3-(prop-2-yn-1-yloxy)aniline or 2,5-dimethoxyaniline) in 100 mM sodium phosphate buffer solution of pH 4.3 was assembled. Hydrogen peroxide added to a final concentration of 3.5 mM. The reaction was initiated by the addition of ybbR-C1A to a final concentration of 25 U mL<sup>-1</sup> (stock solution 1 mg/mL). After the addition of HRP, the reaction was left stirring for 6 h, and then the final solution was dialysed (MWCO of 2000 kDa) against 0.1 M HCl overnight. The remaining solid was washed with water and dried. Solids were analysed by IR spectroscopy.

### 6.2.6 Conducting polymer chemical synthesis

To a 6 mM solution of aniline monomer (aniline, 2-methoxyaniline, 3-(prop-2-yn-1-yloxy)aniline or 2,5-dimethoxyaniline) in 100 mM sodium phosphate buffer solution of pH 4.3, ammonium persulfate was added to a final concentration of 6 mM to initiate the reaction. After the addition of ammonium persulfate, the reaction was left stirring for 6 h, and then the final solution was dialysed (MWCO of 2000 kDa) against 0.1 M HCl overnight. The remaining solid was washed with water and dried. Solids were analysed by IR spectroscopy.

### 6.2.7 Fluorescent labelling of ybbR-C1A

The reaction mixture was prepared as follows:

	Volume	Final concentration
<b>Water</b>	to 50 $\mu$ L	
<b>1M sodium phosphate buffer pH 7.4</b>	2.5 $\mu$ L	50 mM
<b>50mM MgCl<sub>2</sub></b>	10 $\mu$ L	10 mM
<b>Sfp 250mM</b>	1 $\mu$ L	5 mM
<b>ybbR_HRP</b>	13.3 $\mu$ L	20 $\mu$ M
<b>250 <math>\mu</math>M CoA-488 (NEB)</b>	2 $\mu$ L	10 $\mu$ M

**Table 6.7** Fluorescent labelling master mix.

This reaction mixture was then incubated in the dark for 60 minutes at 37°C. SDS-PAGE gel electrophoresis was carried out on the samples and fluorescence detected using a fluorescent gel scanner at wavelength 488nm.

### **6.2.8 Surface Linker synthesis on silicon nitride (AFM probes)**

Silicon nitride surfaces were first cleaned by washing in chloroform (3 x 5 min) and dried in a stream of nitrogen. The surface was then ozone cleaned for 2 h to oxidise the surface. The surfaces were then functionalised<sup>194</sup> by submerging in a pre-degassed solution of ethanolamine hydrochloride (5 M) in DMSO for 20 h. They were then washed in DMSO 1mL (3 x 5 min) then ethanol 1 mL (3 x 5 min) and dried with nitrogen. NHS-PEG-Mal (N-hydroxysuccinimidyl-75-N-(3-maleimidopropionyl)-amido-4,7,10,13,16,19,22,25,28,31,34,37,40,43,46,49,52,55,58,61,64,67,70,73-tetracosaoxapentaheptacontanoate) (1 mg) was dissolved in chloroform (0.5 mL) and the surfaces submerged in the solution for 2 h at RT. After the surfaces were washed with chloroform 1 mL (3 x 10 min) and then dried with nitrogen.

To functionalise with CoA, the PEG-maleimide conjugated surfaces were then submerged in a solution of CoA (10 mM) in 50 mM sodium phosphate pH 7.4 for 4 h. The surfaces were then washed in 50 mM HEPES pH 7.2 (3mL, 3 x 5 min). The remaining maleimides were blocked by incubating in a solution of 2-mecaptoethanol (20 mM) in 50 mM sodium phosphate pH 7.4 for 4 h. The surfaces were then washed in water (3 x 5 min) and submerged in a solution of 2-mecaptoethanol 80 mM in water. Enzyme conjugation was carried out as previously detailed (see section 6.2.7).

### **6.2.9 ABTS assay on silicon nitride surfaces**

Silicon nitride surfaces ( $50\ \mu\text{m} \times 450\ \mu\text{m}$ ) were subjected to conditions previously detailed to produce functional surfaces with immobilised ybbR-C1A. These surfaces were then attached to the side of the wells in a 96 well microtiter plate and 150  $\mu\text{L}$  of assay solution (50 mM sodium acetate at pH 4.5, 0.77 mM hydrogen peroxide, 1.00 mM ABTS) added to each well. Following which, the absorbance at 405 nm was read every 15 s with the plate shaken between each reading.

### **6.2.10 Tip apex CoA confinement on silicon nitride (AFM probes)**

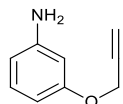
Maleimide-functionalised AFM cantilevers were brought into contact (set point 20 nN) with a surface of a silicon wafer spin coated with CoA, the cantilevers were then scanned over the surface in a  $10 \times 10\ \mu\text{m}$  area (2 s per line) for 1 h at 60 % relative humidity. Any unreacted maleimide groups were then blocked by submerging the cantilever in a 20 mM 2-mercaptoethanol solution for 2 h. The array was then washed in water (3 x 5 min) and submerged in a solution of 2-mercaptoethanol 80 mM in water. Enzyme loading was carried out as previously detailed (section 5.2.7).

### **6.2.11 Single probe biocatalytic nanolithography (on mica and ATP surface)**

In general, AFM probes immobilised with ybbR-C1A were mounted on to the AFM scan head using the conventional AFM probe holder. Either mica or 4-aminobenzenethiol functionalised gold surfaces were mounted at the bottom of a  $1.5 \times 1.5 \times 0.5\ \text{cm}$  fluid well positioned on the sample stage. 0.01-10 mM solution of enzyme substrate (2-methoxyaniline ) in 50 mM acetate buffer at pH 5 sufficient to submerge the surface (approximately 1 mL). 100  $\mu\text{L}$  of this solution was transferred to the probe holder (to ensure liquid-liquid contact. The probe was then brought into contact with the surface and the topography of the surrounding area recorded, hydrogen peroxide was then added to a final

concentration of 0.01-5 mM. The probe was then actuated in a lithographic pattern for a set time (0.1- 300 s) after which the topography of the area was recorded.

### 6.2.12 Synthesis of enzyme substrates: 3-(prop-2-yn-1-yloxy)aniline<sup>195</sup>



3-nitrophenol (2.75 g, 0.0198 mol) was dissolved in diethyl ether (20 mL) at room temperature and potassium carbonate (3.17 g, 0.023 mol) was added. The mixture was stirred for 10 min. After which time propargyl bromide (2.5 mL, 22 mmol) was added, a condenser fixed and the mixture was then heated to reflux for 5 h. Upon completion the reaction was cooled to room temperature and water (5 mL) added to terminate the reaction. The organic phase was washed with water (2x 20 mL), brine (2 x 10 mL) and saturated potassium carbonate solution (20 mL). The organic phase was then dried over anhydrous magnesium sulfate, filtered and the solvent removed under vacuum to yield 1-nitro-3-(prop-2-yn-1-yloxy)benzene (2.409 g, 0.0136 mol, 69 %) as an orange solid and used directly in the next step.

1-nitro-3-(prop-2-yn-1-yloxy)benzene (0.147 g, 0.00083 mol) and iron powder (0.279 g, 5.00 mmol) were suspended in a solution of glacial acetic acid (2 mL), ethanol (2 mL) and water (1 mL). The resulting suspension was sonicated at 30 °C and the reaction was monitored with TLC. Upon completion (2 h), the solution was filtered, the solids washed with ethyl acetate (30 mL). The combined filtrate and washings were partitioned with potassium hydroxide (2 M, 20 mL) and aqueous phase further extracted with ethyl acetate (2 x 25 mL). The combined organic phase washed with brine (2 x 25 mL), followed by water (3 x 50 mL), dried over anhydrous magnesium sulfate, filtered and the solvent removed under vacuum. Flash chromatography (SiO<sub>2</sub>, hexane: ethyl acetate; 2:1) yielded 3-(prop-2-yn-1-yloxy)aniline (0.057 g, 0.00039 mol, 47 %) as a yellow oil. Rf: 0.41 (hexane: ethyl acetate; 2:1), <sup>1</sup>H NMR (400 MHz, CDCl<sub>3</sub>) δ 7.07 (t, J = 8.0 Hz, 1H), 6.39 (ddd, J = 8.2, 2.4, 0.7 Hz, 1H), 6.33 (ddd,



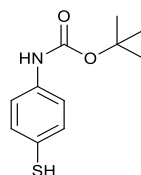
$J = 7.9, 2.1, 0.8 \text{ Hz, 1H}$ ), 6.30 (t,  $J = 2.2 \text{ Hz, 1H}$ ), 4.64 (d,  $J = 2.4 \text{ Hz, 2H}$ ), 3.65 (s, 2H), 2.53 (t,  $J = 2.4 \text{ Hz, 1H}$ );  $^{13}\text{C NMR}$  (101 MHz,  $\text{CDCl}_3$ )  $\delta$  158.77, 147.89, 130.16, 108.81, 104.70, 102.04, 78.89, 75.44, 55.70;  $m/z$  (ESI<sup>+</sup>-TOF) 148.1 (100)  $\text{C}_9\text{H}_{10}\text{NO}^+$  ( $\text{MH}^+$ ), HRMS found 148.0754;  $\text{C}_9\text{H}_{10}\text{NO}^+$  ( $\text{MH}^+$ ) requires 148.0760. Analytical data is consistent with the literature.

### 6.2.13 4-aminobenzenethiol functionalised gold surface preparation

Gold substrates (2 nm titanium adhesion layer, 10 nm gold on aluminasilicate glass microscope slide) were immersed in a freshly prepared 5 mM solution of 4-aminothiophenol in ethanol under an argon atmosphere and allowed to react for 96 h at room temperature. After which the surfaces were washed in ethanol (3x 5 min) followed by sonication in ethanol for 1 minute, further washed with a stream of ethanol (1 min) and dried with a stream of anhydrous nitrogen. Surfaces were kept under vacuum and used within 2 weeks of preparation.

### 6.2.14 4-aminobenzenethiol functionalised silicon oxide surface preparation

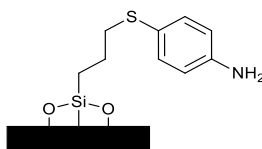
#### 6.2.14.1 *tert*-butyl (4-mercaptophenyl)carbamate<sup>196, 197</sup>



To a stirred slurry of di-*tert*-butyl dicarbonate (0.554 g, 2.5 mmol) and Indium chloride (0.009 g, 0.025 mmol, 1% mol), 4-aminobenzenethiol (0.313 g, 0.0025 mol) was added and heated at 35 °C. The reaction was monitored by TLC and was observed to be complete after 1 h. The resulting reaction mixture was diluted with ethyl acetate (25 mL) and washed with water (3x 25 mL). The organic phase was dried over anhydrous magnesium sulfate, filtered and the solvent removed under reduced pressure. Flash chromatography ( $\text{SiO}_2$ , hexane: ethyl

acetate; 2:1) yielded *tert*-butyl (4-mercaptophenyl)carbamate (0.545 g, 0.0024 mol, 97%) as a white solid. Rf: 0.36 (hexane: ethyl acetate; 2:1), Mp: 179-180°C.  $^1\text{H}$  NMR (400 MHz,  $\text{CDCl}_3$ )  $\delta$  7.39 (d,  $J = 8.7$  Hz, 2H), 7.29 (d,  $J = 8.7$  Hz, 2H), 6.48 (s, 1H), 1.57 (s, 1H), 1.51 (s, 9H);  $^{13}\text{C}$  NMR (101 MHz,  $\text{CDCl}_3$ )  $\delta$  152.60, 138.53, 131.14 (2C), 130.96, 119.05 (2C), 81.02, 28.46 (3C);  $m/z$  (ESI $^+$ -TOF) 226.1  $\text{C}_{11}\text{H}_{16}\text{NO}_2\text{S}^+$  ( $\text{MH}^+$ ). Analytical data is consistent with the literature.

#### 6.2.14.2 4-ATP surface modification



Atomically flat microarray slides were  $\text{O}_2$  plasma cleaned for 1 min immediately prior to use, the surfaces were then immersed in a freshly prepared 1% v/v solution of (3-iodopropyl)trimethoxysilane in anhydrous toluene under an argon atmosphere. The surfaces were allowed to react for 24 h at 80°C. After which the surfaces were washed in anhydrous toluene (3x 5 min) followed by sonication in anhydrous acetone for 1 minute, further washed with a stream of acetone (1 min) and dried with a stream of anhydrous nitrogen. Finally the surfaces were annealed at 130 °C for 10 min.

Freshly prepared (3-iodopropyl)trimethoxysilane functionalised surfaces were immersed in a freshly prepared solution of *tert*-butyl (4-mercaptophenyl)carbamate (50 mM in anhydrous methanol) under an argon atmosphere. The surfaces were allowed to react for 96 h 60 °C. After which the surfaces were washed in with 2-propanol (3x 15 min), acetone (3x 15 min) and dried under a stream of anhydrous nitrogen.

*Tert*-butyl (4-mercaptophenyl)carbamate terminated surfaces were then immersed in a solution hydrochloric acid (4 M in 1,4-dioxane) under an argon atmosphere. The surfaces were allowed to react for 12 h at room temperature. After which the surfaces were washed in

1,4-dioxane (3 x 15 min), acetone (3 x 15 min) and dried with a stream of anhydrous nitrogen. Surfaces were kept under vacuum and used within 2 weeks of preparation.

### 6.2.15 Surface Linker synthesis on polydimethylsiloxane (PDMS) probe arrays

PDMS probe arrays (50  $\mu\text{m}$  or 100  $\mu\text{m}$  pitch) were freshly peeled off the master and oxygen plasma cleaned for 30 s at 200 mTorr. Arrays and an empty glass vial were then immediately placed inside a desiccator under an argon atmosphere and 100  $\mu\text{L}$  (3-aminopropyl)triethoxysilane added to the vial. The vessel was then evacuated to 2-3 Torr and incubated overnight at room temperature. The surfaces were then removed and cured at 110  $^{\circ}\text{C}$  for 10 min, before washing with DMSO (3 x 5 min), rinsing with an ethanol stream and drying under a stream of nitrogen. The surfaces were then submerged in a 5mM solution of Mal-PEG-NHS in DMSO for 2 h at room temperature with gentle agitation. After which they were washed, rinsed and dried as previously. The surfaces were then submerged a solution of CoA (8 mM CoA, 4 mM TCEP in 50 mM sodium phosphate at pH 7.4) for 4 h at room temperature followed by washing with 50 mM sodium phosphate pH 7.4 (3 x 5 min). Remaining maleimides groups were blocked by incubation in a solution of 80 mM 2-mercaptoethanol in 50 mM sodium phosphate at pH 7.4 for 4 h. The surfaces were then washed in 50 mM HEPES pH 7.4 (3x 5 min).

### 6.2.16 ybbR-C1A enzyme immobilisation

The reaction mixture was set up as follows:

	Volume	Final concentration
50mM sodium phosphate pH 7.4	to 100 $\mu\text{L}$	
50 mM $\text{MgCl}_2$	30 $\mu\text{L}$	10 mM
<i>Sfp</i> 250 mM	1 $\mu\text{L}$	5 mM
<i>ybbR-C1A</i>	13.3 $\mu\text{L}$	20 $\mu\text{M}$
TCEP 40 mM	3.75 $\mu\text{L}$	1 $\mu\text{M}$

**Table 6.8** *ybbR-C1A* immobilisation master mix.

Reaction mixture was pipetted on to CoA-functionalised surfaces, incubated at 37 °C for 2 h at 100% relative humidity. Surfaces were then washed with 50mM sodium phosphate, pH 7.4 with 0.5% tween (3x 15 min), 50 mM sodium phosphate, pH 7.4 (3x 5 min) finally rinsing with 50 mM sodium phosphate, pH 7.4. Arrays were stored in 50 mM HEPES pH 7.4 and used within one week. Surfaces were rinsed with water prior to use.

#### **6.2.16 Probe apex CoA confinement on PDMS probe arrays**

An 8 mM CoA solution in water was drop-coated on to half a silicon wafer (4 x 2 cm). A Mal-PEG-NHS functionalised array was then aligned (using auto alignment software) to the clean side of this surface. Upon completion of the alignment the stage was retracted on its z-axis and moved in its y/x-axis until the array was over the drop-coated area. The humidity was set at 40 % and the stage was then moved in its z-axis until contact was observed (using minimum force or visual inspection). Contact was held for 5 min then the stage retracted in its z-axis and the stage moved diagonally on the x/y-axis 10  $\mu$ m. This was repeated twice, following which the array was incubated at 60 % humidity for 2 h. The array was then washed in water (3 x 5 min) and submerged in a solution of 80 mM 2-mecaptoethanol in water. Enzyme loading was carried out as previously detailed.

#### **6.2.17 Activity assay on HRP immobilised PDMS probe arrays**

The ybbR-C1A conjugated arrays were then attached to the bottom wells in a 24-well microtiter plate and 500  $\mu$ L of assay solution (50 mM sodium acetate pH 4.5, 0.77 mM hydrogen peroxide, 1.00 mM ABTS) added to each well. Following which, the absorbance at 405 nm was read every 15 s with the plate shaken between each reading.

### 6.2.18 Multiplexed biocatalytic nanolithography (on 4-ATP surfaces)

In general probe arrays immobilised with ybbR-C1A were rinsed with water and the glass support dried with a stream of nitrogen. The array was then mounted on to the AFM scan head using double-sided tape and the substrate (either 4-aminobenzenethiol functionalised silicon oxide/gold surfaces) was mounted at the bottom of a 1.5 x 1.5 x 0.5 cm fluid well and subsequently on to the sample stage also using double-sided tape. This fluid well was then filled with a 2.6 mM solution of enzyme substrate (2-methoxyaniline or 3-(prop-2-yn-1-yloxy)aniline) in 50 mM acetate buffer at pH 5 sufficient to submerge the surface (approximately 3 mL). Alignment was performed using the described algorithm (as described in section 6.2.21).<sup>133</sup> The array was then retracted and hydrogen peroxide added to a final concentration of 1 mM (4 mL). The array was then very rapidly brought within 10s of nanometres of the surface and patterning commenced with a predefined template to produce the desired pattern using the standard lithography software provided with the AFM (Nanosurf AG, Switzerland). Patterning was undertaken at 60% relative humidity (to prevent evaporation) with a dwell time of 0.5 - 10 s per dot feature (lines were constructed by closely spaced features). Upon completion the array was immediately removed from the solution. The substrate was then removed and washed by submerging in 50 mM acetate buffer pH 5 (3 x 5 min) followed by 1 M HCl (3 x 5 min) and finally water (3 x 5 min); dried under a stream of nitrogen and immediately imaged in lateral force mode.

### 6.2.19 Raman mapping experiments

Lithography was carried out on 4-aminobenzenethiol functionalised gold surfaces using a freshly prepared solution of 2.6 mM 2-methoxyaniline in 50 mM acetate buffer at pH 5. Features were produced with a dwell time of 2 s per dot feature, using a predefined pattern. Upon completion of lithography, surfaces were submerged in 50 mM acetate buffer pH 5 (3 x 5 min) followed 1M HCl (3 x 5 min) and finally water (3 x 5 min) before drying under a stream of nitrogen, and immediately visualised under a Raman microscope using a 532 nm laser.

### **6.2.20 Post lithography fluorescence functionalisation (3-(prop-2-yn-1-yloxy)aniline substrate)**

Post lithography surfaces were then submerged in a solution of 1 mM Azide-fluor 488 (Sigma Aldrich), 0.1 mM copper(I) iodide dissolved in water in complete darkness for 24 h at room temperature. Surfaces were then washed in water (6 x 15 min), dried under a stream of nitrogen and immediately visualised by microscopy with fluorescent excitation at 488 nm

### **6.2.21 Probe array alignment algorithm**

#### **6.2.21.1 Z-position measurement**

The algorithm employed an iterative approach-observe-withdraw-adjust process. For any particular tilt angle, the instrument gradually moves the probes towards the substrate surface to determine the point at which the threshold force is detected by the load cells (typically set at 490  $\mu\text{N}$ ). The algorithm contact between the probes and the surface. The approach is performed in a stepwise manner with the step size defined by a subroutine. Once the amount of force reaches the pre-set threshold, the z-position is stored. The tilt angle is then altered by a pre-set step (typically 50  $\text{m}^\circ$ ) and the next measurement commenced, starting from the stored z-position.

#### **6.2.21.2 The detection of the amount of force.**

In order to detect a clear signal from the force measurements indicating contact with the surface, the AFM scanner is set to oscillate the probes 10  $\mu\text{m}$  along the z-axis every 0.7 s. Under an ADC sampling rate of 25 points per second, all the force data obtained in this single 0.7 s period are saved in an array. The difference between the maximum and the minimum values in an array are determined, denoting the “amplitude”. To avoid interference from background noise (typically  $\pm 49 \mu\text{N}$  in a single 0.7 s period), the difference between the maximum and minimum amplitude is set to 98  $\mu\text{N}$ . Thus, for the pre-set force threshold of 490  $\mu\text{N}$ , only amplitude maxima larger than 588  $\mu\text{N}$  are recorded as contact. In order to

further verify if the desired force threshold has been reached, the measurements of three periods are taken. If all three measurements indicate that the force threshold has been reached, then the z-position is obtained. If the required value is not reached, the probe array is lowered (i.e. z-position is increased) by another step (see below) and the routine repeated.

#### **6.2.21.3 Selection of z-position step lengths.**

The alignment procedure applies several criteria in selecting the z-position step size. When the amount of force measured is below the pre-set 490  $\mu\text{N}$  threshold, a large step length (typically 0.6  $\mu\text{m}$ ) is applied, and when it is between 490  $\mu\text{N}$  and 686  $\mu\text{N}$ , small steps (0.1  $\mu\text{m}$ ) are applied.

#### **6.2.21.4 Tilt angle and data analysis.**

To determine the direction of the tilt adjustment (i.e. whether to increase or decrease the tilt), a routine is included in the algorithm whereby at the start of the optimisation procedure for each axis, three measurements are taken and the gradient of these measurements used to determine the direction of tilt. In the flowchart, a generic angle,  $\psi$ , is used to represent either  $\theta$  (for Steps 1 and 3) or  $\phi$  (for Steps 2 and 4). At the beginning of the alignment, after the initial value of  $\psi$  is given, three measurements of the z-position are performed using large tilt steps of 400  $\text{m}^\circ$  (i.e.  $\psi - 400$ ,  $\psi$  and  $\psi + 400$   $\text{m}^\circ$ ), and thus a series of  $z(\psi_i)$ ,  $i = 1, 2, 3$  is obtained. If  $z(\psi_1) > z(\psi_2) > z(\psi_3)$  and therefore showing a downward trend, that means the maximum value lies on the left side. Hence, a smaller  $\psi$  is then used for the next determination of the z-position. Conversely, if  $z(\psi_1) < z(\psi_2) < z(\psi_3)$ , the maximum value lies on the right side and a larger  $\psi$  is used in the next iteration. This reiteration continues until the conditions  $z(\psi_1) < z(\psi_2)$  and  $z(\psi_2) > z(\psi_3)$  are satisfied, at which point the maximum z-position will lie between  $\psi_1$  and  $\psi_3$ .

Fine optimisation is then performed using a series of z-position determinations with a  $\psi$  step size of  $50 \text{ m}^\circ$  and  $N$  points of data (in this case  $N = 16$ ) between  $\psi_1$  and  $\psi_3$  are recorded. The  $\pm 150 \text{ m}^\circ$  angles are then determined. Thus, starting with  $\phi$  fixed to an arbitrary value in Step 1, the  $N$  points of data are acquired. The data fitted to two lines with the least-squares method, and their intersection calculated as  $(\theta_{\text{optimal}1}, \phi_{\text{arbitrary}})$ . In Steps 2 to 4, the general process is repeated to determine the pairs of angles  $(\theta_{\text{optimal}1} + 150, \phi_{\text{optimal}1})$ ,  $(\theta_{\text{optimal}2}, \phi_{\text{optimal}1} - 150)$  and  $(\theta_{\text{optimal}2} - 150, \phi_{\text{optimal}2})$ , respectively. The final, overall optimised angles are then calculated as the intersection of two lines drawn diagonally between the four points mentioned above.

#### **6.2.22 Polymer pen nanolithography of 16-mercaptohexadecanoic acid on gold substrates.**

The prepared PPL array was cleaned with  $\text{O}_2$  plasma (0.8 mbar) for 30 s. Arrays were inked by coating with 16-mercaptohexadecanoic acid ( $10 \mu\text{L}$ , 5 mM) in ethanol for 1 minute, after which the excess was lightly cleared with a stream of nitrogen. The PPL array and gold substrate were then mounted on the AFM and sample stage, respectively, using double-sided tape.

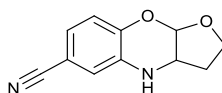
Alignment was performed using the algorithm described, followed by patterning with a predefined template to produce the desired pattern using the standard lithography software provided with the AFM. Patterning was undertaken at 40 % relative humidity at  $20 \text{ }^\circ\text{C}$  with a dwell time of 0.25 s per dot-feature. The gold substrate was then imaged in lateral force mode. Where required, the substrate was subsequently etched for 4 min with a freshly made solution of equal parts 40 mM thiourea, 27 mM Iron (III) nitrate nonahydrate and 100 mM hydrochloric acid. The substrate was then imaged under an optical microscope.



### 6.3 Methods from Chapter 3.

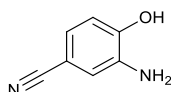
#### 6.3.1 Quinone Imine product standard and precursor synthesis

##### (1) 2,3,3a,9a-tetrahydro-4H-benzo[b]furo[3,2-e][1,4]oxazine-6-carbonitrile<sup>156</sup>



3-amino-4-hydroxybenzonitrile (0.134 g, 0.001 mol), potassium bicarbonate (0.3013 g, 0.003 mol) and 2,3-dihydrofuran (0.350 g 0.005 mol) were combined with stirring in tetrahydrofuran (2 mL) under a nitrogen atmosphere and cooled to 0 °C. A solution of (Diacetoxyiodo)benzene (0.134 g, 0.001 mol) in tetrahydrofuran (4mL), at 0 °C, was then added dropwise over 30 min. After which the solution was monitored with TLC until product formation dissipated (approximately 3 h). The solution was then filtered, the solvent removed under reduced pressure and the residue purified directly by flash chromatography (SiO<sub>2</sub>, hexane: ethyl acetate; 2:1) yielded 2,3,3a,9a-tetrahydro-4H-benzo[b]furo[3,2-e][1,4]oxazine-6-carbonitrile (0.048 g, 0.000237 mol, 23 %,) as an orange solid. <sup>1</sup>H NMR (400 MHz, CDCl<sub>3</sub>) δ 6.98 (dd, J = 8.3, 1.9 Hz, 1H), 6.89 (d, J = 8.3 Hz, 1H), 6.87 (d, J = 1.9 Hz, 1H), 5.38 (d, J = 3.6 Hz, 1H), 4.30 (td, J = 9.0, 3.9 Hz, 1H), 4.16 – 4.00 (m, 3H), 2.21 (dtd, J = 12.3, 7.6, 3.8 Hz, 1H), 1.89 (dq, J = 12.3, 8.9 Hz, 1H). <sup>13</sup>C NMR (101 MHz, CDCl<sub>3</sub>) δ 145.25, 131.40, 123.29, 119.62, 117.87, 117.46, 105.01, 96.52, 68.16, 53.96, 29.48; *m/z* (ESI<sup>+</sup>-TOF) 203.1 C<sub>11</sub>H<sub>11</sub>N<sub>2</sub>O<sub>2</sub><sup>+</sup> (MH<sup>+</sup>). Analytical data is consistent with the literature.

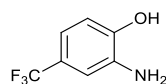
##### (2) 3-amino-4-hydroxybenzonitrile<sup>198</sup>



4-hydroxy-3-nitrobenzonitrile (1.000 g, 0.00609 mol) and palladium on activated charcoal (10 %, 0.102 g) were stirred in methanol (20 mL) under an atmosphere of hydrogen at room

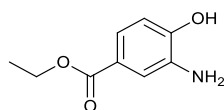
temperature for 24 h. The solution was filtered through Celite, dried over anhydrous sodium sulfate and the solvent removed under vacuum to yield 3-amino-4-hydroxybenzonitrile (0.805 g, 0.00600 mol, 98 %,.) as a brown solid.  $^1\text{H}$  NMR (400 MHz,  $\text{CDCl}_3$ )  $\delta$  7.00 (d,  $J = 1.9$  Hz, 1H), 6.98 (s, 1H), 6.75 (d,  $J = 8.4$  Hz, 1H).  $^{13}\text{C}$  NMR (101 MHz,  $\text{CDCl}_3$ )  $\delta$  142.98, 129.22, 124.06, 121.03, 118.50, 115.40, 103.90;  $m/z$  (ESI $^+$ -TOF) 135.1  $\text{C}_7\text{H}_7\text{N}_2\text{O}^+$  ( $\text{MH}^+$ ). Analytical data is consistent with the literature.

**(3) 2-amino-4-(trifluoromethyl)phenol**<sup>199</sup>



Synthesis was conducted as per the method for **(2) 3-amino-4-hydroxybenzonitrile** using 2-nitro-4-(trifluoromethyl)phenol (1.000 g, 0.00488 mol) yielded 2-amino-4-(trifluoromethyl)phenol (0.836 g, 0.00472 mol, 97 %) as an orange solid.  $^1\text{H}$  NMR (400 MHz,  $\text{CDCl}_3$ )  $\delta$  6.98 (s, 1H), 6.93 (d,  $J = 8.0$  Hz, 1H), 6.75 (d,  $J = 8.1$  Hz, 1H).  $^{13}\text{C}$  NMR (101 MHz,  $\text{CDCl}_3$ )  $\delta$  146.29, 134.71, 123.93, 116.51, 114.68, 113.45, 108.67;  $m/z$  (ESI $^+$ -TOF) 178.0  $\text{CH}_7\text{F}_3\text{NO}^+$  ( $\text{MH}^+$ ). Analytical data is consistent with the literature.

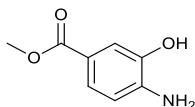
**(4) ethyl 3-amino-4-hydroxybenzoate**<sup>200</sup>



Synthesis was conducted as per the method for **(2) 3-amino-4-hydroxybenzonitrile** using ethyl 4-hydroxy-3-nitrobenzoate (1.000 g, 0.00474 mol) to yield ethyl 3-amino-4-hydroxybenzoate (0.817g, 0.00451 mol, 95%) as a brown solid.  $^1\text{H}$  NMR (400 MHz,  $\text{CDCl}_3$ )  $\delta$  7.45 (d,  $J = 2.0$  Hz, 1H), 7.41 (dd,  $J = 8.2, 2.1$  Hz, 1H), 6.74 (d,  $J = 8.2$  Hz, 1H), 4.32 (q,  $J = 7.1$  Hz, 2H), 1.36 (t,  $J = 7.1$  Hz, 3H).  $^{13}\text{C}$  NMR (101 MHz,  $\text{CDCl}_3$ )  $\delta$  167.26, 148.84,

134.18, 123.17, 122.30, 118.06, 114.63, 77.48, 77.16, 76.84, 60.96, 14.48;  $m/z$  (ESI<sup>+</sup>-TOF) 182.1 C<sub>9</sub>H<sub>12</sub>NO<sub>3</sub><sup>+</sup> (MH<sup>+</sup>). Analytical data is consistent with the literature.

**(5) methyl 4-amino-3-hydroxybenzoate**<sup>201</sup>



Synthesis was conducted as per the method for **(2) 3-amino-4-hydroxybenzoxonitrile** using methyl 4-hydroxy-3-nitrobenzoate (1.000 g, 0.00507 mol) to yield methyl 4-amino-3-hydroxybenzoate (0.786 g, 0.00470 mol, 93 %) as a brown solid. <sup>1</sup>H NMR (400 MHz, CDCl<sub>3</sub>) δ 7.57 (d, J = 1.9 Hz, 1H), 7.50 (dd, J = 8.2, 1.9 Hz, 1H), 6.67 (d, J = 8.2 Hz, 1H), 3.86 (s, 3H). <sup>13</sup>C NMR (101 MHz, CDCl<sub>3</sub>) δ 142.58, 140.48, 124.24, 119.66, 116.38, 114.35, 100.13, 52.02;  $m/z$  (ESI<sup>+</sup>-TOF) 168.1 C<sub>8</sub>H<sub>10</sub>NO<sub>3</sub><sup>+</sup> (MH<sup>+</sup>). Analytical data is consistent with the literature.

### 6.3.2 Quinone Imine enzyme assays methods

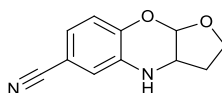
#### 6.3.2.1 General analytical assay procedure

Experiments were performed at a 150 μL per well scale by combining, 2,3-dihydrofuran (100 mM), hydrogen peroxide (2.5 mM) and the desired substituted amino-phenol (2 mM) in 20 mM potassium phosphate buffer pH 7.4 (with 5% v/v 1,4-dioxane to aid the dissolution of the organic amine). 10 μL of HRP (0.001 mg mL<sup>-1</sup>) in 20 mM potassium phosphate buffer pH 7.4) was then added to begin the reaction. Triplicate reactions were shaken at 21 °C, and then terminated at each time point from 0–1320 min by addition of 75 % v/v acetonitrile, 25 % v/v water, 100 mM sodium sulfite, 100 mM ascorbic acid (300 μL). The precipitated protein was then removed by centrifugation. Aliquots (10 μL) of the resulting supernatant were analysed by reversed phase HPLC solvent A = H<sub>2</sub>O + 0.05% TFA, solvent B = CH<sub>3</sub>CN + 0.05% TFA, 0–13 minutes B = 5–95 %, 13–15 minutes B = 95 %).

### 6.3.2.2 General larger scale assay procedure for NMR analysis

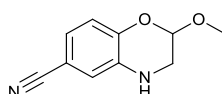
Large scale assays were used to provide enough material to fully characterise enzyme reaction products. These assays were completed on a 30 ml scale. The following conditions were used. 2,3-dihydrofuran (100 mM), hydrogen peroxide (2.5 mM) and the desired substituted amino-phenol (2 mM) in 20 mM potassium phosphate buffer pH 7.4 (with 5 % v/v 1,4-dioxane to aid the dissolution of the organic amine). 2 mL of HRP (0.001 mg/mL in 20 mM potassium phosphate buffer pH 7.4) was then added to begin the reaction. Reactions were shaken at 21 °C and monitored by HPLC until no further product was being formed. Assays were terminated by addition of sodium sulfite (100 mM), lyophilised and the residue purified by flash chromatography (SiO<sub>2</sub>, hexane: ethyl acetate; 2:1).

#### (1) 2,3,3a,9a-tetrahydro-4H-benzo[b]furo[3,2-e][1,4]oxazine-6-carbonitrile<sup>1566</sup>



(0.129 g, 0.00064 mol, 86 %) <sup>1</sup>H NMR (400 MHz, CDCl<sub>3</sub>) δ 6.99 (dd, J = 8.3, 1.9 Hz, 1H), 6.89 (d, J = 8.3 Hz, 1H), 6.86 (d, J = 1.9 Hz, 1H), 5.38 (d, J = 3.6 Hz, 1H), 4.30 (td, J = 9.0, 3.9 Hz, 1H), 4.16 – 4.00 (m, 3H), 2.22 (dtd, J = 12.3, 7.6, 3.8 Hz, 1H), 1.90 (dq, J = 12.3, 8.9 Hz, 1H). <sup>13</sup>C NMR (101 MHz, CDCl<sub>3</sub>) δ 145.37, 131.27, 123.48, 119.54, 117.97, 117.52, 105.06, 96.52, 68.20, 54.05, 29.50; *m/z* (ESI<sup>+</sup>) 203.1 C<sub>11</sub>H<sub>11</sub>N<sub>2</sub>O<sub>2</sub><sup>+</sup> (MH<sup>+</sup>), HRMS found 203.0887; C<sub>11</sub>H<sub>11</sub>N<sub>2</sub>O<sub>2</sub><sup>+</sup> (MH<sup>+</sup>-TOF) requires 203.0820. Analytical data is consistent with the literature.

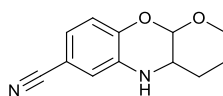
#### (10) 2-ethoxy-3,4-dihydro-2H-benzo[b][1,4]oxazine-6-carbonitrile<sup>1566</sup>



(0.124 g, 0.00061 mol, 82 %) <sup>1</sup>H NMR (400 MHz, CDCl<sub>3</sub>): δ 6.97 (dd, J = 8.3, 1.9 Hz, 1H),

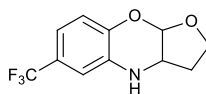
6.86 (d,  $J = 1.9$  Hz, 1H), 6.83 (d,  $J = 8.3$  Hz, 1H), 5.26 (t,  $J = 2.5$  Hz, 1H), 3.92 (qd,  $J = 9.7, 7.1$  Hz, 1H), 3.69 (qd,  $J = 9.7, 7.1$  Hz, 1H), 3.41-3.32 (m, 2H), 1.22 (t,  $J = 7.1$  Hz, 3H).  $^{13}\text{C}$  NMR (101 MHz,  $\text{CDCl}_3$ ), 145.31, 133.86, 123.47, 119.62, 118.59, 117.95, 104.68, 94.90, 64.48, 44.16, 15.12;  $m/z$  (ESI $^+$ ) 205.1  $\text{C}_{11}\text{H}_{13}\text{N}_2\text{O}_2^+$  ( $\text{MH}^+$ -TOF), HRMS found 205.0948;  $\text{C}_{11}\text{H}_{13}\text{N}_2\text{O}_2^+$  ( $\text{MH}^+$ ) requires 205.0970. Analytical data is consistent with the literature.

**(11) 3,4,4a,10a-tetrahydro-2H,5H-benzo[*b*]pyrano[3,2-*e*][1,4]oxazine-7-carbonitrile**<sup>156</sup>

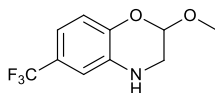


(0.127 g, 0.00058 mol, 79 %)  $^1\text{H}$  NMR (400 MHz,  $\text{CDCl}_3$ )  $\delta$  6.97 (dd,  $J = 8.3, 1.9$  Hz, 1H), 6.88 (d,  $J = 8.3$  Hz, 1H), 6.84 (d,  $J = 1.9$  Hz, 1H), 5.35 (d,  $J = 2.4$  Hz, 1H), 4.00 (ddd,  $J = 11.4, 8.4, 2.9$  Hz, 1H), 3.77 – 3.67 (m, 1H), 3.49 (ddd,  $J = 7.6, 4.2, 2.4$  Hz, 1H), 1.88 – 1.74 (m, 3H), 1.69 – 1.62 (m, 1H).  $^{13}\text{C}$  NMR (101 MHz,  $\text{CDCl}_3$ )  $\delta$  145.26, 132.23, 123.38, 119.62, 117.79, 117.51, 105.00, 94.13, 63.21, 47.60, 26.47, 22.18;  $m/z$  (ESI $^+$ ) 217.1  $\text{C}_{12}\text{H}_{13}\text{N}_2\text{O}_2^+$  ( $\text{MH}^+$ ), HRMS found 217.1045;  $\text{C}_{12}\text{H}_{13}\text{N}_2\text{O}_2^+$  ( $\text{MH}^+$ -TOF) requires 217.0970.

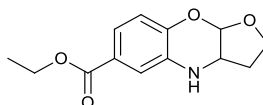
**(12) 6-(trifluoromethyl)-2,3,3a,9a-tetrahydro-4H-benzo[*b*]furo[3,2-*e*][1,4]oxazine**<sup>156</sup>



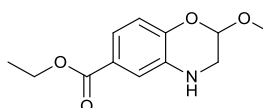
(0.105 g, 0.00042 mol, 76 %)  $^1\text{H}$  NMR (400 MHz,  $\text{CDCl}_3$ )  $\delta$  6.96-6.89 (m, 2H), 6.83 (d,  $J = 1.7$  Hz, 1H), 5.37 (d,  $J = 3.7$  Hz, 1H), 4.30 (td,  $J = 8.9, 3.9$  Hz, 1H), 4.10-4.04 (m, 2H), 2.25-2.17 (m, 1H), 1.91 (dq,  $J = 12.3, 8.8$  Hz, 1H);  $^{13}\text{C}$  NMR (101 MHz,  $\text{CDCl}_3$ )  $\delta$  143.91, 130.67, 125.43, 124.19, 117.22, 115.81, 111.22, 96.30, 67.94, 54.16, 29.52;  $m/z$  (ESI $^+$ -TOF) 246.1  $\text{C}_{11}\text{H}_{11}\text{F}_3\text{NO}_2^+$  ( $\text{MH}^+$ ), HRMS found 246.0748;  $\text{C}_{11}\text{H}_{11}\text{F}_3\text{NO}_2^+$  ( $\text{MH}^+$ ) requires 246.0740. Analytical data is consistent with the literature.

**(13) 2-ethoxy-6-(trifluoromethyl)-3,4-dihydro-2H-benzo[b][1,4]oxazine<sup>156</sup>**

(0.099 g, 0.00040 mol, 71 %) <sup>1</sup>H NMR (400 MHz, CDCl<sub>3</sub>) δ 6.95 (dd, J = 8.3, 1.4 Hz, 1H), 6.87 (d, J = 5.6 Hz, 1H), 6.86 (s, 1H), 5.26 (t, J = 2.5 Hz, 1H), 3.93 (dq, J = 9.8, 7.1 Hz, 1H), 3.90 (s, 1H), 3.70 (dq, J = 9.7, 7.1 Hz, 1H), 3.37 (t, J = 2.5 Hz, 2H), 1.23 (t, J = 7.1 Hz, 3H). <sup>13</sup>C NMR (101 MHz, CDCl<sub>3</sub>) δ 144.16, 133.18, 125.84, 123.83, 117.41, 116.30, 112.77, 94.80, 64.38, 44.48, 15.20; *m/z* (ESI<sup>+</sup>-TOF) 248.1 C<sub>11</sub>H<sub>13</sub>F<sub>3</sub>NO<sub>2</sub><sup>+</sup> (MH<sup>+</sup>), HRMS found 248.0890; C<sub>11</sub>H<sub>13</sub>F<sub>3</sub>NO<sub>2</sub><sup>+</sup> (MH<sup>+</sup>) requires 248.0900. Analytical data is consistent with the literature.

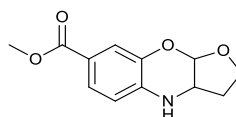
**(15) ethyl 2,3,3a,9a-tetrahydro-4H-benzo[b]furo[3,2-e][1,4]oxazine-6-carboxylate<sup>156</sup>**

(0.105 g, 0.00042 mol, 77 %) <sup>1</sup>H NMR (400 MHz, CDCl<sub>3</sub>) δ 7.39 (dd, J = 8.3, 2.0 Hz, 1H), 7.32 (d, J = 1.9 Hz, 1H), 6.86 (d, J = 8.3 Hz, 1H), 5.39 (d, J = 3.8 Hz, 1H), 4.38 – 4.22 (m, 3H), 4.13 (d, J = 3.9 Hz, 1H), 4.05 (tt, J = 8.5, 5.3 Hz, 2H), 2.16 (dtd, J = 12.4, 7.7, 3.9 Hz, 1H), 1.89 (dq, J = 12.3, 8.9 Hz, 1H), 1.35 (t, J = 7.1 Hz, 3H); <sup>13</sup>C NMR (CDCl<sub>3</sub>, 101 MHz): δ; 166.63, 145.61, 130.15, 124.11, 121.01, 116.77, 115.91, 96.63, 68.00, 60.72, 54.17, 29.26, 14.35; *m/z* (ESI<sup>+</sup>-TOF) 250.1 C<sub>13</sub>H<sub>16</sub>NO<sub>4</sub><sup>+</sup> (MH<sup>+</sup>), HRMS found 250.1074; C<sub>13</sub>H<sub>16</sub>NO<sub>4</sub><sup>+</sup> (MH<sup>+</sup>) requires 250.1070.

**(16) ethyl 2-ethoxy-3,4-dihydro-2H-benzo[b][1,4]oxazine-6-carboxylate<sup>156</sup>**

(0.105 g, 0.00041 mol, 76 %)  $^1\text{H}$  NMR (400 MHz,  $\text{CDCl}_3$ )  $\delta$  7.35 (dd,  $J = 8.4, 2.0$  Hz, 1H), 7.28 (d,  $J = 2.0$  Hz, 1H), 6.76 (d,  $J = 8.3$  Hz, 1H), 5.19 (d,  $J = 2.9$  Hz, 1H), 4.24 (q,  $J = 7.1$  Hz, 2H), 3.86 (dq,  $J = 9.7, 7.1$  Hz, 1H), 3.62 (dq,  $J = 9.7, 7.1$  Hz, 1H), 3.36 – 3.22 (m, 2H), 1.28 (t,  $J = 7.1$  Hz, 3H), 1.15 (t,  $J = 7.1$  Hz, 3H);  $^{13}\text{C}$  NMR (101 MHz,  $\text{CDCl}_3$ )  $\delta$  166.68, 145.83, 132.76, 123.97, 121.45, 117.37, 116.99, 95.16, 64.35, 60.69, 44.55, 15.20, 14.47;  $m/z$  (ESI $^+$ -TOF) 252.1  $\text{C}_{13}\text{H}_{18}\text{NO}_4^+$  ( $\text{MH}^+$ ), HRMS found 252.1230;  $\text{C}_{13}\text{H}_{18}\text{NO}_4^+$  ( $\text{MH}^+$ ) requires 252.124.

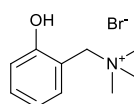
**(18) methyl 2,3,3a,9a-tetrahydro-4H-benzo[b]furo[3,2-e][1,4]oxazine-7-carboxylate<sup>156</sup>**



(0.104 g, 0.00044 mol, 74 %)  $^1\text{H}$  NMR (400 MHz,  $\text{CDCl}_3$ )  $\delta$  7.54 (s, 1H), 7.53 (dd,  $J = 10.9, 1.7$  Hz, 1H), 6.57 (d,  $J = 8.5$  Hz, 1H), 5.33 (d,  $J = 3.7$  Hz, 1H), 4.29 (td,  $J = 8.8, 4.0$  Hz, 1H), 4.10 – 4.00 (m, 2H), 3.84 (s, 3H), 2.24 (ddt, 11.81, 8.01, 3.93 Hz, 1H), 1.93 (dq,  $J = 12.3, 8.7$  Hz, 1H);  $^{13}\text{C}$  NMR (101 MHz,  $\text{CDCl}_3$ )  $\delta$  167.11, 140.12, 135.80, 124.76, 120.06, 118.91, 113.12, 96.05, 67.89, 54.30, 51.84, 30.36;  $m/z$  (ESI $^+$ -TOF) 236.1  $\text{C}_{12}\text{H}_{14}\text{NO}_4^+$  ( $\text{MH}^+$ ), HRMS found 236.067;  $\text{C}_{12}\text{H}_{14}\text{NO}_4^+$  ( $\text{MH}^+$ ) requires 236.092.

**6.3.3 Quinone methide product standard and precursor synthesis**

**(25) 1-(2-hydroxyphenyl)-N,N,N-trimethylmethanaminium bromide<sup>202</sup>**

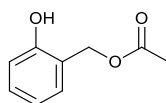


Cyanuric chloride (0.99 g, 0.00536 mol) was added to dimethylformamide (1 mL) and stirred at room temperature, the solution was monitored by TLC until complete consumption of cyanuric chloride was observed. This was followed by addition of dichloromethane (12.5 mL)

and sodium bromide (1g, 0.00971 mol). The mixture was stirred for 10 h whereupon 2-(hydroxymethyl)phenol (0.50 g, 0.00403 mol) was added, stirring was continued at room temperature until the reaction reached completion (as monitored by TLC). The reaction was quenched by dilution with dichloromethane (40 mL) followed by filtration through Celite. The reaction mixture was washed with water (30 mL), hydrochloric acid (1M, 2x 15 mL) and brine (2x 15 mL). The organic layer was then dried over sodium sulfate (at 0 °C) and the solvent removed under vacuum to yield crude 2-(bromomethyl)phenol as a yellow oil. Due to its instability the crude product was used directly in the next step.

Crude 2-(bromomethyl)phenol (0.100 g, 0.00053 mol) was dissolved in ethanol (5 mL) with stirring. Trimethylamine (4.3 M in ethanol) (0.468 mL, 0.0020 mol) was then added dropwise over 1 h. Stirring was continued for 12 h at which time ethyl ether (20 mL) was added to precipitate the salt. The solid was then collected by vacuum filtration and washed with ethyl ether (40 mL) and air dried to yield 1-(2-hydroxyphenyl)-N,N,N-trimethylmethanaminium bromide (0.108 g, 0.00044 mol, 83%) as a white solid. m.p. 170–171°C, <sup>1</sup>H NMR (400 MHz, CDCl<sub>3</sub>) δ 7.33-7.27 (m, 2H), 6.92-6.88 (m, 2H), 4.34 (s, 2H), 2.96 (s, 9H); <sup>13</sup>C NMR (101 MHz, CDCl<sub>3</sub>) δ 156.43, 134.64, 132.65, 120.35, 116.40, 114.52, 52.42, 44.68 (3C); *m/z* (ESI<sup>+</sup>-TOF) 166.1 C<sub>10</sub>H<sub>16</sub>NO<sup>+</sup> (MH<sup>+</sup>). Analytical data is consistent with the literature.

#### (26) 2-hydroxybenzyl acetate<sup>160</sup>

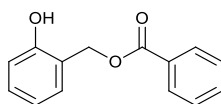


2-hydroxybenzyl alcohol (1 g, 0.008 mol) was dissolved with stirring in dichloromethane (20 mL) under nitrogen and cooled to 0 °C. Followed by dropwise addition of pyridine (623 μL, 0.008 mol) and then ethanoyl chloride (693 μL, 0.008 mol). The reaction was then warmed to room temperature over 15 min and further stirred for 1 h. The reaction mixture was then quenched with a saturated solution of ammonium chloride (20 mL) and the organic layer further washed with a saturated solution of copper sulfate (3 x 20 mL). The organic layer



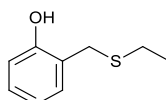
was then dried over anhydrous magnesium sulfate, filtered and the solvent removed under vacuum to yield 2-hydroxybenzyl acetate (1.028 g, 0.00618 mol, 77%) as a colourless oil.  $^1\text{H}$  NMR (400 MHz,  $\text{CDCl}_3$ )  $\delta$  7.46 – 7.27 (m, 2H), 7.11 – 6.88 (m, 2H), 5.12 (s, 2H), 2.11 (s, 3H);  $^{13}\text{C}$  NMR (101 MHz,  $\text{CDCl}_3$ )  $\delta$  173.91, 155.70, 132.39, 131.36, 121.76, 120.72, 118.03, 63.48, 21.07;  $m/z$  (ESI $^+$ -TOF) 167.1  $\text{C}_9\text{H}_{11}\text{O}_3^+$  ( $\text{MH}^+$ ). Analytical data is consistent with the literature.

**(27) 2-hydroxybenzyl benzoate**<sup>203</sup>



Synthesis was conducted as per the method for **(9) 2-hydroxybenzyl acetate**, using 2-hydroxybenzyl alcohol (1 g, 0.008 mol) and benzoyl chloride (1.36 mL, 0.008 mol). Flash chromatography ( $\text{SiO}_2$ , hexane: ethyl acetate; 2:1) yielded 2-hydroxybenzyl benzoate (1.209 g, 0.0053 mol, 66 %) as a colourless oil.  $^1\text{H}$  NMR (400 MHz,  $\text{CDCl}_3$ )  $\delta$  8.07 (dd,  $J$  = 8.4, 1.3 Hz, 2H), 7.58 (tt,  $J$  = 7.5, 1.8, 1.4 Hz, 1H), 7.44 (t,  $J$  = 7.7 Hz, 2H), 7.38 (dd,  $J$  = 7.6, 1.7 Hz, 1H), 7.30 (ddd,  $J$  = 8.2, 7.4, 1.7 Hz, 1H), 6.99 (dd,  $J$  = 8.2, 1.0 Hz, 1H), 6.94 (td,  $J$  = 7.5, 1.1 Hz, 1H), 5.39 (s, 2H).  $^{13}\text{C}$  NMR (101 MHz,  $\text{CDCl}_3$ )  $\delta$  168.93, 155.75, 133.74, 132.39, 131.30, 130.07 (2C), 129.33, 128.57 (2C), 121.86, 120.69, 117.97, 63.86;  $m/z$  (ESI $^+$ -TOF) 229.1  $\text{C}_{14}\text{H}_{13}\text{O}_3^+$  ( $\text{MH}^+$ ). Analytical data is consistent with the literature.

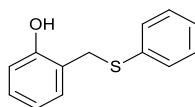
**(28) 2-((ethylthio)methyl)phenol**<sup>204</sup>



2-hydroxybenzyl alcohol (1 g, 0.008 mol) was dissolved with stirring in dichloromethane (20 mL) and cooled to  $-20^\circ\text{C}$ , zinc iodide (1.27 g, 0.004 mol) and propane-1-thiol (0.595 g, 0.0096 mol) were then added. The reaction mixture was stirred for 4 h, after which the

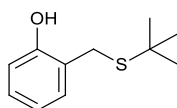
mixture was diluted with dichloromethane (20mL), washed with ice cold water (20 mL) followed by a 10% sodium hydrogen carbonate solution (20 mL). The organic layer was then dried with anhydrous magnesium sulfate, filtered and the solvent removed under vacuum to yield crude product (1.245 g, 0.0074 mol, 93%) as a pale yellow oil. Flash chromatography (SiO<sub>2</sub>, hexane: ethyl acetate; 2:1) yielded 2-((ethylthio)methyl)phenol (1.026 g, 0.0061 mol, 76%,) as a colourless oil. <sup>1</sup>H NMR (400 MHz, CDCl<sub>3</sub>) δ 7.20 (td, J = 7.9, 1.7 Hz, 1H), 7.09 (dd, J = 7.5, 1.4 Hz, 1H), 6.90 (dd, J = 8.1, 1.0 Hz, 1H), 6.86 (td, J = 7.4, 1.2 Hz, 1H), 3.82 (s, 2H), 2.43 (q, J = 7.4 Hz, 2H), 1.23 (t, J = 7.4 Hz, 3H). <sup>13</sup>C NMR (101 MHz, CDCl<sub>3</sub>) δ 155.57, 130.56, 129.20, 122.58, 120.62, 117.27, 32.45, 24.87, 14.34; *m/z* (ESI<sup>+</sup>) 169.1 C<sub>9</sub>H<sub>13</sub>OS<sup>+</sup> (MH<sup>+</sup>-TOF). Analytical data is consistent with the literature.

**(29) 2-((phenylthio)methyl)phenol**<sup>161</sup>



Synthesis was conducted as per the method for **(11) 2-((ethylthio)methyl)phenol**, using 2-hydroxybenzyl alcohol (1 g, 0.008 mol) and benzenethiol (1.058 g, 0.0096 mol). Flash chromatography (SiO<sub>2</sub>, hexane: ethyl acetate; 2:1) yielded 2-((phenylthio)methyl)phenol (1.341 g, 0.0062 mol, 78%) as a colourless crystals. <sup>1</sup>H NMR (400 MHz, CDCl<sub>3</sub>) δ 7.34 – 6.81 (m, 9H), 4.17 (s, 2H). <sup>13</sup>C NMR (101 MHz, CDCl<sub>3</sub>) δ 154.72, 134.76, 130.91(2C), 130.76, 129.25, 129.06 (2C), 127.18, 122.77, 120.92, 116.83, 35.64; *m/z* (ESI<sup>+</sup>) 217.1 C<sub>13</sub>H<sub>13</sub>OS<sup>+</sup> (MH<sup>+</sup>-TOF). Analytical data is consistent with the literature.

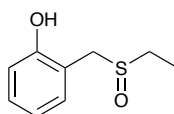
**(30) 2-((tert-butylthio)methyl)phenol**<sup>205</sup>



Synthesis was conducted as per the method for **(11) 2-((ethylthio)methyl)phenol**, using 2-hydroxybenzyl alcohol (1 g, 0.008 mol) and 2-methylpropane-2-thiol (0.866 g, 0.0096 mol).

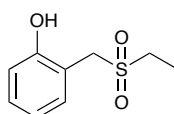
Flash chromatography (SiO<sub>2</sub>, hexane: ethyl acetate; 2:1) yielded 2-((*tert*-butylthio)methyl)phenol (1.021 g, 0.0052 mol, 65 %) as a white solid. <sup>1</sup>H NMR (400 MHz, CDCl<sub>3</sub>) δ 7.22 – 7.11 (m, 2H), 6.91 – 6.81 (m, 2H), 3.86 (s, 2H), 1.36 (s, 9H). <sup>13</sup>C NMR (101 MHz, CDCl<sub>3</sub>) δ 155.65, 130.21, 129.17, 123.15, 120.90, 117.40, 43.84, 30.83, 30.70; *m/z* (ESI<sup>+</sup>) 197.1 C<sub>11</sub>H<sub>17</sub>OS<sup>+</sup> (MH<sup>+</sup>-TOF).

**(31) 2-((ethylsulfinyl)methyl)phenol,<sup>162</sup>**



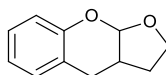
2-((ethylthio)methyl)phenol (0.336 mg, 0.00197 mol) was dissolved with stirring in glacial acetic acid (2 mL) at room temperature, hydrogen peroxide (1 mL, 0.008 mol) was then added dropwise over 15 min. Stirring was continued and the solution was monitored by TLC until complete. Following which the reaction mixture was diluted with water (10 mL) and neutralised with sodium hydroxide (4 M). This aqueous solution was then extracted with dichloromethane (3 x 15 mL), the organic layer dried over anhydrous sodium sulfate, filtered and solvent removed under vacuum to yield a mixture of products. Flash chromatography (SiO<sub>2</sub>, hexane: ethyl acetate; 1:1) isolated 2-((ethylsulfinyl)methyl)phenol (0.077 g, 0.00042 mol, 21 %,) as a colourless oil. <sup>1</sup>H NMR (400 MHz, CDCl<sub>3</sub>) δ 9.30 (s, 1H), 7.23 (t, *J* = 7.7 Hz, 1H), 7.02 (dd, *J* = 12.6, 7.8 Hz, 2H), 6.87 (t, *J* = 7.4 Hz, 1H), 4.12 (dd, *J* = 187.3, 14.1 Hz, 2H), 2.79-2.62 (m, 2H), 1.31 (t, *J* = 7.6 Hz, 3H). Analytical data is consistent with the literature.

**(32) 2-((ethylsulfonyl)methyl)phenol<sup>162</sup>**



This compound was also isolated from the mixture of the reaction to form **(14) 2-((ethylsulfinyl)methyl)phenol**, Flash chromatography (SiO<sub>2</sub>, hexane: ethyl acetate; 1:1) isolating 2-((ethylsulfonyl)methyl)phenol (0.051 g, 0.00025 mol, 13 %,) as a colourless oil. <sup>1</sup>H NMR (400 MHz, CDCl<sub>3</sub>) δ 7.31 (ddd, J = 8.2, 7.4, 1.7 Hz, 1H), 7.21 (dd, J = 7.4, 1.5 Hz, 1H), 7.02-6.97 (m, 2H), 6.82 (s, 1H), 4.35 (s, 2H), 2.98 (q, J = 7.5 Hz, 2H) 1.40 (t, J = 7.5, 3H). Analytical data is consistent with the literature.

**(31) 2,3,3a,9a-tetrahydro-4H-furo[2,3-b]chromene**<sup>206</sup>



o-hydroxybenzyl acetate (0.100 g, 0.00060 mol) was dissolved with stirring in tetrahydrofuran (500 μL) and cooled to -78 °C. Isopropylmagnesium chloride (2.0 M in tetrahydrofuran) (520 μL, 0.107 mg, 0.0010 mol) was added, after 15 min 2,3-dihydrofuran (0.421 g, 0.00601 mol) was then added. The solution was then warmed to room temperature over 16 h after which ethyl acetate (5 mL) was added and the resulting solution was passed through at short plug of silica (3 cm<sup>2</sup> x 2 cm) with ethyl acetate (20 mL). The solvent was then removed under vacuum to yield crude product (0.081 g, 0.00046 mol, 77 %) as a pale yellow oil. Flash chromatography (SiO<sub>2</sub>, hexane: ethyl acetate; 2:1) yielded 2,3,3a,9a-tetrahydro-4H-furo[2,3-b]chromene (0.069 g, 0.00039 mol, 65 %) as a colourless oil. <sup>1</sup>H NMR (400 MHz, CDCl<sub>3</sub>) δ 7.13 (t, J = 7.7 Hz, 1H), 7.07 (d, J = 7.8 Hz, 1H), 6.93 – 6.85 (m, 2H), 5.67 (d, J = 4.9 Hz, 1H), 4.02 (td, J = 8.7, 4.1 Hz, 1H), 3.92 (q, J = 8.2 Hz, 1H), 3.08 (dd, J = 16.1, 5.8 Hz, 1H), 2.80 – 2.67 (m, 2H), 2.05 (ddq, J = 12.5, 8.5, 4.1 Hz, 1H), 1.69 (dq, J = 12.3, 8.6 Hz, 1H). <sup>13</sup>C NMR (101 MHz, CDCl<sub>3</sub>) δ 153.49, 129.19, 127.91, 121.63, 121.41, 117.21, 101.79, 77.48, 77.16, 76.84, 68.30, 38.06, 28.39, 26.47; *m/z* (ESI<sup>+</sup>-TOF) 177.1 C<sub>11</sub>H<sub>13</sub>O<sub>2</sub><sup>+</sup> (MH<sup>+</sup>). Analytical data is consistent with the literature.

#### 6.3.4 Quinone methide general analytical enzyme assay

Experiments were performed at a 150  $\mu\text{L}$  per well scale by combining, 2,3-dihydrofuran (50-200 mM), hydrogen peroxide (0.25-3 mM) and the desired quinone methide precursor (1-5 mM) in 20 mM potassium phosphate buffer pH 5-9 (with 5% v/v 1,4-dioxane to aid the dissolution of the organic substrate). 10  $\mu\text{L}$  of HRP (0.1-0.01 mg/mL in 20 mM potassium phosphate buffer pH 7.4) was then added to begin the reaction. Triplicate reactions were shaken at 21  $^{\circ}\text{C}$ , and then terminated at each time point from 0–1320 min by addition of 300  $\mu\text{L}$  of (75 % v/v acetonitrile, 25 % v/v water, 100 mM sodium sulfite, 100 mM ascorbic acid). The precipitated protein was then removed by centrifugation. Aliquots (10  $\mu\text{L}$ ) of the resulting supernatant were analysed by reversed phase HPLC (solvent A =  $\text{H}_2\text{O}$  + 0.05% TFA, solvent B =  $\text{CH}_3\text{CN}$  + 0.05% TFA, 0–13 minutes B = 5–95 %, 13–15 minutes B = 95 %).

## 6.4 Methods from chapter 4

### 6.4.1 Halogenation assay general assay procedure

All UV-visible data was collected on a Synergy HT Multi-Mode Microplate Reader (BioTek Instruments Inc). Calibration curves were constructed from experiments performed at a 150  $\mu\text{L}$  per well scale by combining, 4-methyl-catachol (0.5 mM), hydrogen peroxide (3 mM) and the desired mixture of aryl-amine substrates (to 0.5 mM final concentration) in 20 mM potassium phosphate buffer pH 7.4 (with 5 % v/v isopropanol to aid the dissolution of the organic amine). 1  $\mu\text{L}$  of HRP (0.1 mg/mL in 20 mM potassium phosphate buffer, pH 7.4) was then added to commence the reaction. The plate was then agitated for 5 minutes and the UV-visible spectra recorded. In all cases, the reactions were performed in triplicate. OriginPro 8 was used for all data analysis, using linear least squares fitting to calculate the calibration curve.

### 6.4.2 HPLC assay analysis

The assay was carried out as per assay conditions section, the reactions were then quenched by the addition of methanol (150  $\mu\text{L}$ ) and precipitate protein was removed by centrifugation. An aliquot (10  $\mu\text{L}$ ) resulting supernatant was the analysed by reversed phase HPLC (solvent A =  $\text{H}_2\text{O}$  + 0.05 % TFA, solvent B=  $\text{CH}_3\text{CN}$  + 0.05 % TFA, 0–13 minutes B = 5–95%, 13–15 minutes B = 95%)

### 6.4.3 Cofactor recycling system enzyme production

Plasmids pET-45b/Fre and pET21b/GDH2 were transformed into BL21(DE3). The resulting cells were plated on LB agar containing Ampicillin (100  $\mu\text{g}/\text{mL}$ ) and incubated overnight at 37 °C. A single colony was picked and inoculated into 5 mL LB containing Ampicillin (100  $\mu\text{g}/\text{mL}$ ) and incubated at 37 °C with 250 rpm shaking overnight. 1 mL of this culture was

taken for plasmid isolation and sequencing. The remaining 4 mL culture was then inoculated into 400 mL of LB media and grown at 37 °C and 250 rpm shaking to an OD<sub>600</sub> of 0.7. The culture was then induced with 0.1 mM β-D-1-thiogalactopyranoside (IPTG) and incubated at 30 °C with 250rpm shaking for three h, the cells were then pelleted (4000 g, 30 min, 4 °C) by centrifugation and used directly for purification

#### **6.4.4 Tryptophan-7-halogenase (RebH) production**

Plasmid pET-28b/RebH was transformed into ArcticExpress(DE3) cells which co-express cold shock proteins chaperonins Cpn10 and Cpn60. The resulting cells were plated on LB agar containing Kanamycin (50 µg/mL) and incubated overnight at 37 °C. A single colony was picked and inoculated into 5 mL LB containing Kanamycin (50ug/mL) and incubated at 37°C and 250rpm shaking overnight. 1 mL of this culture was taken for plasmid isolation and sequencing. The remaining 4 mL culture was then inoculated into 400 mL of LB media and grown at 30 °C with 250 rpm shaking to an OD<sub>600</sub> of 0.7. The culture was then induced with 1 mM IPTG and incubated at 15 °C with 250 rpm shaking overnight, the cells were then pelleted (4000 g, 30 min, 4 °C) by centrifugation and used directly for purification.

#### **6.4.5 Purification of RebH, Fre and GDH2**

Cell pellets were resuspended in 50 mM potassium phosphate buffer with 5 mM imidazole pH 7.4 in a ration of 1:10 wet cell weight to buffer. The resuspended solution was then sonicated 10 cycles at 70 % power for 30 sec with 30 sec intervals. Cell debris was removed from the lysate by centrifugation at 11,000 g for 15 min, the lysate was subsequently filtered through a syringe filter with a 0.22 µm pore size.

All enzymes contained a hexahistidine tag and were subsequently purified on an FPLC using the following procedure; cell lysate was loaded to a HisTrap HP column previously equilibrated with 50 mM potassium phosphate buffer with 5mM imidazole pH 7.4 at a flow rate of 1 mL/min. The column was then washed with 50 mM potassium phosphate buffer

with 20mM imidazole pH 7.4 followed by 50 mM potassium phosphate buffer with 80 mM imidazole pH 7.4. The enzyme was then eluted with 50 mM potassium phosphate buffer with 250 mM imidazole pH 7.4. Fractions containing the enzyme were then pooled. The pooled fractions were then concentrated and buffer exchanged into 50 mM potassium phosphate buffer pH 7.4 containing 10 % glycerol using a centrifugal concentrator MWCO 10 kDa. Proteins were then frozen at -20°C until further use.

#### **6.4.6 RebH-catalysed halogenation**

The reaction mixture for each experiment was prepared in 50 mM potassium phosphate buffer pH 7.4 with 5% v/v isopropanol. 2-Naphthylamine (0.6 mM), NAD (100 µM), FAD (100 µM), NaCl (10 mM), Fre (2.5 µM), GDH2 (5 µM) and glucose (20 mM) were added to make final volume of 300µL in each well of a 96-well microtiter plate (total of 48 wells prepared). The halogenation reactions were initiated by adding RebH (to a final RebH concentration of 25 µM). Reactions were shaken at 21 °C, and then quenched at each time point from 0–1320 min by heating the microtiter plate at 95 °C for 5 min to inactivate the protein. This precipitated protein was then removed by centrifugation. The reactions were conducted in triplicate for each time point. The resulting sample was the spilt into two 125 µL fractions.

#### **6.4.7 RebH-catalysed halogenation assay analysis**

One 125 µL fraction was added to a microtiter plate along with 4-methyl-catechol (0.5 mM, final concentration from a working solution of 200 mM in 50 mM K<sub>2</sub>PO<sub>4</sub> pH 7.4), hydrogen peroxide (3 mM final concentration) and 1 µL of HRP (0.1 mg/mL working solution in 50 mM K<sub>2</sub>PO<sub>4</sub> pH 7.4) was then added to commence the reaction (total volume 150 µL, substrate 0.5 mM). The plate was then shaken for 5 min and the absorption at 516 nm of the 2-naphthylamine adduct measured. Product formation was then quantified by fitting to the absorption to a calibration curve prepared from known concentrations of starting materials

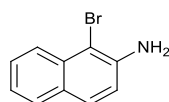


and products with buffer containing all components from the halogenation reaction but omitting RebH.

#### 6.4.8 RebH-catalysed halogenation HPLC Analysis

To the other 125  $\mu$ L fraction, 50 mM potassium phosphate buffer pH 7.4 (25  $\mu$ L) was added to bring the substrate concentration to 0.5 mM (in line with the assay), this was then analysed by HPLC using the same column and solvent gradient as above. Product formation was calculated by fitting peak integration of 2-naphthylamine consumption to a calibration curve prepared from known concentrations of 2-naphthylamine.

#### 6.4.9 Synthesis of 1-bromonaphthalen-2-amine<sup>207</sup>



Naphthalen-2-amine (1.40 mmol, 200 mg) was dissolved in dimethylformamide (20mL) and cooled to 0°C. To the stirred solution *N*-bromosuccinimide (1.40 mmol, 248.8 mg) was then added slowly in several portions. The solution was then warmed to 21 °C and stirred a further 90 minutes. The solvent was then removed by reduced pressure. Dichloromethane (10 mL) and 1M aqueous sodium hydroxide (10 mL) were added and the organic layer removed. The aqueous layer was then extracted with dichloromethane (2 x 10 mL). The organic layers were combined, dried with Na<sub>2</sub>SO<sub>4</sub> and the solvent removed under vacuum to yield crude 1-bromonaphthalen-2-amine (223.5 mg, 1.01 mmol, 72 %) as a black solid. This crude product was then purified by preparative reversed phase HPLC (solvent A = H<sub>2</sub>O + 0.05% TFA, solvent B= CH<sub>3</sub>CN + 0.05% TFA, 0–45 minutes B = 5–95%, 45–50 minutes B = 95%) to yield 1-bromonaphthalen-2-amine as a purple solid. <sup>1</sup>H NMR (400 MHz, CDCl<sub>3</sub>)  $\delta$  8.03 (d, J = 8.4 Hz, 1H), 7.69 (d, J = 7.6 Hz, 1H), 7.63 (d, J = 8.7 Hz, 1H), 7.51 (t, J = 8.4 Hz, 1H), 7.29 (t, J = 8.1 Hz, 1H), 7.01 (d, J = 8.7 Hz, 1H) 2.54 (s, 2H). MS (ESI<sup>+</sup>-TOF) found (MH<sup>+</sup>) 222.5 (50) and 224.5 (50). Analytical data is consistent with the literature.

---

## Chapter 7

### References

1. U. T. Bornscheuer, G. W. Huisman, R. J. Kazlauskas, S. Lutz, J. C. Moore and K. Robins, *Nature.*, 2012, **485**, 185-194.
2. B. M. Nestl, S. C. Hammer, B. A. Nebel and B. Hauer, *Angew. Chem. Int. Ed. Engl.*, 2014, **53**, 3070-3095.
3. M. T. Reetz, *J. Am. Chem. Soc.*, 2013, **135**, 12480-12496.
4. U. T. Bornscheuer and M. Pohl, *Curr. Opin. Chem. Biol.*, 2001, **5**, 137-143.
5. C. M. Clouthier and J. N. Pelletier, *Chem. Soc. Rev.*, 2012, **41**, 1585-1605.
6. J. L. Porter, R. A. Rusli and D. L. Ollis, *ChemBioChem.*, 2015, **17**, 191-267.
7. U. T. Bornscheuer, G. W. Huisman, R. J. Kazlauskas, S. Lutz, J. C. Moore and K. Robins, *Nature.*, 2012, **485**, 185-194.
8. A. T. Bull, A. W. Bunch and G. K. Robinson, *Curr. Opin. Microbiol.*, 1999, **2**, 246-251.
9. T. Hudlicky and J. W. Reed, *Chem. Soc. Rev.*, 2009, **38**, 3117-3132.
10. D. Monti, G. Ottolina, G. Carrea and S. Riva, *Chem. Rev.*, 2011, **111**, 4111-4140.
11. S. W. May, *Curr. Opin. Biotechnol.*, 1999, **10**, 370-375.
12. F. Xu, *Ind. Biotechnol.*, 2005, **1**, 38-50.
13. S. G. Burton, *Trends. Biotechnol.*, 2003, **21**, 543-549.
14. A. W. Munro, P. Taylor and M. D. Walkinshaw, *Curr. Opin. Biotechnol.*, 2000, **11**, 369-376.
15. P. C. Cirino and F. H. Arnold, *Curr. Opin. Chem. Biol.*, 2002, **6**, 130-135.
16. T. L. Poulos, *Curr. Opin. Biotechnol.*, 1993, **4**, 484-489.
17. A. M. Azevedo, V. C. Martins, D. M. Prazeres, V. Vojinovic, J. M. Cabral and L. P. Fonseca, *Biotechnol. Annu. Rev.*, 2003, **9**, 199-247.
18. A. T. Smith and N. C. Veitch, *Curr. Opin. Chem. Biol.*, 1998, **2**, 269-278.
19. S. Colonna, N. Gaggero, C. Richelmi and P. Pasta, *Trends. Biotechnol.*, 1999, **17**, 163-168.
20. M. R. Maurya, *J. Chem. Sci.*, 2006, **118**, 503-511.
21. R. Brigelius-Flohé and M. Maiorino, *BBA-Gen. Subjects.*, 2013, **1830**, 3289-3303.
22. D. Parsonage and A. Claiborne, *Biochemistry.*, 1995, **34**, 435-441.

23. J. T. Rotruck, A. L. Pope, H. E. Ganther, A. B. Swanson, D. G. Hafeman and W. G. Hoekstra, *Science.*, 1973, **179**, 588-590.
24. G. S. Waldo and J. E. Penner-Hahn, *Biochemistry*, 1995, **34**, 1507-1512.
25. T. L. Poulos, *Arch. Biochem. Biophys.*, 2010, **500**, 3-12.
26. M. Hofrichter, R. Ullrich, M. J. Pecyna, C. Liers and T. Lundell, *Appl. Microbiol. Biotechnol.*, 2010, **87**, 871-897.
27. M. Zámocký, B. Gasselhuber, P. G. Furtmüller and C. Obinger, *Cell. Mol. Life Sci.*, 2014, **71**, 4681-4696.
28. L. Duroux and K. G. Welinder, *J. Mol. Evol.*, 2003, **57**, 397-407.
29. C. Obinger, *Arch. Biochem. Biophys.*, 2010, **500**, 1-2.
30. G. Battistuzzi, M. Bellei, C. A. Bortolotti and M. Sola, *Arch. Biochem. Biophys.*, 2010, **500**, 21-36.
31. M. Ayala, R. Roman and R. Vazquez-Duhalt, *Biochem. Biophys. Res. Commun.*, 2007, **357**, 804-808.
32. K. G. Welinder, *Eur. J. Biochem.*, 1979, **96**, 483-502.
33. L. Reimann and G. R. Schonbaum, *Methods Enzymol.*, 1978, **52**, 514-521.
34. N. C. Veitch, *Phytochemistry.*, 2004, **65**, 249-259.
35. F. W. Krainer, R. Pletzenauer, L. Rossetti, C. Herwig, A. Glieder and O. Spadiut, *Protein Expr. Purif.*, 2013, **95C**, 104-112.
36. L. M. Shannon, E. Kay and J. Y. Lew, *J. Bio. Chem.*, 1966, **241**, 2166-2172.
37. L. Näätäsaari, F. W. Krainer, M. Schubert, A. Glieder and G. G. Thallinger, *BMC - Genomics.*, 2014, **15**, 1-16.
38. B. J. Ryan, N. Carolan and C. O'Fagain, *Trends Biotechnol.*, 2006, **24**, 355-363.
39. G. I. Berglund, G. H. Carlsson, A. T. Smith, H. Szoke, A. Henriksen and J. Hajdu, *Nature.*, 2002, **417**, 463-468.
40. B. Y. Yang, J. S. S. Gray and R. Montgomery, *Carbohydr. Res.*, 1996, **287**, 203-212.
41. B. Eggenreich, M. Willim, D. J. Wurm, C. Herwig and O. Spadiut, *Biotechnol. Rep.*, 2016, **10**, 75-83.
42. Y. Shiro, M. Kurono and I. Morishima, *J. Bio. Chem.*, 1986, **261**, 9382-9390.
43. A. Henriksen, A. T. Smith and M. Gajhede, *J. Biol. Chem.*, 1999, **274**, 35005-35011.
44. B. Morawski, Z. Lin, P. Cirino, H. Joo, G. Bandara and F. H. Arnold, *Protein Eng.*, 2000, **13**, 377-384.
45. A. Gumiero, E. J. Murphy, C. L. Metcalfe, P. C. E. Moody and E. L. Raven, *Arch. Biochem. Biophys.*, 2010, **500**, 13-20.
46. M. Zámocký, S. Hofbauer, I. Schaffner, B. Gasselhuber, A. Nicolussi, M. Soudi, K. F. Pirker, P. G. Furtmüller and C. Obinger, *Arch. Biochem. Biophys.*, 2015, **574**, 108-119.
47. K. Yoshida, P. Kaothien, T. Matsui, A. Kawaoka and A. Shinmyo, *Appl. Microbiol. Biotechnol.*, 2003, **60**, 665-670.
48. V. Grigorenko, T. Chubar, Y. Kapeliuch, T. Börchers, F. Spener and A. Egorova, *Biocatal. Biotransform.*, 1999, **17**, 359-379.
49. F. Passardi, C. Cosio, C. Penel and C. Dunand, *Plant. Cell. Rep.*, 2005, **24**, 255-265.
50. M. a. d. I. M. Segura, G. Levin, M. a. V. Miranda, F. M. Mendive, H. M. Targovnik and O. Cascone, *Process Biochem.*, 2005, **40**, 795-800.
51. S. Asad, B. Dabirmanesh, N. Ghaemi, S. M. Etehad and K. Khajeh, *Mol. Biotechnol.*, 2013, **54**, 484-492.
52. O. Spadiut and C. Herwig, *Pharm. Bioprocess.*, 2013, **1**, 283-295.
53. F. W. Krainer and A. Glieder, *Appl. Microbiol. Biotechnol.*, 2015, **99**, 1611-1625.
54. F. W. Krainer, C. Dietzsch, T. Hajek, C. Herwig, O. Spadiut and A. Glieder, *Microb. Cell. Fact.*, 2012, **11**, 22.
55. O. Spadiut, L. Rossetti, C. Dietzsch and C. Herwig, *Protein Expr. Purif.*, 2012, **86**, 89-97.
56. U. Hoch, W. Adam, R. Fell, C. R. Saha-Möller and P. Schreier, *J. Mol. Catal. A: Chem.*, 1997, **117**, 321-328.
57. A. Tuynman, E. H. Schoemaker and R. Wever, *Monatsh. Chem. Chem. Mon.*, 2000, **131**, 687-695.

58. D. Kumar, S. P. de Visser, P. K. Sharma, H. Hirao and S. Shaik, *Biochemistry*, 2005, **44**, 8148-8158.
59. S.-i. Ozaki and P. R. Ortiz de Montellano, *J. Am. Chem. Soc.*, 1995, **117**, 7056-7064.
60. A. M. Klibanov, Z. Berman and B. N. Alberti, *J. Am. Chem. Soc.*, 1981, **103**, 6263-6264.
61. A. van der Vliet, J. P. Eiserich, B. Halliwell and C. E. Cross, *J. Biol. Chem.*, 1997, **272**, 7617-7625.
62. R.-J. Dai, H. Huang, J. Chen, Y.-L. Deng and S.-Y. Xiao, *Chin. J. Chem.*, 2007, **25**, 1690-1694.
63. E. Monzani, R. Roncone, M. Galliano, W. H. Koppenol and L. Casella, *Eur. J. Biochem.*, 2004, **271**, 895-906.
64. C. L. Shaffer, M. D. Morton and R. P. Hanzlik, *J. Am. Chem. Soc.*, 2001, **123**, 8502-8508.
65. R. P. Ferrari, E. Laurenti, L. Casella and S. Poli, *Spectrochim. Acta. Mol. Biomol. Spectrosc.*, 1993, **49**, 1261-1267.
66. K. Matsumoto, H. Takahashi, Y. Miyake and Y. Fukuyama, *Tetrahedron Lett.*, 1999, **40**, 3185-3186.
67. M. d'Ischia, A. Napolitano, K. Tsiakas and G. Prota, *Tetrahedron*, 1990, **46**, 5789-5796.
68. A. Molaei Rad, H. Ghourchian, A. A. Moosavi-Movahedi, J. Hong and K. Nazari, *Anal. Biochem.*, 2007, **362**, 38-43.
69. M. Puiu, A. Răducan, I. Babaligea and D. Oancea, *Bioprocess Biosyst. Eng.*, 2008, **31**, 579-586.
70. D. Ichinohe, T. Muranaka and H. Kise, *J. Appl. Polym. Sci.*, 1998, **70**, 717-721.
71. F. Hollmann, I. W. C. E. Arends, K. Buehler, A. Schallmeyer and B. Bühler, *Green Chem.*, 2011, **13**, 226-265.
72. G. R. Lopes, D. C. G. A. Pinto and A. M. S. Silva, *RSC Adv.*, 2014, **4**, 37244-37265.
73. S. Kobayashi, H. Uyama and S. Kimura, *Chem. Rev.*, 2001, **101**, 3793-3818.
74. S. Kobayashi and H. Higashimura, *Prog. Polym. Sci.*, 2003, **28**, 1015-1048.
75. N. Mita, S.-i. Tawaki, H. Uyama and S. Kobayashi, *Polym. J.*, 2001, **33**, 374-376.
76. H. Uyama, N. Maruichi, H. Tonami and S. Kobayashi, *Biomacromolecules*, 2002, **3**, 187-193.
77. H. Tonami, H. Uyama, S. Kobayashi, T. Fujita, Y. Taguchi and K. Osada, *Biomacromolecules*, 2000, **1**, 149-151.
78. A. G. MacDiarmid, *Angew. Chem. Int. Ed. Engl.*, 2001, **40**, 2581-2590.
79. A. G. MacDiarmid, *Synth. Met.*, 2001, **125**, 11-22.
80. F. Jonas and J. T. Morrison, *Synth. Met.*, 1997, **85**, 1397-1398.
81. B. Wessling, *Synth. Met.*, 1998, **93**, 143-154.
82. B. Wessling, *Synth. Met.*, 1997, **85**, 1313-1318.
83. R. Balint, N. J. Cassidy and S. H. Cartmell, *Acta. Biomater.*, 2014, **10**, 2341-2353.
84. S. Bhadra, D. Khastgir, N. K. Singha and J. H. Lee, *Prog. Polym. Sci.*, 2009, **34**, 783-810.
85. J. Stejskal, I. Sapurina and M. Trchová, *Prog. Polym. Sci.*, 2010, **35**, 1420-1481.
86. W. Liu, J. Kumar, S. Tripathy, K. J. Senecal and L. Samuelson, *J. Am. Chem. Soc.*, 1998, **121**, 71-78.
87. A. L. Cholli, M. Thiyagarajan, J. Kumar and V. S. Parmar, *Pure Appl. Chem.*, 2005, **77**, 339-344.
88. M. Jonsson, J. Lind, T. E. Eriksen and G. Merenyi, *J. Am. Chem. Soc.*, 1994, **116**, 1423-1427.
89. C. Li and M. Z. Hoffman, *J. Phys. Chem. B.*, 1999, **103**, 6653-6656.
90. J. Sakurada, R. Sekiguchi, K. Sato and T. Hosoya, *Biochemistry*, 1990, **29**, 4093-4098.
91. L. I. Krishtalik, *BBA - Bioenergetics*, 2003, **1604**, 13-21.
92. J. Shan, L. Han, F. Bai and S. Cao, *Polym. Adv. Technol.*, 2003, **14**, 330-336.
93. S. Jain, S. P. Surwade, S. R. Agnihotra, V. Dua, P. A. Eliason, G. J. Morose and S. K. Manohar, *Green Chem.*, 2010, **12**, 585-589.
94. P. Walde and Z. Guo, *Soft Matter*, 2011, **7**, 316-331.

95. W. Liu, A. L. Cholli, R. Nagarajan, J. Kumar, S. Tripathy, F. F. Bruno and L. Samuelson, *J. Am. Chem. Soc.*, 1999, **121**, 11345-11355.
96. A. J. Heeger, *Chem. Soc. Rev.*, 2010, **39**, 2354-2371.
97. V. Rumbau, J. A. Pomposo, A. Eleta, J. Rodriguez, H. Grande, D. Mecerreyes and E. Ochoteco, *Biomacromolecules*, 2007, **8**, 315-317.
98. A. Tewari, A. Kokil, S. Ravichandran, S. Nagarajan, R. Bouldin, L. A. Samuelson, R. Nagarajan and J. Kumar, *Macromol. Chem. Phys.*, 2010, **211**, 1610-1617.
99. M. R. Nabid and A. A. Entezami, *J. Appl. Polym. Sci.*, 2004, **94**, 254-258.
100. R. Garcia, R. V. Martinez and J. Martinez, *Chem. Soc. Rev.*, 2006, **35**, 29-38.
101. M. C. Roco, *Curr. Opin. Biotechnol.*, 2003, **14**, 337-346.
102. C. D. O'Connell, M. J. Higgins, S. E. Moulton and G. G. Wallace, *J. Mater. Chem. C*, 2015, **3**, 6431-6444.
103. H. c. M. Saavedra, J. M. Thomas, Z. Pengpeng, C. D. Daniel, A. C. Shelley and S. W. Paul, *Rep. Prog. Phys.*, 2010, **73**, 036501.
104. D. S. Ginger, H. Zhang and C. A. Mirkin, *Angew. Chem. Int. Ed. Engl.*, 2004, **43**, 30-45.
105. R. D. Piner, J. Zhu, F. Xu, S. Hong and C. A. Mirkin, *Science*, 1999, **283**, 661-663.
106. K. Salaita, Y. Wang and C. A. Mirkin, *Nat. Nano.*, 2007, **2**, 145-155.
107. K. Salaita, Y. Wang, J. Fragala, R. A. Vega, C. Liu and C. A. Mirkin, *Angew. Chem. Int. Ed. Engl.*, 2006, **45**, 7220-7223.
108. F. Huo, Z. Zheng, G. Zheng, L. R. Giam, H. Zhang and C. A. Mirkin, *Science*, 2008, **321**, 1658-1660.
109. D. J. Eichelsdoerfer, X. Liao, M. D. Cabezas, W. Morris, B. Radha, K. A. Brown, L. R. Giam, A. B. Braunschweig and C. A. Mirkin, *Nat. Protoc.*, 2013, **8**, 2548-2560.
110. F. Brinkmann, M. Hirtz, A. M. Greiner, M. Weschenfelder, B. Waterkotte, M. Bastmeyer and H. Fuchs, *Small*, 2013, **9**, 3266-3275.
111. A. Kuchler, M. Yoshimoto, S. Luginbuhl, F. Mavelli and P. Walde, *Nat. Nano.*, 2016, **11**, 409-420.
112. J. L. West and N. J. Halas, *Curr. Opin. Biotechnol.*, 2000, **11**, 215-217.
113. Y. Ma, J. Zhang, G. Zhang and H. He, *J. Am. Chem. Soc.*, 2004, **126**, 7097-7101.
114. P. Xu and D. L. Kaplan, *Adv. Mater.*, 2004, **16**, 628-633.
115. P. Xu and D. L. Kaplan, *J. Macromol. Sci., Pure Appl. Chem.*, 2004, **41**, 1437-1445.
116. S. A. M. Carnally and L. S. Wong, *Nanoscale*, 2014, **6**, 4998-5007.
117. X. Luo, V. A. Pedrosa and J. Wang, *Chem. Eu. J.*, 2009, **15**, 5191-5194.
118. R. Garcia, A. W. Knoll and E. Riedo, *Nat. Nano.*, 2014, **9**, 577-587.
119. W. Shim, A. B. Braunschweig, X. Liao, J. Chai, J. K. Lim, G. Zheng and C. A. Mirkin, *Nature*, 2011, **469**, 516-520.
120. D. J. Eichelsdoerfer, X. Liao, M. D. Cabezas, W. Morris, B. Radha, K. A. Brown, L. R. Giam, A. B. Braunschweig and C. A. Mirkin, *Nat. Protocols*, 2013, **8**, 2548-2560.
121. X. Liao, A. B. Braunschweig, Z. Zheng and C. A. Mirkin, *Small*, 2010, **6**, 1082-1086.
122. X. Liao, A. B. Braunschweig and C. A. Mirkin, *Nano Lett.*, 2010, **10**, 1335-1340.
123. L. S. Wong, C. V. Karthikeyan, D. J. Eichelsdoerfer, J. Micklefield and C. A. Mirkin, *Nanoscale*, 2012, **4**, 659-666.
124. L. S. Wong, K. Okrasa and J. Micklefield, *Org. Biomol. Chem.*, 2010, **8**, 782-787.
125. J. Yin, P. D. Straight, S. M. McLoughlin, Z. Zhou, A. J. Lin, D. E. Golan, N. L. Kelleher, R. Kolter and C. T. Walsh, *Proc. Natl. Acad. Sci.*, 2005, **102**, 15815-15820.
126. O. Spadiut, L. Rossetti, C. Dietzsch and C. Herwig, *Protein. Expr. Purif.*, 2012, **86**, 89-97.
127. L. Zhang, H. Peng, J. Sui, C. Soeller, P. A. Kilmartin and J. Travas-Sejdic, *J. Phys. Chem. C*, 2009, **113**, 9128-9134.
128. P. Winget, E. J. Weber, C. J. Cramer and D. G. Truhlar, *Phys. Chem. Chem. Phys.*, 2000, **2**, 1231-1239.
129. J. Yin, A. J. Lin, D. E. Golan and C. T. Walsh, *Nat. Protoc.*, 2006, **1**, 280-285.
130. C. K. Riener, C. M. Stroh, A. Ebner, C. Klampfl, A. A. Gall, C. Romanin, Y. L. Lyubchenko, P. Hinterdorfer and H. J. Gruber, *Anal. Chim. Acta.*, 2003, **479**, 59-75.
131. L. S. Wong, J. Thirlway and J. Micklefield, *J. Am. Chem. Soc.*, 2008, **130**, 12456-12464.

132. E. Abdelhamid, C. David, C. Eulalia, B. François, P.-R. Mateu, A. M. Christopher, T. Francesc and S. Josep, *Nanotechnology.*, 2007, **18**, 485301.
133. S. Wang, J. Hosford, W. P. Heath and L. S. Wong, *RSC Adv.*, 2015, **5**, 61402-61409.
134. N. Tiwari, M. Yue Liu, S. Kulkarni and Y. Fang, *J. Nanophotonics.*, 2011, **5**, 053513-053513-053514.
135. D. Sangamithirai, V. Narayanan, B. Muthuraaman and A. Stephen, *Mater. Sci. Eng. C.*, 2015, **55**, 579-591.
136. P. A. Kilmartin and G. A. Wright, *Synth. Met.*, 1999, **104**, 145-156.
137. M. G. Peter, *Angew. Chem. Int. Ed. Engl.*, 1989, **28**, 555-570.
138. R. W. Van De Water and T. R. R. Pettus, *Tetrahedron.*, 2002, **58**, 5367-5405.
139. M. S. Singh, A. Nagaraju, N. Anand and S. Chowdhury, *RSC Adv.*, 2014, **4**, 55924-55959.
140. V. K. Tandon and H. K. Maurya, *Tetrahedron Lett.*, 2009, **50**, 5896-5902.
141. E. Modica, R. Zanaletti, M. Freccero and M. Mella, *J. Org. Chem.*, 2001, **66**, 41-52.
142. C. C. Nawrat and C. J. Moody, *Angew. Chem. Int. Ed. Engl.*, 2014, **53**, 2056-2077.
143. L. I. Pilkington and D. Barker, *Nat. Prod. Rep.*, 2015, **32**, 1369-1388.
144. X. Jiang and R. Wang, *Chem. Rev.*, 2013, **113**, 5515-5546.
145. W.-J. Bai, J. G. David, Z.-G. Feng, M. G. Weaver, K.-L. Wu and T. R. R. Pettus, *Acc. Chem. Res.*, 2014, **47**, 3655-3664.
146. A. Pezzella, O. Crescenzi, L. Panzella, A. Napolitano, E. J. Land, V. Barone and M. d'Ischia, *J. Am. Chem. Soc.*, 2013, **135**, 12142-12149.
147. D. Xu, A. Chiaroni and M. Largeton, *Org. Lett.*, 2005, **7**, 5273-5276.
148. J. Zhang, C. Taylor, E. Bowman, L. Savage-Low, M. W. Lodewyk, L. Hanne and G. Wu, *Tetrahedron Lett.*, 2013, **54**, 6298-6302.
149. E. Blattes, M.-B. Fleury and M. Largeton, *J. Org. Chem.*, 2004, **69**, 882-890.
150. H. Oikawa and T. Tokiwano, *Nat. Prod. Rep.*, 2004, **21**, 321-352.
151. G. Ulas, T. Lemmin, Y. Wu, G. T. Gassner and W. F. DeGrado, *Nat. Chem.*, 2016, **8**, 354-359.
152. P. J. Tarcha, V. P. Chu and D. Whittern, *Anal. Biochem.*, 1987, **165**, 230-233.
153. D. M. X. Donnelly, F. G. Murphy, J. Polonski and T. Prange, *J. Chem. Soc. Perkin Trans. 1*, 1987, 2719-2722.
154. S. Nicolis, M. Zucchelli, E. Monzani and L. Casella, *Chem. Eur. J.*, 2008, **14**, 8661-8673.
155. J. Ilaš, P. Š. Anderluh, M. S. Dolenc and D. Kikelj, *Tetrahedron.*, 2005, **61**, 7325-7348.
156. N. Bodipati and R. K. Peddinti, *Org. Biomol. Chem.*, 2012, **10**, 1958-1961.
157. L. Mao, S. Luo, Q. Huang and J. Lu, *Sci. Rep.*, 2013, **3**, 3126.
158. J. Auge, *Green Chem.*, 2008, **10**, 225-231.
159. N. L. Weinberg and H. R. Weinberg, *Chem. Rev.*, 1968, **68**, 449-523.
160. R. Rodriguez, R. M. Adlington, J. E. Moses, A. Cowley and J. E. Baldwin, *Org. Lett.*, 2004, **6**, 3617-3619.
161. K. Chiba, J. Sonoyama and M. Tada, *J. Chem. Soc. Perkin Trans. 1*, 1996, 1435-1443.
162. G. Kopf and W. Schwack, *Pest. Sci.*, 1995, **43**, 303-309.
163. M. J. Byrne, N. R. Lees, L.-C. Han, M. W. van der Kamp, A. J. Mulholland, J. E. M. Stach, C. L. Willis and P. R. Race, *J. Am. Chem. Soc.*, 2016, **138**, 6095-6098.
164. C. A. Townsend, *ChemBioChem.*, 2011, **12**, 2267-2269.
165. S. A. Lawrence, *Amines: Synthesis, Properties and Applications*, Cambridge University Press, Cambridge, 2006.
166. M. J. O'Neil, *The Merck Index: An Encyclopedia of Chemicals, Drugs, and Biologicals*, Royal Society of Chemistry, Cambridge, 2013.
167. N. Miyaura and A. Suzuki, *Chem. Rev.*, 1995, **95**, 2457-2483.
168. P. Kovacic and N. O. Brace, *J. Am. Chem. Soc.*, 1954, **76**, 5491-5494.
169. M. Noe, A. Perosa, M. Selva and L. Zambelli, *Green Chem.*, 2010, **12**, 1654-1660.
170. M. A. Fisher and D. Tullman-Ercek, *Curr. Opin. Biotechnol.*, 2013, **24**, 1010-1016.
171. G. W. Huisman and S. J. Collier, *Curr. Opin. Chem. Biol.*, 2013, **17**, 284-292.

172. U. T. Bornscheuer, G. W. Huisman, R. J. Kazlauskas, S. Lutz, J. C. Moore and K. Robins, *Nature*, 2012, **485**, 185-194.
173. C. D. Murphy, *J. Appl. Microbiol.*, 2003, **94**, 539-548.
174. F. H. Vaillancourt, E. Yeh, D. A. Vosburg, S. Garneau-Tsodikova and C. T. Walsh, *Chem. Rev.*, 2006, **106**, 3364-3378.
175. A. Butler and M. Sandy, *Nature.*, 2009, **460**, 848-854.
176. J. T. Payne, M. C. Andorfer and J. C. Lewis, *Angew. Chem. Int. Ed. Engl.*, 2013, **52**, 5271-5274.
177. K.-H. Van Pée and E. Patallo, *Appl. Microbiol. Biotechnol.*, 2006, **70**, 631-641.
178. C. Dong, S. Flecks, S. Unversucht, C. Haupt, K. H. van Pee and J. H. Naismith, *Science.*, 2005, **309**, 2216-2219.
179. E. Yeh, L. C. Blasiak, A. Koglin, C. L. Drennan and C. T. Walsh, *Biochemistry.*, 2007, **46**, 1284-1292.
180. W. S. Glenn, E. Nims and S. E. O'Connor, *J. Am. Chem. Soc.*, 2011, **133**, 19346-19349.
181. E. Verhaeghe, D. Buisson, E. Zekri, C. Leblanc, P. Potin and Y. Ambroise, *Anal. Biochem.*, 2008, **379**, 60-65.
182. L. P. Hager, D. R. Morris, F. S. Brown and H. Eberwein, *J. Biol. Chem.*, 1966, **241**, 1769-1777.
183. C. Wagner, I. M. Molitor and G. M. König, *Phytochemistry.*, 2008, **69**, 323-332.
184. M. Frese, P. H. Guzowska, H. Voß and N. Sewald, *ChemCatChem*, 2014, **6**, 1270-1276.
185. S. Uchiyama, Y. Hasebe, J. Nishimoto, H. Hamana, Y. Maeda and Y. Yoshida, *Electroanalysis.*, 1998, **10**, 647-650.
186. S. Witayakran and A. J. Ragauskas, *Eur. J. Org. Chem.*, 2009, **2009**, 358-363.
187. G. Spyrou, E. Haggard-Ljungquist, M. Krook, H. Jornvall, E. Nilsson and P. Reichard, *J. Bacteriol.*, 1991, **173**, 3673-3679.
188. T. Nagao, T. Mitamura, X. H. Wang, S. Negoro, T. Yomo, I. Urabe and H. Okada, *J. Bacteriol.*, 1992, **174**, 5013-5020.
189. V. Köhler, Y. M. Wilson, M. Dürrenberger, D. Ghislieri, E. Churakova, T. Quinto, L. Knörr, D. Häussinger, F. Hollmann, N. J. Turner and T. R. Ward, *Nat. Chem.*, 2013, **5**, 93-99.
190. D. V. Moiseev, B. O. Patrick, B. R. James and T. Q. Hu, *Inorg. Chem.*, 2007, **46**, 9389-9399.
191. E. Yeh, S. Garneau and C. T. Walsh, *Proc. Natl. Acad. Sci.*, 2005, **102**, 3960-3965.
192. D. G. Gibson, L. Young, R. Y. Chuang, J. C. Venter, C. A. Hutchison, 3rd and H. O. Smith, *Nat. Methods.*, 2009, **6**, 343-345.
193. J. Sambrook and D. Russell, *Molecular Cloning: A Laboratory Manual*, Cold Spring Harbor Laboratory Press, New York, 2001.
194. L. Wildling, B. Unterauer, R. Zhu, A. Rupprecht, T. Haselgrübler, C. Rankl, A. Ebner, D. Vater, P. Pollheimer, E. E. Pohl, P. Hinterdorfer and H. J. Gruber, *Bioconjugate Chem.*, 2011, **22**, 1239-1248.
195. K.-C. Tiew, D. Dou, T. Teramoto, H. Lai, K. R. Alliston, G. H. Lushington, R. Padmanabhan and W. C. Groutas, *Bioorg. Med. Chem. Lett.*, 2012, **20**, 1213-1221.
196. S. V. Chankeshwara and A. K. Chakraborti, *Synthesis.*, 2006, **2006**, 2784-2788.
197. F. Shirini, O. G. Jolodar, M. Seddighi and H. T. Borujeni, *RSC Adv.*, 2015, **5**, 19790-19798.
198. R. Lok, R. E. Leone and A. J. Williams, *J. Org. Chem.*, 1996, **61**, 3289-3297.
199. C.-a. Di, J. Li, G. Yu, Y. Xiao, Y. Guo, Y. Liu, X. Qian and D. Zhu, *Org. Lett.*, 2008, **10**, 3025-3028.
200. J. L. Gal, S. Michaud, M. Gressier, Y. Coulais and E. Benoist, *Bioorg. Med. Chem.*, 2006, **14**, 2904-2909.
201. T. H. M. Jonckers, M.-C. Rouan, G. Haché, W. Schepens, S. Hallenberger, J. Baumeister and J. C. Sasaki, *Bioorg. Med. Chem. Lett.*, 2012, **22**, 4998-5002.
202. C. D. Bray, *Org. Biomol. Chem.*, 2008, **6**, 2815-2819.
203. S. Cao, R. Christiansen and X. Peng, *Chem. Eur. J.*, 2013, **19**, 9050-9058.
204. N. Lebrasseur, J. Gagnepain, A. Ozanne-Beaudenon, J.-M. Léger and S. Quideau, *J. Org. Chem.*, 2007, **72**, 6280-6283.

205. C. K. Lau, H. W. R. Williams, S. Tardiff, C. Dufresne, J. Scheigetz and P. C. Bélanger, *Can. J. Chem.*, 1989, **67**, 1384-1387.
206. N. K. Sharma, F. d. Reinach-Hirtzbach and T. Durst, *Can. J. Chem.*, 1976, **54**, 3012-3025.
207. A. Wasilewska, B. A. Woźniak, G. Doridot, K. Piotrowska, N. Witkowska, P. Retailleau and Y. Six, *Chem. Eu. J.*, 2013, **19**, 11759-11767.



---

**Chapter 8****Appendix.****8.1 ybbR-C1A Sequences****8.1.1 Nucleotide sequence**

ATGGATTCTTTGGAGTTCATTGCATCTAACTTGCTCAATTGACACCTACTTTCTATGAT  
AACTCTTGTCCAAATGTTTCCAACATTGTTAGAGATACAATAGTGAACGAGTTGAGATCC  
GATCCACGTATTGCTGCCTCAATCCTCAGACTGCATTTCCACGACTGTTTTGTTAATGGT  
TGTGATGCTTCCATCTTACTTGATAACACGACATCTTTCAGAACAGAGAAGGACGCATTT  
GGTAATGCTAATTCGGCAAGAGGATTTCTGTAATAGACCGTATGAAAGCAGCAGTGGA  
ATCTGCTTGCCTAGAACTGTTTCGTGTGCTGATTTGTTAACTATCGCAGCTCAACAATC  
AGTAACTCTTGCCGGAGGACCCTCTTGGAGAGTTCCACTAGGACGTCGTGACTCTTTA  
CAGGCTTTTCTGGATCTGGCAAATGCTAACCTGCCAGCACCCCTTTTTCACTTTGCCCA  
ACTTAAGGATAGTTTTAGAAATGTTGGCCTTAATCGTTCAAGCGATTTGGTCGCTCTATC  
CGGTGGTCACACTTTCGGCAAAAACCAATGCAGATTCATTATGGACAGACTATACAAC  
TTTCGAATACTGGACTTCCTGATCCAACCTTTGAATACCACTTACCTGCAAACACTCAGG  
GGTTTGTGCCCTCTTAATGGTAATCTGAGTGCCTTGGTGGACTTCGATTTGAGAACCCC  
TACAATCTTTGACAACAAATACTATGTAACTTAGAAGAGCAAAAGGGTCTGATTCAGAG  
CGATCAGGAGTTGTTCTCCTCCCCAAATGCTACAGACACTATTCCATTGGTAAGGAGTT  
TCGCAAACCTCAACGCAAACCTTTTTCAATGCCTTCGTGGAAGCTATGGATAGGATGGGT

AACATCACCCCGTTAACCGGTACCCAAGGACAGATTAGACTGAATTGTCGTGTCGTCAA  
CTCAAATTCCTTGTTCATGACATGGTGGAAAGTTGTGGACTTTGTTAGCAGCATGCTCG  
AGCACCACCACCACCACCACTGA

### 8.1.2 Protein sequence

MDSLEFIASKLAQLTPTFYDNPCPNVSNIVRDTIVNELRSDPRIAASILRLHFHDCFVNGCDA  
SILLDNTTSFRTEKDAFGNANSARGFPVIDRMKAAVESACPRTVSCADLLTIAAQQSVTLAG  
GPSWRVPLGRRDSLQAFDLANANLPAPFFTLPLQLKDSFRNVGLNRSSDLVALSGGHTFG  
KNQCRFIMDRLYNFSNTGLPDPTLNNTTYLQTLRGLCPLNGNLSALVDFDLRPTIFDNKYYV  
NLEEQKGLIQSDQELFSSPNATDTIPLVRSFANSTQFFNAFVEAMDRMGNITPLTGTQGQI  
RLNCRVVNSNSLLHDMVEVDFVSSMLEHHHHHH\*

## 8.2 Sfp sequences

### 8.2.1 Nucleotide sequence

ATGAAGATTTACGGAATTTATATGGACCGCCCGCTTTCACAGGAAGAAAATGAACGGTT  
CATGTCTTTCATATCACCTGAAAAACGGGAGAAATGCCGGAGATTTTATCATAAAGAAG  
ATGCTCACCGCACCTGCTGGGAGATGTGCTCGTTCGCTCAGTCATAAGCAGGCAGTA  
TCAGTTGGACAAATCCGATATCCGCTTTAGCACGCAGGAATACGGGAAGCCGTGCATC  
CCTGATCTTCCCGACGCTCATTCAACATTTCTCACTCCGGACGCTGGGTCAATTTGCGC  
GTTTGATTCACAGCCGATCGGCATAGATATCGAAAAACGAAACCGATCAGCCTTGAGA  
TCGCCAAGCGCTTCTTTTCAAAAACAGAGTACAGCGACCTTTTAGCAAAAGACAAGGAC  
GAGCAGACAGACTATTTTTATCATCTATGGTCAATGAAAGAAAGCTTTATCAAACAGGAA  
GGCAAAGGCTTATCGCTTCCGCTTGATTCTTTTTCAGTGCGCCTGCACCAGGACGGAC  
AAGTATCCATTGAGCTTCCGGACAGCCATTCCCATGCTATATCAAACGTATGAGGTC  
GATCCCGGCTACAAAATGGCTGTATGCGCCGTACACCCTGATTTCCCGAGGATATCA  
CAATGGTCTCGTACGAAGAGCTTTTATAA

### 8.2.2 Protein sequence

MGSSHHHHHSSGLVPRGSMKIYGIYMDRPLSQEENERFMSFISPEKREKCRRFYHKEDA  
 HRTLLGDVLVRSVISRQYQLDKSDIRFSTQEYGKPCIPDLPAHFNISHSGRWVICAFFDSQPI  
 GIDIEKTKPISLEIAKRFFSKTEYSDLLAKDKDEQTDYFYHLWSMKESFIKQEGKGLSLPLDS  
 FSVRLHQDGQVSIELPDSHSPCYIKTYEVDPGYKMAVCAVHPDFPEDITMVSYEELL\*

### 8.3 RebH Sequences

#### 8.3.1 Nucleotide sequence

ATGGGCAGCAGCCATCATCATCATCACAGCAGCGGCCTGGTGCCGCGCGGCAGC  
 CATATGTCCGGCAAGATTGACAAGATCCTCATCGTCGGCGGCACCGCCGGATGG  
 ATGGCCGCGTCCTATCTCGGCAAGGCCCTGCAGGGCACCGCGGACATCACACTGCTG  
 CAGGCACCCGACATCCCGACGCTCGGGTTCGGCGAGGCCACGATCCCCAATCTGCAG  
 ACGGCGTTCTTCGACTTCTCGGAATCCCGAGGACGAGTGGATGCGGGAGTGCAAC  
 GCGAGCTACAAGGTCGCCATCAAGTTCATCAACTGGCGCACCGCGGGCGAGGGGACG  
 TCCGAGGCCCGCGAGCTCGACGGAGGGCCCGACCACTTCTACCACTCCTTCGGTCTG  
 CTCAAGTACCACGAGCAGATTCCGCTGTGCGACTACTGGTTCGACCGTTCGTACCGGG  
 GGAAGACCGTCGAGCCGTTGACTACGCCTGCTACAAGGAACCCGTCATCCTCGACG  
 CCAACAGGTCACCGCGCAGGCTCGACGGTTCCAAGGTGACGAACTACGCGTGGCACT  
 TCGACGCGCACCTCGTCGCCGACTTCTGCGCCGGTTCGCCACCGAGAAGCTCGGCG  
 TCGCCACGTCGAGGACCGCGTCGAGCACGTCCAGCGCGACGCCAACGGCAACATCG  
 AGTCGGTTCGCACGGCAACGGGGCGTGTCTTCGATGCCGACCTCTTCGTGCGACTGCTC  
 GGGCTTCCGCGGGCTGCTGATCAACAAGGCGATGGAGGAGCCCTTCTCGACATGAG  
 CGATCACCTGCTCAACGACAGCGCCGTGCCACCCAGGTGCCGCACGACGACGACGC  
 GAACGGTGTGGAACCGTTCACCTCGGCGATCGCCATGAAGTCGGGCTGGACGTGGAA  
 GATCCCGATGCTCGGCAGGTTCCGGCACCGGGTACGTCTACTCGAGCCGGTTCGCCAC  
 CGAGGACGAGGCGGTGCGCGAGTTCTGCGAGATGTGGCACCTCGACCCGGAGACCC  
 AGCCCCTCAACAGGATCCGGTTCGGGTTCGGCCGCAACCGGCGCGCGTGGGTTCGGC

AACTGCGTCAGCATCGGCACGTCGTCGTGCTTCGTGGAACCACTGGAGTCGACGGGC  
 ATCTACTTCGTCTACGCCGCGCTGTACCAGCTGGTGAAGCACTTCCCCGACAAGAGCC  
 TCAACCCCGTGCTGACCGCCAGGTTCAACCGCGAGATCGAGACGATGTTTCGACGACAC  
 GCGCGACTTCATCCAGGCGCACTTCTACTTCTCGCCGCGCACGGACACCCCGTTCTGG  
 AGGGCCAACAAGGAGCTGCGCCTGGCGGACGGCATGCAGGAGAAGATCGACATGTAC  
 CGCGCGGGCATGGCGATCAACGCGCCCGCGTCCGACGACGCCAGCTCTACTACGG  
 CAACTTCGAGGAGGAGTTCCGCAACTTCTGGAACAACAGCAACTACTACTGCGTGCTG  
 GCCGGCCTCGGTCTGGTGCCCGACGCACCCTCACCACGCCTGGCGCACATGCCACAG  
 GCGACGGAGTCGGTGGACGAGGTCTTCGGCGCCGTCAAGGACCGGCAGCGGAACCT  
 GCTCGAGACCCTGCCGAGCCTCCACGAGTTCCTGAGGCAACAGCACGGCCGCTGA

### 8.3.2 Protein sequence

MGSSHHHHHSSGLVPRGSHMSGKIDKILIVGGGTAGWMAASYLGKALQGTADITLLQAP  
 DIPTLGVGEATIPNLQTAFFDFLGIPEDWWMRECNASYKVAIKFINWRTAGEGTSEARELDG  
 GPDHFYHSFGLLYHEQIPLSHYWFDERSYRGKTVEPFYACYKEPVILDANRSPRRLDGSK  
 VTNYAWHFDAHLVADFLRRFATEKLGVRHVEDRVEHVQRDANGNIESVRTATGRVFDADL  
 FVDCSGFRGLLINKAMEEPFLDMSDHLNDSAVATQVPHDDDANGVEPFTSAIAMKSGWT  
 WKIPMLGRFGTGYVYSSRFATEDEAVREFCEMWHLDPETQPLNRIRFRVGRNRRRAWVGN  
 CVSIGTSSCFVEPLESTGIYFVYAALYQLVKHFDPKSLNPVLTARFNREIETMFDDTRDFIQA  
 HFYFSPRTDTPFWRANKELRLADGMQEKIDMYRAGMAINAPASDDAQLYYGNFEEEFERNF  
 WNNSNYCVLAGLGLVPDAPSPRLAHMPQATESVDEVFGAVKDRQRNLETLPSTLHEFLR  
 QQHGR\*

## 8.4 Fre Sequences

### 8.4.1 Nucleotide sequence

ATGCATCACCACCACCATCACGTGGGTACCATGACAACCTTAAGCTGTAAAGTGACCTC  
GGTAGAAGCTATCACGGATACCGTATATCGTGTCCGCATCGTGCCAGACGCGGCCTTT  
TCTTTTCGTGCTGGTCAGTATTTGATGGTAGTGATGGATGAGCGCGACAAACGTCCGTT  
CTCAATGGCTTCGACGCCGGATGAAAAAGGGTTTATCGAGCTGCATATTGGCGCTTCT  
GAAATCAACCTTTACGCGAAAGCAGTCATGGACCGCATCCTCAAAGATCATCAAATCGT  
GGTCGACATTCCCCACGGAGAAGCGTGGCTGCGCGATGATGAAGAGCGTCCGATGAT  
TTTGATTGCGGGCGGCACCGGGTTCTCTTATGCCCGCTCGATTTTGCTGACAGCGTTG  
GCGCGTAACCCAAACCGTGATATCACCATTTACTGGGGCGGGCGTGAAGAGCAGCATC  
TGTATGATCTCTGCGAGCTTGAGGCGCTTTTCGTTGAAGCATCCTGGTCTGCAAGTGGT  
GCCGGTGGTTGAACAACCGGAAGCGGGCTGGCGTGGGCGTACTGGCACCGTGTTAAC  
GGCGGTATTGCAGGATCACGGTACGCTGGCAGAGCATGATATCTATATTGCCGGACGT  
TTTGAGATGGCGAAAATTGCCCGCGATCTGTTTTGCAGTGAGCGTAATGCGCGGGAAG  
ATCGCCTGTTGGCGATGCGTTTGCATTTATCTGA

#### 8.4.2 Protein sequence

MHHHHHHVGTMTTL SCKVTSVEAITDTVYRVRV PDAAFSFRAGQYLMVVMDERDKRPF S  
MASTPDEKGFIELHIGASEINLYAKAVMDRILKDHQIVVDIPHGEAWLRDDEERPMILIAGGT  
GFSYARSILLTALARNPNRDITIWGGREEQHLYDLCELEALSLKHPGLQVVPVVEQPEAG  
WRGRTGTVLTA VLQDHGTLAEHDIYIAGRFEMAKIARDLFC SERNAREDR LFGDAFAFI\*

#### 8.5 GDH2 Sequence

##### 8.5.1 Nucleotide sequence

ATGTATACGGATCTGAAGGATAAGGTTGTTGTGGTTACGGGTGGTTCTAAGGGTCTGG  
GTCGTGCGATGGCAGTGCGTTTTGGTCAAGAACAGAGCAAAGTGGTTGTCAACTATCG  
TTCTAATGAAGAAGAAGCACTGGAAGTTAAAAAGGAAATTGAAGAAGCGGGCGGTCAA

GCCATTATCGTCCGCGGCGATGTGACCAAAGAAGAAGACGTGGTTAACCTGGTTGAAA  
CGGCGGTCAAGGAATTTGGCTCACTGGATGTGATGATCAACAATGCCGGTGTGGAAAA  
TCCGGTTCGTACATGAACTGTCGCTGGAAAAGTGAATCAAGTGATTGATACCAACC  
TGACGGGCGCGTTTCTGGGTTACGTGAAGCCATCAAGTACTTCGTTGAAAACGACAT  
CAAGGGCAACGTCATCAATATGAGCTCTGTGCATGAAATGATTCCGTGGCCGCTGTTT  
GTTCACTATGCGGCCTCGAAAGGCGGTATGAAGCTGATGACCGAAACGCTGGCACTGG  
AATACGCTCCGAAAGGTATTCGTGTCAACAATATCGGCCCGGGTGCAATTGATACCCC  
GATCAACGCGGAAAAGTTTGCCGATCCGGAACAACGCGCTGACGTGGAAAGCATGATT  
CCGATGGGCTACATCGGTAAACCGGAAGAAATTGCCAGTGTTGCAGCTTTCCTGGCAA  
GTTCCCAGGCTTCTATGTCACCGGTATCACGCTGTTTGCAGACGGCGGTATGACCAA  
ATACCCGTCTTTCCAAGCTGGCCGCGGTCTCGAGCACCACCACCACCACCACTGA

### 8.5.2 Protein sequence

MYTDLKDKVVVVTGGSKGLGRAMAVRFGQEQSKVVVNYRSNEEEALEVKKEIEEAGGQAI  
VRGDVTKEEDVVNLVETAVKEFGSLDVMINNAGVENPVPSHELLENWNQVIDTNLTGAFL  
GSREAIKYFVENDIKGNVINMSSVHEMIPWPLFVHYAASKGGMKLMTETLALEYAPKGIRVN  
NIGPGAIDTPINA EK FADPEQRADVESMIPMGYIGKPEEIASVAAFLASSQASYVTGITLFAD  
GGMTKYPSFQAGRGLEHHHHH\*